Investigating Cerebellar Mechanisms of Schizophrenia by Using a Pharmacological Mouse Model: Regulation of Voltage-Gated Potassium Channels

Lukasz Lagojda

Institute of Allied Health Sciences

Leicester Institute of Pharmacological Innovation

De Montfort University

This thesis is submitted for the degree of

Doctor of Philosophy

October 2021

“But life is long.
And it is the long run
that balances the short
flare of interest and
passion”.

- Sylvia Plath

Declaration

I hereby declare that except where specific reference is made to the work of others, the contents of this dissertation are original and have not been submitted in whole or in part for consideration for any other degree or qualification at this, or any other institution.

This dissertation is the result of my own work and includes nothing which is the outcome of work done in collaboration, except where specifically indicated in the text. This dissertation contains less than 80,000 words including appendices, bibliography, footnotes, tables, and equations and has less than 150 figures.

Lukasz Lagojda

October 2021

Acknowledgements

First, I would like to congratulate **Dr Lan Zhu** on successfully supervising her first doctoral student. I would like to express my sincerest thanks for her support and the care she has gifted upon me. This thesis would not be possible without her mentorship, for which I will remain forever grateful.

I would also like to acknowledge the whole Neuropharmacology Research Group, which has been a pleasure to work and share ideas with. Special thanks are also directed to the Technical Team for always making things available when they were not.

Lastly, I would like to thank all my friends and family who supported me when things did not look so bright.

Abstract

Schizophrenia is a heterogeneous psychiatric disorder which affects at least 1% of the global population. Its complex pathology involves impaired neuronal communication that leads to the onset of debilitating symptoms affecting behaviour and cognition. Voltage-gated potassium (Kv) channels are fundamental to neuronal communication because of their intricate roles in regulating neuronal excitability, thereby governing information processing in the brain. The cerebellum has a significant influence over how this information is communicated across the brain because of its interconnectivity with virtually all brain regions. To expand our understanding of Kv channels, this thesis investigates the regulation of three alpha subunits of voltage-gated potassium channels Kv2.1, Kv6.4, and Kv3.1b in the cerebellar cortex of a phencyclidine-induced mouse model of schizophrenia and explores their potential role in schizophrenia symptoms.

In Chapter 3 we show using immunohistochemistry that Kv2.1 is expressed in the Purkinje cells and granule cells as membrane-bound clusters in the soma and proximal dendrites, whereas the Kv6.4 are mainly present in the cytosol. Additionally, using proximity ligation we demonstrated for the first time that Kv6.4 arrange with Kv2.1 to form heteromeric channels on the perisomatic

membrane of Purkinje cells. These findings suggest that Kv2.1 and Kv6.4 may act as neuronal ‘transistors’ thereby controlling the frequency of neuronal firing in these cell populations.

In Chapter 4 we describe the behavioural phenotype of our CBA/CA phencyclidine model to include altered exploratory patterns, changes in locomotor activity, and changes in rearing and grooming behaviours. We also observed dysregulation of NMDA-receptor genes in frontal cortex and the cerebellum, and abnormalities in several features of the cerebellum of the model mice. Additionally, we describe the effectiveness of concomitant antipsychotic agents haloperidol and clozapine in attenuating the acute changes in behaviour induced by phencyclidine, and we introduce specific motor function tests to assess cerebellar involvement in the model. Together, these findings support several aspects of face, construct, and predictive validity expected of a schizophrenia model.

Finally in Chapter 5 we investigate the cerebellar regulation of the three Kv subunits in our animal model, where we found Kv2.1 downregulation in the cerebellar cortex which is consistent with findings from human schizophrenia subjects and from animal studies. Strikingly, we found that the Kv6.4 is upregulated in several regions of the cerebellum that was supported by upregulated Kcng4 gene, which may indicate a compensatory mechanism for Kv2.1 loss. Additionally, we observed downregulation of the Kv3.1b in the

granule cell layer of the right cerebellar lateral hemisphere, which may indicate a local functional demand.

In conclusion, this thesis demonstrates, by using a range of behavioural, histological, and biomolecular investigations, the cerebellar pathology resulting from subchronic phencyclidine treatment, and also elucidates the functional role of Kv channels in a schizophrenia-like pathological state.

Table of contents

List of Figures

List of Tables

List of Abbreviations and Acronyms

3rdV	Third ventricle
A	Absorbance
A	Adenine
APD	Antipsychotic drug
b.w.	Bodyweight
BC	Basket cell
BSA	Bovine serum albumin
C	Celsius
C	Cytosine
Cav	Voltage-gated calcium channel
Cb/ CB	Cerebellum
cDNA	Complimentary DNA
CF	Climbing fibre
CLZ	Clozapine
cm	Centimetre
CNS	Central nervous system
COOH	Carboxyl group
C_T	Threshold cycle

CTCF	Corrected total cell fluorescence
D1	Dopamine receptor, type 1
D2	Dopamine receptor, type 2
DAPI	4′,6-diamidino-2-phenylindole
ddH_2O	Double distilled water
DEPC	Diethyl pyrocarbonate
dH_2O	Distilled water
dL	Decilitre
DMT	*N*-*N*-dimethyltryptamine
DNA	Deoxyribonucleic acid
dNTP	Deoxy-NTP
DSM	Diagnostic and statistical manual of mental disorders
DTI	Diffusion tensor imaging
ECL	Enhanced chemiluminescence
EDTA	Ethylenediaminetetraacetic acid
ERBB4	Receptor tyrosine-protein kinase 4
Fc	Frontal cortex
fMRI	Functional magnetic resonance imaging
fps	Frames per second
g	Gram
g	Gravity
G	Guanine
GABA	Gamma-aminobutyric acid
GAD	Glutamic acid decarboxylase

GAPDH	glyceraldehyde 3-phosphate dehydrogenase
GoC	Golgi cell
GrC/ GC	Granule cell
GWAS	Genome-wide association study
Hip	Hippocampus
HLA	Human leukocyte antigen
HLP	Haloperidol
HRP	Horseradish peroxidase
ICD	International classification of diseases
ID	Integrated density
I_k	Inwardly rectifying potassium current
IQR	Interquartile range
kD	Kilo Dalton
kg	Kilogram
Kir	Inwardly rectifying potassium channel
Kv	Voltage-gated potassium channel
LA	Locomotor activity
LN_2	Liquid nitrogen
LSCM	Laser-scanning confocal microscope
LSD	Lysergic acid diethylamide
M.W.	Molecular weight
MAM	Methylazoxymethanol acetate
MF	Mossy fibre
mg	Milligram

MGV	Mean grey value
MHC	Major histocompatibility complex
mM	Millimolar
MRI	Magnetic resonance imaging
mRNA	Messenger RNA
MuIF	Multi-layered fibre
mV	Millivolt
Nav	Voltage-gated sodium channel
ng	Nanograms
NGS	Normal goat serum
NH_2	Amino group
nM	Nanomolar
nm	Nanometre
NMDA	*N*-methyl-D-aspartate
NMDAR	NMDA receptor
NOR	Novel object recognition
NTP	Nucleotide triphosphate
Ø	Diameter
OCT	Optimum cutting temperature
ON	Overnight
PAGE	Polyacrylamide gel electrophoresis
PBST	Phosphate-buffered saline supplemented with Triton
PC	Purkinje cell
PCP	Phencyclidine

PCR	Polymerase-chain reaction
PET	Positron emission tomography
PFA	Paraformaldehyde
pH	Potential of hydrogen
PLA	Proximity-ligation assay
qPCR	Quantitative PCR
RI	Recognition index
RNA	Ribonucleic acid
ROI	Region of interest
RT	Room temperature
RT	Reverse transcription
RT-qPCR	Reverse transcription qPCR
SC	Stellate cell
SD	Standard deviation
SDS	Sodium dodecyl sulphate
SEM	Standard error of the mean
SPET	Single proton-emission tomography
SPECT	Single proton-emission computational tomography
SZ	Schizophrenia
t	Time
T	Thymine
TBST	Tris-buffered saline supplemented with Tween®
TCF4	Transcription factor 4
Th	Thalamus

U	Uracil
UBC	Unipolar brush cell
UV	Ultraviolet
V	Volt
v/v	Volume per volume
VTA	Ventral tegmental area
VRK2	Vaccinia-related kinase
w/v	Weight per volume
WHO	World health organization
α	alpha
β	Beta
γ	Gamma
δ/ Δ	Delta
κ	Kappa
λ	Wavelength
µm	Micrometre

Chapter 1 Introduction

1.1 Schizophrenia

1.1.1 Overview

Schizophrenia is a heterogeneous psychiatric disorder which affects behaviour, emotions, and interferes with how one perceives the real world. Globally, about seven individuals in every one thousand will develop schizophrenia, with men being affected slightly more often compared to women. The median lifetime prevalence of schizophrenia based on a meta-analysis of systematic reviews of data from 46 countries is currently estimated at around 0.4%, though the estimates vary significantly between regions (McGrath et al., 2008), and despite the relatively low prevalence, the condition was ranked as the 12th amongst 310 of the most disabling injuries and diseases worldwide (Vos et al., 2017) with global cases rising from 13.1 million in 1990 to 20.9 million in 2016 (Charlson et al., 2018). The name schizophrenia is derived from Greek words *schizein* (σχίζειν, meaning 'to split') and *phrēn*, (φρεν, meaning 'mind') because in the early

observations the illness was characterised by a ‘disconnection of the psychic function’. This, however, has led to misconceptions that the disorder is characterised by a split personality, which is not true; schizophrenia is a complex syndrome which manifests itself with a wide array of symptoms that cluster into distinct (but not necessarily independent) core categories (**Figure 1-1**; **Table 1-1**). The *positive* and *aggressive* symptoms relate to an excessive or distorted normal experience, such as hallucinations or delusions, and a generalised hostility towards others. Contrarily, the negative and affective symptoms relate to a reduced normal experience, or a lack thereof, which is manifested by a loss of motivation or reduced speech, apathy, and signs of depression or suicidality. On another hand, the cognitive symptoms, which can also be related to a reduced normal experience, refer to the deficits in executive function or abridged mental flexibility that become progressively more debilitating as the disorder continues (Serper, 2011; Ellenbroek, 2016; Siddi et al., 2019).

Schizophrenia is often referred to as a *spectrum disorder* because its symptoms overlap with several other psychiatric conditions with seemingly analogous features, such as the delusional disorder, which is characterised by the manifestation of isolated delusional thinking that persists in the absence of other psychotic features (i.e., positive symptoms), or the schizoaffective disorder, which usually presents with the same symptoms as

schizophrenia but moreover, the affected also experience major mood episodes that range from extreme mania to severe depression, which is the hallmark feature of bipolar disorder (Biedermann and Fleischhacker, 2016). Nonetheless, very few patients present with such elaborate symptoms; therefore, both manuals emphasise the significance of rather nebulous warning signs such as anxiety or depression, changes in behaviour, becoming withdrawn from normal social life, and problems with concentrating.

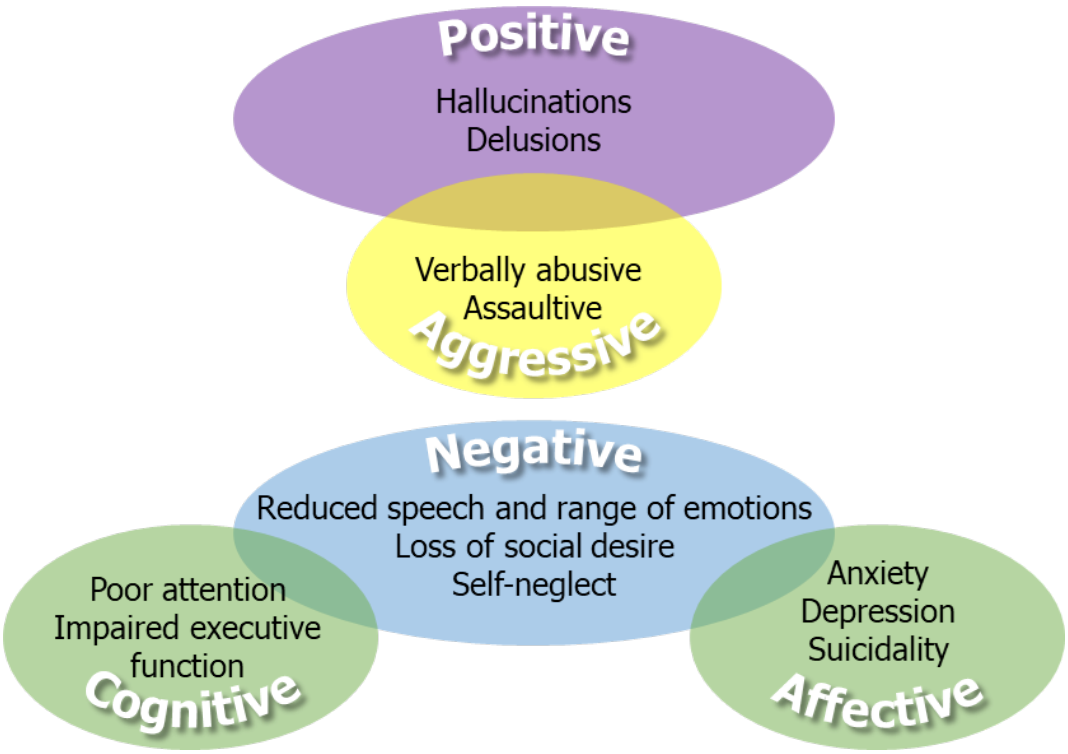

Figure 1-1 Diagram shows clustering of schizophrenia symptoms.

Schizophrenia encompasses distinct domains of symptoms which may overlap and need to be differentiated. E.g., the negative and affective symptoms often develop alongside each other and overlap significantly, so that depression can be easily misunderstood for generalised loss of social desire or apathy.

Table 1-1 Definitions of symptoms in schizophrenia. Summarized form DSM-5 and ICD-10.

Positive symptoms
Reflect the excess or distortion of normal experience, including: • Hallucinations, most commonly auditory but also visual, olfactory, and tactile. • Delusions, which develop among personal themes, such as a belief of being followed; thought broadcasting and insertion, such as a belief that thoughts and actions are a result of external force or person. • Thought disorder, which is manifested by disorganised thinking and an inability to use language coherently.
Negative symptoms
Reflect a reduced or the lack of normal experience, including: • Loss of motivation and self-neglect. • Loss of interest in social life. • Reduced speech and diminished emotional expression.
Affective symptoms
May often present alongside negative symptoms, including: • Depression. • Increased stress and anxiety. • Suicidal thoughts or behaviours.
Aggressive symptoms
A general dislike or hostility in a wide range of situations, such as: • Inability to participate in a dispute without an exaggerated emotional input. • Use of abusive language and verbal threats. • Willingness to inflict harm.
Cognitive symptoms
Develop along with longstanding struggle with negative symptoms, and include: • Deficits in executive function. • Impaired working and spatial memory. • Abridged mental flexibility and poor selective attention.

At diagnosis, however, auditory-verbal hallucinations accompanied by a failure to appreciate, or the lack of insight, that the symptoms occur as a result of the illness are the most common features present in newly diagnoses cases. These hallucinations usually involve one or more actors which are frequently abusive and criticise actions of the affected individual. Thus, people who experience hearing voices, frequently attempt to make sense of their hallucinatory experiences, which may result in delusional thinking or strange beliefs, such as being central to some form of conspiracy or threat (Picchioni and Murray, 2007; Jablensky, 2010).

1.1.2 **Aetiology**

Despite the continuous efforts to explain the aetiological bases of schizophrenia, our knowledge regarding its origins remains scarce. Mounting evidence suggests a complex synergic interplay between genes and the environment (Henriksen, Nordgaard and Jansson, 2017). There is ample evidence which indicates a strong familial link for schizophrenia. In fact, data from twin studies suggest that schizophrenia heritability can be estimated within a range of 41-87%, that also reflects the genetic proximity between the relative and the proband (Cannon et al., 1998; Sullivan, Kendler and Neale, 2003; Lichtenstein et al., 2009). Similarly, studies examining nutritional deficiencies and adverse life events at various stages of development have made strong causal links to schizophrenia (and other

psychiatric disorders), which emphasise that epigenetic factors underlie an equally important contribution to developing schizophrenia as does genetic predisposition (McGrath, Brown and St Clair, 2011).

Genetic factors

Our understanding of the genetic compound was recently expanded with the advancement of genome-wide association (GWA) studies, which predict that common-gene variants contribute to almost half of its genetic component (Lee et al., 2012; Welter et al., 2014). The first success of schizophrenia GWA studies unveiled that allele in the vicinity of the *ZNF804A* gene may influence the risk to a broader psychotic phenotype (O'Donovan et al., 2008). Future efforts identified several other genes, including the *TCF4* involved in early neural differentiation (Purcell et al., 2009), and the *ERBB4 and NRG1* genes involved in neuronal development (Shi et al., 2009), which supported the notion that, to some extent, schizophrenia arises due to aberrant developmental processes. Some analyses of post-mortem brain samples showed substantial reductions in the numbers of synaptic spines in several structures, including the subiculum, the striatum, and the temporal, auditory, and prefrontal cortices, compared to matched controls (Roberts et al., 1996; Garey et al., 1998; Rosoklija et al., 2000; Glantz and Lewis, 2000; Sweet et al., 2009; Konopaske et al., 2014), which could suggest earlier involvement of

neurogenetic factors; however, these may occur at any stage of schizophrenia. The first large-scale GWA study by the Schizophrenia Working Group of Psychiatric Genomics Consortium (2014) involved 36,989 affected individuals and 113,075 healthy controls. The authors investigated over 9.5 million gene variants, and 128 independent associations were found within 108 loci with genome-wide significance to schizophrenia. This enabled the identification of a growing number of genes such as *KCTD13, PAK6,* and *CNTN4* involved in synaptic function, the *GRIN2A*, *CLCN3*, *SRR*, and *GRIA1* genes widely involved in glutamatergic neurotransmission, the *CACNA1C*, *CACNB2*, *RIMS1* and *CACNA1* genes involved in the neuronal calcium signalling, as well as the *DRD2* gene coding for the dopamine D2 receptor, which at this time remains the primary target for current antipsychotic medications (Ripke et al., 2014; Foley, Corvin and Nakagome, 2017). Furthermore, eleven rare copy-number variants, including duplications at genomic locations: 1q21.1, 7q11.23, 15q11.2-13.1, 16p13.1 and 16p11.2; and deletions at 1q21.1, 3q29, 15q11.2, 15q13.3, and 22q11.2, *NRXN1* have shown strong associations with schizophrenia, with approximately 2.5% of patients suffering from the disorder and 0.9% healthy controls carrying a mutation in at least one of these loci (Rees et al., 2014). Moreover, some of the regions found to be associated with schizophrenia are located on the Chromosome 6 which contains genes coding for the major histocompatibility complex, human leukocyte antigen and the

complement C4 proteins – illustrating that the genes yet to be mapped seem to converge on the pathways of the inflammatory mechanisms of the immune system, thus emphasising the significance of environmental factors (Shi et al., 2009; Donnelly et al., 2012; Sekar et al., 2016).

Environmental factors

Infectious agents

The first documented speculation addressing the environment as a contributing factor to schizophrenia dates back to the reports of causal relationships between bacterial infections and psychoses mentioned in 1896 fifth edition of Kraepelin's *"Psychiatrie. Ein Lehrbuch für Studirende und Aerzte"* (Noll, 2007). Such relationships were also first reported involving viral infections a decade following the 1918 influenza pandemic (Graves, 1928), whereas more recent studies reported significant associations in schizophrenia patients with other human infections, including Borna-disease virus, human herpesvirus 2, or human endogenous retrovirus W, *C. psittaci*, *C. pneumoniae* (Torrey et al., 2006; Yolken and Torrey, 2008; Li et al., 2013; Gutiérrez-Fernández et al., 2015), and *T. gondii* (Monroe, Buckley and Miller, 2015). It is also worth to mention in the light of the Coronavirus Disease 19 (COVID-19) pandemic that a possible epidemic of neuropsychiatric complications may follow. COVID-19 has already taken an immense toll on human life and the list of complications following the

infection is rapidly expanding. One retrospective study conducted 30 years after the 1957 influenza A2 outbreak, O'Callaghan et al. (O'Callaghan et al., 1991) reported the highest birth-rate of schizophrenia patients that was about five months following the peak of the outbreak; however, the scepticism at the time was the uncertainty of whether respiratory viruses can infect nerve cells. It is been now well established for almost two decades that respiratory viruses including human coronaviruses can infect and reside dormant in the brain tissue (Jacomy and Talbot, 2003), and several anti-coronavirus antibodies were found in newly diagnosed schizophrenia compared to healthy controls (Severance and Yolken, 2020), thus, suggesting that human coronavirus infections may influence the onset of neuropsychiatric disorders in susceptible individuals.

Nutritional deficiencies

Retrospective studies of famines, such as those which occurred in the Netherlands and China allowed for identification of causal relationships between inadequate food intake and a multitude of later life-onset conditions, including psychiatric disorders. Susser and colleagues (1992) demonstrated that in the aftermath of the Dutch Winter Hunger in 1944 and 1945, the incidence of schizophrenia in the adults whose mothers were exposed to the famine increased near two-fold. Similar retrospective studies confirmed these findings from the records of Han population exposed to the

Great Chinese Famine in years 1959-1961 (St Clair et al., 2005; Xu et al., 2009). Since then, several specific nutrient deficiencies were proposed to partake in the increased risk of schizophrenia, including Vitamin D, iron, or folic acid.

A study of a 1966 birth cohort in Northern Finland found a reduced risk of developing schizophrenia in adult males who received Vitamin D supplementation during their first year of life (McGrath et al., 2004), whereas data from ecological studies that explored the associations between schizophrenia and the season of child delivery showed an increased incidence of schizophrenia in adults born in winter/spring (Torrey et al., 1997), and an increased prevalence of the disorder was reported in populations inhabiting higher latitudes (Davies et al., 2003; Saha et al., 2006). Furthermore, studies of migrant populations show that dark-skinned people, who are naturally more inclined to Vitamin D deficiency, are at an increased risk of psychosis compared to other ethnic groups (Cantor-Graae and Selten, 2005; Dealberto, 2010).

Iron is an essential cofactor for many enzymes involved in dopamine, serotonin, and norepinephrine synthesis, and iron deficiency has been associated with decreased dopamine receptor pruning (Beard, 2003; Beard, 2008). Iron is also an important cofactor for cholesterol and lipid synthesis, which may partially attribute to the disruptions in myelination following

prenatal iron deficiencies, given that such disruption has been observed in schizophrenia (Todorich et al., 2009; Roussos and Haroutunian, 2014). Insufficient iron intake during pregnancy has been long associated with behavioural, cognitive, and motor abnormalities (Walter et al., 1989; Lozoff et al., 2006; Lukowski et al., 2010) which resemble those observed in children who developed schizophrenia adulthood.

Folic acid is an important micronutrient used for the biosynthesis of thymidine and purines essential for RNA and DNA synthesis. It also plays a role in the synthesis of some of the essential amino acids required to produce proteins. This makes it particularly crucial during periods of rapid development, such as pregnancy (Hansen and Inselman, 2014). Homocysteine is an amino acid involved in the metabolic cycle of folic acid, and its levels increase consistently as folic acid levels decline, making it a useful proxy for measuring folic acid intake using stored sera, as folic acid degrades over time. This amino acid was found to act as a partial antagonist for the glycine site of the *N*-methyl-D-aspartate (NMDA) receptor when glycine levels are within the physiological range, which is consistent with the glutamate receptor hypofunction in schizophrenia (Numata et al., 2015). In a population-based California study, maternal serum samples of women who gave birth between 1959-1967 were assayed for levels of homocysteine and compared to matched controls, and their offspring followed up for schizophrenia from 1981 – 1997. The authors found a

significant 2.39-fold increased risk of developing schizophrenia in adults whose mothers had elevated serum homocysteine during their third trimester (Brown et al., 2007).

Adverse life events

Exposures to traumatic events in early life including psychological and physical abuse, parental substance abuse, poverty, sexual abuse, or parental loss are generally associated with negative outcomes, including increased risk to several psychopathologies (Morgan and Fisher, 2007). People exposed to childhood trauma are at an increased risk of developing major depression, post-traumatic stress disorder, substance abuse, anxiety disorder, and eating disorders (Üçok et al., 2015), and there is an increasing body of evidence suggesting that adverse childhood events influence the risk of developing schizophrenia. Meta-analyses of large study cohorts established that exposures to adverse events in general increases the risk of psychosis in later life up to 2.8- to 3-fold, with emotional abuse being the largest risk-factor (Varese et al., 2012; Şahin et al., 2013). Additionally, a study suggested that children who display antecedents of schizophrenia or those with schizophrenia family history are more likely to be exposed to daily stressors and adverse life events compared to their peers, further suggesting that the vulnerability to psychosis may be associated with the extent to which young people react to environmental stimuli (Cullen et al.,

2014). In a London and Nottingham study, the authors identified significant associations between maternal child abuse, maternal antipathy, and a lack of supporting figure during childhood with a greater risk of developing a psychotic disorder (Fisher et al., 2010), whereas a 2016 South London study involving first-episode psychosis hospital admissions between 2006-2010, the authors found significant associations between childhood sexual abuse, childhood physical abuse, parental separation and the first-episode psychosis (Ajnakina et al., 2016). Adverse childhood events also appear to be associated with worse positive symptoms in the clinically ill, compared to schizophrenia patients with no prior childhood trauma and are found to be associated with remission of negative symptoms (Harrison and Fowler, 2004; Lysaker et al., 2005; Lysaker and LaRocco, 2008; Cohen et al., 2012).

Individuals exposed to severe social stressors, whether young or adult, are more likely to develop some form of psychotic illness. As proposed by the *social defeat theory*, losing a confrontation in any type of hostile dispute among humans is itself an observed association between vulnerability factors (e.g., urban upbringing or being part of the migrant population) and the likelihood of developing the schizophrenia in later life. Furthermore, social stressors are often perceived to be more severe amongst the marginalised and excluded ethnic or social groups and may potentiate any underlying environmental or genetic risk for schizophrenia (Susser and Patel, 2014). Although the cause is unknown, it is evident that

urban birth or upbringing elevates the risk of schizophrenia in the adult offspring. The largest study to date involved birth cohorts between 1942-1978 in the Netherlands that were followed up for psychiatric admissions between 1972-1992. In this three-tier analysis based on population densities, the authors found that children born in the highest population density category were twice as likely to develop schizophrenia compared to their peers from lower density municipalities (Marcelis et al., 1998). A similar study from Denmark based on a five-tier analysis reported that individuals living in the high-tier urbanisation were at a 1.4-fold increased risk of developing schizophrenia, whereas individuals from the lowest tier were at 0.82-fold reduced risk. Additionally, the authors found that for individuals in each fixed urbanicity tier and at their 15th birthday the risk of schizophrenia increases together with the increasing risk at birth. This suggests a dose-response relationship between the exposure to the urban environment and the risk of the disorder in later life (Pedersen and Mortensen, 2006). Interestingly, in another Danish study of children born between 1985-2003, the authors used data on the availability of green spaces, such as public parks and courts. The study found that children living in the lowest decile of available green spaces, such as the inner city, were at 1.5-fold increased risk of developing schizophrenia in adulthood compared to children living in the highest decile, such as suburbs, suggesting that exposure to green space in childhood could provide a novel

risk-decreasing mechanism for schizophrenia in highly developed urban environments (Engemann et al., 2018). This forms an interesting suggestion, as densely populated areas are known to increase the incidence of communicable diseases. Therefore, as schizophrenia seems to be triggered by infections, it would be interesting to study if this disorder may be ‘passed’ onto others within largely populated areas.

Migration and the refugee crisis are amongst the largest humanitarian challenges in the modern world, with an estimated 258 million international migrants due to geopolitical disputes such as war (Who: World Health Organization, 2013). The literature concerning psychoses in migrant population dates back to the 1932 study of Norwegian emigration to the United States, wherein these population associations were found between schizophrenia and poor social adaptation (Ödegaard, 1933), and there are consistent reports of an elevated incidence of schizophrenia and other psychotic disorders in peoples emigrating from war-torn countries following the World War II (Hitch and Rack, 1980), the Hungarian uprising (Mezey, 1960), the collapse of the Soviet Union (Polyakova and Pacquiao, 2006), and the breakup of Yugoslavia (Mollica et al., 1999). Similarly, economic uncertainty forced far-away populations to migrate groups to Western Europe, including the Caribbean immigrants to the United Kingdom (Harrison et al., 1997), Moroccan and Surinamese immigrants to the Netherlands (Selten, Slaets and Kahn, 1997; Selten et al., 2001), and East

African immigrants to Sweden (Zolkowska, Cantor-Graae and McNeil, 2001), which all presented an elevated risk of schizophrenia. In recent years, violence and crime in the Mesoamerica, Sub-Saharan Africa and devastation in the Middle East resulted in the forceful displacement of over 68 million people ((Who: World Health Organization, 2013). In a study of immigrants in Ontario, Canada, refugee status was an independent predictor for psychoses amongst any migrant groups, which carried a 1.27-fold increased risk, with highest rates specifically for refugees from East Africa, and South Asia (Anderson et al., 2015). A 2016 study of 1.3 million people in Sweden, found that refugee status carried an elevated 2.9-fold risk of developing schizophrenia and other psychoses, and non-refugee migrants from similar regions of origins were at 1.7-fold risk, compared to native-born Swedish population (Hollander et al., 2016).

Recreational drugs use

Psychosis may occur during intoxication or withdrawal of psychoactive substances; thus, a history of substance abuse is itself considered a predictor of schizophrenia (Cannon et al., 2008). Regular amphetamine users are at an up to three-fold increased risk of developing the disorder (McKetin et al., 2010), and some authors demonstrated a dose-response relationship (Ujike and Sato, 2004; McKetin et al., 2013). Interestingly, the use of cannabis is the greatest single risk-factor, despite that it only induces

transient psychotic states (Núñez and Gurpegui, 2002). In a Danish study, up to 50% of patients who were previously treated for cannabis-induced psychosis developed schizophrenia after a 3-year follow-up (Arendt et al., 2005), and these findings were replicated in a Finnish study, which reported 46% of previous cannabis-induced psychoses converted to any schizophrenia-spectrum disorder. At the same time, other psychoactive substances including amphetamines, hallucinogens and opioids had a significantly lower conversion rate (Niemi-Pynttäri et al., 2013). Furthermore, cannabis users are twice more likely to develop schizophrenia compared to poly-drug users despite being twice less likely to present with substance-induced psychosis – further emphasising the risk carried by cannabis use (Rognli et al., 2015).

1.1.3 Pathogenesis

Schizophrenia disorder is a neurodevelopmental disorder because the pathological changes observed in a schizophrenic brain are driven by processes that occur long before the first frank symptoms of the disorder develop – beginning during gestation, which progress into adulthood (Stachowiak et al., 2013). Therefore, the clinical and pathophysiological course of schizophrenia is best presented as four stages that represent the major events leading to the manifested endophenotype (**Figure 1-2**).

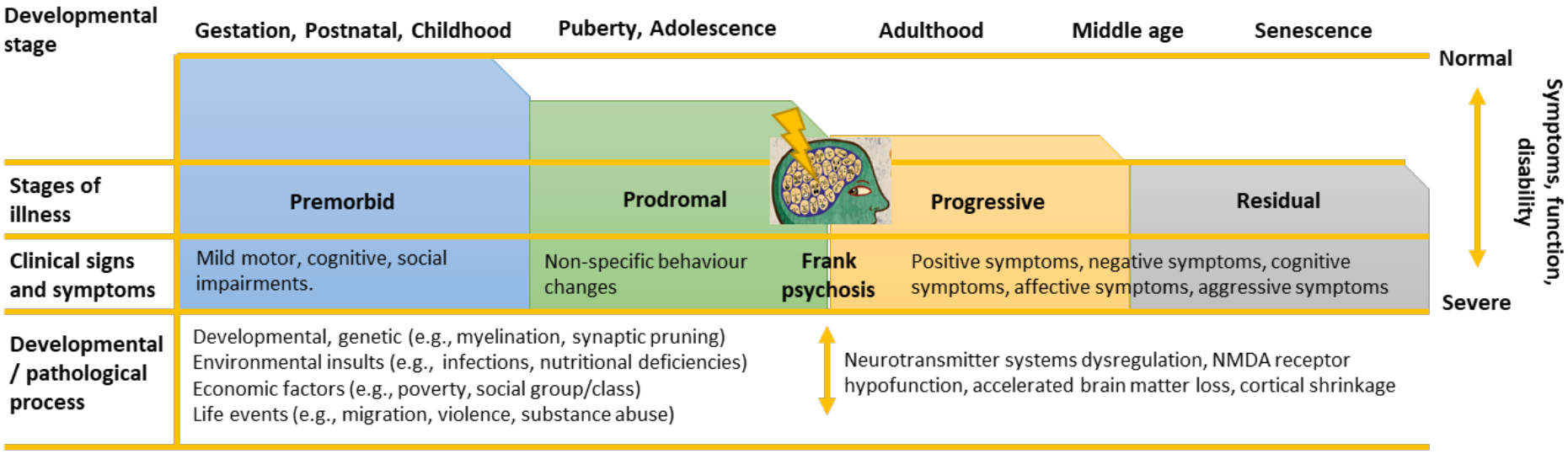

Figure 1-2 Diagram illustrates the clinical and pathological course of schizophrenia.

Here the development of shcizophrenia is presented as four stages; the premorbid and prodromal stage which involve 'backdoor' events that contribute to the later onset of clinical symotoms. First frank psychosis which occurs around the age of early adulthood marks the beginning of the progressive stage during which treamtent is implemented to stabilise positive symptoms and improve the negative symptoms as well as to minimise the cognitive effects. Adapted from Lieberman et al., 2001 and updated for accuracy.

The Progressive and Residual Stage

The role of neurotransmitter systems

The first psychotic episode is driven by disrupted neurotransmitter systems, where the neurochemical imbalance influences the behavioural and perceptual changes observed in schizophrenia. Our understanding of the bases of this imbalance has advanced in the past decades, and several neurotransmitter systems were proposed to partake in the underlaying pathophysiology (**Table 1-2**). However, the disrupted signalling of dopamine and glutamate are regarded as the most influential notions behind schizophrenia symptoms.

The dopamine hypothesis

The foundations of the dopamine hypothesis of schizophrenia were laid following the discovery that neuroleptics increase the metabolism of dopamine in animals (DELAY, DENIKER and HARL, 1952; Carlsson and Lindqvist, 1963). At the time, majority of the research focused on the ability of amphetamines to increase synaptic levels of monoamines, which culminated in the findings of the clinical effectiveness of neuroleptics and their affinity for dopamine receptors, thus the original hypothesis was also called the dopamine receptor hypothesis (Seeman and Lee, 1975; Creese, Burt and Snyder, 1976). However, this also suggested that schizophrenia

was a manifestation of a generalised hyperdopaminergic state, which was inconsistent with the developing research. The affinity of the antipsychotic drug clozapine for the D2 receptor is only one-tenth that of chlorpromazine. However, clozapine is far more effective than chlorpromazine in treating psychosis (Richelson, 1984; Claghorn et al., 1987); or that brain 3-H-spiroperidol (a dopamine receptor binding indicator) levels did not increase following clozapine administration in rat, which implicated that clozapine does not increase dopamine sensitivity (Seeger, Thal and Gardner, 1982; Lee and Tang, 1984). The original hypothesis was revisited by Davis et al. (Davis et al., 1991) after mounting evidence from human and animals posed that amphetamines and neuroleptics also affect other monoamine systems and that there was no clear indicator of the locus of this dopaminergic anomaly in the schizophrenic brain. The levels of dopamine and homovanillic acid (a metabolite of dopamine), and dopamine receptor density in the brains of schizophrenia patients were inconsistent across different brain regions such as the temporal, cingulate, and frontal cortices, the putamen, the caudate nucleus, the nucleus accumbens (Rasetti et al., 2009), and the amygdala (Bacopoulos et al., 1979; Mackay et al., 1982; Reynolds, 1983; Seeman et al., 1987; Hess et al., 1987; Toru et al., 1988). Further research found evidence of regional dopamine regulation, such as the striatal dopamine dysregulation during psychosis, where an increase in dopamine release was reported in the acute schizophrenia patients

following amphetamine challenge (Laruelle et al., 1996), and such increase was later positively correlated with the severity of psychotic symptoms with subsequent response to dopamine antagonists (Abi-Dargham et al., 2000). Conversely, schizophrenia was also associated with a reduction of dopamine receptor availability (Laruelle et al., 1999), and early positron-emission tomography (PET) studies found reduced activation of D1 receptor in the prefrontal cortex of schizophrenia patients, which was correlated with the severity of negative symptoms and reduced cognitive performance (Terasaki et al., 1997). Thus, the concept of a generalised hyperdopaminergic state has been reinvented as a regional dopamine imbalance and, with developing evidence from further research, two dopamine pathways involved in the symptomology of schizophrenia were developed (**Figure 1-3**). Subsequent evidence from functional magnetic resonance (fMRI) studies have linked schizophrenia symptoms in all domains to altered activation patterns of specific cortical and subcortical regions. For example, salience processing is dependent on the signals from midbrain dopaminergic projections to the ventral striatum and dorsolateral prefrontal cortex, and positive symptoms have been characterised by abnormal salience processing and the emergence of visual hallucinations. PET studies have consistently revealed increased striatal uptake of 18-fluorine dihydroxyphenylalanine tracer in patients with psychosis (Fusar-Poli and Meyer-Lindenberg, 2013; Fusar-Poli et al., 2013), and the striatal

uptake was previously linked to prefrontal activity (Meyer-Lindenberg et al., 2002). Abnormal activation and connectivity in the auditory and speech cortices have been also correlated with the emergence of auditory hallucinations (Sommer et al., 2008; De Weijer et al., 2013). Dopamine abnormalities linked to the persistence of negative symptoms were found in the regions responsible for social cognition, emotional regulation, and reward processing. For example, the activity of regions forming the 'social brain', including the temporoparietal junction, prefrontal cortex, and amygdala was shown to be abnormal in schizophrenic individuals and these abnormalities are also thought to be linked to the prominent deficits in social cognition which occur at later stages of disease progression (Rasetti et al., 2009).

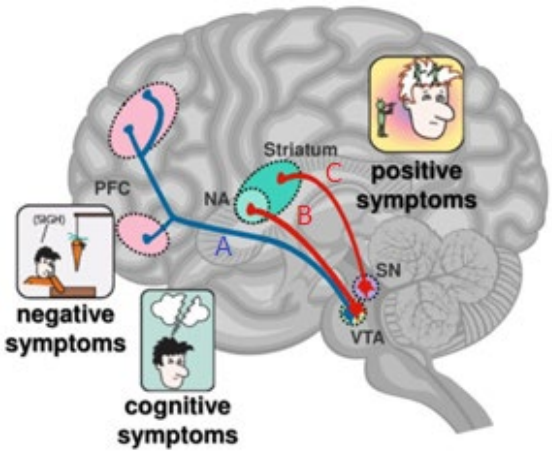

Figure 1-3 Dopamine pathways underlying the symptoms of schizophrenia.
Hypoactivation of the mesocortical pathways (A) results in the manifestation of negative and cognitive symptoms, whereas hyperactivation of the mesolimbic (B) and nigrostriatal (C) pathways results in positive symptoms. Increased DA input shown in red; decreased dopamine DA input shown in blue: DA, dopamine; SN, substantia nigra; VTA, ventral tegmental area; NA, nucleus accumbens; PFC, prefrontal cortex. Adapted from (Stahl, 2013).

Table 1-2 Neurotransmitter systems dysregulated in schizophrenia.

Dopaminergic
Amphetamines (including methamphetamine) and cocaine increase synaptic levels of dopamine; antipsychotic drugs D2 receptor blockade; increased D2/D3 receptor density in SZ; elevation in DA synthesis (Howes, McCutcheon and Stone, 2015)
Glutamatergic
NMDA-R antagonists produce SZ-like symptoms in man and exacerbate symptoms in clinically ill; altered NDMA-R subtype expression; anti-NDMAR encephalitis presents with SZ-like symptoms; GWA studies identified sites associated with glutamatergic neurotransmission; neurophysiological studies found aberrant glutamate activity in SZ patients (Uno and Coyle, 2019)
GABAergic
GABA receptor expression and reduced GABAergic cell types in the brains of SZ patients and overall GABA system changes during adolescence (Lewis et al., 1999; Pratt et al., 2012); disturbances in working memory appear to emerge from gamma oscillatory activity in PCF (Dienel and Lewis, 2019).
Serotonergic
Hallucinogens can induce perceptual disturbances, agitation, and anxiety similar to symptoms seen in a first psychotic episode (Geyer and Vollenweider, 2008); functional crosstalk between $mGlu_2$ and $5\text{-}HT_{2A}$ in animal models have been described (Shah and González-Maeso, 2019).
Endocannabinoid
Acute cannabis or THC administration may induce psychotic states and cognitive impairment in regular users as well as exacerbate symptoms of SZ in those already affected (Fakhoury, 2017).
Nicotinic
α4 and α7 nicotinic receptors are reduced in *post-mortem* brains of SZ patients (Ripoll, Bronnec and Bourin, 2004), and nicotine was reported to improve PPI in NMDA receptor antagonist models of psychosis (Domino, Mirzoyan and Tsukada, 2004). Recently α7 receptor was suggested a potential target for treating cognitive decline in SZ (Jones, 2018)

Abbreviations: SZ, schizophrenia; PPI, prepulse inhibition.

The glutamate hypothesis

In contrast to the limited range of dopaminergic neurotransmission which is localised mainly to the striatum (Simpson, Kellendonk and Kandel, 2010) and dorsolateral prefrontal cortex (Lesh et al., 2011), the notion of a wider-reaching glutamate neurotransmission based on clinical and neurochemical, and further supported by genetic findings was proposed – suggesting a hypofunction of the glutamatergic signalling compromised NMDA receptors (**Figure 1-4**; (Coyle, 1996; Coyle, 2006; Thomas L. Schwartz, Shilpa Sachdeva and Stephen M. Stahl, 2012).

Glutamate activity accounts for between 60-80% of neuronal metabolic demand of the brain (Rothman et al., 2003). It acts as the principal excitatory neurotransmitter and mediates rapid transmission in the CNS two types of glutamate receptor, including the ionotropic and metabotropic glutamate receptors, which play profound roles in neurotoxicity, neurocognition and neuroplasticity, and balance GABA release – the principle inhibitory neurotransmitter in the brain (Tsai et al., 1995; Kessels and Malinow, 2009; Gordon, 2010).

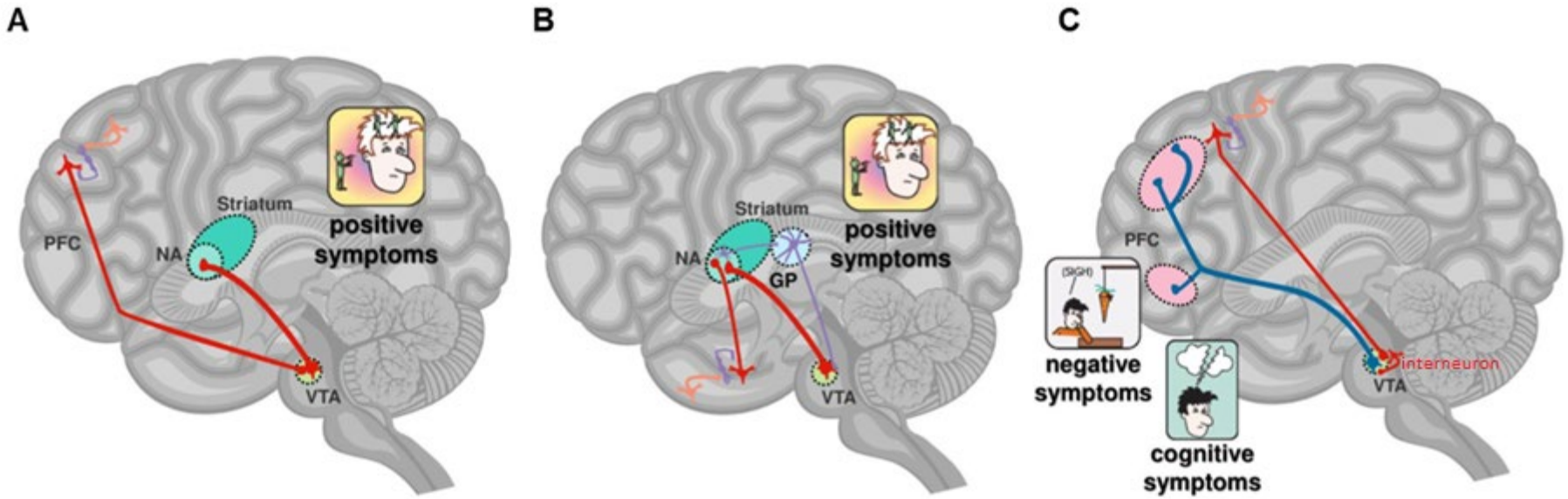

Figure 1-4 Neuronal pathways to schizophrenia symptoms as implicated by the glutamate hypothesis.

NMDA receptor hypoactivation in cortical interneurons (A) and the ventral hippocampus (B) can lead to hyperactive mesolimbic dopamine pathway, which contributes to positive symptoms. NMDA receptor hypoactivation in cortical interneurons may also lead to hypoactive mesocortical dopamine pathway, thus contributing to the negative and cognitive symptoms (C). Red, glutamatergic neuron; Purple, GABAergic neuron; Orange, cortical pyramidal neuron; Blue, dopaminergic neuron. Abbreviations: PFC, prefrontal cortex; NA, nucleus accumbens; VTA, ventral tegmental area; GP, globulus pallidus. From (Stahl, 2013).

Clinical and pharmacological evidence

One early report that drew attention to glutamate involvement in the clinical course of schizophrenia involved a study where glutamic acid was used to treat catatonic schizophrenics, resulting in a higher level of reactivity and motor control compared to non-treated group (Kitzinger and Arnold, 1949), preceding even that of dopamine involvement. The first fundamental discovery, however, was the ability of NMDA receptor antagonist phencyclidine (PCP) and ketamine to produce psychotic symptoms in man. The effects of PCP persist beyond the end of usage, and they are accompanied by a progressive withdrawal and poverty of speech, whereas cognitive deficits resembling some aspects of those observed in late-stage schizophrenia also appear in recreational PCP users (Morgan, Muetzelfeldt and Curran, 2009), and psychosis-like symptoms are also present in chronic ketamine users (Morgan and Curran, 2006). Most importantly, administration of these compounds to drug-naïve schizophrenia patients exacerbated their symptoms, while relapses in medicated subjects are observed (John H Krystal et al., 1994; Malhotra et al., 1996; Coyle, 2006). Furthermore, the psychotomimetic effects of NMDA receptor antagonists persist in the absence of dopamine antagonists (John H Krystal et al., 1994), and often without dopamine activity as a whole (Carlsson and Carlsson, 1990; Moghaddam et al., 1997), suggesting that the hypofunction of NDMA

receptors that is independent of D2 receptors may explain schizophrenia features in each symptom domain.

More recently, anti-NMDA receptor encephalitis, which is an autoimmune condition caused by anti-NMDA receptor autoantibodies against the extracellular domain of the NMDA receptor, has been considered to lead to the internalisation of postsynaptic NMDA receptor clusters – thus causing NMDA receptor downregulation (Dalmau et al., 2007; Warren, Siskind and O'Gorman, 2018). The condition manifests with atypical behaviour, abnormal speech, seizures, catatonia, psychotic features that include hallucinations and delusions, and cognitive impairment (Zandi et al., 2011). Moreover, a study reported that 6.5% of psychoses that fulfilled the criteria for schizophrenia diagnosis also showed immunoreactivity against anti-NMDA receptor IgG autoantibodies (Irani et al., 2010).

Post-mortem studies

Some of the first evidence for indirect glutamate involvement in schizophrenia also comes from *post-mortem* neurochemical findings, which revealed brain region-dependent variabilities in transcript and protein expression of NMDA receptor subtypes (Kristiansen et al., 2007). For example, the reduction in NR1 subunit mRNA density in the superior temporal cortex of schizophrenic brains significantly correlated with the

severity of cognitive symptoms (Humphries et al., 1996), and similar findings were reported for the NR1 (as well as metabotropic glutamate receptor subunits GluR1 and GluR7) in the superior frontal cortex (Sokolov, 1998). Despite that the overall findings regarding glutamate receptor density remain inconsistent (Conn, Lindsley and Jones, 2009; E. McCullumsmith et al., 2012), a recent meta-analysis concluded that both the mRNA and protein of the NR1 subunit was significantly decreased relative to controls in the prefrontal cortex of the post-mortem schizophrenic brain, whereas the same analysis found no consistent statistically significant changes in the cortical GluN2 (A, B, or D) mRNA or protein expression in the schizophrenic brain, relative to controls, while a decreasing trend in prefrontal cortical NR2C mRNA expression was reported (Catts et al., 2016). These changes in NMDA receptor expression could also be due to abnormal glutamate receptor trafficking (Funk et al., 2009), and aberrant receptor localisation as opposed to generalised receptor deficit (Hammond et al., 2014). Numerous NMDA receptor-associated postsynaptic density proteins were reported in *post-mortem* samples of schizophrenia, including increased mRNA (but downregulated protein expression) of PSD-93 and PSD-95 in the anterior cingulate gyrus (Kristiansen et al., 2006; Kristiansen et al., 2007). Several studies also reported that levels of glutamate and N-acetyl-asparty-glutamate (NAAG) and the activity of glutamate carboxypeptidase-2 (GCP-2) were altered in schizophrenia samples. The

NAAG is a neurotransmitter that is catabolised by the GCP-2 enzyme into N-acetylaspartate and glutamate. It acts as both endogenous mGlu3 and NMDA receptor antagonist. An elevated NAAG and reduced glutamate level, as well as reduced GCP-2 activity in schizophrenia, further supports that NAAG-mediated signalling contributes to the hypofunction of NMDA receptor in schizophrenia (Tsai et al., 1995; Ghose et al., 2009; Bergeron and T. Coyle, 2012; Balu, 2016).

In-vivo neuroimaging

The development of non-invasive neuroimaging technologies paved a way to visualising brain structures and their activity *in-vivo*. Several techniques, including positron emission tomography (PET), proton magnetic resonance spectroscopy (^{1}H-MRS), and single-photon emission computed tomography (SPECT), amongst others, were used to investigate the NMDA receptor deficit in schizophrenia (Lanzenberger and Kasper, 2005; Uno and Coyle, 2019). First such evidence came from SPECT study describing reduced NMDA-receptor binding in the right hippocampus of non-medicated subjects following ketamine challenge, and the authors also demonstrated that this reduced binding was modulated toward normality following treatment with both typical and new generation antipsychotics (Pilowsky et al., 2006). First findings from ^{1}H-MRS studies revealed that ketamine administered acutely to healthy volunteers lead to a significant increase in

glutamine – a marker of glutamatergic transmission, which marginally correlated to cognitive performance (Rowland et al., 2005). Meanwhile in schizophrenia, (Merritt et al., 2016) (2016) in their recent meta-analysis identified significant increase in glutamatergic transmission within the limbic system, glutamine levels in the thalamus, glutamate indices increase in the basal ganglia, and Glx (glutamine + glutamate) levels in the medial temporal lobes and basal ganglia. However, a key limitation to ^{1}H-MRS studies of glutamate is that this technique, as opposed to PET/SPECT, does not distinguish between extracellular or intracellular compartments, nor between extra- and intra-neuronal compartments (Poels et al., 2014).

Genetic findings

As mentioned in **Section 1.1.2**, several genes closely related to glutamatergic neurotransmission as well as its downstream mediators, including *GRIN2A* (NR2A), *GRIA1* (AMPA receptor GluA1), *SSR* (SR), and GRM3 ($mGlu_3$) were found to be enriched in schizophrenia using the genome-wide association approach (Ripke et al., 2014; Ohi et al., 2016; Horwitz et al., 2019). Other studies also identified an increased volume of rare gene variants in form of both single nucleotide polymorphisms and *de novo* copy number variants, where the latter exert significantly larger effect (Pocklington et al., 2015; Kushima et al., 2017). Furthermore, recently accumulating evidence also support a role for rare loss of function (LoF)

variants. A screening study for the exonic mutations of NMDA receptor subunits in autism spectrum disorder and schizophrenia found forty mutations, where two were identified as *GRIN2C* (NR2C) and *GRIN2D* (NR2D) rare LoF mutations – supporting the notion that LoF variants within the glutamatergic system increase the risk of schizophrenia (Yu et al., 2018),

The integrated model

The evidence for the role of dopamine in positive symptoms is compelling, while the involvement of dopamine in negative and cognitive symptom is less clear, for which glutamatergic model involving NMDA receptor hypofunction seems to have a more solid basis (Howes, McCutcheon and Stone, 2015). However, it is important to note that systems do not work on their own. The evidence for other neurotransmitters is becoming equally relevant (**Table 1-2**). Most notably GABA, which is the primary inhibitory neurotransmitter in the brain that has been reported to be involved in the pathophysiology of some aspects of schizophrenia in both basic and clinical neuroscience research (Benes et al., 2007). GABAergic interneurons are the key players in rhythm-generating networks in the brain, and the synchronisation of neuronal oscillations is fundamental to the mechanisms of perception, memory, and consciousness. Several abnormalities, including aberrant neural synchrony (Uhlhaas and Singer, 2010), abnormal

gamma oscillations (Cardin et al., 2009), and impaired working memory were observed in schizophrenia (Lewis and Gonzalez-Burgos, 2006). Simultaneously, adjunctive GABA agonists were shown to be efficacious in improving the core symptoms of schizophrenia, although it is unclear in what ways GABA system interacts with other neurotransmitter systems, which requires further efforts to elucidate the relationships between these systems (Wassef, Baker and Kochan, 2003; Yang and Tsai, 2017).

Brain morphology

The advent of neuroimaging techniques confirmed altered brain volumes in first-episode schizophrenia, and it is now generally recognised, thanks to multiple meta-analyses, that reductions in grey and white matter across various brain regions, and whole-brain volume, as well as ventricular enlargement, are the neuroanatomical hallmarks of the disorder (Wright et al., 2000; Honea et al., 2005; Steen et al., 2006; Arnone et al., 2009; Morgan, Muetzelfeldt and Curran, 2009; Haijma et al., 2013; Van Erp et al., 2016). Changes in gyrification, cortical thickness, and subcortical shapes are largely localised to the anterior cingulate, the bilateral insula, as well as the thalamus, hippocampus, and amygdala (Crossley et al., 2009), and reductions of grey matter volume, especially in the temporal lobes, advance with the duration of illness (Vita et al., 2012). However, due to the absence of distinct boundaries separating schizophrenia from other neuropsychiatric

disorders in general and their immense heterogeneity, no circumscribed functional or anatomical abnormalities specific to schizophrenia have been identified (Linden, 2012; Fornito, Bullmore and Zalesky, 2017).

In the past two decades, multiple studies also applied neuroimaging techniques to compare human brain at various stages of schizophrenia (Chung and Cannon, 2015). The development of 'high-risk' strategies shed light on the understanding of some of the functional and structural changes around schizophrenia onset, whereas prospective studies in individuals who carry risk genes, such as children of parents diagnosed with schizophrenia, siblings, or co-twins that do not manifest with prodromal symptoms, have largely shown decreases in white matter volume across a wide gamut of brain regions including the prefrontal cortex (Hao et al., 2009), the cingulate gyrus (Muñoz Maniega et al., 2008), the hippocampus (DeLisi et al., 2006; Hao et al., 2009), and the parietal lobe (Hoptman et al., 2008; Gogtay et al., 2012). All these studies showed that high-risk individuals who converted to schizophrenia show a much steeper rate of grey matter volume loss compares to the non-converters, as well as matched healthy controls.

1.1.4 Treatment and Management

Pharmacotherapy interventions

The aim of pharmacotherapy in schizophrenia is mainly three-fold: 1) to minimise the symptoms in first-episode psychosis; 2) to facilitate the overall

functional recovery from a psychotic outbreak; and 3) to reduce the risk of relapses and readmission to secondary care facilities. Antipsychotic drugs are mainly effective at alleviating positive symptoms, while their effectiveness on treating the negative symptoms is only partial. Agents which block post-synaptic dopamine D2 receptors are the backbone of treatment, and are classically categorised as either first-generation antipsychotics, such as haloperidol or sulpridine, or second-generation antipsychotics, such as risperidone and olanzapine, or third-generation antipsychotics, including aripiprazole and cariprazine, which also partially agonise dopamine receptors in special circumstances (Stępnicki, Kondej and Kaczor, 2018).

First-generation antipsychotics

The history of antipsychotic treatment dates back to the 1950 when the neuroleptic chlorpromazine was synthesised as a result of research on antihistamines by the French chemist Paul Charpentier (López-Muñoz et al., 2005). The action of first-generation (typical) antipsychotics is achieved mainly by D_2 receptor antagonism. However, due to the lack of specificity in any dopaminergic pathway, typical antipsychotics lead to a wide range of side effects, particularity causing an elevated prolactin level, and extrapyramidal symptoms, such as pseudo parkinsonism, akathisias, or dyskinesias, which result from D_2 blockade in the tuberoinfundibular and nigrostriatal pathways, respectively. Although typical antipsychotics can

effectively alleviate positive symptoms, high dose may induce secondary negative and cognitive symptoms by antagonising D_2 receptors in the mesocortical pathways, thus, appropriate dosing is achieved mainly by trial and error. Another side effects on the CNS include drowsiness, vertigo, sedation caused by the antihistaminic activity, or disturbed sleep, amongst others. Typical antipsychotics may also act on the α1 adrenergic receptor, which can cause hypotension and cardiovascular effects, including tachycardia, arrythmias, chest pains, and palpitations were also reported. Additionally, gastrointestinal effects, including nausea, constipation, and weight gain are also the common culprits of non-compliance (Stępnicki, Kondej and Kaczor, 2018; Blackman and MacCabe, 2020).

Second-generation antipsychotics

The second-generation (atypical) antipsychotics, such as clozapine, arrived nearly 40 years after the synthesis of chlorpromazine. Clozapine was discovered in the Sandoz laboratory (Crilly, 2007), and as an atypical antipsychotic it is both dopamine and serotonin receptor antagonist. It binds to dopamine receptors $D_{1\text{-}5}$, although with ten times higher affinity to D_4 receptors compared to D_2 receptors. The antagonising effect on D_4 and 5-HT_{2A} contributes to the lower prevalence of extrapyramidal side effects and decrease of negative symptoms. However, clozapine is only used to treat treatment-resistant forms of schizophrenia, where no satisfactory response with at least two other drugs was achieved. Its limitation is due to the

tendency to cause life-threatening agranulocytosis, thus the control of white blood cells each week within the first six months of treatment is necessary (Strange, 2001; Stępnicki, Kondej and Kaczor, 2018).

Third-generation antipsychotics

The newest groups of antipsychotic agents have been individualised based on their mechanisms of action on the dopamine receptor. The third-generation antipsychotics are partial D_2 agonists. For example, aripiprazole in the presence of high dopamine concentrations competes for the D_2 receptor, which results in partial dopamine receptor antagonisms, leading to clinical benefits, such as reduced positive symptoms. Contrarily, when extracellular dopamine concentration is low in circuits that govern negative symptoms and cognitive function, aripiprazole can bind to and partially agonise dopamine receptors, leading to improved clinical state; thus, aripiprazole has been also named the “dopamine stabiliser” (Tamminga, 2002; Mailman and Murthy, 2010).

The advent of new antipsychotic drugs in clinical practice contributed to lowering the probability of extrapyramidal side effects; however, the advantage of atypical over typical antipsychotics and their clinical effectiveness is still widely debated. In some patients, the older drugs are more effective while in others the newer drugs resulted in better outcomes. Patients who are undergoing management with typical

antipsychotics, have no troublesome side effect, and are clinically sound should not be changed to atypical medications unless they begin experiencing extrapyramidal side effects. Patients with poor compliance to treatment may be offered depot preparations to facilitate dosing regiments (Agius, 2010).

Non-pharmacological approaches

Several psychological treatments are offered to improve functioning and prevent relapse. Unfortunately, their availability is often limited by the lack of specially trained therapists. Systematic reviews have shown that cognitive behavioural therapy (CBT) is helpful to reduce persistent negative symptoms and to improve insight. Psychoeducation, which aims to improve the communication between family members has shown an effect in reducing stress and raises awareness in all the people involved. Emerging evidence suggests that pharmacotherapy in combination with psychological interventions, such as CBT can lead to reductions in long-term distress caused by treatment-resistant hallucinations and delusions, improving medication adherence, and preventing relapses (Rector and Beck, 2012; Hofmann et al., 2012; Blackman and MacCabe, 2020).

Treatment resistance

To date, there has been no agreement on the definition of treatment-resistant schizophrenia. However, the authors of a landmark randomised-controlled clinical trial which investigated the effects of clozapine vs. chlorpromazine in patients that did not respond to treatment defined treatment resistance as *"minimum three periods of treatment with antipsychotic medications for at least two different classes at adequate doses for an adequate period of time with no relief and no period of good functioning over the previous five years"* (Kane et al., 1988). These criteria remain in some of the most frequently cited randomised-controlled trials investigating treatment-resistant schizophrenia, although overall heterogeneity in the criteria used exists (Conley and Buchanan, 1997; Sensky et al., 2000).

In 1939, electroconvulsive therapy (ECT) was introduced to treat schizophrenia as a replacement for seizures induced chemically. The procedure involves the induction of a fit by applying electric stimuli to the cranium with electrodes placed bilaterally on the scalp (Endler, 1988). Today, ECT is administered in its modified form which includes anaesthesia and muscle relaxants to reduce the possibility of adverse outcomes such as limb and spinal fractures resulting from convulsion (Sinclair et al., 2019).

Prognosis

Although it appears that schizophrenia affects men and women rather equally, men have a more abrupt and earlier age of onset, experience more negative symptoms, and face a poorer prognosis with an overall lower rate of full recovery. Between 20-50% of patients will make a fully functional recovery, and 20% will never experience another psychotic episode. However, the estimates including social recovery were only 13.5%. Those patients that fail to comply with treatment, experience frequent relapses, or present with aggressive symptoms are often sanctioned under the mental health act and institutionalised until their symptoms stabilise (Jääskeläinen et al., 2013; Eagles, 2017). Nonetheless, it is vital to stress that schizophrenia pharmacotherapy is mainly effective at targeting the positive symptoms, whereas progress on reducing other important features of schizophrenia has not significantly advanced. The negative symptoms usually become apparent after psychosis has remitted, and the effectiveness of the therapeutic approaches which are limited to psychological, social, and family support, and their long-term benefit remains unreliable (Jauhar et al., 2014). Patients who adhere poorly to the antipsychotic regime or those in frequent relapse cycles usually gain little advantage, as progress made on improving these symptoms is often lost following a concurrent psychotic episode. Persisting negative symptoms

contribute greatly to the cognitive decline, which frequently requires more costly rehabilitation (Patel et al., 2014; Eagles, 2017).

1.1.5 Animal Models of Schizophrenia

Animal models are used in research as approximations of human conditions in non-human subjects with the intent to advance the understanding of a disease or to improve treatment options (Forrest, Coto and Siegel, 2014). Neuropsychiatric disorders, including schizophrenia, involve psychopathologies of uniquely human traits including thought and reasoning, and the characteristic features of schizophrenia such as auditory hallucinations or delusional thinking are not possible to be directly modelled in animals. This greatly subjective nature of this condition, combined with a lack of diagnostic tests, biomolecular markers, and access to brain tissue *in vivo* makes it redundant to say that studying psychiatric disorders in non-human subjects poses a great challenge. Nonetheless, the development of animal models with relevance to schizophrenia is continually advancing in efforts to elucidate the basic biology underlying this condition (Young, Zhou and Geyer, 2010; Heckers et al., 2013; Ripke et al., 2014; Kumar et al., 2015). Animal models used to study schizophrenia are generated by either: 1) pharmacologically inducing a schizophrenia-like state; 2) disrupting the developmental pathways, thereby leading to misguided brain development; or 3) by manipulating one or more genes known to play significant roles in

the disorder. Nevertheless, owing to the complexity of schizophrenia and its developmental nature, no single model can produce symptoms within each domain, and at every stage of the disease.

Developmental models

Neurodevelopmental models allow to investigate processes which lead to the development of schizophrenia during the prodromal stage of the disease, thus have a potential for the identification of prophylactic strategies to prevent the development of psychosis (Powell, Risbrough and Geyer, 2003). Developmental models involve manipulating the environment, such as inducing stress, and anxiety by socially isolating young pups from their littermates, or more commonly, by administering drugs to animals during prenatal or early post-natal periods and studying the offspring in the course of its development (Jones, Watson and Fone, 2011; Winship et al., 2019).

One such form involves physical interreference in brain development, such as inducing lesions to the ventral hippocampus in rat on post-natal day 7 by locally injecting the excitotoxin ibotenic acid or tetrodotoxin, which lead to an array of abnormalities that are consistent with schizophrenia and which emerge at various times following puberty (Tseng, Chambers and Lipska, 2009). Similarly, the gestational methylazomethanol (MAM) model involves administration of MAM to pregnant dams on gestational day 17 (Moore et al., 2006). MAM is an antiproliferative and

antimitotic agent that methylates the DNA (Matsumoto and Higa, 1966), and exerts effect specifically on neuroblasts (Cattabeni and Di Luca, 1997). Gestational MAM offspring show increased volumes of lateral and third ventricles, decreased parvalbumin neurons in limbic and cortical areas, and increased response to MK-801 (a non-competitive NMDA receptor antagonist several times more potent than PCP), amongst others (Moore et al., 2006).

A second form of developmental interventions may include inducing maternal immune activation (MIA) in pregnant dams by inoculating them with infectious agents, such as viral polyionosine-polycytidylic acid (poly I:C), and consequently, studying the effect on the offspring (Reisinger et al., 2015). Compelling evidence suggests that primate and rodent offspring to mothers who underwent MIA during pregnancy show a wide range of neurochemical, electrophysiological, anatomical, and behavioural changes that are consistent with schizophrenia (Howland, Cazakoff and Zhang, 2012; Zhang et al., 2012; Meyer, 2014; Dickerson et al., 2014; Machado et al., 2015; Paylor et al., 2016).

Pharmacological models

Drug-induced models in schizophrenia research are frequently generated with either dopamine enhancers, such as amphetamine or apomorphine, or with non-competitive NMDA receptor antagonists, such as ketamine,

PCP, or MK-801. As explained previously, amphetamine-induced psychosis in man is a well-known adverse effect of its recreational use, which is proposed to result from an increased synaptic dopamine produced as result of the drug. Acute, chronic, and intermittent administration of amphetamine to rodents increases synaptic dopamine levels, and induces exaggerated locomotor activity and exaggerated response to acute stimulant challenge, which reflect those in the positive symptom domain of schizophrenia (Featherstone, Kapur and Fletcher, 2007; Robert E Featherstone et al., 2008). Chronic amphetamine treatment also induces some cognitive impairment such as reduced reasoning and problem-solving, which is measured by the attentional set-shifting task; however, the regiment lasts five weeks (Fletcher et al., 2007). However, amphetamine fails to induce negative-like symptoms, such as deficit in social interaction (Sams-Dodd, 1998), and it appears to induce some aspects resembling prefrontal cortical-related cognitive dysfunction only partially, with hippocampal function being unaffected (Robert E. Featherstone et al., 2008). That is, amphetamine induces psychotic-like effects and changes but does not reliably exert an effect on negative symptoms and cognitive performance. In fact, (Lindenmayer et al., 2013) proposed that it is worth exploring whether treating selected groups of patients with stimulants could reduce negative symptoms.

As mentioned, the use of PCP in humans induces psychotic symptoms that are clinically indistinguishable from those observed in schizophrenia, including hallucinations, social withdrawal, and impaired mental flexibility. As opposed to dopamine enhancers, NMDA receptor antagonists have been very efficacious at producing schizophrenia-like features in all symptom domains. PCP in rodents does not only induce changes indicative of positive symptoms, such as increased locomotor activity or spontaneous ambulation, but also impairs social interaction and significantly reduces several indices of cognitive performance (Cadinu et al., 2018). However, the effects of NMDA receptor antagonists vary between strains (Mouri et al., 2012), and are both dose- and treatment duration-dependant (Hiyoshi et al., 2014; Neill et al., 2014). PCP models are often used as tools in pre-clinical neuroscience and pharmacology research for testing new APDs candidates (Castañé, Santana and Artigas, 2015); however, no standardised model exists. A More detailed account on PCP models of schizophrenia will be introduced in **Chapter 4**, where we discuss our findings on the phenotype induced by a subchronic PCP treatment in CBA/Ca mouse strain.

Genetic models

Advances in schizophrenia genetics allowed for identifying a wide range of genomic regions, and later candidate genes, with high probability to be involved in the disorder. This in turn facilitated attempts at generating more

sophisticated models that target specifically the very blueprints of the disorder. For example, a deletion on chromosomal locus 22q11.2 is associated with approximately 1% of schizophrenia patients. The symptoms attributed to 22q11.2 deletion, as well as the cognitive deficits and treatment response do not differ from other schizophrenia cases (Bassett et al., 2005). Mice with microdeletion at analogous 22q11.2 recapitulate the main neuroanatomical findings in 22q11.2 carriers, including enlarged ventricles and reduced cortical and subcortical volumes (Stark et al., 2008; Ellegood et al., 2014). Behavioural studies reveal that 22q11.2 microdeletions induce deficits in fear conditioning, PPI, and impaired spatial memory (Karayiorgou, Simon and Gogos, 2010).

DISC1 is a gene for Disc1 (disrupted-in-sczhiophrenia-1) synaptic protein involved in pre- and post-natal neuronal development. Mutation in *DISC1* is considered highly penetrant risk for schizophrenia, although the evidence is conflicting (Sullivan, 2013). Mice with partial loss of Disc1 protein function have brain morphology that is consistent with schizophrenia, including reduced cortical thickness and volume, and enlarged ventricles. Additionally, reduced immunoreactivity for parvalbumin in interneurons has been found in medial prefrontal cortex and hippocampus, which is consistent with human *post-mortem* findings (Jaaro-Peled, 2009). Disc1-deficitent mice show striking hyperactivity and reduced volitional behaviours, although other metrics, locomotor activity, reduced

PPI, or differences in cognitive abilities and extent of negative symptoms show conflicting results (Clapcote et al., 2007; Hikida et al., 2007; Lipina et al., 2013; Rees et al., 2014).

Glycine and D-serine are physiological NMDA-receptor agonists binding to constitutional NR1 subunit of all types of NMDA receptors. D-serine was shown to preferentially activate the NDMA receptor in adult, and several genes that demonstrate associations in studies on schizophrenia are related to D-serine including the *SRR*, *DAO*, and *G72* (Labrie, Wong and Roder, 2012). Interestingly, the genes involved in D-serine formation (*SRR*; serine racemase) and catabolism (*DAO*) can be easily manipulated; mice deficient in serine racemase have lower brain levels of D-serine and show behavioural abnormalities resembling those in schizophrenia (Labrie, Fukumura, et al., 2009). Conversely, inactivation of *Dao* gene enhances reversal learning, which suggest improvement of the cognitive deficits (Labrie, Duffy, et al., 2009). Lastly, the insertion of the human *G72* gene into mice has resulted in several cognitive and behavioural aspects resembling those observed in schizophrenia (Otte et al., 2009).

1.2 Voltage-Gated Ion Channels

Nearly seven decades ago, the pioneering works of Hodgkin and Huxley (Hodgkin and Huxley, 1952) on the giant squid axon established that the generation and propagation of action potentials in electrically excitable cells is absolutely dependent on the ionic currents of sodium and potassium. These currents are governed by a vast repertoire of functionally complex, yet structurally simple, transmembrane proteins, which undergo exceptionally rapid conformational changes; the voltage-gated ion channels transform from an impermeable structure to a highly permeable pore to facilitate energetically favourable, selective passage of ions across the lipid bilayer according to their electrochemical gradient at a rate close to the diffusion limits. Without ion channels, the lipid membranes of cells and cell organelles would present an excessively energy-demanding barrier for any ion to pass (Roux, 2017), thus preventing any intercellular information being transmitted at velocities necessary to sustain response to environmental stimuli, and also raising a question whether a lack of ionic currents would allow for complex life to develop (Anderson and Greenberg, 2001).

Structure of voltage-gated ion channels

The first characterised voltage-sensitive ion channel was the Na^+ channel purified from the electrocytes of electric eels (Agnew et al., 1978). Several years later, (Noda et al., 1984) established its complete amino acid

sequence, describing 24 repeating sequences within four distinct motifs of the structure, and hypothesised that this entity must arrange within the bilipid membrane in some form of a pseudo symmetric fashion to allow the flow of ions. Three years past, the first Ca^{2+} channel was isolated and purified from rabbit skeletal muscle, and its complete structure showed a strikingly similar composition to that of Na^{+} channels (Takahashi et al., 1987; Leung, Imagawa and Campbell, 1987). In the same year, a K^{+} channel sequence was deducted for the first time from the fruit fly *D.melanogaster*, where the authors described a single unit with six similar membrane-spanning segments (Tempel et al., 1987). Several decades later it is understood that most voltage-gated ion channels are formed by either one α-subunit that is a continuous polypeptide composed of four domains, such as in the case of Nav and voltage-gated calcium (Cav) channels; or four α-subunits containing a single domain each, as in case of Kv and HCN channels (**Figure 1-5**).

The α-subunits of voltage-gated ion channels share common evolutionary ancestry, thus inherit a similar basic structure; each domain is typically composed of six α-helical transmembrane segments and within each α-domain, the fourth transmembrane segment, S4, contains arginine-rich sequence that is primarily responsible for detecting changes in the membrane potential. The re-entrant pore loop is a short sequence located

between segments S5 and S6, which together form the narrowest part of the pore that defines its ion selectivity (Lai and Jan, 2006).

Auxiliary subunits of ion channels

The α-subunits of voltage-gated ion channels often form macromolecular complexes with a variety of accessory subunits (often represented as α_2, β, γ, δ) and other proteins which diversify their function. For example, there are five β-subunits associated with Nav channels that are involved in modulating Nav channel kinetics, gating, and localisation of the ion channel pore (O'Malley and Isom, 2015; Bouza and Isom, 2018). On the other hand, there are three distinct types of auxiliary subunits for Cav channels. The first two types are comprised of several combinations of α_2-β and α_2-δ (formed by individual α_2, and distinct splice variants of β, and δ-subunits), while γ-subunits comprise the third type (Wang et al., 2002).

The Kv channel family has thus far the largest number of associated accessory subunits. They include Kv β-subunits (Kvβ); calcium-sensing Kv channel-interacting proteins (KChIPs); Kv channel-associated protein (KChAP); The 14-3-3 proteins (named after chromatography fraction number and their relevant gel position); and the KCNE-encoded proteins. Although enlisting the functions of all of them would be beyond the scope of this thesis, it is worth to mention that several Kv accessory subunits increase the functional diversity of Kv2 and Kv3 channels. For example, the

KChaP protein increases Kv1.3, Kv2.x, and Kv4.3 currents amplitude in *Xenopus* oocytes but it does not affect the activation and inactivation kinetics of these channels. (Kuryshev et al., 2000). Meanwhile, the *KCNE1-KCNE3*-encoded proteins were shown to modulate Kv3.1- and Kv3.2-mediated currents by slowing their activation and deactivation and inactivation kinetics (Lewis, McCrossan and Abbott, 2004) and *KCNE1* and *KCNE2*-encoded regulate the gating properties of Kv2.1 in cultured human cardiomyocytes (McCrossan et al., 2009). The physiological importance of KCNE-encoded proteins has been underscored by the fact that mutations in KCNE genes have been linked to numerous human disorders, including sensorineural deafness or periodic paralysis. Moreover, SNPs in KCNE-coding regions were shown to alter the sensitivity to channel block by several drugs (Li, Sung and McDonald, 2006).

The functional diversity of Kv2 channels is greatly expanded further by the modulatory properties of the α-subunits from subfamilies Kv5-6 and Kv8-9, which do not form functional tetramers one their own. Instead, they arrange with the Kv2-type channels to alter their biophysical properties (Bocksteins and Snyders, 2012). Although these subunits are in fact Kv channel subunits of their own, they are also auxiliary subunits in this regard. A more comprehensive introduction to these subunits will be presented on later pages of this chapter, as well as in **Chapter 3**.

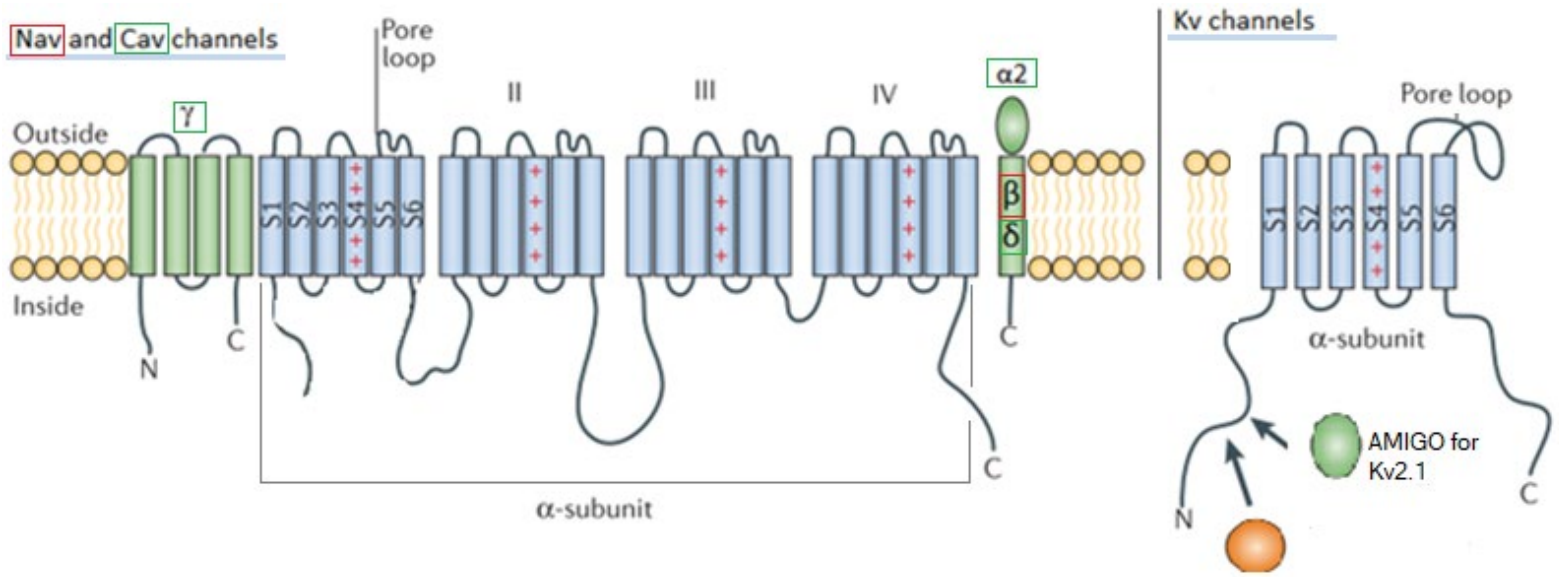

Figure 1-5 Structural topography of voltage-gated ion channels.

Voltage-gated sodium (Nav) and calcium (Cav) channels are formed of a continuous polypeptide which forms the four structural domains (I-IV), each containing six membrane-spanning segments (S1-S6). The fourth segment (S4) is a prominent voltage sensor, whereas the pore loop located between segments S5 and S6 comprises the pore-forming region through which ions flow. The β-subunits (for Nav) and γ or δ -subunits (for Cav) assemble with the Nav or Cav α-subunits, respectively. The voltage-gated potassium channels (Kv) are formed of four identical or similar α-subunits that are and individual single domain. The Kv1 have intracellular β-subunits which interact with the N termini. The Kv4 channels have two associated proteins: a single-span membrane protein DPPX and the intracellular KChIP protein. Adapted using (Lai and Jan, 2006) and updated for accuracy.

Function of voltage-gated ion channels

The most apparent function of voltage-gated ion channels is to produce electrochemical activity in cells which is accountable for a range of physiological roles, including the senses, movement, or the cognitive functions. However, the quest to fully comprehend the functional heterogeneity of voltage-gated ion channels is an ongoing struggle. There are over 350 distinct ion channels expressed in the mammalian brain alone and a great majority of those are essential to normal biology which is evidenced by the vast repertoire of disorders related to them (George, 2005; Kullmann, 2010; Kim, 2014). Although the functional properties of individual voltage-gated ion channels are yet to be elucidated, the general functional 'mapping' of voltage-gated ion channels within neurons is now easier to understand (**Figure 1-6**; **Table 1-3**). In a hypothetical model neuron that receives multiple excitatory and inhibitory presynaptic stimuli, the activation of glutamatergic receptors induces excitatory post synaptic potentials (EPSPs) which propagate through the dendritic arbour *via* cyclic activation of Nav and Kv channels, and hyperpolarisation-activated cyclic nucleotide-gated (HCN) cation channels located on the dendritic processes, which control the course and the extent of passive spread of action potentials (APs). The dendrites may also undergo depolarisation AP back propagation from the axon that is activated by different Nav, Kv, and Cav

channels, and this phenomenon might signal recent synaptic excitation and influence synaptic plasticity that leads to long-term depression or long-term potentiation (Colbert, 2002; Magee and Johnston, 2005).

Action potentials in the somatodendritic region, including inhibitory post synaptic potentials (IPSPs) from fast-spiking GABA interneurons, summate on the soma where the probability of further AP generation is determined. At the axon initial segment (AIS), the Nav and certain Kv channels, including the Kv2, determine the subthreshold properties for initiating APs, which are then propagated along the axon toward the presynaptic terminals where Kv1-type and Cav channels govern neurotransmitter release. Axons that are myelinated contain nodes of Ranvier, which allow the APs to ‘jump’ between each node through saltatory conduction that increases the velocity of APs. Here, the Nav, Kv3.1, and Kv7-type channels permit the currents to propagate from one node to another and to initiate new AP in the subsequent node, with additional help of certain Kv1-type channels located at the juxtaparanodal junctions to increase the reliability of APs at the nodes and to reduce the excitability during remyelination (Rasband et al., 1998; Black, Waxman and Smith, 2006; Tian et al., 2014; Trimmer, 2015).

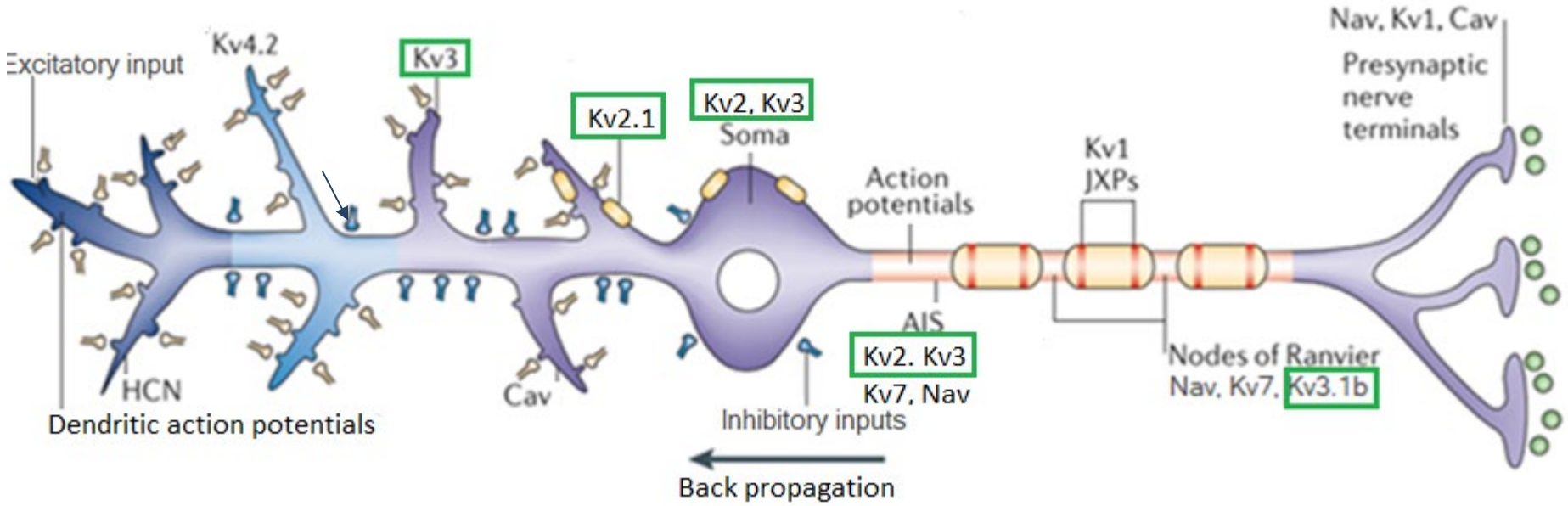

Figure 1-6 Simplified diagram showing localisation of voltage-gated ion channels in distinct neuronal domains of a model neuron.

The neuron receives multiple excitatory and inhibitory input. Nav channels are generally located in the presynaptic nerve terminals, the nodes of Ranvier, and the axon initial segment (AIS). Kv channels are distributed throughout the neuron, although specific subtypes localise to particular regions of neuros, (e.g., Kv1-type cluster within the axonal regions, whereas majority of Kv2- and Kv3-type channels are found within the somatodendritic region and dendrites, respectively; however, some Kv3.1b are also present at the nodes of Ranvier. Cav channels are located near the presynaptic nerve termini where they trigger neurotransmitter release. Kv channel that are located in dendrites contribute to controlling back propagation, whereas strong dendritic potentials may generate dendritic action potentials. Adapted from (Lai and Jan, 2006) and (Trimmer, 2015).

Table 1-3 Distribution and brief function of voltage-gated ion channel subtypes in central nervous system neurons

Channel subtype	Distribution	Function
Nav1.1	Dendrites; soma; AIS; NR	*Dendrites*: dendritic spikes, boosting EPSPs; *AIS:* AP generation, found mostly in GABAergic interneurons; *NR:* saltatory conduction.
Nav1.2	Dendrites; soma; AIS; unmyelinated axons, axon terminals	*Dendrites:* dendritic spikes, boosting EPSPs; AP back propagation, found mostly in glutamatergic neurons; *axon terminals*: activation of Cav2 channels during exocytosis.
Nav1.6	AIS; NR	*AIS:* AP initiation; NR: saltatory conduction.
Kv1.1	Dendrites; soma; AIS; JXPs; axon terminals	Delayed activation during APs; membrane repolarisation; limits firing frequency and amplitude; delayed activation after APs; *Axon terminals*: controls Cav2-mediated neurotransmitter release.
Kv2-type	Dendrites; soma	Delayed activation during APs; repolarisation of APs; delayed activation after APs. Shape delayed rectifier currents; *AIS*: maintain AP amplitude by regulating interspike potentials during high frequency firing.
Kv3-type	Proximal dendrites; soma; NR	Delays initiation of APs; slows firing frequency of neurons; slows fast-spiking of some GABA interneurons. Shape transient A currents
Kv4-type	Distal dendrites; soma	Delays initiation of APs; limits back propagation of APs. Shape

Channel subtype	Distribution	Function
		transient A currents
Kv7.2-3	Dendrites; soma; AIS; NR	Govern subthreshold excitability and responsiveness of neurons to synaptic input
KCa	Dendrites; soma	Contribute to membrane repolarisation and governs after-hyperpolarisation thus leading to spike frequency adaptation. Activated via Ca^{2+}
Cav1-type	Dendrites; soma	Activate KCa; trigger dendritic spikes; boosts EPSPs. Shape L currents
Cav2.1	Dendrites; soma; axon terminals	Activates KCa; triggers dendritic spikes; exocytosis. Shape P/Q currents
Cav3-type	Dendrites; soma	Triggers rhythmic burst firing by low-threshold spikes; activation of KCa. Shape T currents
HCN-type	Dendrites (proximal < distal)	Maintain membrane potentials near resting membrane potentials; dampens IPSPs and EPSPs; feedback mechanisms for counteracting depolarisation and hyperpolarisation

Abbreviations: AIS, axon initial segment; NR, node of Ranvier; EPSP, excitatory post synaptic potential; AP, action potential; KCa, Calcium-activated potassium channel; GABA, γ-aminobutyric acid; HCA, hyperpolarisation-activated cyclic nucleotide-gated; IPSP, inhibitory post synaptic potential. Adapted using Child and Benarroch (2014) and Trimmer (2015).

1.2.1 Voltage-Gated Potassium Ion Channels

Potassium ion channels facilitate flux of K^+ across the plasma membrane down their electrochemical gradient. Amongst the distinct types of K^+ channels encoded by over 80 genes, the voltage-gated potassium channels (Kv) are the most diverse members of voltage-gated ion channel superfamily (Alexander et al., 2017). In human, the Kv α-subunits are encoded by 40 genes and are grouped into twelve subfamilies based on the amino acid sequence homology of their S1-S6 segments (**Table 1-4**).

Table 1-4 Voltage-gated K^+ channel family α-subunits.

Subunit	Gene names	Other names
Kv1.1-8	KCNA1-7, KCNA10	*Shaker*
Kv2.1-**2**	**KCNB**1-**2**	*Shab-related*
Kv3.1-4	**KCNC1**-4	*Shaw-related*
Kv4.1-3	KCND1-3	*Shal-related*
Kv5.1	KCNF1	*Modifier, KvS*
Kv6.1-**4**	**KCNG**1-**4**	*Modifier, KvS*
Kv7.1-5	KCNQ1-5	
Kv8.1-2	KCNV1, KCNV2	*Modifier, KvS*
Kv9.1-3	KCNS1-3	*Modifier*
Kv10.1-2	KCNH1, KCNH5	*EAG1, EAG2*
Kv11.1-3	KCNH2, KCNH6, KCNH7	*ERG1, ERG2, ERG3*
Kv12.1-3	KCNH8, KCNH3, KCNH4	*ELK1, ELK2, ELK3*

Channels in bold are the focus of this thesis. Adapted from Allen et al. (2020)

Unlike the substantially smaller repertoire of Nav and Cav channels, whose sole roles are to initiate and propagate action potentials, and to release Ca^{2+} into presynaptic terminals, the Kv channels play much more diverse physiological roles. In neurons, Kv function can be broadly grouped into either: 1) keeping neuronal excitation within limits; 2) shaping the amplitude and frequency of APs; and 3) controlling the APs and functional properties of neurons (Anderson and Greenberg, 2001; Köhling and Wolfart, 2016). The contribution of Kv channels to controlling these properties depends on their concerted subcellular localisation within the plasma membrane (i.e., dendrites, soma, axons), as well as within the membrane sub-compartments (e.g., dendritic spines, AIS, nodes of Ranvier, presynaptic termini).

The α-subunits which form actual conductance pores include the members of subfamilies Kv1-4, Kv7, and Kv10-12. For example, the Kv1-type channels are low voltage-activating and are mainly located in the axons of cerebellar, hippocampal, and thalamic neurons. Although they do not influence the first AP, they do increase the threshold for subsequent APs to ascertain correct AP propagation (Jan and Jan, 2012). Contrarily, the Kv7-type channels are expressed in in various combinations in neurons where they mediate M-currents which raise the threshold for firing of APs. In contrast, the α-subunits of Kv5, Kv6, Kv8, and Kv9 subfamilies are electrically silent (hence their name ‘silent Kv’ [KvS] subunits). Alike any other Kv channel, each KvS displays its unique characteristics but

collectively, all KvS subunits share three common features: 1) they are incapable of producing electrically functional channels on their own; 2) they interact with Kv2-type channels to form heterotetrametric functional channels; and 3) they modulate the biophysical properties of Kv2 channels (Bocksteins and Snyders, 2012; Bocksteins, 2016). The first characteristic has been studied extensively in Y2H models and FRET experiments, which have showed consistently that the KvS subunits fail to interact with themselves at the T1 domains (Post, Kirsch and Brown, 1996; Stocker, Hellwig and Kerschensteiner, 1999; Zhu et al., 1999; Ottschytsch et al., 2002; Kerschensteiner, Soto and Stocker, 2005; Schnitzler et al., 2009). Furthermore, while all functional Kv subunits contain PXP motif within their S6 segment, which is thought to be responsible for the formation of a hinge within the S6 helical structure that is necessary for channel gating (Del Camino et al., 2000; Labro et al., 2003), the KvS subunits lack the second proline residue within the PXP motif. However, restoration of the second proline residue within the PXP motif of Kv6.3 channel in Kv2.1 background did not restore the channel functionality, suggesting that the structural difference in PXP motifs between Kv and KvS subunits perhaps does not affect the KvS function (Ottschytsch et al., 2005). Similarly, the mechanisms by which KvS subunits form heterotetrametric Kv2-type channels have been studied extensively in the last two decades. First report of KvS interacting with other Kv subunits come from a 1996 study, where (Hugnot et al.,

1996)realised that when the Kv8.1 is co-expressed with Kv2 and Kv3.4 subunits, the Kv2- and Kv3-mediated currents were diminished. The next decade, a specific stoichiometric configuration was reported, where for majority of Kv2.1/9.3 heterotetrameric arrangements, one Kv9.3 subunit assembled with three Kv2.1 subunits (Kerschensteiner, Soto and Stocker, 2005), which challenged the notion at that time which posed that Kv2.1 channels arrange as dimers of dimers (Tu and Deutsch, 1999). The KvS subunits do not heteromerise outside the Kv2 subfamily to form functional Kv channels on plasma membrane because, for Kv6.4 and Kv2.1 at least, the specific co-assembly depends on both the interaction between the COOH terminus of the Kv6.4 and NH_2 terminus of the Kv2.1 (Bocksteins et al., 2014). Functionally, the KvS subunits alter the biophysical properties of Kv2 channels, thus modulating the Kv2-mediated currents. Heterotetrameric Kv2/KvS channels display changes in activation, deactivation, and/or inactivation kinetics (as well as voltage-dependence thereof); and changes in current density (Bocksteins and Snyders, 2012; Bocksteins, 2016). Distinct KvS subunits may affect the biophysical properties of Kv2 channels *via* different mechanisms; for example, the Kv6.1 may cause a shift in Kv2.1 voltage dependence of inactivation of around 50 mV towards the hyperpolarised direction relative to that of Kv2.1 homotetramers by promoting Ca^{2+}-calmodulin dependent dephosphorylation (Salinas et al.,

1997; Kramer et al., 1998) because Kv6.1 binds to calmodulin which senses intracellular Ca^{2+} levels (O'Connell et al., 2010).

The Kv2.1 and Kv6.4 channels

The Kv2 subfamily is comprised of two members. The Kv2.1 was isolated in 1989 using cDNA expression cloning (Frech et al., 1989), and the Kv2.2 was sequenced three years later in Snyder's lab (Hwang et al., 1992). Antibody-based detection and RNA expression studies have shown that, in terms of tissue distribution, the Kv2 are the most ubiquitous of all Kv channels. They are widely expressed in hippocampal and cortical neurons (Du et al., 1998; Bishop et al., 2015), spinal α motor neurons (Muennich and Fyffe, 2004), and dorsal root ganglia (Tsantoulas et al., 2014), but also, in retinal and retinal bipolar cells (Yazulla and Studholme, 1998), gastrointestinal (Epperson et al., 1999) and arterial smooth muscle (Amberg and Santana, 2006), cardiac myocytes (O'Connell, Whitesell and Tamkun, 2008), testes, (Regnier et al., 2017), and pancreatic β-cells (Fu et al., 2017; Greitzer-Antes et al., 2018). The Kv2.1 is the more profusely expressed of the two subunits (Hwang, Cunningham, et al., 1993; Hwang, Fotuhi, et al., 1993), and it is also the more ubiquitously expressed one in mammalian brain, and the only Kv2-type channel expressed in cerebellar neurons (Hwang, Fotuhi, et al., 1993). The Kv2.1 plays essential roles in numerous processes depending on its conductive and non-conductive properties. For example, studies of cultured

rat hippocampal and cortical neurons showed the Kv2.1 underlies a major component of the delayed rectifier K^+ current in these cell types (Murakoshi and Trimmer, 1999; Bekkers, 2000; Korngreen and Sakmann, 2000), and it was shown to have a significant influence on AP width in hippocampal neurons during high-frequency stimulation (Du et al., 2000). Studies of Kv2.1 knock-down with a pore-mutant or antisense gene expression suggested that the effect of Kv2 channel activity in cortical or hippocampal neurons is only minimal during single APs, as shape of APs is not affected by reduced or absent Kv2.1 channels (Du et al., 2000; Guan, Armstrong and Foehring, 2013). Additionally, while Malin and Nerbonne (Malin and Nerbonne, 2002) reported that the Kv2 can also contribute to the repolarisation of wide APs in sympathetic neurons, the loss of channel in both sympathetic and hippocampal neurons disrupted the maintained repetitive or tonic firing (Du et al., 2000; Malin and Nerbonne, 2002; Guan, Armstrong and Foehring, 2013). Mutations in Kv2.1-coding gene *KCNB1* in humans were linked to epilepsy (Thiffault et al., 2015). One such form includes the early infantile epileptic encephalopathy (EIEE), a progressive hereditary encephalopathy that manifests itself in early childhood. Although EIEE develops during embryonic periods, it is remarkably uneventful during gestation until first seizure develops during childhood, following which motor and cognitive defects become evident (Torkamani et al., 2014; Saitsu et al., 2015). In that respect, a study of *Kcnb1*$^{-/-}$ knock-out mice reported a

phenotype that is strikingly hyperactive and display an increased susceptibility to chemically induced seizures, consistent with the role for Kv2.1 as a suppressor of neuronal activity (Speca et al., 2014). Furthermore, the *KCNB1* gene is located at locus 20q13.13, and common risk variants for schizophrenia were found within close vicinity of this chromosomal location (Ripke et al., 2014). In that respect, the *Kcnb1*$^{-/-}$ knock-out mice generated by Speca and colleagues also showed schizophrenia-related abnormalities, including locomotor hyperactivity and deficits in spatial learning. An even more striking schizophrenia-like phenotype was observed in AMIGO knock-out (KO) mice. AMIGO is a Kv2.1 auxiliary subunit that constitutes an integral part of the Kv2.1 channel complex in the brain (Peltola et al., 2011). The behavioural manifestations consisted of increased locomotor activity and sensitivity to NMDAR antagonist MK-801 which were normalised by application of clozapine. Moreover, the authors observed reduced PPI and impaired mental flexibility and working memory – emphasising the potential role of Kv channels as targets for antipsychotic treatment development. Moreover, mutant mice lacking the AMIGO protein showed ~50% reduction in Kv2.1 protein expression and a concurrent significantly lower I_K current densities compared to WT mice, further emphasising the importance of accessory subunits in Kv channel function (Peltola et al., 2016).

As introduced briefly in **1.2.1**, the non-conducting or 'silent' Kv (KvS) α-subunits cannot assemble to form functional channels on their own but they must interact selectively with Kv2-type channels to form Kv2/KvS tetramers, which was demonstrated to cause a hyperpolarising shift in the Kv2.1 activation and deactivation kinetics in transfected cell lines (Bocksteins and Snyders, 2012; Pisupati et al., 2018). The expression patterns of KvS subunits are restricted to specific tissue types as opposed to the ubiquitously expressed Kv2 subunits, thus it is expected that the function of KvS α-subunits is to tune local Kv2-mediated currents to meet the tissue-specific demands (Bocksteins, 2016). From a developmental perspective, the *Kcng4* gene is expressed in hollow organs in developing zebrafish, such as the ear, eye, and brain ventricular system (Jędrychowska and Korzh, 2019). In adult mammals, the Kv6.4 is expressed in the testes. For example, in a transgenic mouse generated in Snyder's lab, Regnier and colleagues showed that in comparison to WT animals, the *Kcng4*$^{-/-}$ mice are sterile, and the little spermatozoa produced are immobile due to disturbed spermatogenesis (Regnier et al., 2017). The Kv6.4 is also highly co-expressed in the uterine sensory neurons where it decreases neuronal excitability, thus potentially contributing to analgesic effects during labour. In that respect, a cohort of women experiencing lower pain during first child delivery was identified to carry a rare polymorphism in the *KCNG4* gene causing a single mutation in the in the Kv6.4 selectivity filter (Lee et al.,

2020). Furthermore, a missense mutation L360P in the *KCNG4* gene was found in a migraine cohort (Lafrenière and Rouleau, 2012), and recently, the *KCNG4* was amongst 12 new candidate genes involved in multiple sclerosis (Vilariño-Güell et al., 2019).

The Kv6.4 is particularly interesting because data from the Allen Brain Atlas show that in adult mice, the *Kcng4* expression appears to be highly localised to the thalamus and the cerebellum. Moreover, the *Kcng4* expression is seemingly higher compared to *Kcnb1* (**Appendix A2**), which postulates possible non-conductive functions. In fact, the structural and supportive roles of Kv2.1 and Kv6.4 became well documented in the past two decades. The Kv2.1 exists in two separate populations: one that is dispersed freely on the plasma membrane and contains the electrically active channels, and a second population that forms highly dense clusters, which are non-conducting (Johnson, Leek and Tamkun, 2019). For example, the non-conducting Kv2.1 were implicated in exocytosis, where Lotan and colleagues found that the Kv2.1 facilitated vesicle release from neuroendocrine cells *via* interaction with syntaxin which was independent of K^+ flux (Singer-Lahat et al., 2007; Feinshreiber et al., 2010). Furthermore, Tamkun's lab found that around 80% of Kv1.4 and Kv2.1 insertion events to the plasma membrane in cultured hippocampal neurons occurs within the Kv2.1 cluster perimeter, suggesting that these microdomains may act as trafficking hubs (Deutsch et al., 2012; Fox, Loftus and Tamkun, 2013).

The Kv3.1b channel isoform

The Kv3 channel subfamily is comprised of four members, from Kv3.1 to Kv3.4, and each member exists in multiple isoforms based on distinct mRNA splice variants, which diversifies their susceptibility to regulation by accessory subunits and the ways in which they interact with cytoplasmic signalling pathways. However, one distinctive feature amongst all Kv3-type channel variants which differentiates them from other electrically active Kv α-subunits is that the Kv3 channels open at more positive potentials and their response to change in voltage is very rapid. Moreover, upon repolarisation, their deactivation rates are ten times faster compared to most Kv channels. Therefore, the Kv3-type channels are major determinants of high-frequency neuronal activity, and consequently, they are expressed in brain regions where the neuronal populations are required to generate APs with microsecond precision to assure realistic representation of the temporal patterns of synaptic inputs, such as the auditory system and the cerebellum (Rowan et al., 2016).

The Kv3.1-coding gene *KCNC1* was first cloned from neuroblastoma-glioma hybrid cells (Yokoyama et al., 1989), although the main functional roles of Kv3.1 were found to be within the nervous system. The Kv3.1 become active only when the membrane potentials become more positive than -10 mV, thus they remain closed at typical membrane potentials but

open rapidly once the APs reach their peak (Grissmer et al., 1994). The Kv3.1 underlie a typical delayed rectifier K^+ current and undergo little inactivation during depolarisation that last less than one second although their inactivation response is substantial once the depolarisation is extended to many seconds (Kanemasa et al., 1995). A key biophysical feature essential to the biological role of Kv3.1 is the swiftness in which they close once the membrane returned near resting potential, which results in a minimal refractory period in neurons in which the Kv3.1 are responsible for repolarisation. In *situ* hybridisation and antibody-based detection studies revealed that Kv3.1 are expressed in a subset of neurons which fire at high rates, such as parvalbumin-positive hippocampal and cortical interneurons, cerebellar granule cells, thalamic reticular nuclear neurons (Perney et al., 1992; Sekirnjak et al., 1997; Wang et al., 1998), but also in several auditory nuclei (Perney et al., 1992; Si Qiong J. Liu and Kaczmarek, 1998; Li, Kaczmarek and Perney, 2001). The Kv3.1 exists in two major isoforms, the Kv3.1a and Kv3.1b (Luneau et al., 1991). Both isoforms appear to be expressed in the same neurons; however, for many neurons the Kv3.1a is only dominant in early development, whilst the Kv3.1b is the dominant in adult neurons (S. Q.J. Liu and Kaczmarek, 1998; Si Qiong J. Liu and Kaczmarek, 1998). The subcellular localisation of Kv3.1b targets the axon initial segment, which has the greatest influence on AP generation (Xu et al., 2007). As introduced briefly on previous pages, the Kv3.1b colocalises with

Nav channels along myelinated axons where it plays an integral role in saltatory conduction of APs (Devaux et al., 2003; Kim and Rutherford, 2016). In cortical and hippocampal parvalbumin-positive interneurons, however, the Kv3.1b is restricted to proximal dendrites, soma, axon hillock, unmyelinated axonal membranes, and presynaptic axon terminals (Sekirnjak et al., 1997; Ozaita et al., 2002).

Although the Kv3-type channels are mostly associated with facilitating high rates of APs, it has recently become clear that they also play a major role in neurotransmitter release. A comprehensive body of evidence including recordings from presynaptic terminals combined with pharmacological studies have established that APs in presynaptic terminals are shaped by Kv3-type currents in auditory brainstem neurons (Wang and Kaczmarek, 1998; Ishikawa et al., 2003; Nakamura and Takahashi, 2007), cerebellar neurons (Southan and Robertson, 2000; Ritzau-Jost et al., 2014; Rowan et al., 2016), cortical interneurons (Goldberg et al., 2005), and hippocampal neurons (Alle, Kubota and Geiger, 2011; Hoppa et al., 2014).

The dysfunction of Kv3-type channels has been linked to several neurological diseases in humans including spinocerebellar ataxia (Zhang and Kaczmarek, 2016), epilepsy (Nascimento and Andrade, 2016; Kim et al., 2018), and foetal alcohol syndrome (Tavian, De Giorgio and Granato, 2011). For the Kv3.1, a recurrent *de novo* mutation R320H in the *KCNC1* gene

which removes a single arginine residue in the S4 voltage sensor results in a dominant-negative non-functional channels which suppress the amplitude of Kv3-mediated currents once they assemble into heterotetramers with wild-type Kv3.1 α-subunits. Individuals affected by this mutation manifest with progressive myoclonus epilepsy, ataxia, action myoclonus (Muona et al., 2015). For this, suppression of all Kv3.1-type channels in cortical neurons of chronic epileptic rats by application of low concentrations of 4-aminopyridine induced seizure-like activity in brain slices (Zahn et al., 2008; Zahn et al., 2012). However, Ho and colleagues demonstrated that both homozygous and heterozygous Kv3.1-deficient mice, despite a distinct behavioural phenotype, but present with no seizures (Ho, Grange and Joho, 1997). Other studies have also proposed that reduced Kv3.1 expression may prompt seizures in animals. For that, Lee and colleagues found around 50% reduction in Kv3.1b immunoreactivity in hippocampal neurons of seizure-prone gerbils with a smaller reduction in Kv3.2, but no reduction in several other Kv channels, including Kv3.4 which suggested that the Kv3-type channels, particularly the Kv3.1b are involved in setting seizure threshold (Lee et al., 2009). Furthermore, Kv3.1b channels have been indirectly implicated in schizophrenia. Reduced gamma frequency oscillations, which required a synchronous activity in cortical GABAergic interneurons that express Kv3-type channels, have been associated with cognitive impairments in schizophrenia (Lewis et al., 2012). Two years later,

Yanagi and colleagues found significantly reduced Kv3.1b in parietal and prefrontal cortex in post-mortem samples of unmedicated schizophrenia patients, while Kv3.2 levels remained unchanged. Moreover, the authors found no significant difference in Kv3.1b expression in those brain regions in samples from subjects that underwent therapy, which suggested that antipsychotic medications are able to restore Kv3.1 (Yanagi et al., 2014).

Recent decades saw a growing number of voltage-gated ion channels recognised as important contributors in the underlying pathology of neuropsychiatric disorders, including schizophrenia (**Table 1-5**). However, owing to the very multifaceted genetic architecture of psychiatric disorders, the characterisation of associations between them and the ion channel genes proves very complicated, and the characterisation and individual expression patterns remain to be described in every disease and supported with substantial evidence from model animals. As forementioned in this section, the Kv2 channels are unique in the sense that they are the only Kv α-subunits capable of forming functional channels with members of KvS subfamilies, and their roles have been implicated in several human psychiatric conditions. Moreover, the Kv3-type channels are of special interest in schizophrenia due to their intricate roles in controlling gamma frequency oscillations, which have been shown to be desynchronised in unmedicated patients.

Table 1-5 Voltage-gated potassium channels implicated in neuropsychiatric disorders.

Disorder	Protein	Gene	Locus	Reference
ASD, autoimmune psychiatric disorder, bipolar disorder, schizophrenia.	Kv1.1 Kv2.1 Kv3.1 Kv7.3 Kv11.1 Kir3.1	*KCN1A* *KCNB1* *KCNC1* *KCNQ3* *KCNH2* *KCNJ3*	12p13.32 20q13.13 11p15.18q24 7q36.12q24.1	(Sklar et al., 2011; Sicca et al., 2011; Grube et al., 2011; Sanders et al., 2012; Kristensen, Sandager-Nielsen and Hansen, 2012; Yamada et al., 2012; Zhang et al., 2013; Yanagi et al., 2014; Ripke et al., 2014; Peltola et al., 2016; Latypova et al., 2017; Pisupati et al., 2018)

1.3 The Cerebellum

1.3.1 Anatomy

The cerebellum is a region of the brain known for its role in coordinating motor function, posture, and balance. Its name is a diminutive of the Latin word *cerebrum* (meaning 'little brain'); despite the small size which is approximately one-tenth of that of the cerebrum, the cerebellum contains nearly 80% of total brain neurons. The structure is located in the posterior cranial fossa where it sits dorsal to the brainstem and inferior to the occipital lobes. The gross anatomical features of the cerebellum reveal the anterior, the posterior, and the flocculonodular lobes, which are separated by two fissures (**Figure 1-7**). The primary fissure separates the anterior and posterior lobes while the posterolateral fissure separates the posterior and the flocculonodular lobes. Furthermore, the cerebellum is functionally divided into three zones. The cerebrocerebellum (lateral zones), which is comprised of the lateral hemispheres, receives input from the cerebral cortex and it is mainly involved in motor planning. The spinocerebellum (the intermediate and medial zones) is comprised of the central vermis and paravermis and receives proprioceptive information from the dorsal column of the spinal cord and is responsible for motor control. The vestibulocerebellum, which is comprised of the flocculonodular lobe receives information from the visual cortex and vestibular nuclei and is

responsible for ocular movement and balance (Haines and Mihailoff, 2018). The cerebellar connections to other parts of the nervous system run through cerebellar tracks located within three pairs of cerebellar peduncles. The superior cerebellar peduncle (*brachia conjunctiva*) connects the midbrain, the middle cerebellar peduncles (*brachia pontis*) connect the pons, and the inferior cerebellar peduncle (restiform bodies) connect the medulla (D'Angelo, 2018).

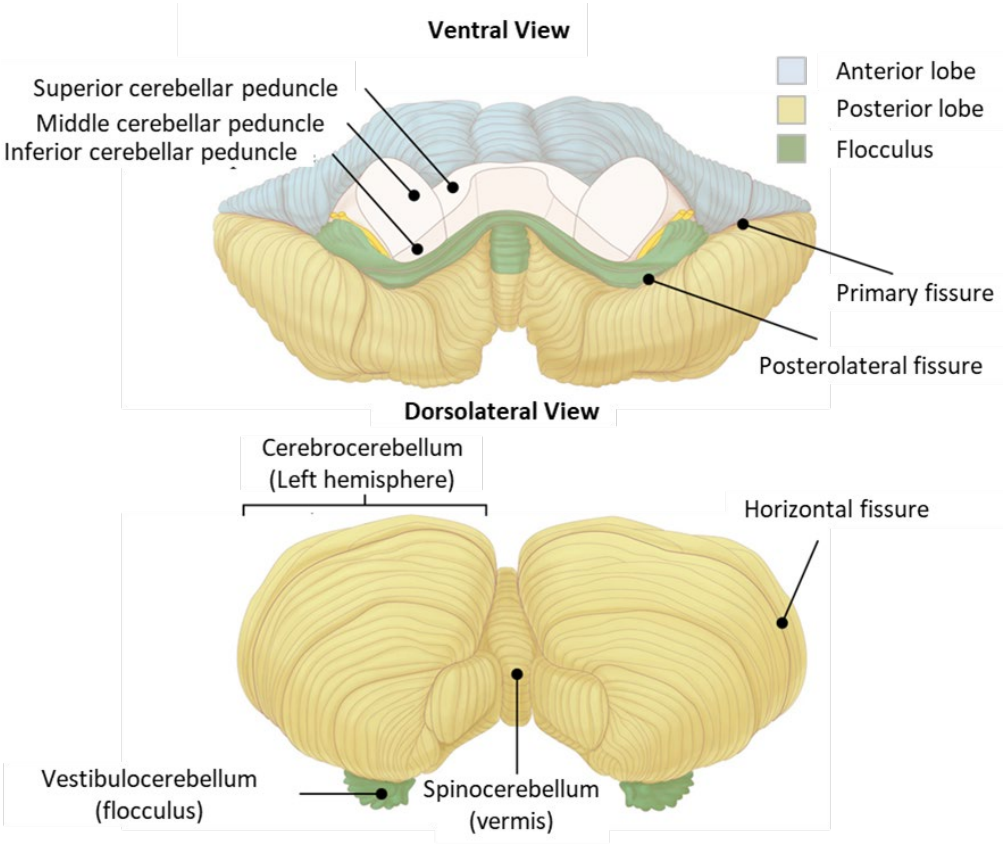

Figure 1-7 Gross anatomical features of the cerebellum.

Top, ventral view showing cerebellar lobes and cerebellar connections to the brainstem; bottom, a dorsolateral view showing lateral hemispheres, vermis, and flocculus. Adapted from (AMBOS, n.d.).

The lobes of the cerebellum are further divided into ten smaller lobules that are identified using Roman numerals I–X, and its corresponding lateral counterparts are assigned the prefix 'H' (**Figure 1-8**). The lobules II–X of the vermis have corresponding lateral hemispheres lobules HII – HX, while the vermal lobule I does not have a corresponding hemisphere part in man. The anterior lobe contains lobules I–V and HII–HV, and the posterior lobe allocates lobules VI–IX and HVI–HIX, whereas the flocculus consists of lobule X and lateral hemispheres HX. Perhaps the most striking gross anatomical feature of a mammalian cerebellum is its folial arrangement. Each cerebellar lobule is arranged into a series of ridges of the cerebellar cortex that are continuous from hemisphere the midline of the superior surface (D'Angelo, 2018).

Superimposed on the lobules are three principal zones on each side of the cerebellum that are defined based on their afferent and efferent connections: the medial zone, the vermis (from Latin word *vermin*, meaning 'worm') is a narrow strip of cortex extending from the anterior lobe to the flocculus; the intermediate zone (the paravermis) is adjacent to the vermis and extends from the anterior to the posterior lobe but has little representation in the flocculus; and the lateral zones (the lateral hemispheres) that comprise the largest part of the cerebellar cortex, and involve the anterior and posterior lobes, and the flocculus (Voogd and

Marani, 2016). Beneath the cerebellar cortex lie four pairs of deep cerebellar nuclei embedded in the white matter core (**Figure 1-8**).

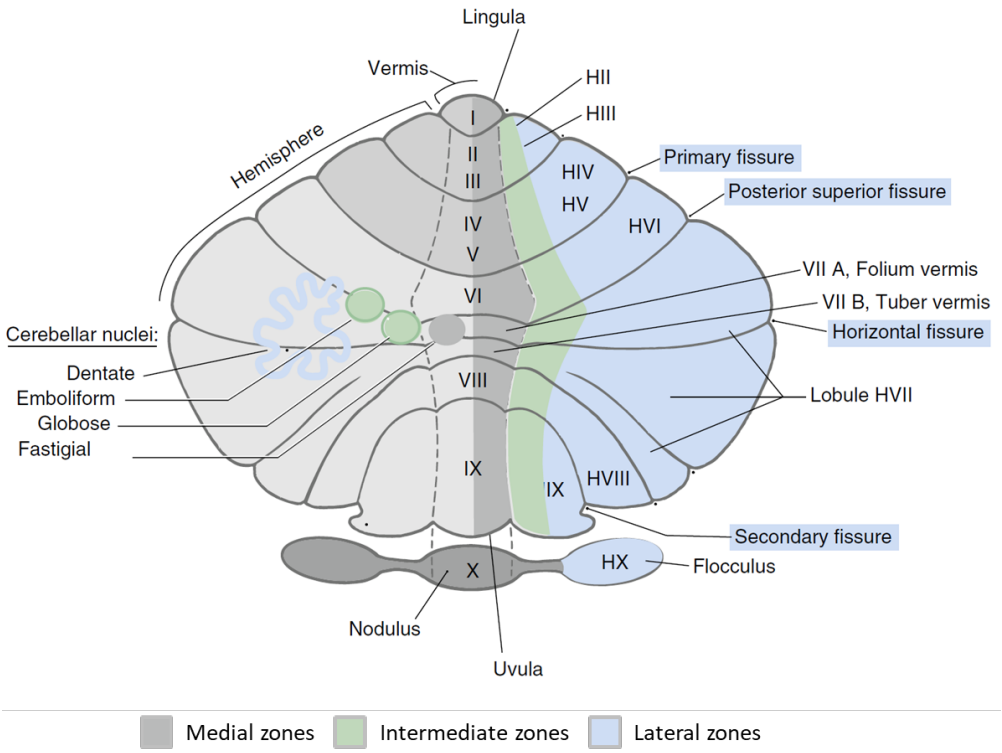

Figure 1-8 Unfolded view of the cerebellum.

The image shows cerebellar lobules with assigned Roman numerals in the vermal part and their lateral counterpart with prefix 'H'. The principal zones are depicted on the right, and on the left, the deep cerebellar nuclei within the medulla are colour-coded to depict their location within the corresponding principal zones. Adapted from (Haines and Mihailoff, 2018)).

The fastigial nuclei which are located adjacent to the midline are functionally related to the overlaying medial zone. They are mainly involved in communicating with the vestibular nuclei and interpreting body motion in a spatial plane and are involved in modulating the saccadic eye movement

(Brooks and Cullen, 2009). Located laterally to the fastigial nuclei lie two interposed nuclei: the globose nucleus and the emboliform nucleus which are functionally related to the intermediate zones of the cerebellar cortex. The interposed nuclei receive efferent fibres from the anterior lobe and feed information to the red nucleus the superior cerebellar peduncle to regulate the strength of proximal limb muscles, but it was also found to be involved in Pavlovian conditioning and eye-blink response (Clark, Zhang and Lavond, 1992; Krupa and Thompson, 1997). Located laterally to the emboliform nucleus on each side lie the dentate nuclei which are functionally related to the lateral zones of the cortex and their size correlates with the large size of the lateral hemispheres.

The cerebellar cortex and medulla

Just like the gross anatomy, the cerebellar microarchitecture is also highly uniform, and each portion of the structure shares a similar basic microcircuitry (Sillitoe and Joyner, 2007). The outermost part of the cerebellum, the cerebellar cortex, contains several types of densely packed cell types that are arranged into three distinct layers (**Figure 1-9**).

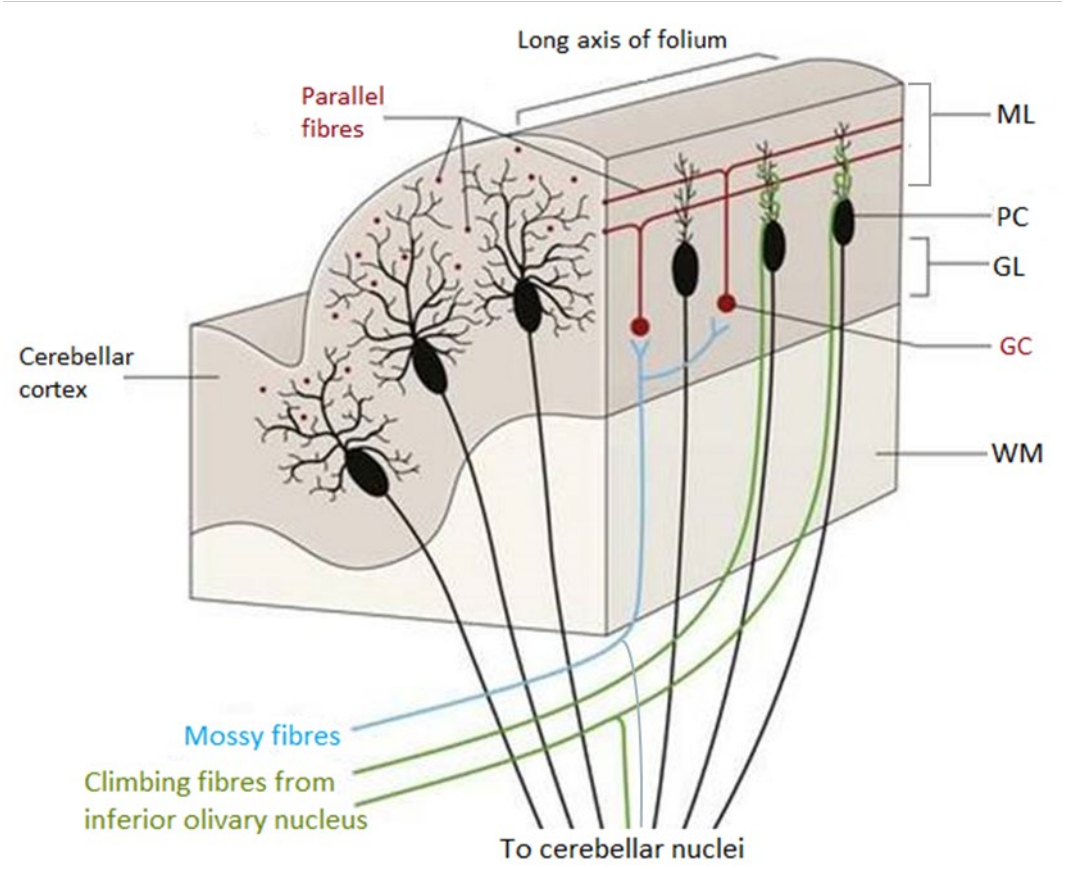

Figure 1-9 Illustration showing cross-section of a cerebellar folium.

The image depicts the cytoarchitecture of the cerebellar cortex with its afferent and efferent connections. The Purkinje cell is the primary neuron receiving numbered afferents and it is the only cortical output cell. The main cerebellar input is achieved *via* mossy fibres and climbing fibres. PC, Purkinje cell; ML, molecular layer; GL, granular cell layer; GC, granular cell; WM, white matter. Generated using BioRender®.

The middle-most layer is home to the large (~50 μm in diameter) somata of linearly arranged PCs which form a border between the molecular and granular layers. From each PC stems an elaborate, fan-shaped dendritic tree that projects into the molecular layer. The primary dendrite is the trunk of the tree and gives rise to secondary dendrites that branch into numerous

tertiary dendrites. These secondary and tertiary dendrites form terminal branchlets at which synaptic contacts are formed. PCs are GABAergic and the only cortical output cells whose axons penetrate through the granular layer to inhibit target neurons in the vestibular and cerebellar nuclei (Larramendi and Lemkey-Johnston, 1970).

The granular layer is home to three main cell types. The most numerous are the granule cells which are small (~8 μm) glutamatergic neurons and are the primary excitatory cells in the cerebellum. Their axons ascend to the molecular layer to form parallel fibres which latch onto the PCs and form synapses with the spiny branches of the tertiary branchlets. Unipolar brush cells (UBC) are the second type of neuronal cells found in the granule layer and together with the granule cells comprise the only excitatory cell types in the cerebellar cortex. UBCs do not exceed 14 μm in size, and they form a single dendritic structure arising from the soma that resides in the granule cell layer and diverges into 2 – 4 rosettes which are contacted by dendrites of other unipolar brush cells, granule cell dendrites, and Golgi cell axons. Unlike granule cells, which are ubiquitous in every part of the cerebellar granule layer, the UBCs are scarce and are reside predominantly in the vermis, areas adjacent to the flocculus, and the lateral hemisphere lobules HVI–HVIII (Lu, Hartmann and Bower, 2005; Mugnaini, Sekerková and Martina, 2011). Golgi cells are the third type of neuronal cells found in the granule layer and are noticeably larger (~25 μm) than

granule cells and UBCs. These cells are primarily found adjacent to PCs and their axons diverge into the granule cell layer to form synapses with granule cell dendrites.

The molecular layer is the outermost layer and contains significantly less neuronal cell bodies compared to the granule layer. It is mainly composed of a vast network of PC dendrites and parallel fibres that originate in the granule cells, although it is home to two intrinsic cell types: stellate cells which are found in the outermost regions of the molecular layer, and basket cells which are located immediately above the PCs. Both cell types are similar in size and receive glutamatergic inputs from the parallel fibres, although where stellate cells form synapses with dendritic projections of the PCs, the basket cells also form ‘baskets’ around PC soma.

Cerebellar connectivity

Input to the cerebellum arrives from a wide range of sources. Some project directly the vestibulocerebellar and spinocerebellar pathways, whereas others arrive indirectly *via* numerous central pathways. The afferent fibres arrive in the cerebellar cortex *via* three types of cortical terminals. The mossy fibres (nucleocortical fibres), which originate in the deep cerebellar nuclei and carry information from a range of other nuclei in the pons, medulla, and the spinal cord, and exert glutamatergic impulses to the Golgi

cells and the granular cell dendrites. The information that arrives from these nuclei is delivered to the specific cerebellar nucleus that is associated with the particular cortical zone (e.g., the dentate nuclei receive afferents *via* the middle cerebellar peduncle through the pontocerebellar axons which originate in the pontine nuclei). The second type of afferents comprises the climbing fibres. The inferior olive in the medulla oblongata is the only source of cerebellar afferents that terminate as climbing fibres in the cerebellar cortex. The climbing fibres carry information from the cerebellar nuclei that arrived *via* olivocerebellar fibres from the inferior olivary nuclei. Similarly, the signals carried by olivocerebellar fibres arrive at the specific nucleus where they excite the cerebellar nuclear neurons, which is then relayed to the appropriate parts of the cerebellar cortex. Climbing fibres terminate within the molecular layer, entwining upon the PC dendritic tree where they make synaptic contact with the smooth branchlets of PC processes to excite the PC (Sotelo, 2004; Hashimoto and Kano, 2005). The third type of afferent fibres originates in several locations and display diffuse termination. These fibres have a similar 'multi-layered' morphology in the cerebellum thus, their identities are based on their intricate molecular characteristics. The multi-layered fibres include serotonergic fibres originating in the raphe nuclei (Dieudonné, 2001); noradrenergic fibres from the locus coeruleus (Abbott and Sotelo, 2000); and the cholinergic fibres originating in pedunculopontine nucleus (Jaarsma et al., 1997).

1.3.2 Function

The cerebellum is undoubtedly the most elegant of all brain regions. Its uniform anatomy and ornately arranged cytoarchitecture may only imply elaborate functions. The cerebellum communicates and consolidates information from multiple regions of the brain, including the spinal cord (Manzoni, 2007), vestibular nuclei (Meng et al., 2014), the brain stem (Nowak et al., 2007), and the cerebral cortex (Hoover and Strick, 1999; Kelly and Strick, 2003). The cerebellum is most known for its roles in coordinating movement, posture, and balance. Almost two centuries ago, Flourens (Flourens, 1842) demonstrated that damage to the cerebellum in pigeons impaired their ability to fly due to the loss of coordination of voluntary wing movements, not because of muscle weakness. Today we understand that the cerebellum compares *intention* with *execution* to compensate for the ongoing errors in anticipation of their occurrence, which generates a precise predictive motor control observed in all vertebrates (D'Angelo, 2018). However, the more elusive function of the cerebellum involves its roles in emotion and cognition. One line of evidence posing at cerebellar involvement in higher cognitive tasks arises form developmental and evolutionary biology; high primates other than humans lack the capacities for abstract thinking, complex language, and sophisticated social constructs. In those species two brain regions are considerably smaller compared to humans – the frontal cortex and the cerebellum (Passingham,

Toni and Rushworth, 2000). Furthermore, there is significant input from anatomical studies illustrating point-to-point connectivity between cerebellum and other brain regions including frontal and parietal cortex which provide significant evidence to support the idea that the cerebellum is involved in neural circuits which perform higher cognitive tasks. Tract-mapping studies in mice demonstrated exact connectivity between the cerebellum and multiple cortical regions *via* the cortical-cerebellar-thalamic-cortical circuit (CCTCC), providing strong evidence of bidirectional connectivity with structures of high neuropsychiatric interest, such as the prefrontal cortex, the limbic lobes, the septal nuclei, and numerous hypothalamic and thalamic nuclei (Andreasen, 1999; Ivry et al., 2002; Ito, 2008; Habas et al., 2009; Stoodley, Valera and Schmahmann, 2012).

In humans, eye-blink conditioning studies demonstrated impaired time production and perception (Keele and Ivry, 1990; Akshoomoff and Courchesne, 1992) and impaired associative learning (Attwell et al., 2002) in subjects with cerebellar damage. Furthermore, cerebellar insult may produce symptoms similar to those observed in psychiatric disorders, such as poverty of speech or mutism (Orefice et al., 1999; Rekate et al., 1985). More recently, cerebellar vermis has been implied in learning during mental recall of emotional personal episodes or during unconditioned or conditioned association involving emotions (Strata, 2015). Additionally, *in vivo* neuroimaging studies have shown that cerebellum activates during a

variety of mental activities, such as facial recognition, emotional attribution, directed attention, and numerous types of memory (Allen et al., 1997; Seidler et al., 2002; Kim, Ugurbil and Strick, 1994). For that, in addition to disorganised movement and coordination, patients with severe cerebellar injuries also present with emotional alterations and cognitive deficits (Villanueva, 2012).

1.3.3 The Cerebellum in Schizophrenia

The current literature provides a wide range of insights into cerebellar involvement in schizophrenia. First, it is worth to mention that schizophrenia patients often manifest with neurological soft signs (NSS) which are subtle impairments in motor coordination, balance, sequencing of complex motor acts, and sensory integration (Heinrichs and Buchanan, 1988). If we considered all patients with schizophrenia, the prevalence of abnormal NSS is over 50%, while only about 5% of controls show such abnormalities (Chan and Chen, 2007). Furthermore, there is an increasing body of evidence of cerebellar involvement in higher cognitive functions, and an ever more case studies reporting the concurrence of psychosis and cerebellar pathologies (Mignarri et al., 2014; Trikamji, Singh and Mishra, 2015; Tréhout et al., 2019). For example, Keshavan and colleagues (2003) compared the scores for repetitive motor tasks abnormalities and brain volumes in schizophrenia patients and healthy volunteers, and found that

the scores were higher amongst schizophrenia patients compared to the controls, and the higher scores were associated with smaller volumes of the left association cortex. Authors of another study compared the signs in several neurological dimensions between schizophrenia and mood disorder subjects, and healthy controls, and patients with schizophrenia presented with higher prevalence of coordination disorders compared to the other groups, which seem to reflect fronto-cerebellar dysfunction. Furtermore, studies using MRI techniques found associations between clinical correlates of cognitive performance in schizophrenia and significantly reduced cerebellar volume (Levitt et al., 1999), and diminished cerebellar vermis volume (Nopoulos et al., 1999), whereas the posterior superior cerebellar vermis was found to be singificantly smaller in male schziophrenia patients comapred to controls (Okugawa et al., 2002), and progressive loss of ceberellar volume was reported in patients with childhood onset of the disease (Keller et al., 2003), as well as in patients manifesting with predominantly positive symptoms (Nopoulos et al., 2001). Furthermore, reduced cerebellar cortex and vermis activity in schizophrenia was demonstrated using fMRI techniques during several cognitive tasks including attention and memory (Crespo-Facorro et al., 2007) such as social interference (Andreasen, Calage and O'Leary, 2008). However, research into the exactpathological processess in the schizoiphrenic cerebellum is still in its infancy.

A key neuroanatomical feature in schziophrenia pathophysiology involves alterations in the cortico-thalamic-cerebellar circuit (CTCC) – a constellation of tracts connecting the looped neural pathways which link the thalamus to the cerebral cortex and the cerebellar nuclei *via* the superior cerebellar peduncle (Koziol et al., 2014). Neuroimging methods found patterns of both hypo- and hyperconnectivity in the CTCC and the occurrence of psychotic featues in patients as young as nine to eleven year-old, which suggested that the alterations precede the onset of more serious pathology (Karcher et al., 2019). Furthermore, several studies have described longitudinal associations between alterations in CTCC connnectivity and the progression or the conversion of symtpoms to psychosis in groups at high clincial risk (Anticevic et al., 2015; Bernard, Orr and Mittal, 2017; Cao et al., 2018). However, Ramsay (2019) in his recent meta-analysis failed to establish consistent changes in CTCC associated with psychoses, acknowledge the methodological limitations posed by functional analysis techniques. Additionally, the directionality of the effects, whether hyper- or hypoconnectivity in subjects with with psychisis relative to control groups vary across the studies thus posing a challenge in the interpreting of these results (Moberget and Ivry, 2019). Interestingly, the hypoconnectivity appears to be more profound in the areas involved in cognitive processes such as the crus I and crus II, whereas the hyperconnecitvity might be asosciated with snesorimotor regions (Shinn et al., 2015).

Chapter 2 Materials and Methods

2.1 Animal Procedures

All experimental procedures in this study were carried out in strict accordance with the UK Home Office regulations under the Animals (Scientific Procedures) Act 1986, Procedure Individual Licence (PIL) and Project Licence, and De Montfort University guidelines on animal welfare. All efforts were made to minimise the number of animals used in the study and their suffering.

2.1.1 Housing and Monitoring

The subjects were male CBA/Ca mice purchased from Charles River at 5-6 weeks of age. This mouse strain is the most commonly used strain in British scientific and pre-clinical research. It also has low incidence of spontaneous mammalian cancer and is known for its longevity, yet the effects of PCP on this strain remains to be reported. Additionally, our collaborator at University of Leicester use CBA/Ca strain for their research on auditory brain stem and hearing. They have also generated several lines of

transgenic CBA/Ca mice that can be potentially useful for us in the future. The animals were randomly allocated into groups of 3 or 4 mice per cage upon arrival and allowed one week of acclimation in the new environment. The mice were housed in a holding room in a natural light/dark cycle (lights on at 07^{30} for 12 hours). The average room temperature (RT) was 22°C and the average humidity was 40%. All animals underwent daily inspection for signs of health deterioration and their weight was recorded each morning throughout the study. All drugs were administered *via* intraperitoneal injections on the alternate side of the abdomen to minimise pain and distress. The animals were provided standard laboratory chow and freshwater *ad libitum* and were allowed moderate or no environmental enrichment, depending on the experiment design.

2.1.2 Study Design and Treatments

Subchronic study

To induce the pharmacological mouse model of schizophrenia, the animals were administered with phencyclidine (PCP; 5.0 mg/ kg b.w.) twice a day (early morning and late afternoon) for seven days or received an equal volume of 0.9% saline, followed by a seven-day washout period (i.e., drug-free.) as described previously (Brigman et al., 2009)

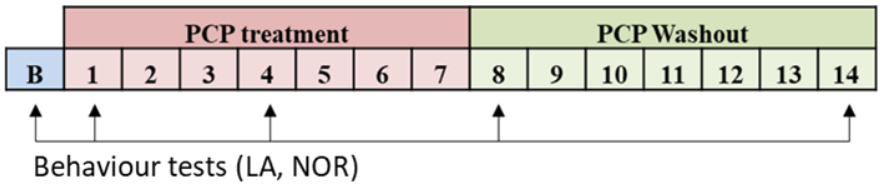

Figure 2-1 Subchronic study design.

The total study duration was 15 days including baseline. The animals were administered either PCP or saline during the first seven days, followed by seven days of washout. The behaviour tests were carried out at baseline and/or days 1, 4, 8, and 14.

Acute reversal study

The acute study was designed to investigate the behavioural changes in a model of acute psychosis and the extent to which these changes were reversed with concomitant administration of antipsychotic medication. Forty animals were randomly allocated into four groups of equal size and received either:

1. Normal saline (0.9%); or
2. PCP (10 mg/ kg b.w.); or
3. PCP (10 mg/ kg b.w.) + Haloperidol (0.03 mg/kg b.w.); or
4. PCP (10mg/ kg b.w.) + Clozapine (0.003 mg/kg b.w.).

The PCP dose has been used previously and was shown to induce alterations in locomotor activity and stereotypical behaviours (Mansbach, 1989; Sams-Dodd, 1996). The animals underwent a battery of behaviour tests at baseline and on the day 30 minutes after treatment, which included open field tests and motor coordination tests.

2.1.3 Animal Behaviour Tests

Tests were performed to assess behavioural changes induced by PCP in both studies. The antipsychotic medications were used to study the reversal of the acute changes induced by PCP in the acute study only. The tests measured cognitive performance and general locomotor activity in an open field; the novel-object recognition test adapted from Leger *et al*. (Leger et al., 2013) was used to measure recognition memory, and locomotor activity test adapted from Samson (2015) was used to investigate features relative to positive symptoms such as stereotypy, or stress and anxiety features, such as withdrawal. Motor coordination tests adapted from Filali *et al*. (Filali et al., 2015), which included the performance on a horizontal bar and a vertical pole were performed in the acute study only. All test in the open field were aimed to be completed within forty minutes of administration for each animal as plasma concentrations of PCP peak approximately 30 minutes following dosing, and acute effects last up to two hours (Michael Owens et al., 1990). The animals were handled with care to stress or anxiety - each animal was removed from their home cage using both hands and placed in the open field arena facing away from the experimenter.

Open Field Tests

The open-field test is a common method for assessing general locomotor activity, exploratory behaviours, and anxiety in rodents (Perals et al., 2017), where these behaviours can be measured both qualitatively and quantitatively. The open-field test is commonly used as a tool for assessing sedative or stimulant effects of compounds, thus variations of the open field test are included in virtually any thorough investigation of rodent behaviour in a neuroscience laboratory (Andreasen, 1999; Gould, Dao and Kovacsics, 2009). The original open field test was developed by Hall and Ballachey (Hall and L, 1932) with the intention to measure activity in rodents and their willingness to explore the surroundings. In principle, the open field test is conducted in a test arena, which is an enclosure that may be either circular, square, or rectangular, and that includes surrounding walls to prevent an escape. The behaviour can be assessed manually or with the aid of video-tracking systems. In this thesis, a free video-tracking software MouseMove (Samson et al., 2015) and a commercial EthovisionXT package (Noldus, Spink and Tegelenbosch, 2001) were used. However, behaviours such as rearing, or defaecation were recorded manually as they could not be readily captured using an automated system. The primary outcome of interest in the open field test is the locomotor activity, which is measured in metrics such as travel distance, time in motion, rotatory preference, or rearing. Some outcomes, particularly time spent in the centre, defaecation, and

activity within the first 5 minutes are related to emotions, such as stress, anxiety, or fear.

The novel object recognition test (NOR) is a modified version of the open field test that involves introducing novel objects to the test arena and quantifying the time spent by an animal exploring each of the objects. In the NOR test, an animal is exposed to two identical objects simultaneously with the expectation that it spends near-equal time exploring both objects. Following an intersession interval, one of the identical objects is replaced with a new, novel object. Since rodents are naturally inclined to explore new objects, it is anticipated that the animal spends more time exploring the novel object relative to the old one (Leger et al., 2013). The test is commonly used to gather useful information about the curiosity (Sih, Bell and Johnson, 2004) as well as different kinds of neophobia (Greggor, Thornton and Clayton, 2015). Furthermore, measuring the response of animals to novel objects can be used to test memory. The novel object recognition test is based on the visual-paired comparison task widely used in humans and non-human primates to test different aspects of non-declarative memory (Rose et al., 2013; Zhang et al., 2019). One such well-studied aspect is recognition memory, which depends on structural integrity and connectivity of diencephalic structures and the medial temporal lobe (Squire and Dede, 2015).

Open Field Acquisition System

The initial open field tests in this project were conducted in a custom-built test arena adapted from Samson *et al*. (Samson et al., 2015). The arena was constructed from two sheets of corrugated plastic secured together using sprayable glue and nylon tie straps; a white sheet was used to form the base of the arena and a black sheet was arranged to form a circular wall 76 cm in diameter and 40 cm in height. The assembled arena was secured to a wheeled garment rail using nylon tie straps. A bicycle wheel was secured in the middle of the top rail with a screw for a webcam attachment and to support a white bathroom curtain used to obstruct the field of view of the animals (**Figure 2-2**). Video recordings were acquired at a rate of 25 frames per second with a basic USB webcam connected to a Windows PC equipped with Debut Video Capture and Screen Recorder (NCH Software, USA). The open field tests in the acute study were conducted in a rectangular guinea pig cage base, 50 cm in length and 40 cm in width. The videos were acquired using a generic PC webcam connected to a Windows PC equipped with EthovisionXT video-tracking software (Nodulus, USA).

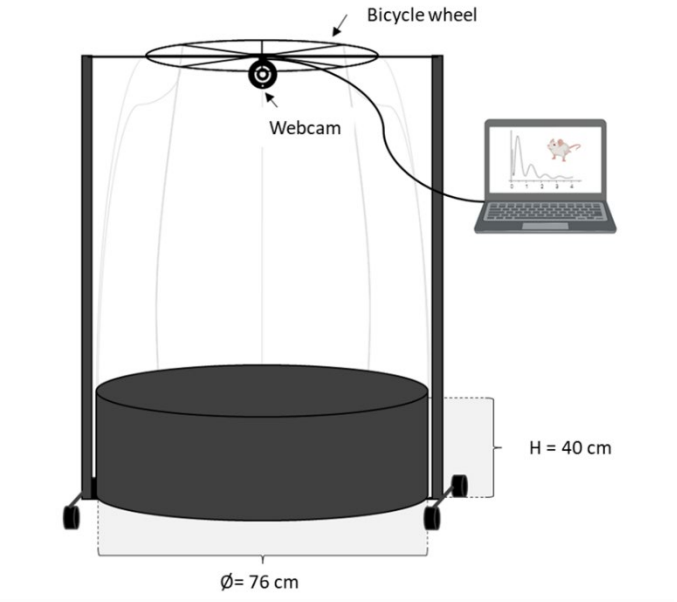

Figure 2-2 Illustration showing the custom-built open-field arena.

Locomotor Activity Test Procedure

The animals were transferred from the housing room to the procedure room in their home cages and allowed 30 minutes within their home cages to acclimatise to the procedure room. The arena was cleaned with 70% *v/v* ethanol to minimise olfactory cues before introducing each animal. Each animal was acclimatised to the test arena for three consecutive days before the test day by allowing to explore the arena for ten minutes each day to minimise stress-induced bias. On the test day, each animal was reintroduced to and placed in the arena and their behaviour in the open field recorded for 10 minutes and the video files saved to an external hard drive. The number of droppings and urination attempts were recorded

manually during cleaning the arena in preparation for the next animal (not discussed).

Novel-Object Recognition Test Procedure

The arena was cleaned, and the animals underwent acclimation as in locomotor activity test procedure. The NOR test consisted of a familiarisation session, and a test session performed after a 24-hour (in the subchronic study) or 2-hour (in the acute study) intersession interval. In the familiarisation session, two identical flasks filled with distilled water were placed on an imaginary line along the arena diameter 15 cm away from the wall on opposite ends of the line (in the subchronic study) or 10 cm on opposite ends of an imaginary midline (in the acute study) as depicted in **Figure 2-3**.

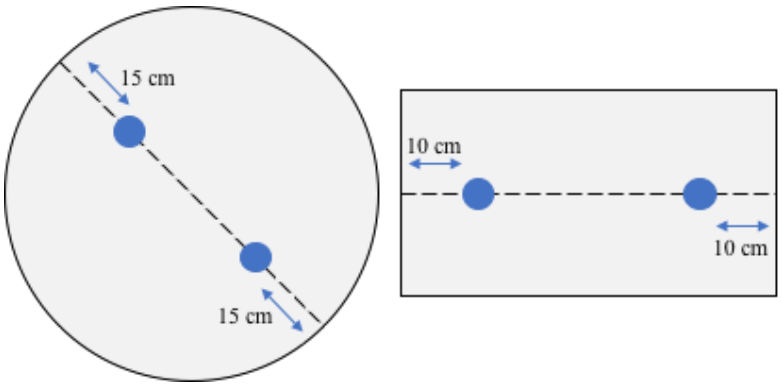

Figure 2-3 Illustration shows the placement of two objects in the arena during NOR test.

On the left, the circular arena used in the subchronic study. On the right, the rectangular arena used in acute treatment. The dotted line represents the imaginary line on which the objects shown in blue are placed.

Each animal was introduced in the centre of the arena between the two objects and with their head facing away from the experimenter. The behaviour was recorded for 10 minutes, and each video saved to an external hard drive. During the test session, one of the identical water-filled flasks was replaced with a Lego® bricks tower in an alternating manner for each consecutive animal (i.e., Flask 1 replaced for Animal 1; Flask 2 replaced for Animal 2, Flask 1 replaced for Animal 3, etc.), and each animal reintroduced to the centre of the arena between the two objects. The behaviour was recorded for 10 minutes, and the video files saved.

Open-Field Test Data Analysis

In the first instance, the obtained video files were prepared for analysis using a semi-automated analysis system that consisted of an ImageJ pre-processing macro and MouseMove software (see Samson *et al.*, 2015 for detailed protocol). In brief, the ImageJ pre-processing macro was used to generate the *x, y* coordinates of each animal in each video, after which the macro exported these coordinates into text files. Each text file was then imported into MouseMove software so that after calibrating the open field spatial and temporal parameters accordingly, the generated analysis results including animal accumulative trajectories were exported. For the NOR test the *x, y* coordinates of the two objects on the imaginary line in the NOR test were recorded, and a 4 cm radius around these objects was set in

MouseMove software and the data regarding objects exploration within the perimeter of these zones were exported to a spreadsheet.

Each of the acquired video files above was reanalysed using EthovisionXT video-tracking software for consistency with future studies. In brief, a new EthovisionXT project file was created, and the number of trials was set correspondingly to the number of videos. Information for each trial, including “Animal ID”; “Cage number”; “Treatment group”; and “Study Day” was tabulated. Each trial was acquired from the previously recorded video files. Data analysis parameters were defined after the acquisition of all trials and output was autogenerated by the software.

For the NOR test only, two arena settings were created: one for the familiarisation session, and one for the test session. Two-centimetre inclusion zones were defined around the objects within the arena. The animal detection settings were selected to recognise the nose of the animal within the perimeter of the defined zones. The time spent within the zones with the nose facing toward the objects was used to calculate the exploration time-based *Discrimination ratio*, which was used as the primary outcome measure to reflect the recognition of a novel object as compared to a familiar one (Bevins and Besheer, 2006).

The data generated using MouseMove and EthovisionXT data were populated in IBM™ SPSS® for statistical analysis. For the locomotor activity

analyses, the statistical test of choice was the Two-Way Mixed Analysis of Variance (ANOVA) with treatment (two levels; Vehicle and PCP) as the between-subject independent variables, and time points (five levels; Baseline, Day 1, Day 4, Day 8, Day 14; or three levels [Baseline, Day 1, and Day 14 for NOR test]) as the within-subjects independent variables were used to test the effect of time, the effect of treatment, and the interaction between them on locomotor activity parameters (e.g., overall mobility, travel distance, etc.). The data in all cells of the design were checked for any significant outliers, and the assumptions of normality and homogeneity of variance were tested. Transformations of data using either the square root or log were performed to meet the assumptions of normality and homogeneity of variance where necessary (Hinton, 2014). The data forms, either original or transformed, which violated the least assumptions were selected for statistical analysis and discussed. In the NOR test, the statistical test of choice was the two-tailed t-test or Mann-Whitney U mean ranks test, depending on data distribution.

All graphs were generated using GraphPad PRISM. Although the locomotor activity data were first generated using MouseMove, only the data generated using EthovisionXT will be discussed.

Motor Coordination Tests

The mice in the acute study were challenged on the horizontal bar and vertical pole to test their motor coordination. The horizontal bar was a wooden ruler 20 cm in length, 1 cm in width, and 0.2 cm in thickness that was secured with Blue Tack between the opposite walls of the animal home cage to form a bridge. The vertical pole was a cylindrical iron funnel stand 60 cm in height and 1 cm in diameter. The pole was wrapped in masking tape for grip support and placed in the centre of the animal home cage during the test. The home cage was cushioned with bubble wrap during the vertical pole test to prevent injury to the animal in case of falling from the top of the pole.

Procedure for the Horizontal Bar test

The mice were held singlehandedly facing toward the experimenter and the base of the tail held between the thumb and the index finger. Each mouse was placed under the centre of the bar and the tail released when all four paws grasped the bar and mouse hang upside-down. Latencies before falling and righting were recorded in a single 3-trial session with 120 seconds for each trial, and a 15-minute interval between each trial, during which the animals were returned to the home cage. If a mouse did not reach the criterion (i.e., did not fall or stand upright), 120 seconds was

entered to the dataset. The best score out of the three trials was retained and used for analysis.

Procedure for the Vertical Pole test

The vertical pole challenge consisted of two variations including climbing and descending. In the first variant, the mice were placed in the middle of the pole with its head facing upward and released when all four paws grasped it. The latencies to reach the top of the pole and the latencies to fall were recorded. In the second variant, the mice were placed near the top of the pole with their head facing upwards and released when all four paws grabbed it. The latencies to climb down the length of the pole, as well as latencies to fall, were recorded.

Both test variations were carried out in a single 3-trial session with a 2-minute trial period, and a 15-minute interval between each trial. If a mouse did not reach the criterion (i.e., did not reach the top or did not fall), 120 seconds was tallied. As previously, the best score out of the three trials was retained and used for analysis.

Motor Coordination Data Analysis

The data were populated in GraphPad PRISM for data analysis. The statistical test of choice was the two-tailed unpaired t-test or Mann-Whitney U mean ranks test, depending on data distribution.

2.1.4 **Brain dissection**

All animals were culled by cervical dislocation after the last behavioural test. The head was detached from the body using scissors, and the skull exposed with a midline incision to the skin using a scalpel blade and pulled laterally. The brain was exposed by making an incision along the midline from the caudal part of the intraparietal bone and removing the bones using small surgical forceps after subsequent mediolateral cuts to the anterior part of the frontal bones. The cranial nerves were severed with a small spatula as the brain was scooped out onto a pre-chilled dissection platform lined with filter paper and pre-frozen PBS slurry. The platform was an iron-free metal block that was half-submerged in an icy water bath.

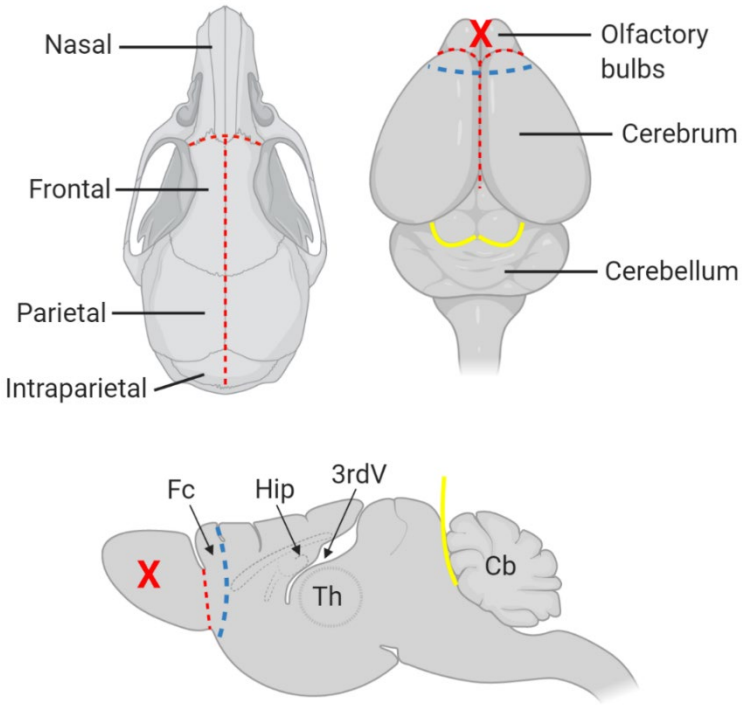

Figure 2-4 Illustration showing the location of incisions in brain dissection.
Top left depicts mouse skull and top right depicts a mouse brain with incision shown in red dotted lines. Incision line for frontal cortex is shown in blue. The yellow line shows the spatula location for separating the cerebellum. The bottom image shows the midsagittal view. Abbreviations: Fc, frontal cortex; Hip, hippocampus; Th, thalamus; Cb, cerebellum; 3rdV, third ventricle. Graphic generated using bioRENDER.

Collection of Tissue Samples

For western blotting and PCR, the samples were collected into Eppendorf tubes and either transported on ice for immediate processing or snap-frozen on dry ice. In brief, the olfactory bulbs were removed and discarded. The frontal cortex was collected from the anterior 2 mm of the cerebrum by a cut with a ten-degree angle to the coronal section tilting anteriorly. The cerebellar peduncles were transected by inserting a small spatula between the cerebellum and the brainstem to detach the cerebellum. The two

cerebral hemispheres were separated with a single cut along the midline. On each cerebral hemisphere, the thalamus and hypothalamus were dissected out together by inserting the edge of a small spatula into the opening of the third ventricle. The connected hypothalamus was separated by incising the mammillothalamic tract and discarded. After the thalamus and hypothalamus were removed, the hippocampus was disconnected from the cortex with a spatula.

Preparation of Frozen Tissue Blocks.

This procedure was performed in preparation for later tissue cryosectioning. The cerebrum and the cerebellum were dissected as described in the previous section. The lateral hemispheres of the cerebellum were then dissected by making a midsagittal cut on each side of the vermis, approximately 1.5 mm laterally from the midline. Each cerebellar region and each cerebral hemisphere were placed in an individual freezing mould with the cross-section facing down. The mould, which was half-filled with Scigen O.C.T. compound cryostat embedding medium (23-730-625; Fisher Scientific, UK) was immediately submerged in an LN_2-filled dewar using a custom-made holder for approximately 30 seconds or until the LN_2 ceased to boil whilst making sure the LN_2 did not enter the mould. The blocks were transported on dry ice to -80°C freezer for storage.

2.2 Nucleic Acid and Protein Extraction

2.2.1 Protein Extraction

Freshly dissected tissue samples including cerebellum, frontal cortex, thalamus, and hippocampus were homogenised with 1 mL Trizol reagent (15596026; Fisher Scientific, UK) per region in 1.5 mL centrifuge tubes using a cordless motor (Kimble, USA) and reusable pellet pestles (Z359947; Merck, UK). The tubes of homogenate were left to incubate at RT for 5 minutes to allow complete dissociation of nucleoprotein complexes, and a 0.2 mL of chloroform was added. The tubes were secured and inverted gently for 15 seconds after which they were incubated for 3 minutes at RT to allow the precipitate to form. The samples were then centrifuged at 14,000 x *g* for 15 minutes in a Sorvall Legend Micro 17R temperature-controlled centrifuge (Thermo Scientific, UK) pre-set to 4°C. The phase separation resulted in the formation of three layers containing RNA, DNA, and organic compounds as illustrated in **Figure 2-5**.

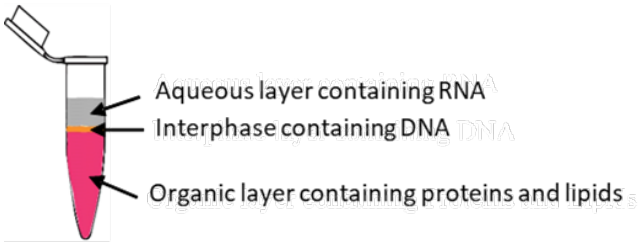

Figure 2-5 Illustration of Trizol® phase-separated layers.

2.2.2 RNA Isolation and Purification

After the phase separation, 0.3 mL of the aqueous layer was transferred each into an RNase-free tube on ice, and 0.5 mL of isopropanol was added to the tube and incubated on ice for 10 minutes, then centrifuged at 12,000 x *g* for 10 minutes at 4°C. The tubes containing the aqueous layer and isopropanol were inspected to ensure the RNA pellet was formed, and the supernatant was carefully discarded into a waste container and the excess blotted onto a tissue. The RNA pellets were washed with 1 mL of 75% *v/v* ethanol in their tubes using a bench-top vortex and centrifuged at 7,500 x *g* for 5 minutes at 4°C. The supernatant was discarded, and the ethanol wash repeated twice. The RNA pellets were dissolved in 0.5 mL of DEPC-treated water, and each assessed for purity and RNA concentration using NanoDrop Lite™ (ThermoFisher Scientific, USA) spectrophotometer. In brief, the machine was calibrated using DEPC-treated H_2O before each reading. A 1 µL sample was applied to the machine for estimation. A reading of $A_{260/280}$ between 1.8 and 2.1 indicates RNA purity acceptable for most applications. The RNA concentration of each sample was noted, and samples diluted to a working concentration of 100 ng/µL with DEPC-treated water.

2.2.3 DNA Precipitation

Any remnants of the aqueous phase overlying the interphase from the Trizol separation were removed and 0.3 mL of 100% ethanol was added to each tube and incubated for 3 minutes at RT. The samples were then centrifuged at 2000 x *g* for 10 minutes at 4°C to pellet the DNA. The phenol-ethanol supernatant was transferred into a fresh 2.0 mL tube for protein isolation and the DNA pellet was stored in 100% ethanol at -80°C.

2.2.4 Protein Precipitation and Solubilisation

Proteins were precipitated and solubilised using a modified protocol as described by Kopec et al. (Kopec et al., 2017); a 1.5 mL of isopropanol was added to the protein-containing phenol-ethanol supernatant and incubated for 10 minutes at RT, then centrifuged at 12,000 x *g* for 10 minutes at 4°C to pellet the proteins, and the supernatant discarded. The protein pellet was dislodged in 250 µl 95% ethanol by probing the pellet with a sterile pipette tip and mixing the contents gently. The samples were centrifuged for 5 minutes at 7600 x *g* at 4°C, and the supernatant discarded. Additional wash with 250 µL of 95% ethanol was performed as above. After decanting, the protein pellet was air-dried for 10 minutes. The dry pellets were dislodged in 100 µL of optimised lysis buffer (20 mM EDTA, 140 mM NaCl, 5% SDS) supplemented with 1 mM activated NaOv form Santa Cruz RIPA lysis buffer

system (sc-24948; Santa Cruz Biotechnology, USA), and Roche cOMPLETE™ ULTRA protease inhibitor cocktail (5892970001; Merck, UK). The tubes with the dislodged protein samples were closed and secured with office tape to prevent popping open and placed on a heating block. The samples were incubated for a minimum 30 minutes at 100°C to ensure complete solubilisation of proteins. The protein samples were allowed to reach RT for 5 minutes before estimating the protein concentrations.

2.2.5 Estimation of Total Protein Concentrations

Protein samples of known concentrations were prepared by dissolving bovine serum albumin (BSA) in distilled water, in a range of concentrations from 0.0 – 1.0 mg/mL at increments of 0.1 mg/mL, and 1.5 mg/mL. Five microlitres of these protein samples were then loaded onto a 96-well plate in triplicates, and 150 µL of Bradford reagent (10495315; Fisher Scientific, UK) was added to each sample well. Each plate was swirled gently and allowed to incubate for 10 minutes at RT. The optical density for each well was measured at 595 nm wavelength using a uQuant™ microplate reader (BioTek, USA). The obtained absorbance values were used to generate the plot shown in **Figure 2-6**. The graph equation $y = mx + c$ was used to determine the concentrations of the test samples.

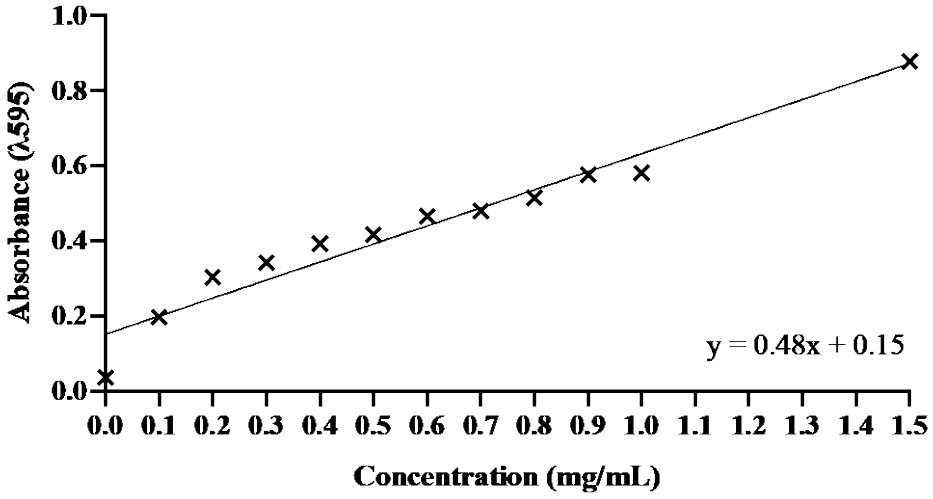

Figure 2-6 Simple linear regression of BSA absorbance at 595 nm wavelength.
The protein samples were measured at concentrations 0.0 – 1.0 mg/ mL at 0.1 increments, and 1.5 mg/mL.

2.3 Western blot

2.3.1 Overview

Western blot is one of the most ubiquitously used protocols in biomolecular science research. It is a valuable tool for qualitative assessment of single proteins and post-translational protein modifications, and with recent technological advancements in detection methods, western blot transformed as a popular semi-quantitative tool for investigating changes in protein expression (Lee, 2007b). The technique utilises gel electrophoresis to separate a complex mixture of protein in a sample, which are then transferred to and immobilised on a membrane. The membrane is then probed with primary antibodies that are specific to the target antigen, and horseradish peroxidase (HRP)-conjugated secondary antibodies that specifically detect the primary antibodies. These antibodies are then visualised using specialised equipment after addition of chemiluminescence reagent, as illustrated in the general workflow in **Figure 2-7**. A western blot sample is prepared by mixing a protein sample with a detergent, such as sodium dodecyl sulphate (SDS) which denatures the three-dimensional structure of the protein into a primary strand. The SDS is a negatively charged molecule with a 12-carbon tail that is esterified to a sulphate group. The SDS binds to positively charged groups of denatured proteins strand and thus covers them with net-negative charges and confers the proteins

negative charges in a charge-to-mass ratio to allow proteins with different molecular weight to be separated with the current during gel electrophoresis. After the proteins are separated on a gel, they are transferred onto a membrane, such as the nitrocellulose membrane used in this work.

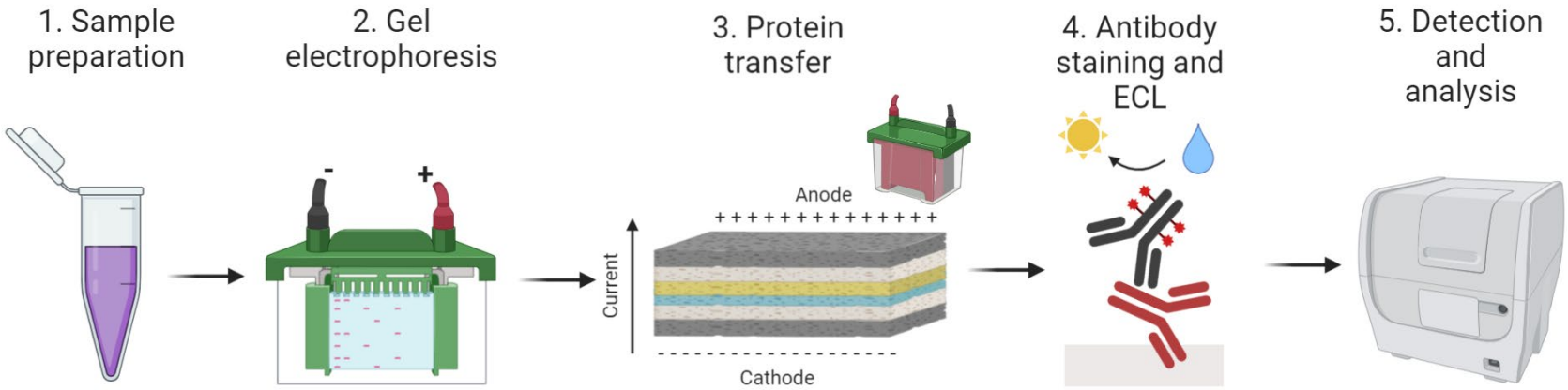

Figure 2-7 General western blot workflow.

1. The extracted protein sample is mixed with electrophoresis buffer containing SDS and boiled; 2. The sample is loaded onto a polyacrylamide gel and resolved in an electrophoresis tank; 3. The resolved gel is arranged in a transfer cassette (from cathode: sponge, filter paper, gel, membrane, filter paper, sponge), which is then placed in a transfer module within the electrophoresis tank and current applied to facilitate transfer from membrane onto the gel; 4. The membrane is incubated with blocking buffer, primary antibody, HRP-conjugated secondary antibody, and a solution of luminol and hydrogen peroxide to enable detection; 5. The membrane is placed in a detection chamber equipped with a camera to capture the light emitted from the membrane-bound proteins.

During this stage, the gel and the membrane are ‘sandwiched’ so that the current flow can carry the net negatively charged proteins toward the anode, during which they are trapped within the pores of the membrane and immobilised. After the transfer is complete, the membranes are inspected for transfer quality by applying a temporary dye, such as Ponceau S for the success of transfer and artefacts such as potential air bubbles. However, it does not allow to assess transfer efficiency (i.e., how much protein has transferred from the gel onto the membrane). This may be especially important when investigating low abundance proteins of high molecular weight (M.W.) as those proteins transfer at a lower rate compared to low M.W. proteins and therefore may require more time or a higher voltage to fully migrate from the gel onto a membrane. Transferred gels can be stained with protein stains such as Coomassie blue, although this requires additional labour, which might not be ideal in a research-intensive setting. Recently, a stain-free technology has been developed and proved to be a superior method to traditional staining (Rivero-Gutiérrez et al., 2014). Stain-free gels contain a trihalo compound within the gel moiety that covalently binds tryptophan residues as the proteins migrate down the gel, and after the gel is exposed to ultraviolet light, the tryptophan-trihalo adduct emits fluorescence and enables the detection of proteins without the use of stains (**Figure 2-8**). Moreover, the proteins continue to emit fluorescence

after transfer which allows ensuring transfer quality without Ponceau S staining, and stain-free images of the total protein content in each lane can be used to quantify the amount of protein in each lane.

After the proteins transferred successfully, the membrane is incubated with a blocking solution such as tris-buffered saline containing either non-fat milk or BSA, which is used to minimise non-specific binding. Following the blocking step, the blocking solution is replaced with the solution containing diluted primary antibody that is specific to the target antigen, and the membrane is incubated with the antibody usually overnight at 4°C or 1 - 2h at RT to allow maximal antibody-antigen binding. After the primary antibody incubation, the membrane is treated with a secondary antibody that is conjugated to a reporter enzyme horseradish peroxidase (HRP). After the secondary antibody incubation, the membrane is treated with a luminol solution in peroxide, where the HRP enzyme catalyses a photogenic reaction at the secondary antibody binding site and the emitted light can be captured using a chemiluminescent imager (Kurien and Scofield, 2006).

Since the amount of total protein loaded onto each lane in the gel cannot be precisely controlled, it must be normalised to a form of control. A loading control has traditionally been one of the structural proteins, whose expression was assumed to remain constant regardless of treatment, such

as β-actin, tubulin, or glyceraldehyde 3-phosphate dehydrogenase (GAPDH). However, it has been shown that some experimental conditions can affect the amount of this protein in the cell (Colella et al., 2012), and this poses a risk of collecting inaccurate data. A total amount of protein in each lane is a far superior control for normalisation to the traditional approaches (Gilda and Gomes, 2013; Rivero-Gutiérrez et al., 2014). Therefore, the use of structural protein in this thesis was eventually discontinued in favour of total protein contents calculated from stain-free blot images.

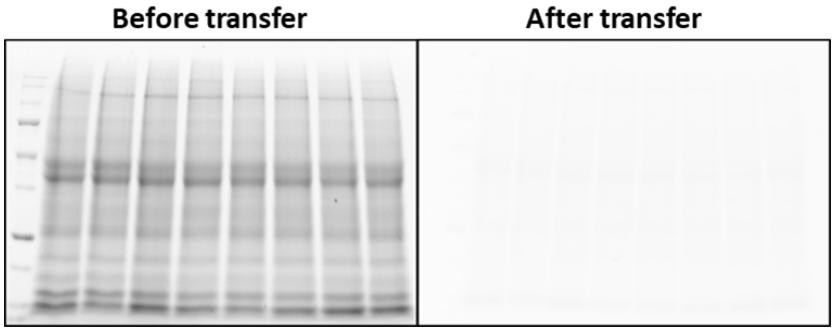

Figure 2-8 Resolved proteins on a stain-free polyacrylamide gel.
The figure shows images of the same polyacrylamide gel taken before and after protein transfer. The image on the left shows fully resolved samples in each lane. The image on the right shows the only negligible amount of protein left on the membrane after transfer.

2.3.2 Electrophoresis sample preparation

The previously protein solubilised protein samples were mixed with an equal volume of electrophoresis sample buffer (sc-286962; Santa Cruz Biotechnologies, USA) and heated in a water bath at 95°C for 10 minutes.

The samples were then either used immediately or made aliquots were stored at -20°C for future use.

2.3.3 Preparation of Solutions

- Running buffer (25 mM Tris, 192 mM glycine, 3.5 mM SDS) was prepared by dissolving 3.03 g Trizma®, 14.4 g glycine, and 1 g SDS in 800 mL dH_2O, and the volume adjusted to 1000 mL.
- Transfer buffer (48 mM Tris, 39 mM, 20% Methanol) was prepared by dissolving 5.82 g Trizma® and 2.93 g glycine in 200 mL methanol and volume adjusted to 1000 mL with dH_2O.
- Tris-buffered saline (20 mM Tris, 151 mM, pH 7.4) supplemented with 0.1% Tween (TBST) was prepared by dissolving 2.4 g Trizma® and 8.8 g NaCl in 800 mL dH_2O and mixing 1 mL of Tween®20 (T2700-500ML; Merck, UK), and the volume adjusted to 1000 mL.

2.3.4 SDS-PAGE

The boiled electrophoresis samples were allowed to reach RT for 5 minutes before loading the gels, or the frozen electrophoresis samples were briefly heated at 95°C for 2 minutes before the procedure. The samples were resolved using a Bio-Rad Mini-PROTEAN® tank on 12% Mini-PROTEAN® TGX™ Stain-free™ Precast Protein Gels (4568046; Bio-Rad, UK) in running buffer. The gel cassettes were assembled in the tank and approximately

800 mL of the running buffer was poured over the cassettes. The assembly was checked for leakages, and each gel loaded with 5 µL of Precision Plus Protein™ Kaleidoscope™ Standards (1610375; Bio-Rad, UK) in the first lane, 10 µL of sample buffer only as a negative control in the last lane, and 10 µg of sample protein in each of the remaining wells, making sure that test and control samples were loaded on the same gel. The tank was then assembled with the lid and electrodes, and resolved for 15 minutes at 150 V, followed by an additional 45-60 minutes at 130 V using a Bio-Rad power pack.

2.3.5 **Stain-free imaging**

The cassettes were opened, and the resolved gels placed in a tray with dH_2O. The gels were imaged on a stain-free imaging tray using a Bio-Rad Gel-doc™ EZ® connected to a Windows PC equipped with ImagLab™ software. In brief, a new protocol was created selecting the “Stain-free” option in the ImageLab software. The gels were then activated for 5 minutes each and exposed to UV light for 0.9-1.5 seconds, making sure the images produced were not over-exposed. The exposure times were used to image the gels at the same exposure times after protein transfer.

2.3.6 **Protein transfer**

The proteins on the resolved gels were transferred onto a GE Healthcare Amersham™ Protran™ nitrocellulose membrane (15209804; Fishers Scientific, UK) using a Bio-Rad Mini-PROTEAN® tank, assembled with a Mini Trans-Blot® transfer module. Each component of the transfer sandwich; two fibre pads, two sheets of filter paper and a piece of nitrocellulose membrane were soaked in refrigerated transfer buffer. The sandwich cassette was placed on a tray with its black portion facing down and layered with fibre pad; filter paper; nitrocellulose membrane; stain-free gel; filter paper; and fibre pad. Any air bubbles that have formed within the sandwich were expelled using a roller. The cassettes were installed into the transfer module and placed in the tank. Pre-frozen ice pack was placed in the tank and the refrigerated transfer buffer was poured over the modules until near-fully submerged making sure that the buffer does not reach the electrodes on the transfer module. To further minimise overheating, the tank was placed inside a polystyrene box filled with icy water. The lid with the power cables was attached to the tank, and the system was left to run for 60 minutes at 100 V. After the transfer was completed, the stain-free images of the gels were taken at the same exposure times as before the transfer. Stain-free images of the blotted membranes were also taken and inspected for artefacts and used later in immunostaining analysis.

2.3.7 Immunostaining

Each membrane was placed in a staining cassette and blocked in 5 mL TBST containing 5% *w/v* protease-free BSA (11423164; Fisher Scientific, UK) or 5% *w/*v skim milk powder (70166; Merck, UK) in TBST for 1h at RT on a shaker. The blocking solution was then replaced with 5 mL solution containing primary antibodies shown in **Table 2-1**, and the membrane incubated overnight at 4ºC on a shaker in a cold room. The following day each membrane was washed 3 times in TBST for 5 minutes each at RT. The membranes were then incubated in 5 mL solution containing HRP-conjugated secondary antibodies shown in **Table 2-1** for 2h at RT on a shaker.

Table 2-1 Antibodies used in western blotting.

Antibody	Host/type	Dilution	Reference / Supplier
Kv2.1	Mouse	1:500	75-014, Antibodies Inc.
Kv6.4	Rabbit	1:500	ab155772, abcam
anti-Mouse HRP	Goat IgG	1:2000	sc-2005, Santa Cruz
anti-Mouse HRP	Goat IgG	1:2000	ab205719, abcam
anti-Rabbit HRP	Goat IgG	1:2000	sc-2004, Santa Cruz
anti-Rabbit HRP	Goat IgG	1:2000	ab205718, abcam

2.3.8 **Blot Imaging and Analysis**

The membranes were washed three times for 5 minutes each time in TBST. Enhanced chemiluminescence (ECL) reagent was freshly prepared during the final wash by mixing equal volumes of solution A (luminol solution) and solution B (peroxide solution) of the Clarity™ Western ECL Substrate (170-5061; Bio-Rad, UK) with a minimum final volume of 1 mL per 125 mm^2 of the membrane. The membranes were incubated in the detection reagent for 3-5 minutes at RT on a rocking platform, after which they were sealed in a plastic cling film to prevent drying. The images were obtained with GeneGnomeXRQ (Syngene, USA) chemiluminescence imaging system connected to a Windows PC. The obtained images were quantified using ImageJ (NIH, USA). The data was populated in GraphPad PRISM for analysis. The statistical test of choice was the two-tailed t-test or the Mann-Whitney U test of mean ranks, depending on data distribution.

2.4 Immunohistochemistry

2.4.1 Overview

Immunohistochemistry, like western blotting, uses the antibody-antigen binding principle to target specific proteins. However, where protein blots seek a protein in a complex sample, immunohistochemistry allows detecting a target protein in a tissue section preserving most of the cytoarchitecture. Therefore, the investigation is extended to cellular and subcellular localisations of such proteins. In preparation for immunohistochemistry, the tissues are collected fresh and snap frozen as blocks. The frozen blocks are then sectioned using a cryostat microtome to the desired thickness and, as in this work, are collected onto glass slides coated with poly-L-lysine that promotes adhesion of the tissue to the slide by attracting negatively charged amino acids (Katchalski, Grossfeld and Frankel, 1947; Yavin and Yavin, 1974). Alternatively, 'floating sections' might be collected into welled plates. The sections are then treated with a fixative, such as paraformaldehyde. Fixation might be also performed *in vivo* by perfusing a deeply anaesthetised animal before the collection of tissues. Paraformaldehyde reacts with a wide range of functional groups forming intermolecular and intramolecular cross-linked species; thus, preserving and stabilising the tissue morphology from decomposition by inactivating proteolytic enzymes and protecting the samples from infection. Fixation also

strengthens the sample to prevent damage from mechanical stress to which the samples are exposed to during immunohistochemistry procedure. A variety of fixation methods were developed (**Table 2-2**), and the usability of each depends on the type of the sought-after target and tissue it originated.

Table 2-2 Common fixatives and their target antigens.

Sample Type or Antigen	Fixative
Most proteins, peptides, and enzymes of low M.W.	4% *w/v* paraformaldehyde (PFA) 4% *w/v* PFA-1% *w/v* glutaraldehyde 10% neutral-buffered formalin
Delicate tissues	Bouin's fixative
Small molecules (i.e., amino acids)	4% *w/v* PFA-1% *w/v* glutaraldehyde
Blood-forming organs (i.e., spleen, liver, bone marrow); connective tissue	Zenker's solution Helly's solution
Nucleic acids	Carnoy's solution
Large protein antigens (i.e., immunoglobulins)	100% ice-cold methanol 100% ice-cold acetone
Ideal for electron microscopy	4% *w/v* PFA-1% *w/v* glutaraldehyde 1% *w/v* osmium tetroxide

Adapted from ThermoFisher Scientific.

The molecular crosslinks formed by paraformaldehyde often mask the antigenic epitopes on the tissues thus preventing the antibodies from recognising and binding to the target antigen (Hoffman et al., 2015), hence antigen epitope retrieval may be necessary. The retrieval involves

incubating the fixed sections in acidic buffers at high temperatures, as used in this work, or by treating the fixed sections with solutions containing digestive enzymes. This allows for enough of the crosslinks to break and expose the epitopes, allowing them to be recognised by the antibodies (Scalia et al., 2017). Once the tissue sections are fixed and antigen-retrieved they must be layered and incubated with a blocking solution to prevent any potential non-specific antibody binding. The blocking solution this work contained BSA and normal goat serum in phosphate-buffered saline. The serum must be derived from the animal species the secondary antibody was raised as opposed to the animal species of the primary antibody. If done otherwise, the secondary antibody would also detect the non-specifically bound serum antibodies on the tissue resulting in unwanted background signal. It is also important to consider whether the target antigen is located extracellularly or intracellularly. Antibodies do not readily diffuse across the cell membrane, thus a detergent such as Triton X-100 used in this work must be included in the blocking solution to permeabilise the membrane. Once the sections are blocked and permeabilised, the blocking solution is replaced with primary antibodies diluted in the blocking buffer and incubated at the optimal conditions for the specific antibody used, which is determined experimentally (e.g., overnight at 4ºC). The slides are then washed and layered with a solution containing diluted secondary antibodies that are conjugated to a fluorophore and counter-stained with a

nuclear dye (Ramos-Vara, 2017). Imaging involves the use of a microscope equipped with a specialised light source that provides intense, near-monochromatic illumination. A specific filter cube allows the fluorophore-conjugated to the secondary antibody to be excited at a specific wavelength, which in turn emits light at a longer wavelength to be captured by the attached camera. More advanced imaging involves the use of a laser-scanning confocal microscope (LSCM) that instead of a typical light source, the LSCM is equipped with a high-powered laser and scanning mirrors which allow capturing a series of images that can be reconstructed into a three-dimensional model (**Figure 2-9**).

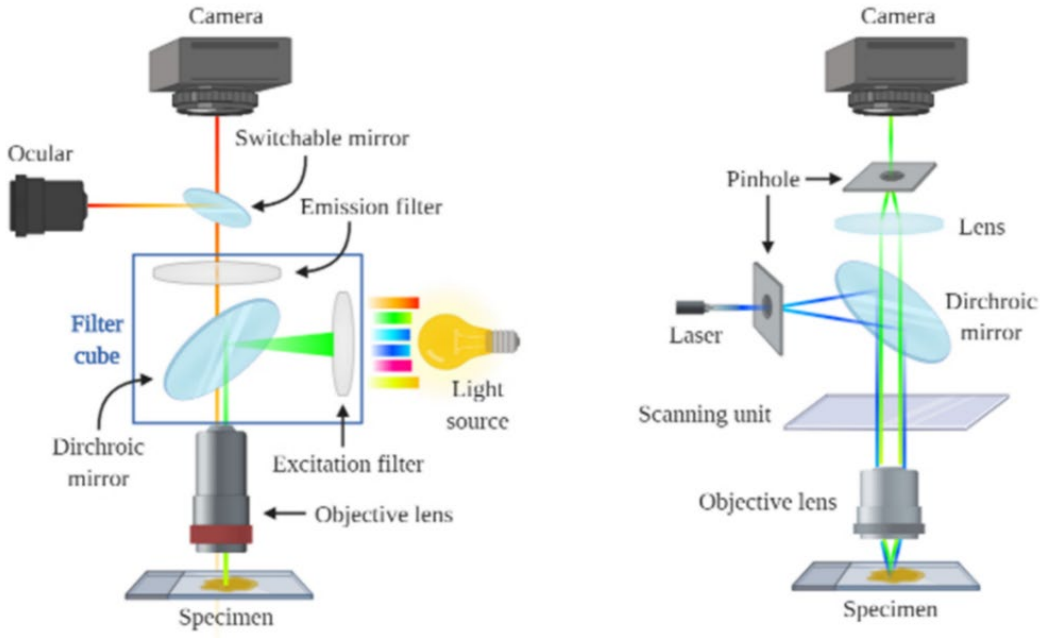

Figure 2-9 Comparison of key components of fluorescence (left) and a confocal microscope (right).

2.4.2 Preparation of frozen sections

The fresh-frozen tissue blocks were sectioned using OTF5000 series cryostat (Bright Instruments, UK). The chamber temperature was set to -14°C the night before and the specimen mount temperature was set to and -12°C. The tissue blocks were transferred from -80°C storage and allowed approximately 30 minutes inside the cryostat chamber for the block to equilibrate with the chamber temperature and were subsequently mounted onto the cutting chuck using OCT medium. The cryostat blade cutting angle was set to 15° from the vertical plane, tilting toward the tissue block. The tissue blocks were trimmed at 20 µm until the entire tissue was visible. Subsequent 12-, 20-, and 40-micron cerebellar sagittal sections were collected onto poly-*L*-lysine-coated microscope slides (10219280; Fisher Scientific, UK). Approximately every 15th collected section was rapidly stained with haematoxylin to ensure the correct slice position and satisfactory tissue morphology. The tissues were either proceeded with immunofluorescence or stored at -20ºC for future use.

2.4.3 Preparation of Solutions

- Phosphate-buffered saline (137 mM NaCl, 10 mM H_3PO_4, 2.7 mM KCl, pH 7.4) was prepared by dissolving 1 Oxoid™ Phosphate Buffered Saline Tablet (BR0014G; Fisher Scientific, UK) in every 100 mL of ddH_2O.

- Paraformaldehyde solution (4%) was prepared by heating 800 mL PBS to 50ºC in a beaker in a fume hood and adding 40 g of PFA powder (158127; Sigma, UK). The milky PFA solution was stirred ensuring the temperature did not exceed 60ºC. Small aliquots of 5M NaOH was added to the solution using a disposable pipette until the PFA solution cleared, and the beaker was left aside to reach RT. The PFA solution volume was then adjusted to 1000 mL with PBS and pH adjusted to 6.9. The solution was chilled to 4ºC and used immediately, or 50 mL aliquots were made in plastic tubes and stored at -20ºC.
- Citrate buffer (10 mM) was prepared by dissolving 1.92 g citric acid in 800 mL ddH_2O and stirred. The pH was adjusted to 6.0 and ddH_2O added to a final volume of 1000 mL.
- PBS supplemented with 0.1% Triton (PBST) was prepared by mixing 1 mL of Triton™ X-100 (9002-93-1; Fisher Scientific, UK) in 1000 mL PBS.
- BSA stock (10% *w/v*) was prepared by mixing 1 g of BSA powder in 10 mL PBST. Made aliquots were stored at -20ºC for future use.
- Blocking solution was prepared by mixing 600 µL PBST, 200 µL 10% BSA, 200 µL normal goat serum (S-100; Vector Labs, UK) per each 1mL solution.
- DAPI counterstain (300 nM) was prepared by diluting 4 µL DAPI (D1306; ThermoFisher Scientific, UK) in 150 mL PBS in a Duran bottle and shaken vigorously.

2.4.4 Tissue Fixation and Antigen Retrieval

In a fume hood, 150 mL of ice-cold 4% PFA was poured into a slide box and the slides placed inside in a slide rack. The box was secured with a lid and placed in the refrigerator to incubate for 10 minutes at 4ºC. After the incubation, the slide rack was moved into a new box and the used PFA discarded into a non-chlorinated waste container. The slides were then washed 3 times in fresh PBS for 10 minutes each time at RT on a shaker. Antigenic epitopes were retrieved for all primary antibodies. In a fume hood, 500 mL citrate buffer was heated in a beaker to 95°C on a hot plate. After the final PBS wash, the rack with slides was placed vertically in the beaker with citrate buffer, ensuring the tissue faced upwards to prevent potential damage to the tissues by rising water vapour bubbles during heat treatment. The beaker was covered with aluminium foil and the temperature maintained at 95-100°C for 20 minutes. The beaker was then placed in the sink with running tap water and allowed to cool down to ~70°C. The citrate buffer was discarded into a waste non-chlorinated waste container and the rack with slides was washed in PBS 3 times for 5 minutes each time on a shaker at RT.

2.4.5 Immunostaining

The tissue sections were blocked against non-specific binding in blocking solution. The excess PBS was blotted off the slides on to a tissue and two

parallel lines were drawn with ImmEdge® pen (H-1400; Vector Labs, UK) perpendicularly to both edges of the glass slide, enclosing the tissue section within a hydrophobic barrier around 1cm in width. The slides were placed in a ddH_2O-flooded humidity chamber and each slide layered with 200 µL of blocking solution within the drawn enclosure. The chamber was assembled with the lid and the slides were incubated in the chamber for 2h at RT. The primary antibodies were diluted in the blocking solution and the blocked slides were blotted off onto a tissue. The slides were layered with 200 µL diluted primary antibody solution and incubated. The slides were then washed 3 times in PBS for 20 minutes each time at RT on a shaker. The secondary antibodies were diluted in blocking solution in minimal lighting condition to prevent potential photo-bleaching. The excess PBS was blotted off the washed slides were on to a tissue and the slides were layered with 200 µL of secondary antibody solution. Antibodies used in the study as well as their incubation times are listed in **Table 2-3**.

Following secondary antibody incubation, the excess antibody solution was blotted off the slides on to a tissue and the slides were washed 3 times in PBS for 20 minutes each time. After the final wash, the slides were washed in a solution containing DAPI counterstain for 5 minutes. The slides were then washed 3 times in PBS for 5 minutes each time. After the final wash, the excess wash solution was blotted off the slides and the slides dried around the tissue sections with blotting paper. The slides were

mounted with coverslips using either VECTASHIELD® HardSet™ Antifade Mounting Medium (H-1400; Vector Laboratories, UK) or VECTASHIELD® Antifade Mounting Medium (H-1000; Vector Laboratories, UK; The glass coverslips were placed on a blotting paper and 20 µL mounting medium was pipetted in the centre of each slip. Each slide was placed on a coverslip with the tissue portion facing down and pressed down to expel the excess mounting medium and. The mounted slides were then cleaned around the coverslip and sealed using clear nail varnish.

Table 2-3 Antibodies used in histochemistry work.

Antibody	Host	Reference/Source	Dilution/Conditions
Kv2.1	Mouse	75-014, Antibodies Inc.	1:1000; ON at 4°C
Kv6.4	Rabbit	ab155772, Abcam	1:500; ON at 4°C
Calbindin D28K	Rabbit	ab11426, Abcam	1:500; 48h at 4°C
Kv3.1b	Rabbit	APC-014, Alomone	1:500; ON at 4°C
anti-Mouse AF*488	Goat	A-11001, Life Sciences	1:1000; 2h at RT
anti-Rabbit AF 488	Goat	A-11008, Life Sciences	1:2000; 2h at RT
anti-Rabbit AF 555	Goat	A-21428, Life Sciences	1:1000; 2h at RT

ON, overnight; *AF, Alexa Fluor®; RT, room temperature.

2.4.6 Fluorescence Microscopy

Microscopy was completed using Leica fluorescence imaging system which consisted of a Leica DM2000 fluorescence microscope equipped with a Leica DFC365 FX camera that was connected to a Windows PC, and the micrographs were taken with x4, x40, and x40 (or 100x oil-immersion lens) and saved in Leica LAS X software. Micrographs were taken at constant brightness and exposure time for each blue, green, and red channel for each objective lens to maintain comparability between the captured images.

2.4.7 Laser-scanning Confocal Microscopy

Confocal microscopy was undertaken at the Advanced Imaging Facility (University of Leicester) with the support of Dr Kees Straatman. The acquisition of images was performed using an Olympus FV1000 confocal laser scanning system with an inverted IX81 motorised microscope equipped with 60×/1.35NA objective (Olympus).

2.4.8 Quantification of Fluorescent Signal

The fluorescent signal was quantified using ImageJ. The images were imported into ImageJ by dragging the image into the software interface. Region of interest (ROI) manager was opened from the “Analyze” → “Tools” menu. Areas of interest (i.e., Purkinje cells, granular cell layer regions) were selected using the selection tools (i.e., freeform, or

rectangular). A rectangular selection of background was selected in 10 different areas. The selected areas of interest and background were added to the ROI manager by clicking ‘add’ on the ROI manager window. From the “Analyze” menu, measurements were set to include the “integrated intensity” and “mean grey value,” and the measurements taken by choosing the “Measure” option in the “Analyze” menu. A new pop-up window opened with the measurements of the selected regions. The values were copied to a spreadsheet and average *mean grey value* was calculated from all background readings. The corrected total cell fluorescence (CTCF) was calculated using the formula:

$CTCF - ID\ (CELL\ AREA\ \times BACKGROUND\ MGV,$ where:

ID = integrated density; MGV = average mean grey value

The CTCF values were calculated for all collected images and populated in IBM SPSS and GraphPad PRISM. The statistical test of choice to compare the control and treated samples was the two-tailed unpaired t-test or Mann-Whitney U test of mean ranks, depending on data distribution.

2.5 Reverse-Transcription Quantitative Real-Time PCR

2.5.1 Overview

Quantitative real-time polymerase-chain-reaction (qPCR) is a major advancement of the PCR technique that enables consistent detection and measurements of gene products. Unlike other variants of the PCR technique, qPCR incorporates spectrofluorometry to detect the increase in the amount of DNA by measuring the proportional increase in the intensity of fluorescent signal after each PCR cycle. This obviates the need for gel electrophoresis or post-PCR sample handling, and therefore it minimises the possibility of sample contamination and increases the efficiency of high throughput (Bustin et al., 2005). The reverse-transcription qPCR (RT-qPCR) assay typically involves two steps:

1. Revers-transcription of RNA into their complementary DNA (cDNA) strands, which form a template for the PCR assay.
2. Simultaneous amplification of the cDNA using PCR and detection of PCR products and its quantitation in real-time.

The reverse transcription is, quite literally, the opposite of the normal cellular transcription of the DNA into RNA. The cDNA strand is produced from an RNA template using reverse-transcriptase enzymes that utilise this

template and random primers complementary to the 3'-end of the RNA to direct the synthesis of cDNA. The reverse-transcription components which include the reaction buffer, deoxyribonucleotide-triphosphates (dNTPs), the RNA template, the reverse transcriptase enzyme, and random primers are combined in a test tube and the reaction is catalysed in a typical thermocycler. The reaction mixture is first heated to 25°C for 5 minutes, which activates the reverse transcriptase enzyme and allows the random primers to anneal to the RNA strands. The mixture is then heated further to 37°C for two hours, where the enzymes reverse-transcribe the primed RNA strands into their cDNA strands. After the cycle is complete, the sample is heated to 85°C to deactivate the RT enzyme which terminates the reaction (Jalali, Zaborowska and Jalali, 2017). The produced cDNA template is then used in a separate reaction, where the genetic material is amplified and quantified in real-time. The amplification and quantitation are carried out in a specialised thermocycler equipped with a spectrofluorometer that measures the fluorescent signal of a dye after each PCR cycle. A single qPCR run includes 40 PCR cycles which involve three main stages:

1. Denaturation stage, where the sample is heated to 95°C to break apart hydrogen bonds and to activate the polymerase enzyme.
2. Annealing stage, where the mixture is cooled to between 40-65°C to allow the specific forward and reverse primers to hybridise complementary pairing on the opposite sides of the DNA strand.

3. Extension stage, where the sample is heated toward the optimal temperature for the polymerase enzyme to bind to the primer-template complex and assemble a new cDNA strand using the dNTPs contained in the mixture.

After each cycle, the copied sequence forms a double-stranded helix which binds the reporter dye, and its fluorescence is measured at the end of each cycle, (i.e., in real-time). The amount of fluorescence is directly proportional to the amount of newly synthesised DNA (**Figure 2-10**).

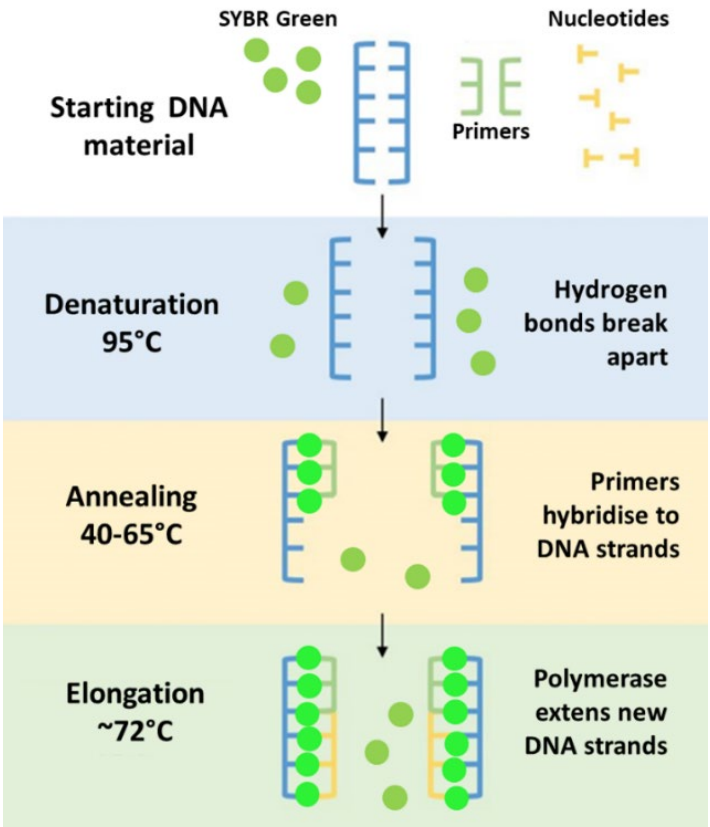

Figure 2-10 Illustration shows the three stages in a qPCR cycle.

The reporter dye is floating freely in the reaction mixture and only emits low levels of fluorescence. As a new DNA strand is synthesised the dye binds to the newly formed double-stranded helix and gets excited, which causes it to fluoresce.

Because the reporter dye SYBR green binds to any double-stranded DNA, including artefacts such as primer-dimers, the primers must be specifically designed to amplify only the target gene sequence. For that reason, a *melt curve* analysis is required to validate the assay and to ensure specific amplification took place. This is achieved at the end of a qPCR assay, where the reaction mixture is incrementally heated from 60-95°C during which the fluorescence is measured continuously. As the temperature increases, the double-stranded helix dissociates, and the fluorescence signal decreases proportionally (Robin, 2006). The temperature at which a double-stranded helix dissociates completely depends on its intrinsic length or GC content, hence a single peak in a meal curve analysis indicates the amplification of a single product (**Figure 2-11**).

The obtained fluorescence values are plotted onto a graph with the fluorescence values on the y-axis and the corresponding cycle number on the x-axis as presented in **Figure 2-12**. Each qPCR reaction is characterised by its *threshold cycle* (C_T) at which the fluorescence exceeds the background level (Wong and Medrano, 2005). A lower C_T indicates a greater number of a starting material. This correlation permits precise calculation of the target molecules over a wide dynamic range, while still retaining the specificity and sensitivity of a conventional end-point PCR (Schmittgen and Livak, 2008).

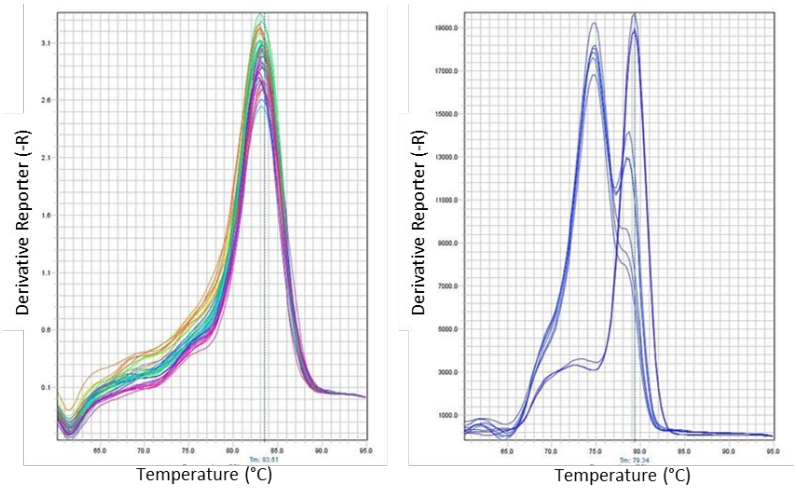

Figure 2-11 Representative graphs showing fluorescence intensity values during melt curve analysis of PCR products for *KCNB1* gene amplified using two pairs of primers.
The peaks indicate the temperature at which the double-stranded DNA is fully dissociated. On the left, the observed melting temperatures for each sample peak at near-identical values, suggesting the primer pair used produced single product. The inconsistencies observed on the right suggest the presence of multiple distinct amplicons, thus indicating the primers used are not specific.

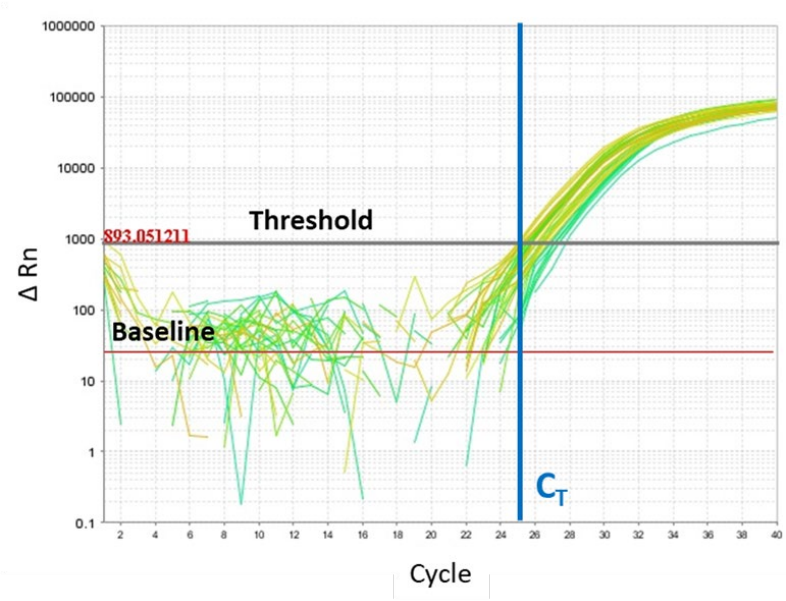

Figure 2-12 Amplification plot of a qPCR assay.
The baseline refers to the background fluorescence before the detectable amplification occurs. The threshold denotes the amount of fluorescence above the baseline and is expressed as three standard deviations above the mean background values.

Quantitative gene expression can be presented either as an absolute copy number of a particular gene or the relative expression of a gene. The absolute gene quantitation is used to measure the exact number of gene copy, such as viral load count, whereas relative gene expression, as studied in this thesis, can be used to measure any changes in gene expressions between two or more experimental conditions (Chen et al., 2005). Absolute gene quantitation compares the PCR results to a standard curve, whereas relative gene expression uses one or more control genes to correct for the variability between PCR reactions. The most commonly used method of presenting relative gene expression is the 'ΔΔ Ct' method first described by Livak and Schmittgen (Livak and Schmittgen, 2001) that allows presentation of data as an expression fold-change. It can be used to compare the expression of a gene between two samples, as depicted by the equation below:

$$\Delta\Delta\ C_T = \frac{2^{CT(target,untreated)-CT(reference,untreted)}}{2^{CT(target,treated)-CT(reference,treated)}}$$, were

$C_T(target, untreated)$ is the C_T value for the target gene of a control sample,

$C_T(reference, untreted)$ is the C_T value for the reference gene of a control sample,

$C_T(target, treated)$ is the C_T value for the target gene of a treated sample,

$C_T(reference, treated)$ is the C_T value for the reference gene of a treated sample.

2.5.2 Primer Selection and Specificity Validation

Pre-designed KiCqStart® SYBR® Green primers (**Table 2-4**) were obtained from Merck (UK) and their specificity for target mRNA transcripts were computationally validated using BLAST™, and their aptitude for primer-dimer formation was simulated *in silico* using uMelt™. The dry probes were diluted to 100 µM stock concentration in DEPC-treated H_2O according to manufacturer technical datasheet.

Table 2-4 Oligonucleotide primers sequences used in this thesis.

Gene	Primer sequence (5'– 3')	Amplicon size (bp)
Actb	F: GATGTATGAAGGCTTTGGTC R: GAGACCAATAAAAGTGCACA	96
Kcnb1	F: AGTCTCACCTTCTCTTCATC R: CCACATCTCTAAGGAGGAAA	136
Kcng4	F: TTCTTCTCATTTCCCCCTAC R: CTTCCTAAAACAAGCGACAG	198
Grin1	F: TGTGGAATTCAATGAGGATG R: CACCAGACTAAAGATAGTGACA	196
Grin2b	F: CTGGTGACCAATGGCAAGCATG R: CTTCTTAGAGCCATTCAGTG	139
Grin2c	F: TCGGTGAGGTATACTACAAG R: GATTATAGACTTCTCTGTGCCT	147

Abbreviations: bp, base pairs; F, forward; R, reverse

2.5.3 cDNA Synthesis (Reverse transcription)

Complimentary DNA strands were synthesised using High-Capacity cDNA Reverse Transcription Kit (4368814; ThermoFisher Scientific, UK). The reaction mix was prepared as follows:

Per 20 µL single reaction:

- MultiScribe™ Reverse Transcriptase: 0.5 µL
- dNTP mix: 0.8 µL
- Reverse Transcriptase buffer: 2.0 µL
- Random Primers: 2.0 µL
- DEPC-treated H_2O: 4.7 µL
- Total sample RNA: 10.0 µL

The reaction was carried out in a Hybaid thermal cycler (Thermo Scientific, UK). The cDNA cycle was optimised as follows:

Settings	**Step 1**	**Step 2**	**Step 3**	**Step 4**
Temperature	25°C	37°C	85°C	4°C
Time	5 minutes	2 hours	5 minutes	hold

2.5.4 Real-time Quantitative PCR

PCR primer mix (10 µM) was prepared by combining 10 µL of forward and 10 µL reverse primer for each gene in 980 µL of DEPC-treated H_2O in an

individual tube for each gene. Reaction Master Mix for each gene was then prepared by mixing, per single 13 µL-reactions:

- 10 µM primer mix, 3 µL.
- SYBR® green, 7.5 µL.
- DEPC- treated H_2O, 2.5 µL.

In a 96-well plate, 1 µL of previously synthesised cDNA (10 µM) for each sample was pipetted in triplicates into individual wells (e.g., wells A1, A2, A3 each contain the same sample cDNA). Subsequently, 10 µL of Reaction Master Mix for each gene was added to their corresponding wells. The plates were sealed and centrifuged in a plate mixer for 1 minute before placing in the thermocycler. The RT-qPCR reaction was carried out in StepOne Real-time PCR thermocycler (Applied Biosystems, UK) with the following settings:

Stage 1 (Pre-cycle)	**Stage 2 (PCR, 40 cycles)**	**Stage 3 (Melt curve)**
• 50°C, 2 minutes • 95°C, 10 minutes	• 50°C, 15 seconds • 75°C, 1 minute	• 50°C - 95°C at 0.3°C increments

2.5.5 Relative Gene Expression Analysis

The relative gene expressions were calculated using the Livak method as described in **Section 2.5.1**. The data were populated in GraphPad PRISM. The statistical test of choice was the unpaired t-test or Mann-Whitney U test of mean ranks, depending on data distribution.

2.6 Proximity-ligation Assay

2.6.1 Overview

Proximity-ligation assay (PLA) is a novel biomolecular technique that permits *in situ* detection of interactions between two proteins that are endogenously co-expressed within a short distance. The procedure combines the elements of antibody-antigen binding and polymerase chain-reaction to produce a signal in a histological sample or cell culture that can be detected, measured, and quantified using fluorescence or confocal microscopy (Söderberg et al., 2008; Weibrecht et al., 2010). The traditional immunohistochemical protocol is restricted to co-localisation of target proteins by producing an overlay image of separate fluorescence channels, thus only allowing for a visual overlap of the investigated proteins without the certainty of significant physical interactions taking place. On the contrary, the PLA exploits the proximity of two proteins to produce a signal only if the two are present within 40 nm distance (i.e., interacting with one another). Several techniques have been established to investigate protein-protein interactions, including the common co-immunoprecipitation (Lee, 2007a) or the more sophisticated fluorescence-based assays, such as fluorescence resonance energy transfer (Edidin, 2003). While each method presents with its own limitations, the PLA assay offers significant advantages over other approaches; most importantly, it allows for detection

of endogenous protein with high specificity and sensitivity (Fredriksson et al., 2002; Söderberg et al., 2006). Additionally, PLA does not depend on cloning of genes or other genetic modifications of the cells, thus it can be used as clinical diagnostic tool (Bagchi, Fredriksson and Wallén-Mackenzie, 2015).

As illustrated in **Figure 2-13**, the assay requires a tissue section (or cultured/harvested cells) to be fixed, permeabilised, and blocked against non-specific binding using low-affinity antibodies, followed by incubation with two primary antibodies that are specific against the target protein, and which are raised in different species (e.g., one mouse and one rabbit). The PLA assay then introduces two hybrid probes which are secondary IgG antibodies conjugated to RNA primers: one forward and one reverse (e.g., anti-mouse reverse [or 'minus'] primer, and anti-rabbit forward [or 'plus'] primer). The tissues are then treated with a ligation solution which introduces a DNA loop containing nucleotide sequences complementary to the forward and reverse primers. This DNA loop will be attached to the section if the two primers exist in close proximity. Subsequent step involves rolling-circle amplification which is achieved by incubating the tissues with amplification solution containing polymerase enzyme, oligos, and detection dye. The amplified signal can be then detected using fluorescence or confocal microscopy.

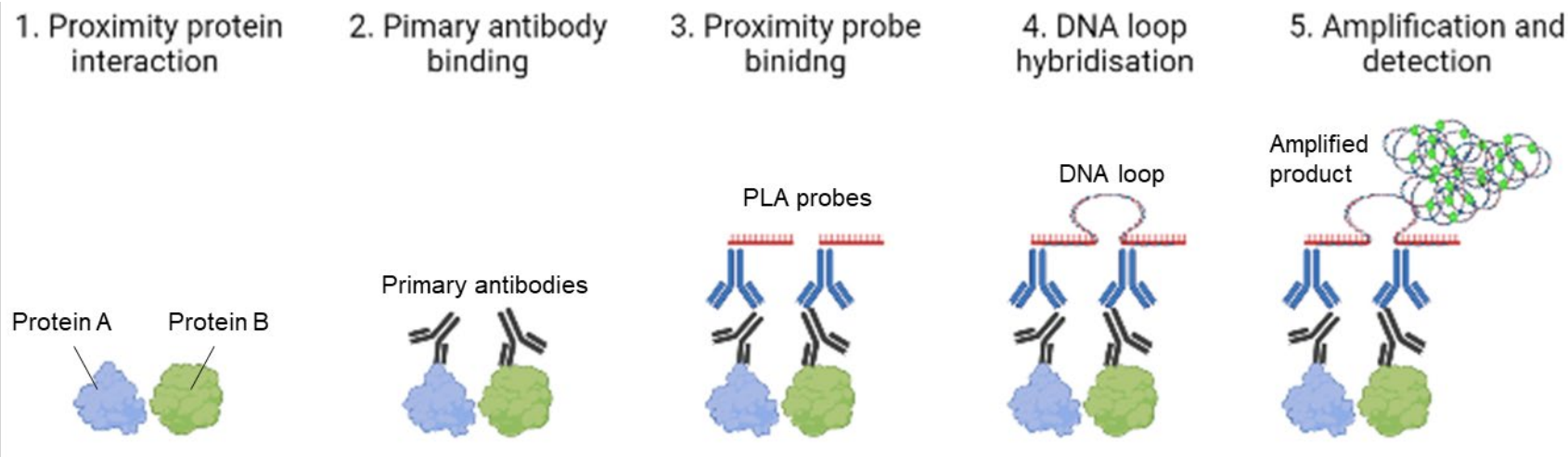

Figure 2-13 Diagram showing the key steps in proximity ligation assay.
A histological sample with an assumed proximity interaction is selected and the target antigens probed with specific primary antibodies. The PLA probes containing primer sequences are then introduced to detect the primary antibodies, after which a circular DNA loop is hybridised to the primers. This DNA loop serves as an anchorage for rolling disc amplification. The amplified product contains a fluorescent dye that can be detected using fluorescence or confocal microscopy. Created in BioRender.com

2.6.2 Antibody Staining

Frozen tissue sections (12 microns) were fixed, antigen-retrieved blocked and incubated with primary antibodies as previously described in **Section 2.**

2.6.3 Probe Hybridisation

Stock probe solution was prepared from concentrated PLA probes (Anti-rabbit PLUS [DUO92002; Merck, UK] and Anti-mouse MINUS [DUO92004; Merck, UK]). The probes were vortexed gently and diluted in five parts of antibody diluent (DUO82015; Merck, UK). Probe Master Mix was prepared by mixing, per single 40 µL reaction:

- 8 µL stock anti-rabbit PLUS solution
- 8 µL stock anti-mouse MINUS solution
- 24 µL antibody diluent

The primary antibody was tapped off the slides and washed two times in 1x Wash buffer A for 10 minutes each. The excess wash buffer was tapped off and slides loaded with 40 µL of probe master mix and incubated in a pre-heated humidity chamber for 1 hour at 37°C.

2.6.4 Ligation

Working concentration ligation buffer was prepared by diluting the stock ligation solution (DUO82009; Merck, UK) in five parts of ddH_2O. The ligation mixture was prepared by mixing, per single 40 µL reaction:

- 8 µL of diluted ligation buffer
- 32 µL ddH_2O per single reaction.

The probe master mix was tapped away from the slides and washed two times for five minutes each in 1x wash buffer A at RT. Ligase enzyme (DUO92102; Merck, UK) was diluted in the ligation buffer at 1:40 ratio. The slides were then loaded with 40 µL of ligase/buffer solution each, and incubated in a pre-heated humidity chamber for 30 minutes at 37 °C.

2.6.5 Amplification

Working concentration amplification buffer was prepared by diluting the stock solution (part of DUO92102; Merck, UK) in five parts of ddH_2O. Amplification mix was prepared by combining, per single 40 µL reaction:

- 8 µL of diluted ligation buffer
- 32 µL ddH_2O per single reaction

The ligase solution was tapped off and the slides washed two times for five minutes each in 1x wash buffer A at RT. Polymerase enzyme (part of

DUO92102; Merck, UK) was added to the amplification buffer at 1:80 ratio, and the slides loaded with 40 µL of amplification solution and incubated in a pre-heated humidity chamber for 100 minutes at 37 °C. The samples were then washed two times in 1x Wash Buffer B for 10 minutes each at RT, and a final wash in 0.01 x wash buffer B supplemented with 300 nM DAPI for one minute. The slides were then cover-slipped using a non-hardening mounting medium (H-1000; Vector Labs, UK) and sealed with clear nail polish.

2.6.6 Imaging and Data Analysis

Slides were imaged as described in **Section 2.4.6**. Micrographs were processed using ImageJ software (NIH, USA). In brief, the sealed slides were imaged at 400 x and 1000 x magnification using dry and oil-immersed objective lens, respectively. The slides acquired at 1000 x magnification were taken at three focal planes and stacked together to compose one image.

Chapter 3 Expression and distribution of Kv2.1 and Kv6.4 in The Cerebellar Cortex

3.1 Introduction

The cerebellum is a brain region composed of two lateral hemispheres and a central vermis which are connected to the rest of CNS by afferent and efferent fibres traversing through three pairs of cerebellar peduncles (Sotelo, 2004). The structure plays major roles in fine-tuning motor and ocular control, balance, posture, as well as memory, perception, and cognition (Koziol et al., 2014b). These functions are maintained by the neuronal cell populations distributed across the foliated cerebellar cortex, which receive sensory information and compute corrective instructions that are relayed back to the appropriate areas of the CNS (Beckinghausen and Sillitoe, 2019). Although an interplay between all cerebellar neurones is central to achieving these functions, two types of cells within the cerebellar

cortex are of key importance: 1) the granule cells (GCs) which receive cortical input *via* mossy fibres; and 2) the Purkinje cells (PCs) which receive input from the GCs *via* parallel fibres and from the climbing fibres of the inferior olive. These inputs modulate PC activity, and in turn, the PCs generate the sole output from the cerebellar cortex, thereby eliciting significant influence over the downstream neuronal events in other areas of the CNS (Ito, 2006). The optimal function of the cerebellum depends on the synchronous activity of these two cell populations which is tightly controlled by the organised inhibitory and excitatory stimuli, largely governed by the intrinsic conductance determined by ion channel activity (Sillitoe and Joyner, 2007).

As introduced in **Chapter 1.2**, voltage-gated K^+ channels (Kv) are expressed in all excitable cells where they are critical for the maintenance of membrane excitability, thereby contributing significantly to the information processing within the nervous system (Smolin et al., 2012; Tsantoulas et al., 2012; Tsantoulas et al., 2014; Calvo et al., 2016). In the mammalian brain, individual Kv channel subtypes are responsible for regulating discrete aspects of neuronal function depending on several factors, such as their biophysical properties, their subcellular localisation, or their susceptibility to neuromodulation (Trimmer, 2015). The Kv2.1 are ubiquitously expressed throughout the brain where they produce the majority of the delayer rectifier current (Klemic et al., 1998). These Kv2.1-

mediated currents influence the homeostatic regulation of Ca^{2+} influx and neuronal excitability during high frequency repetitive firing. The functional diversity of Kv2.1 channel is expanded by a number of modulatory subunits (Bocksteins, 2016). The Kv6.4 appears particularly elusive as *in situ* hybridisation data from the Allen Institute suggests that in mouse, cerebellar levels of mRNA of the Kv6.4-coding gene *Kcng4* are ten times that of the Kv2.1-coding *Kcnb1* (**Appendix A2**), raising a possibility of a Kv6.4 reservoir in cerebellar neurons with a role yet to be elucidated.

Several functional Kv channels have been characterised in the cerebellum, including the Kv1-type (Chung et al., 2001; Chung et al., 2005; William et al., 2012), the Kv3-type (Joho et al., 2006; Veye, Snyders and De Schutter, 2013), and the Kv4-type (Strassle et al., 2005; Amarillo et al., 2008). Despite its profound effect on neuronal function, the expression of Kv2.1 channel has so far been only studied in cultured cerebellar GCs (Jiao et al., 2007; Zhuang et al., 2012; Wang et al., 2014), and although Kv2.1 has been reported in cerebellar PCs previously (Hwang, Cunningham, et al., 1993), its subcellular localisation remains to be reported. At the same time, no KvS subunits have yet been described in the cerebellum despite their important contribution to Kv2.1 channel physiology.

3.2 Aims

In this chapter, we aim demonstrate the expression patterns of Kv2.1 and Kv6.4 subunits in the two main neuronal populations of the cerebellar cortex, and the interaction between these two subunits *in-situ*.

3.3 Materials and Methods

This study used five animals in total. Three mice were used for histological study, whereas the remaining two animals were used for western blotting. This section aims to provide a brief summary of the methods employed, whereas elaborated description of the methodology used to include preparation of solutions, brain dissection, etc. is contained in **Chapter 2**.

3.3.1 Animal work

Twelve-week-old male CBA/Ca mice weighing 22-26 g were sacrificed by cervical dislocation, decapitated, and their brains removed. For western blotting, the frontal cortex, hippocampus, thalamus, and the cerebellum were dissected and snap-frozen in Eppendorf tubes using LN_2 and kept on dry ice. For histological studies, the cerebellum and cerebrum were dissected form the remaining three animals and snap frozen in OCT medium-filled cryostat blocks. All samples were moved to -20°C short-term storage before processing.

3.3.2 Western blotting

The dissected brain regions were homogenised in RIPA buffer using a Dounce homogeniser and centrifuged for 10 minutes at 4°C. The resulting supernatant was mixed with an equal volume of electrophoresis sample buffer and boiled for 10 minutes at 95°C. The boiled samples were allowed to reach RT and were loaded onto 12% polyacrylamide gels and resolved for 15 minutes at 150 V, and further 45 minutes at 130 V. The gels were washed once in dH_2O, and the proteins were transferred from the gels onto nitrocellulose membranes for 30 minutes at 100 V. The membranes were incubated in Ponceau S stain for 5 minutes to assess the quality of protein transfer. Each membrane was then washed in 1% glacial acetic acid for 5 minutes, and subsequently washed two times in dH_2O for 5 minutes each. The membrane to be probed for Kv2.1 was blocked in 3% BSA in TBST, and the membrane to be probed for Kv6.4 was blocked in 3% skimmed milk in TBST for one hour each at RT. The membranes were then incubated with anti-Kv2.1 (75-014; Antibodies Inc.; 1:1000) anti-Kv6.4 (ab155772, Abcam; 1:500) in 3% BSA and skimmed milk, respectively, overnight at 4°C. After three 10-minute washes, the membrane probed for Kv2.1 was incubated with HRP-conjugated goat anti-mouse antibody (sc-2005, Santa Cruz) diluted at 1:2000 in 3% BSA and incubated for 1 hour, whereas the membrane probed for Kv6.4 was incubated with HRP-conjugated goat-anti-rabbit antibody (sc-2004, Santa Cruz) diluted at 1:2000 in 3% skimmed milk

for 1 hour. After three ten-minute washes at RT, the membranes were incubated in ECL solution for 3-5 minutes then sandwiched between two transparent sheets of plastic and the images were taken in a chemiluminescence chamber connected to a desktop PC.

3.3.3 Immunohistochemistry

The sections were made using a cryostat microtome and collected onto poly-L-lysine-coated microscope slides, and fixed in 4% PFA buffer for 10 minutes at 4°C then washed 3 times in PBST at RT. The antigens were retrieved in 20 mM citrate buffer for 20 minutes at 95°C and washed as previously. Next, the sections were incubated in a solution containing BSA and normal goat serum for 2 hours at RT, and incubated with anti-Kv2.1, anti-Kv6.4 antibodies overnight at 4°C, and anti-Calbindin D28K for 48 hours at 4°C; the diluted anti-Calbindin D28K antibody was applied overnight and replaced with a solution containing both the diluted anti-Calbindin D28K and anti-Kv2.1 antibodies for the second night, and the slides washed as previously. The sections were then incubated with appropriate AlexaFluor®-conjugated antibodies for 2 hours at RT and washed. The slides were then incubated with 300 nM DAPI diluted in PBS for 5 minutes. The slides were washed and mounted with coverslips using antifade mounting medium and sealed using clear nail polish. Micrograph images were taken with a Leica fluorescence system and processed using ImageJ.

3.3.4 Proximity ligation assay

Twenty-micron thick cerebellar sagittal sections were fixed, antigens retrieved, blocked, and slides incubated with anti-Kv2.1 and anti-Kv6.4 overnight as described in **Section 3.2.3**. The slides were then washed two times in Wash Buffer A and incubated with diluted anti-mouse MINUS and anti-rabbit PLUS probes at 37°C for 1h. After incubation, the slides were washed as previously and incubated with ligation solution at 37°C for 30 min. After subsequent washes, the sections were incubated with amplification solution at 37°C for 100 min. The slides were then washed two times in 1 x Wash Buffer B and a final wash in 0.01 x Wash Buffer B with added DAPI. The slides were then cover slipped and sealed using clear nail varnish. The images were taken at 200 x, 400 x, and 1000 x magnification and processed using ImageJ.

3.3.5 Fluorescence intensity plots

To investigate the subcellular localisation of Kv2.1 and Kv6.4, plots of AlexaFluor® fluorescence intensities were generated. Micrographs were imported into ImageJ and the ‘Line Tool’ was used to draw across the representative cells to be measured. Subsequently, ‘Plot Profile’ option was selected from the ‘Analyse’ menu, and ‘Live’ button was selected from the plot options. The drawn line was then moved accordingly to select the most suitable area to present on the graph. The plot data was then copied by

clicking ‘More’ button and ‘Copy All Data.’ The data which included raw grey values of the pixels along the line was then pasted into an Excel spread sheet and a new line graph created.

3.4 Results

We employed a combination of western blotting, immunohistochemistry, and PLA to study the expression of voltage-gated K^+ channel subunits Kv2.1 and Kv6.4 proteins in the cerebellum, their cellular and subcellular localisations, as well as the localisation and interaction between these two channel subunits *in-situ*.

Western blotting confirms the presence of Kv2.1 and Kv6.4 proteins in the cerebellum

First, we used western blotting to confirm whether the two proteins are detectable in the cerebellum. The immunoblots in **Figure 3-1** demonstrate the detected Kv2.1 and Kv6.4 proteins in samples obtained from two animals. These samples included three control regions of known protein expression, and the cerebellum. Although not quantified, the chemiluminescent bands suggest a high-to-medium level of Kv2.1 in the frontal cortex, the hippocampus, and the thalamus, and a moderate level in the cerebellum. For the Kv6.4, the bands indicate very low expression levels

in the frontal cortex, whereas a moderate level of expression in the hippocampus, thalamus, and the cerebellum is observed.

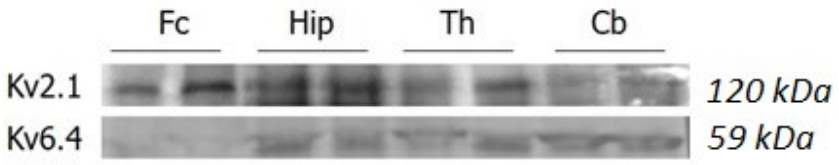

Figure 3-1 Both Kv2.1 and Kv6.4 are widely expressed in the brain, including the cerebellum.

The immunoblots show varying levels of Kv2.1 and Kv6.4 expression in different areas of mouse brain. Abbreviations: Fc, frontal cortex; Hip, hippocampus; Th, thalamus; Cb, cerebellum.

Kv2.1 is present in the granular cell layer and the Purkinje cells but not in the cells of the molecular layer

We then investigated the expression of Kv2.1 in cerebellar cortex using immunohistochemistry with a combination of confocal and fluorescence microscopy, which allowed us to determine that the Kv2.1 is present in within the granule cell layer (GCL), and the PCs. The confocal images presented in **Figure 3-2** illustrate the distribution of Kv2.1 in those regions across a section of cerebellar vermis, where the Kv2.1 (green) is observed as bright puncta approximately 1-2 μm in size. While the morphology of the cells in the GCL cannot be readily established, the Kv2.1 is evidently expressed in the PC soma as evidenced by their large cell bodies. Furthermore, we speculate that the Kv2.1 is present in the proximal dendrites of PCs, which are observed as extensions rising into the ML that

are approximately 2 μm in diameter and of varying lengths and seemingly extend up to ~100 μm into the ML.

We then proceeded to establish the subcellular localisation of Kv2.1 in the GCs and PCs. The example micrographs presented in **Figure 3-3** depict the Kv2.1 detected within GCL that is manifested as micron-sized clusters. The plot in Panel G shows the intensity of AlexaFluor®488 fluorescence measured along the line in Image E. The adjacent peaks indicate a higher level of fluorescence on the membrane, suggesting that the majority of Kv2.1 reside in or near the plasma membrane. A similar pattern is observed in PCs (**Figure 3-4**A-C). The Kv2.1 also exist as bright puncta although here their size appears to vary between 1-2 μm. The measured fluorescence intensity presented in Panel G indicates that majority of Kv2.1 in PCs are also localised to or near the plasma membrane. Furthermore, our imaging confirms that within PCs, the Kv2.1 is present in proximal dendrites (**Figure 3-4**D-F), which is observed as extensions from the apical surface of the PC soma that rise into the ML.

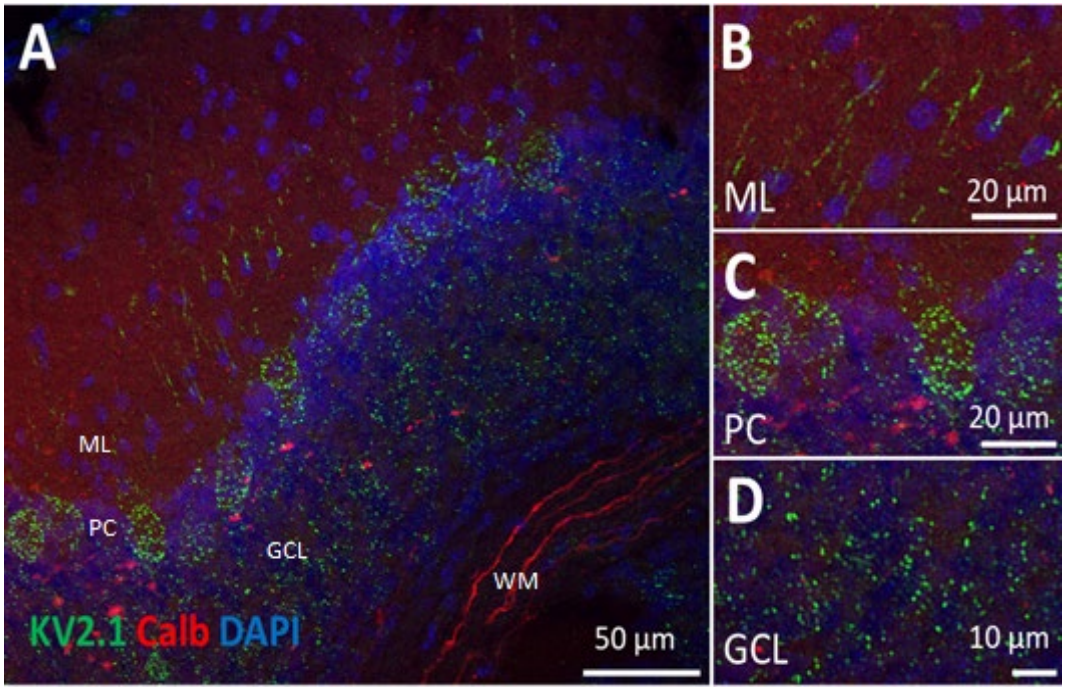

Figure 3-2 The Kv2.1 is widely expressed in cerebellar Purkinje cells and in the granular cell layer.

A. Immunofluorescent staining of a sagittal section of cerebellar vermis with Kv2.1 (green), CalbindinD28k (red) and the nuclei (blue). The Kv2.1 is observed in all three layers of the cerebellar cortex. B-D show an enlarged view of the three layers from panel A. The Kv2.1 is expressed as clusters on the surface of PC somata, and as dispersed clusters across GCL. In the ML, the Kv2.1 is observed as extensions which arise from the PC somata. Calbindin D28K (red) was used to selectively stain PCs; the nuclei were counterstained with DAPI. Abbreviations: ML, molecular layer; PC, Purkinje cell; GCL, granular cell layer; WM, white matter.

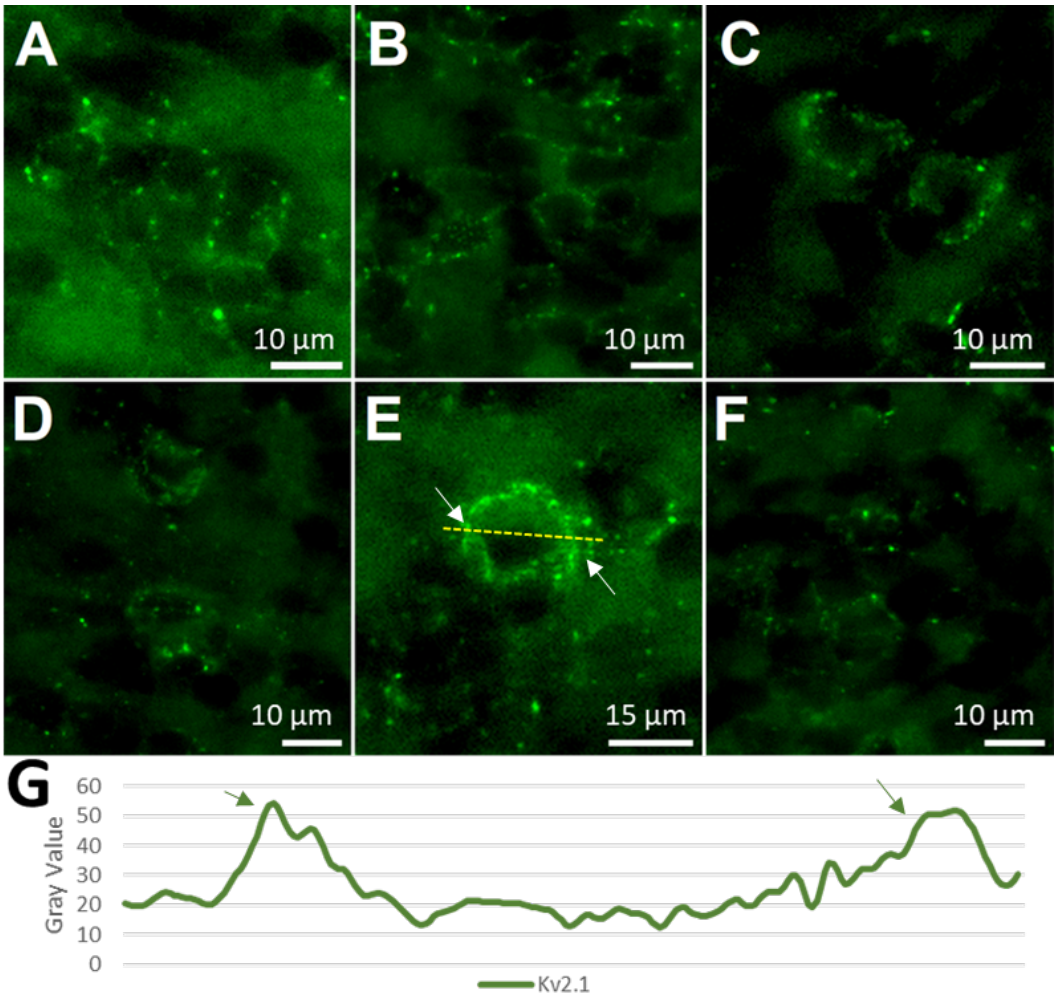

Figure 3-3 The Kv2.1 shows clustered expression on the granular cell plasma membranes.

Images A-F are examples of immunofluorescent staining of cerebellar granule cells showing various levels of punctuate expression of Kv2.1 with visible micron-sized clusters. In G, a plot of fluorescence intensity corresponding to Kv2.1 expression measured along the line indicated in E suggests a high expression on the plasma membrane of granule cells. The arrows indicate the plasma membrane in E and its corresponding high intensity peaks in G.

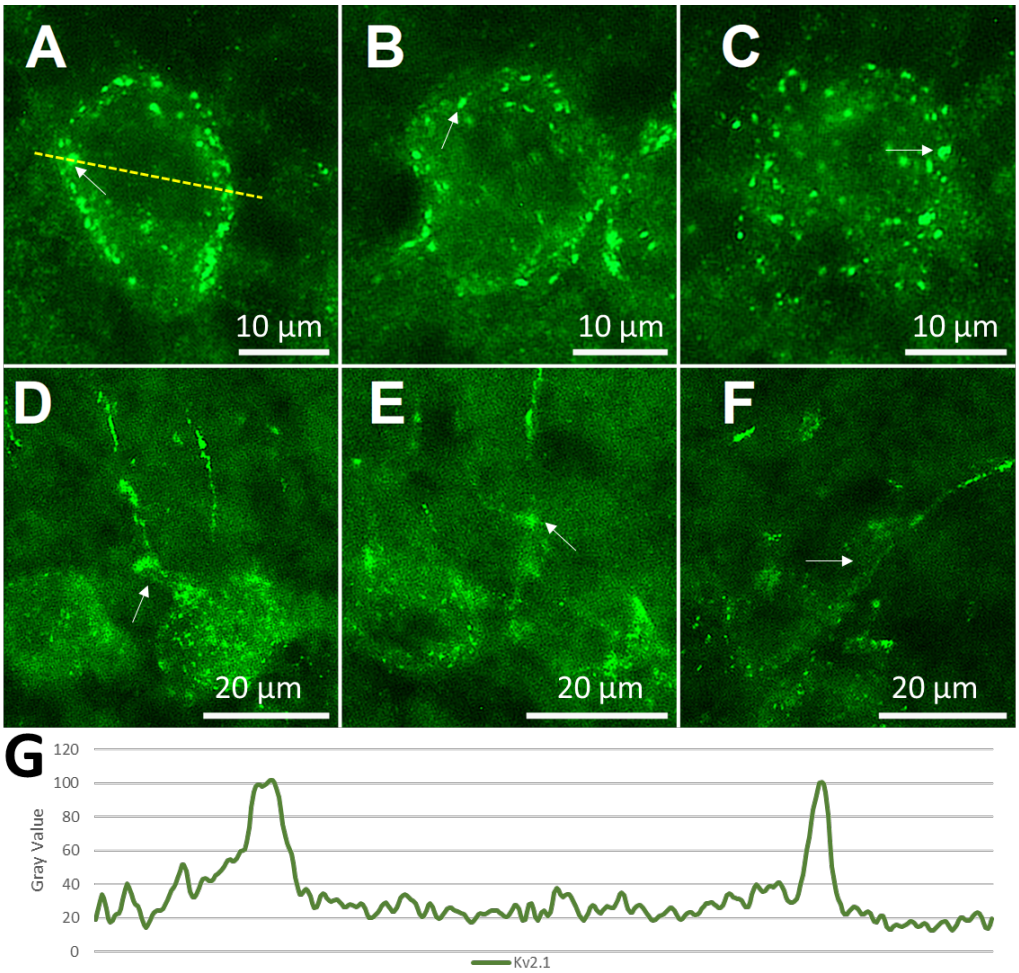

Figure 3-4 The Kv2.1 is expressed in both clustered and dispersed forms in different portions of cerebellar Purkinje cells.

A-C. Immunofluorescent staining of PCs shows a primarily punctuate (~2micron, arrows) pattern of Kv2.1 in PC somata. The arrows in D-F indicate Kv2.1 presence in proximal dendrites. In G, the plot of fluorescence intensity corresponding to Kv2.1 expression measured along the line indicated in A suggests Kv2.1 is highly expressed on the cell membranes.

Kv6.4 is present in cell populations within each layer of the cerebellar cortex

Unlike the Kv2.1 subunits, Kv6.4 appear to be present in all three layers of the cerebellar cortex; the fluorescence micrograph presented in **Figure 3-5** illustrate a profuse expression in PCs, whereas Kv6.4 presence in GCL and ML appears to be low. Further investigation into the subcellular localisation of Kv6.4 revealed a discrete expression pattern compared to Kv2.1. The micrographs of representative neurons form GCL presented in **Figure 3-6** illustrate Kv6.4 (green) within the cells observed as faint objects without conclusive morphological features, which might be due to the abundant background fluorescence which masks the true signal at the current focal plane. However, the control section presented in Micrograph C acquired using the same parameters as the test samples indicates no autofluorescence, thus suggesting a low level of Kv6.4 presence in these cells. We also measured the fluorescence emitted from these cells to deduct its subcellular location. The plot in Panel G shows variable signal intensity corresponding to Kv6.4 expression across a dotted line indicated in Image A. The graph shows four repeating sets of an incremental increase of fluorescence that is followed by a decrease in signal intensity, and each set is separated by a less distinct but sudden drop in brightness. This may indicate that in the each of the four cells the Kv6.4 is expressed at either the plasma membrane or the cytosol at similar levels, or that it is present within

the cytosol only. In addition, the micrograph presented in Panel F sows the nuclei in the GCL, which are observed as a blue amorphous mass due to the vast number of GC present and tight packing. This, in addition to the incomplete separation between Kv6.4 intensities in Panel G, serves as a plausible argument to claim that the cells observed here are indeed GCs.

For the PCs, the subcellular localisation of Kv6.4 also appears to be somatic and no indications of its presence in other compartments are observed. The micrographs in **Figure 3-7** illustrate this abundant expression in representative PCs. While there are no clear indicators of formed clusters, each PC manifests some degree of regional variability in brightness. This is interpreted from the plot in Panel G, where the fluorescence corresponding to Kv6.4 expression measured along the line indicated in Image C suggests an abundant cytosolic reservoir of Kv6.4 in PC soma with an increased fluorescence in one part of the cell.

We also detected some Kv6.4 immunoreactivity in the ML. However, as the GCL, this region shows high background fluorescence, which complicates our ability to make thorough observations. We focused our analysis on the upper portions of the ML which houses cerebellar stellate cells (SCs). As presented on the micrographs in **Figure 3-8**, the Kv6.4 in these cells appear as faint puncta that are dispersed randomly in the cell soma with no indicators of expression within other cellular compartments.

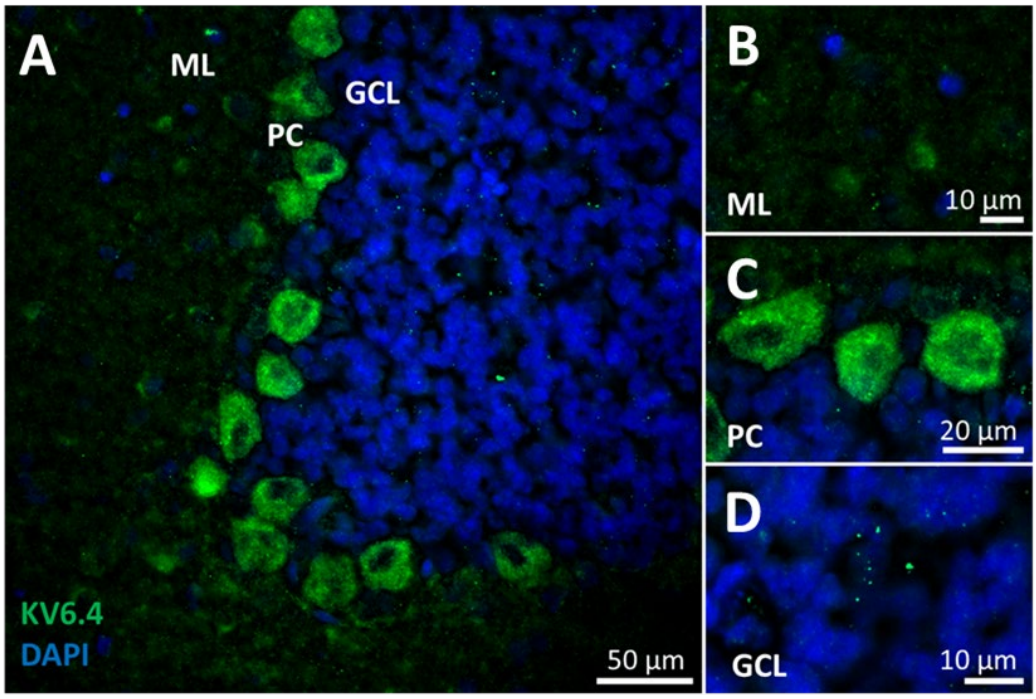

Figure 3-5 The Kv6.4 is predominantly expressed in cerebellar Purkinje cells.

A. Immunofluorescent staining of a sagittal section of cerebellar vermis with Kv6.4 (green) and the nuclei (blue). A variable expression of Kv6.4 (green) is observed in all three layers of the cerebellar cortex that is most prominent in the PCs. Images B-D show an enlarged view of the three layers. The Kv6.4 expression is abundant in the cytoplasm of PC soma and not obvious in both ML and GCL. The nuclei were counterstained with DAPI. Abbreviations: ML, molecular layer; PC, Purkinje cell; GCL, granular cell layer.

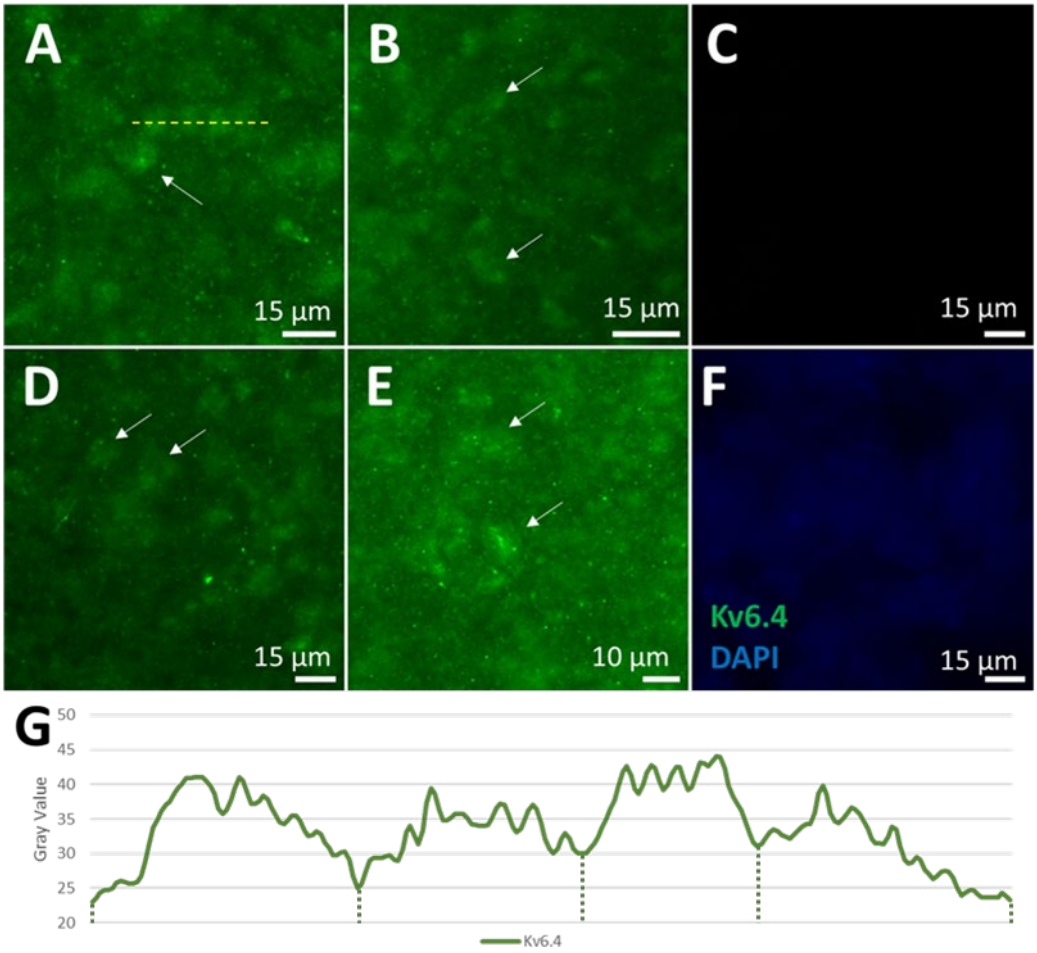

Figure 3-6 The Kv6.4 displays a very low expression the granular cell layer.

The immunofluorescent staining of Kv6.4 (green) in granule cell somata that is significantly masked due to the abundant background fluorescence. However, the plot of fluorescence intensity corresponding to Kv6.4 expression measured across the four cells indicated by the line in Image A suggests that Kv6.4 is expressed might be largely expressed intracellular. Images B, D, and E depict further examples of Kv6.4-immunoreactive cells in the GCL. Arrows indicate the immunoreactive cells. Nuclei (blue) are counterstained with DAPI. Images C and F are primary antibody-negative controls.

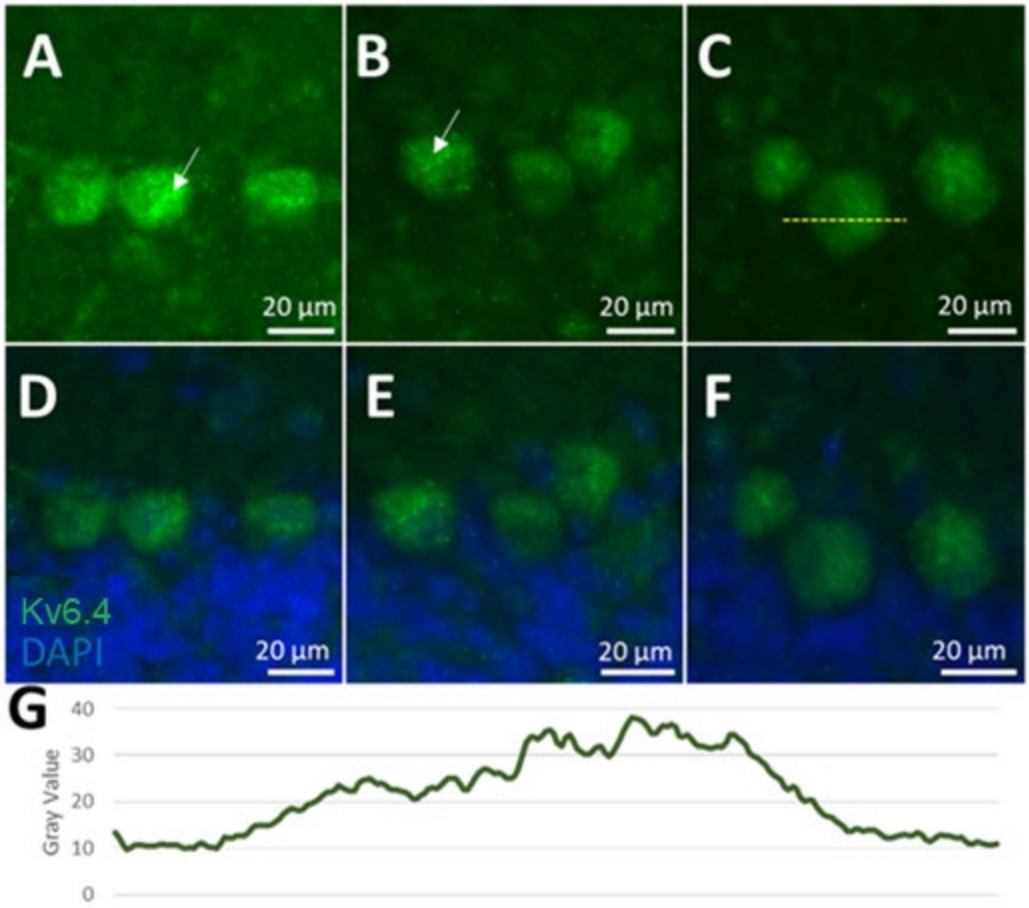

Figure 3-7 The Kv6.4 is expressed exclusively in Purkinje cell soma.

A-F. Immunofluorescent staining of sagittal sections of cerebellar vermis show high expression of Kv6.4 (green) in the somatic cytoplasm of PCs. G. Line profile of fluorescence intensity as indicated by the dashed line in panel C, suggesting cytosolic expression of Kv6.4. Nuclei (blue) are counterstained with DAPI.

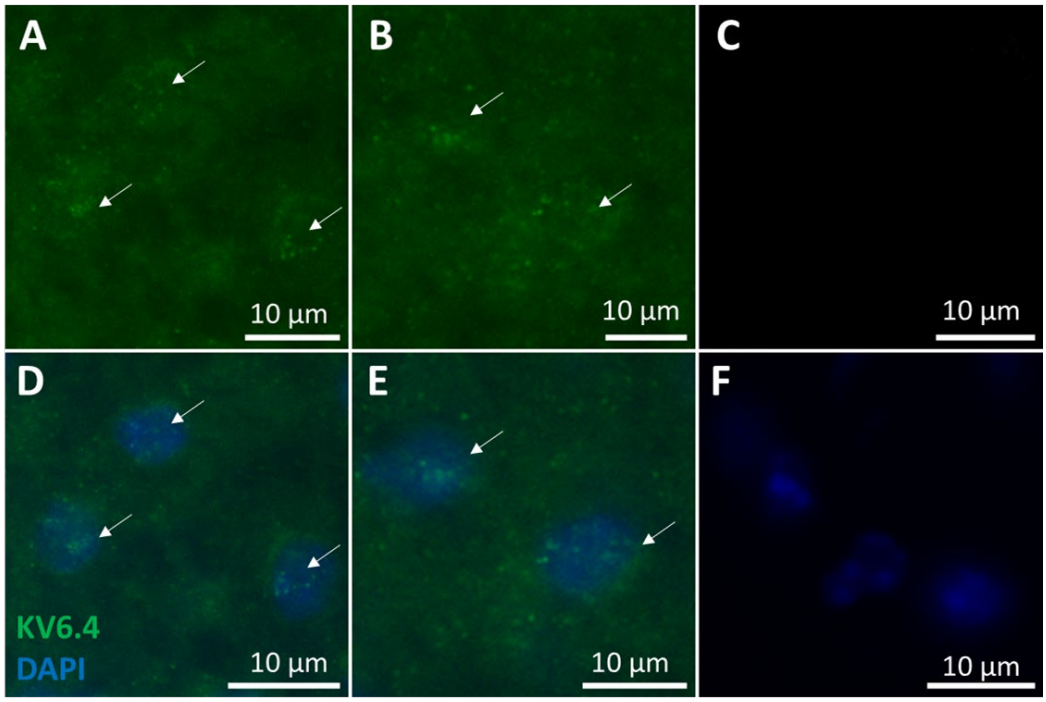

Figure 3-8 The Kv6.4 shows evidence of clustered expression in cerebellar stellate cells.

Immunofluorescent staining of cerebellar stellate cells for Kv6.4 (green) and nuclei (blue). The micrographs A and B show examples of presumed Kv6.4 present in cerebellar stellate cells and their DAPI-stained counterparts (D and E). The arrows indicate the Kv6.4 aggregates observed, which could suggest either cytosolic reservoir of Kv6.4 in the soma or a membrane expression. Images C and F are primary antibody-negative controls.

Kv2.1/Kv6.4 co-assemble in Purkinje cell soma

After establishing the distinct expression patterns of the two subunits in cerebellar cortical neurons, we asked whether they arrange to form functional heterotetramers. To answer this question, we first used double immunostaining to detect Kv2.1 and Kv6.4 in a single cell simultaneously. The micrographs presented in **Figure 3-9** shows the two channel subunits detected in two separate PCs. The overlay images of Kv2.1 and Kv6.4 depict no change in observed colour to a more yellow hue within the clusters which would indicate increased Kv6.4 expression in cluster region. Furthermore, there was no observed increase in fluorescence intensity corresponding to Kv6.4 with the cluster regions in Panel E. Therefore, the ability of Kv2.1 to form functional heteretetramers with Kv6.4 in PCs *in vivo* could not be established.

Because of the high abundance of Kv6.4 in Purkinje cells which appears to be significantly higher compared to Kv2.1, we were convinced that these two channel subunits must combine together in one form or another. Therefore, we investigated this further using a proximity ligation assay (PLA), which allows detecting interactions between two proteins *in situ*. Unlike the fluorescent double staining technique which only detects the colocalisation of two protein in a sample tissue, the PLA assay allows for the detection of physically interacting proteins, thus assuming functional

relevance. The micrographs in **Figure 3-10** show fluorescence micrographs taken at various magnifications. Image A shows a chain of PCs that are reactive for Kv2.1/Kv6.4 interactions seen in (orange). Images B-E depict single PCs each taken at 1000x magnification using oil immersion lens in grey scale. Each PC was imaged at three focal planes that were stacked together to compose a detailed view of the cell features as oil immersion often tends to generate blur. In this view we can clearly deduct that Kv2.1/Kv6.4 interactions are present in PC soma; however, it is not clear whether these occur on the membrane or within the cytosol. The interacting proteins are seen as bring punctate on the soma which are more likely to be expressed on the plasma membrane. Images F-H are controls. Nuclei (blue) were counterstained with DAPI. No interactions were found within the GCL or M (not shown).

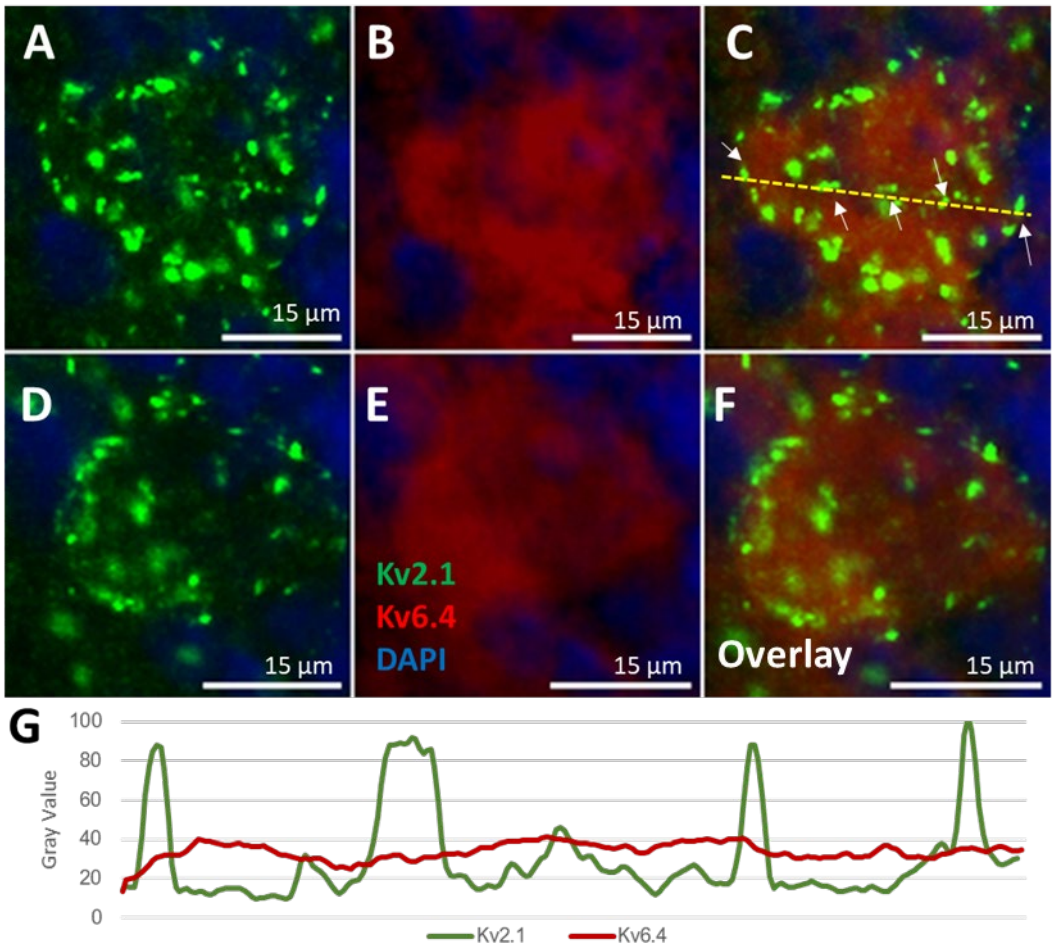

Figure 3-9 The Kv2.1 and Kv6.4 are express in the PC soma but show no evidence of colocalisation.

A-F. Immunofluorescent staining of cerebellar PCs with Kv2.1(green); Kv6.4 (red), and the nuclei (blue). G. Fluorescence line profile plot of Kv2.1 and Kv6.4 expression along the dashed line as indicated in the overlay image in panel C suggests no colocalisation of Kv2.1 and Kv6.4.

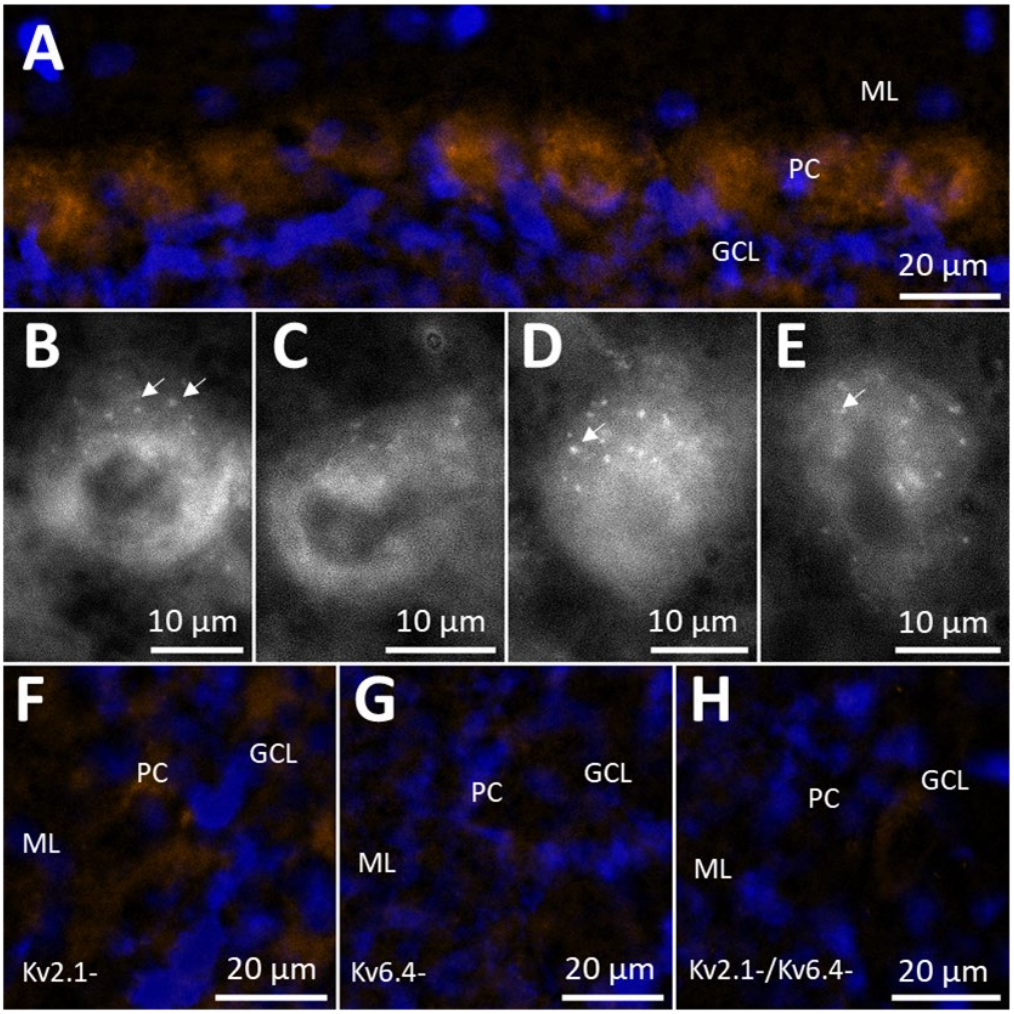

Figure 3-10 The Kv2.1 and Kv6.4 interact to form Kv2.1:Kv6.4 channels in cerebellar Purkinje cells *in situ*.

A. Pseudocoloured micrograph showing a portion of molecular layer (top), Purkinje cell layer (middle) and a portion of granular cell layer (bottom). Images B-E show interacting Kv2.1 and Kv6.4 subunits as bright puncta (arrows) in individual PC soma. Images F-H show primary antibody-negative controls. A was taken at 400 x magnification using dry lens. Images B-G were taken at 1000 x magnification using oil-immersion lens at three focal planes and stacked using ImageJ. Control images F-H were taken at 200 x magnification using dry lens. Abbreviations: ML, molecular layer; PC, Purkinje cell; GCL, granular cell layer. Scalebars: A, 20µm; B-G, 10µm; H-J, 20µm.

3.5 Discussion

In order to understand the intricate roles of Kv channels in cerebellar physiology it is important to establish the expression patterns of Kv channel subtypes in cerebellar neurones. In this study we showed that the Kv2.1 and Kv6.4 are expressed in distinguished patterns in the two main excitatory and inhibitory neuron types within the cerebellar cortex. For Kv2.1, this subunit is localised to the plasma membrane and exists primarily as micron-sized clusters on the soma of GCs, whereas the clusters observed in PCs are also present in proximal dendrites, and their size appears to vary between 1-2 μm. Additionally, a subpopulation of diffused Kv2.1 channels also appears to exist in PCs. The expression pattern observed here is largely consistent with studies conducted on hippocampal neurons as well as transfected cell lines. For example, Murakoshi and Trimmer (1999) were the first to attribute the discrete localisation of Kv2.1 clusters to soma and proximal dendrites in cultured rat hippocampal neurons. In the same study, by blocking the Kv2.1 channel activity using anti-Kv2.1 antibodies, whole-cell-patch-clamp recordings from transfected COS-1 cells and mouse fibroblasts established that Kv2.1 forms a major component of the slowly activating delayed rectifier current, which is important for somatodendritic excitability (Klemic et al., 1998). The same lab established the localisation of Kv2.1 in cultured hippocampal glutamatergic pyramidal cells and GABAergic interneurons which were differentiated by their

immunoreactivity for glutamic acid decarboxylase (GAD) (Antonucci et al., 2001). There they observed that microclusters of Kv2.1 formed on the soma and proximal portions of dendrites of the GAD-negative excitatory neurons, while the GAD-positive interneurons expressed larger proportions of significantly bigger macroclusters – consistent with our observations in the inhibitory PCs. In the same decade, similar findings were reported in both cultured and intact hippocampal neurons (Misonou, Mohapatra and Trimmer, 2005; O'Connell et al., 2006; Misonou, Thompson and Cai, 2008; Mulholland et al., 2008). Additionally, Tamkun's lab demonstrated that the Kv2.1 also accumulate in the axon initial segment (AIS) of both native and transfected cultured hippocampal neurons (Sarmiere, Weigle and Tamkun, 2008). However, this observation was made only for GAD-negative cells, whereas the AIS of GABAergic interneurons did not contain Kv2.1 in their plasma membranes. This is partially consistent with our findings in PCs, where no evidence of Kv2.1 in AIS was observed, suggesting that Kv2.1 may not play a role in the action potential initiation in the PCs as it does in glutamatergic neurons; however, we were not able to confirm whether Kv2.1 is present in the AIS of GCs, which remains to be investigated. It is important to add that Kv2.1 clusters are dynamic structures, and their state depends on phosphorylation; these clusters are highly phosphorylated in neurons at rest but an increase in neuronal activity by, for example, induction of hypoxia and kinate-induced seizures *in vivo*, or by glutamate

stimulation in cultured neurons leads to a calcineurin-dependant dephosphorylation (Misonou et al., 2004; Misonou et al., 2006). This in turn triggers de-clustering of Kv2.1 accompanied by a hyperpolarising shift in voltage-dependant activation of Kv2.1, thus leading to suppressed homeostatic neuronal firing (Misonou et al., 2004; Mohapatra et al., 2009). This function poses particularly interesting implication for PCs, considering that the Kv2.1 may not be present in the AIS. A single PC receives sustained excitatory input from multiple GCs *via* parallel fibres and from the inferior olive *via* mossy fibres. At the same time, the PC axon is the only output route from the cerebellar cortex (Haines and Mihailoff, 2018); therefore, it can be speculated that, the Kv2.1 may serve as suppressors of neuronal activity with no influence over neuronal firing.

Although the kinetic properties of virtually all known Kv channels have been characterised (Ranjan et al., 2019), confounding factors exist which make it difficult to attribute the properties of Kv channels to the expression of particular Kv α-subunits *in vivo*. Perhaps the most problematic has been established almost thirty years ago in early research which revealed that most of Kv subunits *in vivo* are expressed as heteroteramers (Sheng et al., 1993; Wang et al., 1993; Scott et al., 1994). Furthermore, the biophysical properties of all Kv channels are to some extent modulated by accessory and other interacting proteins. In fact, the Kv channels are associated with the largest number of accessory subunits (discussed in

Section 1.2.1). In the case of Kv2.1, their properties are further extended by arranging with several α-subunits from KvS channel subfamilies. In our study we investigated the co-expression of Kv2.1 and the electrically silent Kv6.4, and made two notable observations: 1) Contrarily to Kv2.1, the Kv6.4 showed a robust cytosolic expression that is strictly localised to the soma of GCs and PCs, and some evidence of Kv6.4 in SCs was also observed; 2) we showed that the two subunits form Kv2.1/Kv6.4 heteroteramers in PCs but not in other cells of the cerebellar cortex. For the latter, Kv6.4 in model systems was demonstrated to exert several modulatory properties over the Kv2.1, including a decreased current density (Bocksteins et al., 2009), and altered biophysical properties of Kv2.1 channel, resulting in ~40 mV hyperpolarising shift in voltage dependence of inactivation with little effect on activation kinetics (Bocksteins et al., 2012; Stas et al., 2015). This could further support our previous argument about the potential role of Kv2.1, that Kv2.1/Kv6.4 channels act to further suppress the neuronal activity. The former findings, however, may pose important implications for the current status *quo* of KvS subunits. Based on our understanding of the KvS properties from studies in transfected cells, the feature which distinguishes them from other Kv α-subunits is their inability to form electrically active channels on their own (Bocksteins and Snyders, 2012). The Kv6.4 plays a regulatory role by joining the electrically active Kv2.1 α-subunit to form Kv2.1/Kv6.4 channels with variable content (Bocksteins, 2016). Although

disparities exist with regards to the predominant stoichiometric configuration Kv2.1: Kv6.4 heteromers (Pisupati et al., 2020), these exist in 2:2 and 3:1 ratio for Kv2.1: Kv6.4 per single channel (Pisupati et al., 2018; Möller et al., 2020). Therefore, if KvS co-assemble only with Kv2 α-subunits while being unable to tetramerise with their own subfamily members, what is the role of such abundant cytosolic pool of Kv6.4? It can be speculated that this pool is necessary to allow fast recruitment of Kv2.1/Kv6.4 to the plasma membrane in response to rapid changes in physiological demands, which will be discussed further in **Chapter 5**.

3.6 Conclusion

The cerebellar expression of Kv2.1/Kv6.4 has only been studied in granule cell cultures; therefore, this study provided the first insights into the expression of these two channel subunits in mouse. Here, we demonstrated that Kv2.1 and Kv6.4 display a similar pattern of expression compared to previous reports in other brain regions, but most importantly, we provided the first evidence of *in-situ* interaction between these two proteins in intact neurons.

Chapter 4 Generation and Validation of The Phencyclidine CBA/Ca Mouse Model of Schizophrenia

4.1 Introduction

As discussed in **Section 1.1**, schizophrenia manifests itself with an array of symptoms broadly categorised as positive, negative, and cognitive. Although the pathogenesis of the disorder is very complex, and various extents of dysregulation in several neurotransmitter systems are supported by compelling evidence from both animal and human studies, the dysregulation of the glutamatergic system is believed to be the key component in the onset of symptoms in each of the symptom domain. The hypothesis of glutamate hypofunction in schizophrenia stemmed from the observations of the psychotomimetic effects of *N*-methyl-D-aspartate (NDMA) receptor antagonists ketamine and phencyclidine (PCP) in healthy individuals and their ability to exacerbate schizophrenia symptoms in the clinically ill (Hammond et al., 2014).

PCP was first discovered in the 1920s as a novel surgical anaesthetic. Despite being relatively easy to produce and possessing very promising anaesthetic properties, its medicinal use was short-lived due to the profound adverse effects; patients recovering from surgery often manifested with perceptual disturbances, delusional thinking, impaired speech, agitation, and disordered behaviour (Luby et al., 1959). However, some of its less-debilitating effects, such as reduced inhibition, state euphoria and increased response to audio-visual stimulation (i.e., music and light/ colours) allowed it to thrive as a popular recreational drug under the street name ‘angel dust’ (Bertron, Seto and Lindsley, 2018). Regular angel dust enthusiasts were repeatedly misdiagnosed with schizophrenia because the effects produced by long-term PCP use are clinically indistinguishable from those experiencing a first psychotic episode (Allen and Young, 1978; John H. Krystal et al., 1994). These remarkably parallel experiences between schizophrenia patients and those who reach for angel dust recreationally made PCP of major interest to neuroscientists.

As presented in **Figure 4-1**, the principal pharmacological action of PCP is the non-competitive antagonism of NMDA glutamate receptors (Anis et al., 1983). However, the antagonising potential for several other ion channels including the Nav and Kv channels (Vincent et al., 1983; ffrench-Mullen and Rogawski, 1989), and nicotinic acetylcholine receptors (Oswald, Bamberger and McLaughlin, 1984), as well as several other membrane

proteins, including the opioid σ-receptors (Contreras et al., 1988), and noradrenaline and dopamine transporters have been reported – although to a much lesser extent (Garey and Heath, 1976; Pubill et al., 1998). The action of PCP at these sites may partially contribute to its distinct psychotomimetic profile, considering that those affected demonstrate compromised potassium channel function, elevated dopamine levels in limbic regions, and reduced nicotinic receptor activity in the central nervous system (Morris, Cochran and Pratt, 2005).

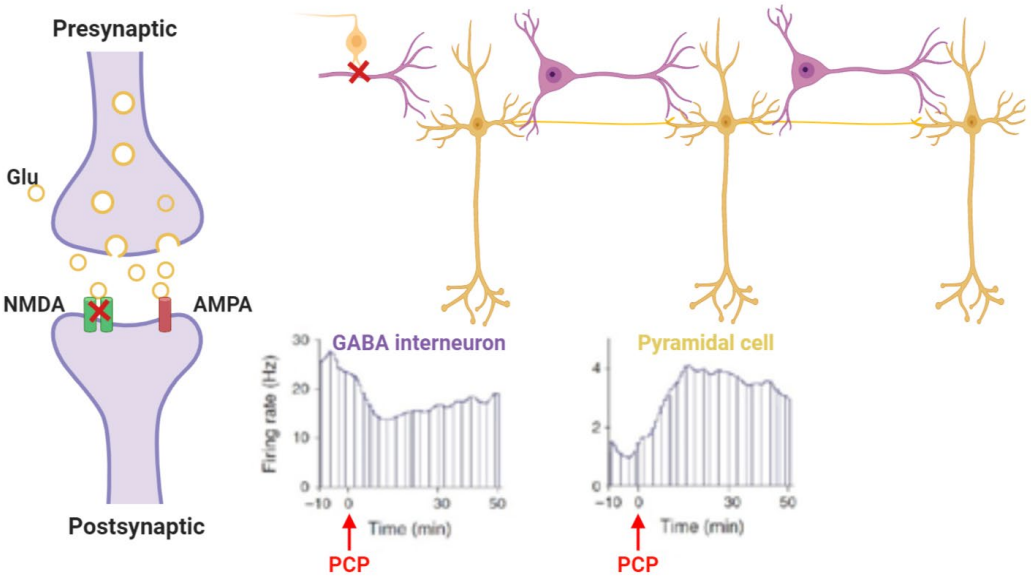

Figure 4-1 Simplified diagram illustrating the pharmacological action of PCP.
PCP selectively antagonises the ionotropic *N*-methyl-D-aspartate (NMDA) receptors which results in a reduced firing rate of γ-aminobutyric acid (GABA) interneurons. Under physiological conditions, GABA interneurons inhibit the activity of excitatory neurons, such as the pyramidal cells of the cortex, hippocampus, or amygdala. This disinhibition results in an increased firing rate of these neurons and affects dopamine homeostasis which contributes to the development of the psychotropic effects experienced by PCP users.

This distinct pharmacological profile of PCP and its effects in humans has naturally led to the use of this agent in animals to investigate which effects may have translational value for the particular symptoms of schizophrenia-spectrum disorders. To date, the behavioural phenotypes, as well as their biomolecular and anatomical correlates in models produced by various treatment regimens, have been well characterised in recent literature (Jones, Watson and Fone, 2011; Castañé, Santana and Artigas, 2015; Winship et al., 2019). For example, acute PCP administration elicits increased ambulation and stereotyped behaviours which are thought to resemble positive symptoms in humans (Kalinichev et al., 2008), and social isolation, which is thought to correlate to negative symptoms (F Sams-Dodd, 1996), and impaired pre-pulse inhibition as well as decreased indices of cognition in rodents (Egerton et al., 2005). However, based on the clinical observations of long-term PCP use, the subchronic and chronic treatments might be used to more faithfully represent the symptoms observed in schizophrenia. That is because repeated or intermittent administration of PCP does not normally induce spontaneous hyperlocomotion but the exposure to subsequent doses results in an exaggerated locomotor response (Scalzo and Holson, 1992; Xu and Domino, 1994; Hanania, Hillman and Johnson, 1999; Fletcher et al., 2005; McLean, Woolley and Neill, 2010), and these effects in animals mimic the early clinical

observations where positive symptoms are present in individuals when PCP is on-board (Luby et al., 1959; Cohen et al., 1962).

Inducing schizophrenia-like state in animals intends to investigate the features of the distinct endophenotypes produced by various treatment regiments rather than attempting to model the disorder as a whole, as classification of the individual behavioural effects of these treatments together with the pathophysiological correlates represent a crucial step towards elucidating the very biological components of the disorder; it also allows to rapidly monitor disease progression that would otherwise be not possible in humans, as well as it enables the development of novel treatment strategies (Winship et al., 2019). However, the lack of consensus within the scientific community regarding a standard model species and strain is an ongoing issue, thus more work is needed in categorising these endophenotypes. For that, the animal models or model candidates must undergo rigorous testing to validate whether the treatment reliably reflects the changes observed in man. This is commonly achieved by seeking to satisfy the validity of face, construct, and prediction (Jones, Watson and Fone, 2011). Face validity refers to the core behavioural symptoms that an animal should mimic, such as stimulant sensitivity, decreased social interaction, and cognitive impairment. The model construct is considered valid when the model presents similar structural, neurochemical, or biomolecular defects to those seen *post-mortem* in humans, such as the

loss of synaptic connectivity, genetic alterations, mesolimbic DA hypofunction, mesocortical DA hyperfunction, or cortical glutamate dysfunction. In this chapter, we will test this triad of face, construct, and predictive validity, and in this context, our findings will be discussed.

4.2 Aims

This study tested the effects of both subchronic and acute PCP treatment on several aspects of animal behaviour and the cerebellar expression of genes of interest in juvenile mice. Specifically, we investigated the effect of subchronic PCP administration on the performance in the open field, and the recognition memory, and the long-term effect of PCP on cerebellar morphology. We also investigated the effects of acute PCP treatment on the performance in the open field, as well as motor coordination and the ability of concomitant administration of haloperidol or clozapine with PCP to reverse these changes.

4.3 Materials and Methods

This study used 56 animals in total. Sixteen animals were used for the subchronic study, and forty animals were used in the acute reversal study. This section will consider each method briefly. For an elaborated description of housing conditions, behavioural setup, tests employed, as

well as tissue harvesting and solutions preparations, please refer back to **Chapter 2.1**.

4.3.1 Drug Treatment

Animals in the subchronic study were randomly selected into two groups:

1. The treatment group was administered with PCP; 5.0 mg/kg b.w. twice a day (total dose 10 mg/ b.w.) for seven days, followed by a seven-day drug-free period.
2. The control group was administered with an equal volume of physiological saline (0.9% NaCl) twice a day for seven days, followed by a seven-day drug-free period.

Animals in the acute reversal study were randomly allocated into four groups of equal size and received a single injection of either:

1. Normal saline (0.9%); or
2. PCP (10 mg/ kg b.w.); or
3. PCP (10 mg/ kg b.w.) + Haloperidol (0.03 mg/kg b.w.); or
4. PCP (10mg/ kg b.w.) + Clozapine (0.003 mg/kg b.w.).

4.3.2 Behaviour tests

The tests performed in both the subchronic study, and the acute reversal study included manual scoring (e.g., rearing, and grooming events, vocalisations, number of droppings), and automated recording (i.e., locomotor activity in the open field). The two cerebellar-specific tests which used manual scoring have been implemented to investigate motor

coordination in the acute reversal study. For detailed descriptions of the test procedures please refer to **Section 2.1.3**.

4.3.3 Animal work

In brief, the animals were sacrificed following the final behaviour test by cervical dislocation, and then decapitated, and brains removed. For quantitative PCR, the frontal cortex and the cerebellum were dissected and snap-frozen in Eppendorf tubes using LN_2. For immunohistochemistry, the dissected cerebellum samples were snap-frozen in OCT medium-filled cryostat blocks. All samples were moved to -20°C short-term storage before processing.

4.3.4 RT-qPCR

Frontal cortex and cerebellum samples were homogenised, and RNA was extracted as described in **Section 2.2**. Complimentary DNA (cDNA) strands were synthesised using a High-Capacity cDNA Reverse Transcription Kit (Cat. 4368814; ThermoFisher Scientific, UK) in a Hybaid thermal cycler (Thermo Scientific, UK). The primer pairs used for amplification of *Grin1*, *Grin2*, and *Grin3* genes are listed in **Table 2-3**. A 10 µM PCR primer mix was prepared separately for each studied gene by diluting 10 µL of forward and reverse primer stock in 980 µL water. A reaction mix was then prepared for each gene by combining the primer mix for each gene with

SYBR green assay reagent and DEPC-treated water. In triplicates, a 96-well plate was loaded with 1 µL of the previously synthesised cDNA and 10 µL of the reaction mixture was added to the corresponding wells. The plates were then sealed and centrifuged using a plate mixer for one minute before being placed in a StepOne Real-time PCR thermocycler (Applied Biosystems, UK). The thermocycler settings are presented in **Section 2.5.4**. Relative gene expression was calculated using the Livak method, as described in **Section 2.5.1**

4.3.5 Immunohistochemistry

Cerebellar sections made previously were fixed in 4% PFA buffer for 10 minutes at 4°C then washed 3 times in PBST at RT, and antigens were retrieved in 20 mM citrate buffer for 20 minutes at 95°C then washed as above. The tissues were permeabilised and non-specific binding sites were blocked with blocking buffer containing BSA and NGS in TBST for 2 hours at RT, then the blocking solution was replaced with diluted anti-Calbindin D28K antibody and incubated for 48 hours at 4°C and washed. The slides were then layered with diluted AlexaFluor®488 secondary antibody and incubated for 2 hours at RT.

4.3.6 Cerebellar measurements

Purkinje Cell Density

The linear densities of Purkinje cells were estimated from images of Calbindin D28K-stained sections taken with x10 objective lens. Each micrograph was imported separately into the software by dragging the image into ImageJ interface. The “cell counter” tool was launched from the “Plugins” menu and each Purkinje cell was counted by clicking on it, and the total cell number in each image was copied to a spreadsheet. Subsequently, the length of Purkinje cell layers was measured by drawing the Purkinje cell layer with a “Segmented line” tool and choosing “Measure” → “Analyze.” For each image, the total Purkinje cell number was divided by the Purkinje cell layer length and the data were expressed as the average cell number per mm length. The density data were populated in IBM SPSS and GraphPad PRISM. The statistical test of choice to compare the control and treated groups was the two-tailed independent t-test or the Mann-Whitney U test of mean ranks, depending on data distribution.

Purkinje Cell Size

Purkinje cell size was estimated from images of Calbindin D28K-stained sections taken with x40 objective lens. The images were imported into ImageJ and the region of interest (ROI) manager was launched from the “Analyze” → “Tools” menu. Purkinje cell somas were selected in each

image using a free-form selection tool, and the cells were added to the ROI manager by clicking 'add.' Measurements of the selected cells were taken by selecting the "Measure" option from the "Analyze" menu. A new "Results" window opened, from which the column including the areas of the cell somas was copied to a spreadsheet. The area measurements were used to calculate the cell body diameter by employing the formula of a hypothetical circle:

$A = \pi r^2$, thus

$r = \sqrt{\frac{A}{\pi}}$, and

$\emptyset = 2r$, where: A = area; r = radius; and Ø = diameter.

The calculated values were populated in GraphPad PRISM. The statistical test of choice to compare the control and treated samples was the two-tailed unpaired t-test or the Mann-Whitney U test of mean ranks, depending on data distribution.

Cerebellar Cortex Thickness

Cerebellar cortical thickness was measured in the granular cell layer and the molecular layer using ImageJ. The images were imported, and a straight-line tool was used to draw a line distal from the Purkinje cell toward the outer molecular layer boundary, and distal from Purkinje cell toward the granular cell layer boundary, and the distance measured by selecting "Measure" from the "Analyze" menu. The measurements were populated in

GraphPad PRISM for analysis. The statistical approach involved the two-tailed unpaired t-test or Mann-Whitney U test, depending on data distribution.

4.4 Results

4.4.1 Effect of subchronic PCP on mouse behaviour

We employed a battery of behaviour tests an analysed several parameters to test the face of the model. Although we found that PCP treatment evoked audible vocalisations in majority of the animals, we were not able to record and therefore distinguish the frequencies at which the calls were made. Majority of meaningful 'conversations' between rodents, such as mating calls or sounds emitted during distinct affective states are expressed at ultrasonic frequencies (Knutson, Burgdorf and Panksepp, 2002; Portfors, 2007; Portfors and Perkel, 2014); therefore, these findings will not be considered, and are included in the **Appendix A3** instead. The reader will also find with several other findings, including animal weight analysis and number of droppings produced.

PCP induces changes in normal grooming and rearing.

Our first analysed observation during locomotor activity measurements were the counts of grooming and rearing events in each 10-minute session (**Table 4-1**; **Figure 4-2**). Statistically significant differences in the number of grooming events in the PCP group was found across time points ($\chi^2_{(4)}$ = 19.6, p = .0007, Friedman test). A post-hoc analysis with Dunn's multiple comparison revealed that the number of grooming events was significantly higher on day 1 compared to baseline (5.38 ± 0.26 vs. 2.25 ± 0.25; Z = 3.95, p = .0008). We also found statistically significant difference in the frequency of rearing among time points within the PCP group ($\chi^2_{(4)}$ = 25.54, p = .0001; Friedman test), and the Dunn's multiple comparison analysis revealed that the mice reared more frequently on day 4 (9.88 ± 0.48 vs. 5.00 ± 0.38; Z = 2.85, p = .04) compared to baseline, and gradually subsided on day 14 (4.63 ± 0.42 vs. 5.00 ± 0.38; Z = 3.08, p = 0.02).

Table 4-1 Grooming and rearing events in the PCP group during subchronic treatment.

	Grooming events
Comparison	**Mean ± SEM, Significance^**
Baseline vs. Day 1	2.25 ± 0.25 vs. 5.38 ± 0.26; $p < .0001$
Baseline vs. Day 4	2.25 ± 0.25 vs. 3.88 ± 0.30; $p = .3280$
Baseline vs. Day 8	2.25 ± 0.25 vs. 4.63 ± 0.53; $p = .0914$
Baseline vs. Day 14	2.25 ± 0.25 vs. 3.25 ± 0.45; $p > .0999$
	Rearing events
Comparison	**Mean ± SEM, Significance^**
Baseline vs. Day 1	5.00 ± 0.38 vs. 3.13 ± 0.30; $p = .9688$
Baseline vs. Day 4	5.00 ± 0.38 vs. 9.88 ± 0.48; $p = .0443$
Baseline vs. Day 8	5.00 ± 0.38 vs. 6.63 ± 0.60; $p = .9999$
Baseline vs. Day 14	5.00 ± 0.38 vs. 4.63 ± 0.42; $p > = .0999$
Day 4 vs. Day 14	9.88 ± 0.48 vs. 4.63 ± 0.42; $p = .0205$

^, Dunn's correction within PCP groups. Values are mean ± SEM. N = 8

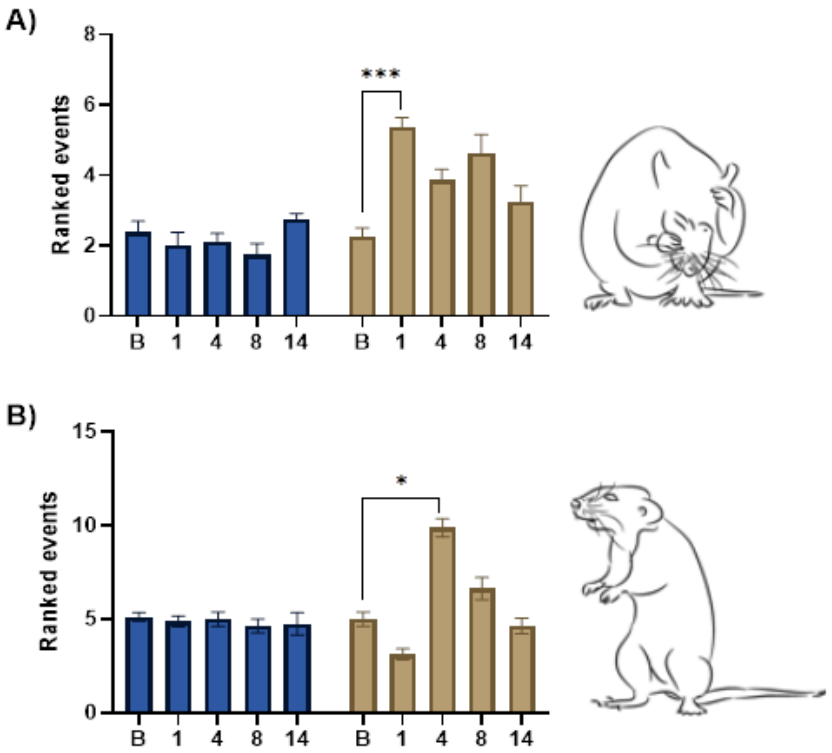

Figure 4-2 Grooming and rearing behaviours recorded across the study duration (please refer to Figure 2-1).

The graphs in A and B show mean ranks ± SEM of grooming and rearing frequencies, respectively, listed in Table 3-3. *, *p* = .04; ***, *p* = .0001 (Friedman test with Dunn's correction); N = 8 in each group. The images in A and B illustrate grooming and rearing, respectively.

Effects of PCP on general locomotor activity.

The locomotor activity data were subjected to analysis using a two-way mixed ANOVA (2x5) with treatment (2 levels; vehicle and PCP) as the between-subjects independent variables, and time points (5 levels) as the within-subjects independent variable to test the effect of treatment, time, and the interaction between them on each of the parameters examined at baseline, day 1, day 4, day 8, and day 14 of the course (**Table 4-2**).

The analysis revealed a significant effect of time on motion/ trial duration ($F_{(2.82,\ 39.46)}$ = 7.86, p < .001; Greenhouse-Geisser correction), and a significant effect of interaction between the treatment and the time on motion/ trial duration ($F_{(2.82,\ 39.46)}$) = 7.32, p = .01; Greenhouse-Geisser correction), and further univariate test on the simple main effects of treatment on motion / total time within each time point showed that the PCP-treated animals were statistically significantly less active on day 1 compared to control animals (0.42 ± 0.03 vs. 0.65 ± 0.02; $F_{(1,\ 14)}$ = 31.03, p < .0001), and the PCP-treated animals were also significantly less active on day 8 compared to the control animals (0.58 ± 0.02; $F_{(1,\ 14)}$ = 8.94, p = .01), whereas no statistically significant difference in overall mobility between the two groups was detected on baseline, day 4, nor day 14 (**Figure 4-3**A).

Further two-way ANOVA with the same design revealed a significant effect of time on both the travel distance ($F_{(2.34,\ 32.70)}$ = 7.67, p = 0.001; Greenhouse-Geisser correction), and on travel speed ($F_{(2.32,\ 32.46)}$ = 7.33, p < 0.005; Greenhouse-Geisser correction), and a significant effect of interaction between treatment and time on both the travel distance ($F_{(2.34,\ 32.70)}$ = 4.85, p < 0.05; Greenhouse-Geisser correction) and on travel speed ($F_{(2.32,\ 32.46)}$ = 4.83, p < 0.05; Greenhouse-Geisser correction).

A subsequent univariate test on the simple main effect of treatment on the two variables within each time point revealed that the PCP-treated

animals travelled significantly less on day 1 compared to control animals (16.2 ± 1.9 cm vs. 27.8 ± 4.0; $F_{(1, 70)} = 9.59$, $p < 0.005$) but travelled significantly more on day 4 compared to control animals (52.6 ± 7.9 cm; $F_{(1, 70)} = 5.91$, $p < 0.05$), which subsided on day 8 ($F_{(1, 70)} = 3.83$, $p > 0.05$) and day 14 ($F_{(1, 70)} = 0.03$, $p > 0.05$) as shown in **Figure 4-3**B.

Similarly, the PCP-treated animals travelled significantly slower on Day 1 compared to control animals (2.90 ± 0.35 cm/s vs. 6.37 ± 0.35 cm/s; $F_{(1, 70)} = 9.59$, $p < 0.005$) but travelled significantly faster on day 4 compared to control animals (9.28 ± 1.38 cm/s; $F_{(1, 70)} = 5.89$, $p < 0.05$), which also subsided on day 8 ($F_{(1, 70)} = 3.82$, $p > 0.05$) and Day 14 ($F_{(1, 70)} = 0.03$, $p > 0.05$) as depicted in **Figure 4-3**C.

We also observed stereotyped circling behaviour, measured by the number of rotations made in each session (**Table 4-3**; **Figure 4-4**). The analysis detected a significant effect of time on rotation counts ($F_{(4, 56)} = 12.88$, $p < 0.001$), and a significant effect of interaction between time and treatment on rotation counts ($F_{(4, 56)} = 13.48$, $p < 0.001$). The univariate analysis on the simple main effects of treatment on rotation counts within each time point showed that the animals in the PCP group made significantly more rotations on day 1 (25.50 ± 9.64 vs. 12.38 ± 3.07; $F_{(1, 70)} = 18.06$, $p < 0.001$) and day 4 (39.75 ± 10.25 vs. 15.25 ± 5.90; $F_{(1, 70)} = 62.92$,

$p < 0.001$) compared to the control animals, which subsided on day 8 ($F_{(1, 70)} = 0.02$, $p > 0.05$) and day 14 ($F_{(1, 70)} = 1.02$, $p > 0.05$).

Table 4-2 Summary of PCP effects on locomotor activity in the open field

			Travel distance (m)
	Vehicle (N = 8)	**PCP (N = 8)**	**Significance**
Baseline	27.8 ± 4.0	30.4 ± 4.0	$p = .985$
Day 1	36.0 ± 1.9	16.2 ± 1.9	$p < .001$
Day 4	37.1 ± 7.9	52.6 ± 7.9	$p = .167$
Day 8	41.1 ± 2.4	28.6 ± 2.4	$p = .010$
Day 14	45.1 ± 3.9	44.0 ± 3.9	$p = .712$
			Travel speed (cm/ s)
	Vehicle (N = 8)	**PCP (N = 8)**	**Significance**
Baseline	4.91 ± 0.69	5.36 ± 0.69	$p = .683$
Day 1	6.37 ± 0.35	2.90 ± 0.35	$p = .003$
Day 4	6.56 ± 1.38	9.28 ± 1.38	$p = .018$
Day 8	7.25 ± 0.42	5.06 ± 0.42	$p = .054$
Day 14	7.78 ± 0.68	7.59 ± 0.68	$p = .860$
			Motion time/ trial duration
	Vehicle (N = 8)	**PCP (N = 8)**	**Significance**
Baseline	0.61 ± 0.03	0.61 ± 0.04	$p = .985$
Day 1	0.65 ± 0.02	0.42 ± 0.03	$p < .001$
Day 4	0.63 ± 0.05	0.74 ± 0.06	$p = .167$
Day 8	0.67 ± 0.02	0.58 ± 0.02	$p = .010$
Day 14	0.69 ± 0.03	0.70 ± 0.02	$p = .712$

Values represent mean ± SEM.

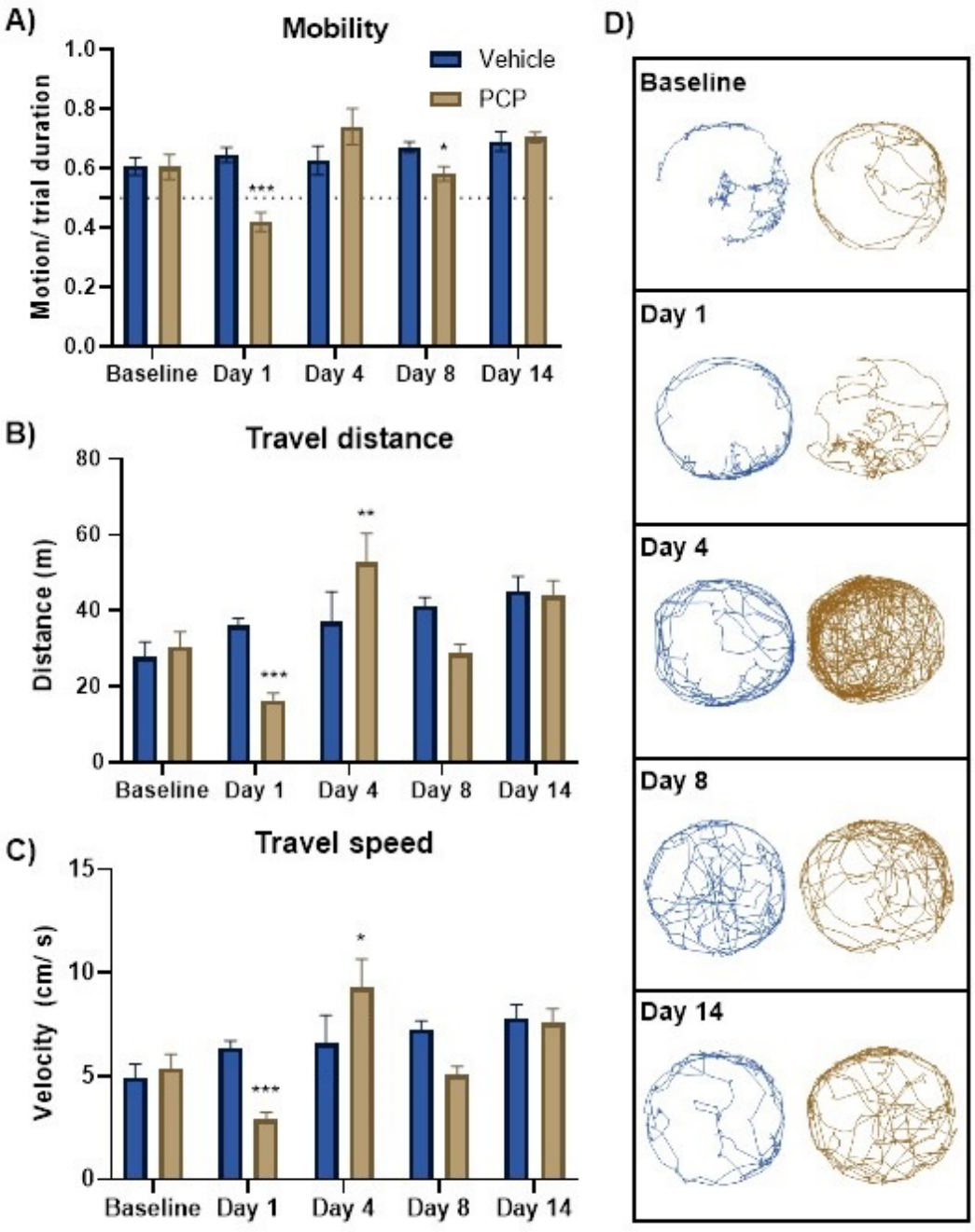

Figure 4-3 Effect of subchronic PCP treatment on the mouse locomotor activity. Graphs show mean values ± SEM. *, $p < .05$; ** $p < .01$; ***, $p < .001$ (Two-way mixed ANOVA with pairwise comparison); N = 8 in each group. In A, the horizontal dotted line represents even inclination to movement and station.

Table 4-3 Comparison of rotation counts between the vehicle and PCP groups.

			Rotation counts
	Vehicle (N = 8)	**PCP (N = 8)**	**Significance**
Baseline	13.38 ± 3.96	14.75 ± 3.69	p = .6581
Day 1	12.38 ± 3.07	25.50 ± 9.64	p < .0001
Day 4	15.25 ± 5.90	39.75 ± 10.25	p < .0001
Day 8	14.37 ± 4.00	14.00 ± 4.47	p = .9043
Day 14	17.13 ± 7.36	14.00 ± 4.47	p = .3154

Values represent mean ± SEM.

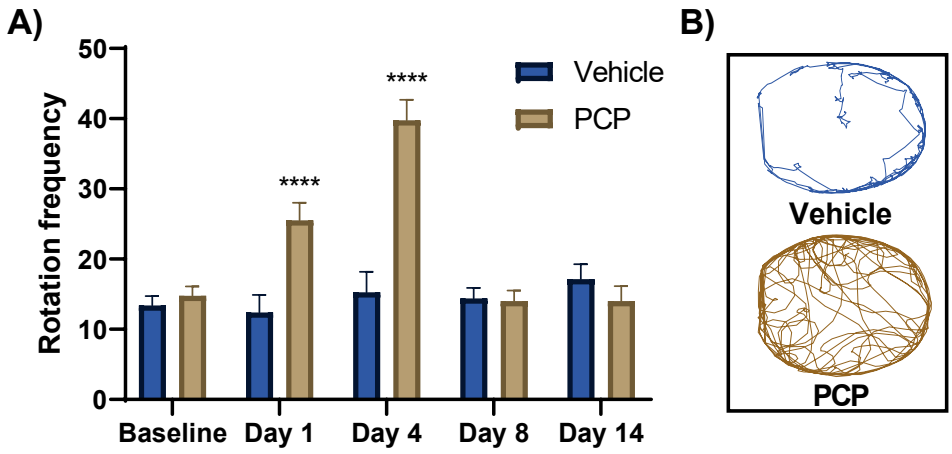

Figure 4-4 Mouse stereotypical circling behaviours during PCP treatment.
The graph (A) shows increased rotation counts in the PCP-treated animals on days 1 and 4. Bars show mean values ± SEM. ****, p = .0001 (Two-way mixed ANOVA with pairwise comparison); N = 8 in each group. In B, representative trajectories from a vehicle- and a PCP-treated animal on day 1.

Lastly, we investigated the effects of PCP on the time the animals spent in the centre zone and the periphery of the test arena. The two-way mixed ANOVA with the same design showed no significant effect of time ($F_{(2.85, 39.89)}$ = 2.56, p > 0.05), the effect of the treatment ($F_{(1, 14)}$ = 2.91, p > 0.05), or the

effect of interaction between treatment and time on the time spent in the centre zone ($F_{(2.85, 39.89)}$ = 2.45, p > 0.05). While the two-way mixed ANOVA also did not detect a significant effect of time on the time spent in the outer zone ($F_{(4, 56)}$ = 2.08, p > 0.05), there was a significant effect of the treatment on the time spent in the outer zone ($F_{(1, 14)}$ = 5.10, p < 0.05), and a significant effect of interaction between the treatment and time on the time spent in the outer zone ($F_{(4, 56)}$ = 3.19, p < 0.05) within the PCP group (**Figure 4-5**; **Table 4-4**). Subsequent univariate test on the simple effect of time within the PCP group showed a significant difference in the time spent in the centre zone among all time points ($F_{(4, 70)}$ = 3.99, p < 0.01). The pairwise comparison shows that PCP treated animals spent significantly less time in the centre zone on day 1 compared to baseline (311.2 ± 60.2 s vs. 434.5 ± 28.4 s; p < 0.01) and remained low on day 4 (348.1 ± 48.3 s; p < .03) and then subsided on day 8 (443.6 ± 25.2; p > 0.05) and day 14 (447.7 ± 17.0; p > 0.05). Univariate test on the simple effect of treatment within each time point shows on day 1 and day 4, PCP treated animals spent significantly less time in the periphery than the control animals ($F_{(1, 70)}$ = 8.48, p < 0.01, and $F_{(1, 70)}$ = 5.14, p < 0.05, respectively). At other time points, there is no significant difference in time in the periphery between 2 groups of animals (p > 0.05).

Table 4-4 Summary of time spent in the centre and the outer zone of the test arena, and between-group comparison at each time point. Values represented as mean ± SEM.

			Time in centre zone (s)
	Vehicle (N = 8)	**PCP (N = 8)**	**Significance^**
Baseline	73.1 ± 27.9	132.5 ± 28.5	$p > .005$
Day 1	126.4 ± 43.4	247.8 ± 57.3	$p > .005$
Day 4	115.8 ± 34.8	216.1 ± 44.5	$p > .005$
Day 8	157.3 ± 25.2	121.5 ± 25.9	$p > .005$
Day 14	193.5 ± 14.9	132.2 ± 48.0	$p > .005$
			Time in outer zone (s)
	Vehicle (N = 8)	**PCP (N = 8)**	**Significance&**
Baseline	493.6 ± 26.8	434.5 ± 28.4	$p = .190$
Day 1	441.2 ± 22.7	311.2 ± 60.2	$p = .005$
Day 4	449.2 ± 20.6	348.1 ± 48.3	$p = .026$
Day 8	413.0 ± 21.9	443.6 ± 25.2	$p = .495$
Day 14	390.3 ± 11.7	447.7 ± 17.0	$p = .202$

^, Univariate analysis of $\log_{10}$-transformed data; &Original data

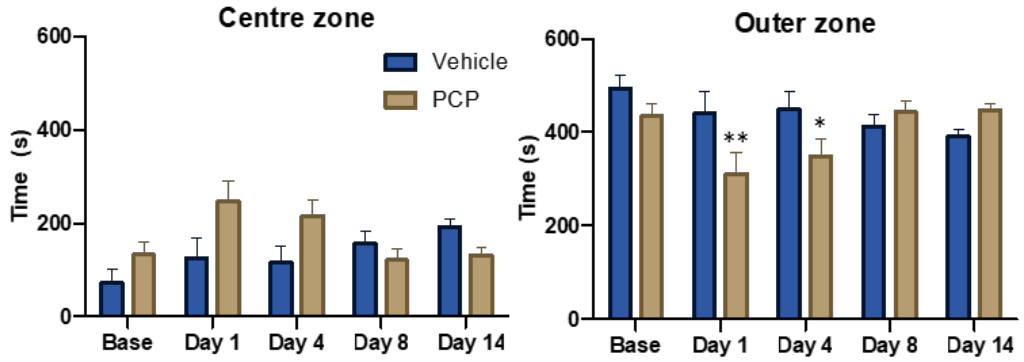

Figure 4-5 Effect of PCP on zonal preference in the locomotor test arena.

The average time spent in the centre zone (left) and in the periphery (right) of the arena during a 10-minute exploration. Bars represent mean ± SEM. *, $p < .05$; **, $p < .01$ (Univariate test on the simple main effect of treatment within each time point); N = 8 in each group.

Effect of PCP on recognition memory

The analysis of mouse performance in the two-object novel object recognition test showed no statistically significant difference in retention index between the vehicle- and PCP-treated animals at baseline ($t_{(14)}$ = 0.90, p = .28), on day 1 ($t_{(12)}$ = 0.53, p = .61), or on day 14 ($t_{(14)}$ = 0.30, p = .77; unpaired t-test). Surprisingly, the control animals at each time point did not favour the novel object over the familiar object when challenged (**Table 4-5**; **Figure 4-6**).

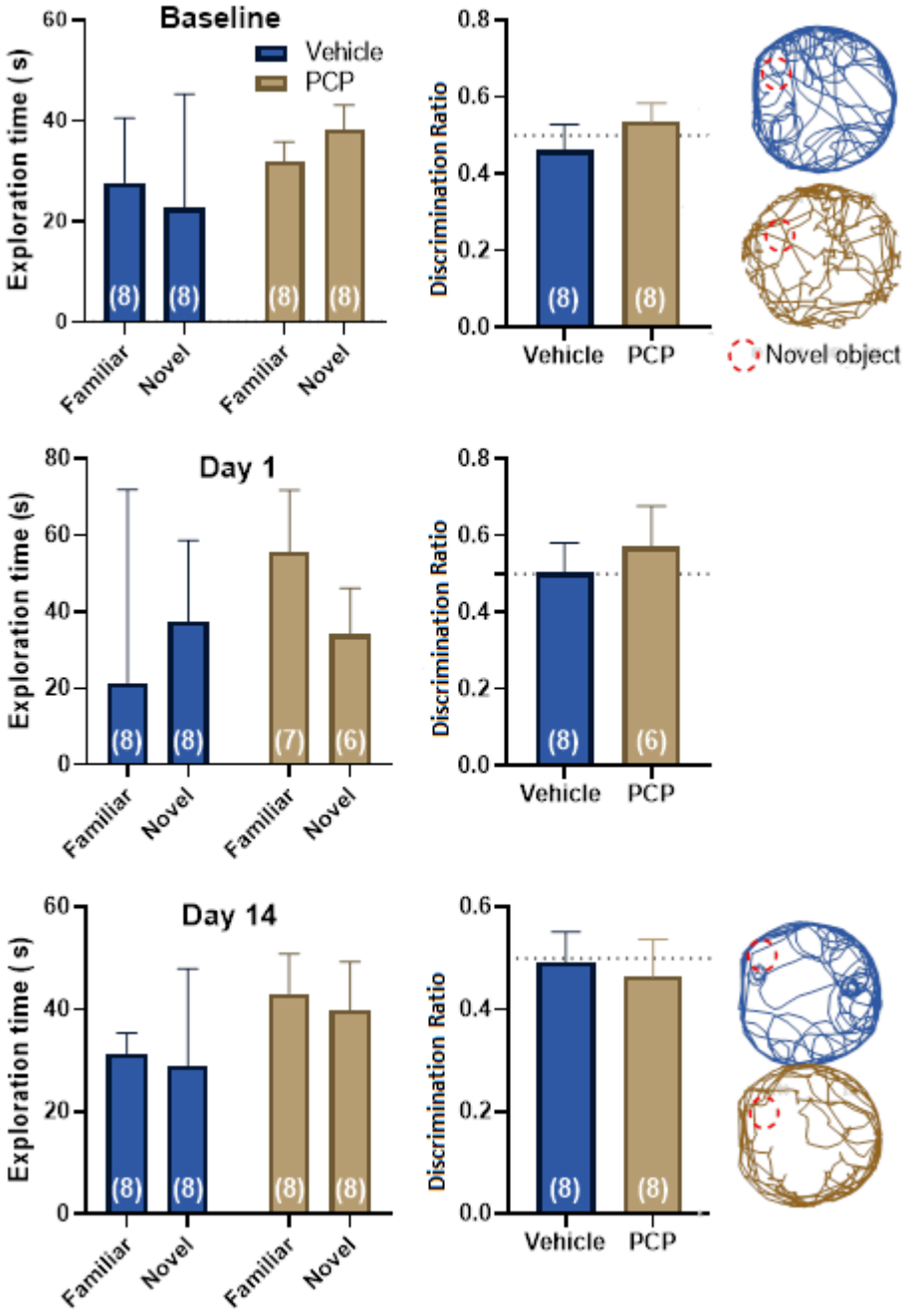

Figure 4-6 Effect of PCP on performance in novel object recognition test.

Graphs on the left show exploration times of familiar and novel object in both treatment groups. For the exploration times, the graphs show median ± IQR for the vehicle group and mean ± SEM for the PCP group. Discrimination ratio show mean ± SEM; statistical significance was tested using unpaired t-test. The number in each column indicate the number of animals used in that group.

Table 4-5 Comparison of NOR test results between vehicle- and PCP-treated animals.

	Discrimination Ratio	
	Vehicle vs. PCP	**Significance**
Baseline	0.46 ± 0.07; N = 8 vs. 0.54 ± 0.05; N = 8	p = .3838
Day 1	0.50 ± 0.08; N = 8 vs. 0.57 ± 0.11; N = 6	p = .6069
Day 14	0.49 ± 0.06; N = 8 vs. 0.46 ± 0.07; N = 8	p = .7691

4.4.2 Regulation of NMDA receptor subunit genes in the subchronic PCP model

Another important component in testing an animal model is validating the model construct by investigating several variables such as the biochemical alterations present in the disease. As introduced in **Section 1.1.3**, there is mounting evidence from both animal and post-mortem human studies supporting dysfunction of NMDAR subtypes. We therefore applied real-time quantitative PCR to investigate the lasting effect of PCP on the expression of genes coding for NMDA receptor subunits NR1, NR2B, and NR2C in the frontal cortex and in the cerebellum after the washout period.

The PCP treatment induced differential regulation of these genes in the frontal cortex and the cerebellum (**Table 4-6**; **Figure 4-7**). In the frontal cortex the *Grin2b* gene was significantly downregulated in the PCP animals compared to controls (1.01 ± 0.06 vs. 0.85 ± 0.07; p = .0468), and a non-significant reduction in downregulation of *Grin2a* gene was observed (1.04 ± 0.10 vs. 0.83 ± 0.24; p = .0756), whereas no effect on *Grin2c* expression was observed. On the contrary, the *Grin1 g*ene was statistically significantly upregulated in the cerebellum of PCP-treated animals (1.41 ± 0.09 vs. 1.02

± 0.25; *p* = .0044). At the same time, no significant dysregulation was observed for either *Grin2b* or *Grin2c*.

Table 4-6 Comparison of RT-qPCR data for NMDA receptor genes between vehicle- and PCP-treated animals in frontal cortex and cerebellum.

		Frontal cortex
Gene	**Vehicle vs. PCP**	**Significance**
Grin1	1.04 ± 0.10, N = 8 vs. 0.83 ± 0.24, N = 7	$t_{(13)}$ = 1.525, *p* = .0756
Grin2b	1.01 ± 0.06, N = 8 vs. 0.85 ± 0.07, N = 8	$t_{(13)}$ = 1.810, *p* = .0468
Grin2c	1.06 ± 0.14, N = 7 vs. 1.21 ± 0.21, N = 7	$t_{(12)}$ = 0.607, *p* = .2776
		Cerebellum
Gene	**Vehicle vs. PCP**	**Significance**
Grin1	1.02 ± 0.25, N = 8 vs. 1.41 ± 0.09, N = 8	$t_{(13)}$ = 3.037, *p* = .0044
Grin2b	1.03 ± 0.24, N = 7 vs. 1.21 ± 0.13, N = 7	$t_{(14)}$ = 1.072, *p* = .1510
Grin2c	1.05 ± 0.13, N = 8 vs. 0.87 ± 0.08, N = 8	$t_{(14)}$ = 1.191, *p* = .1268

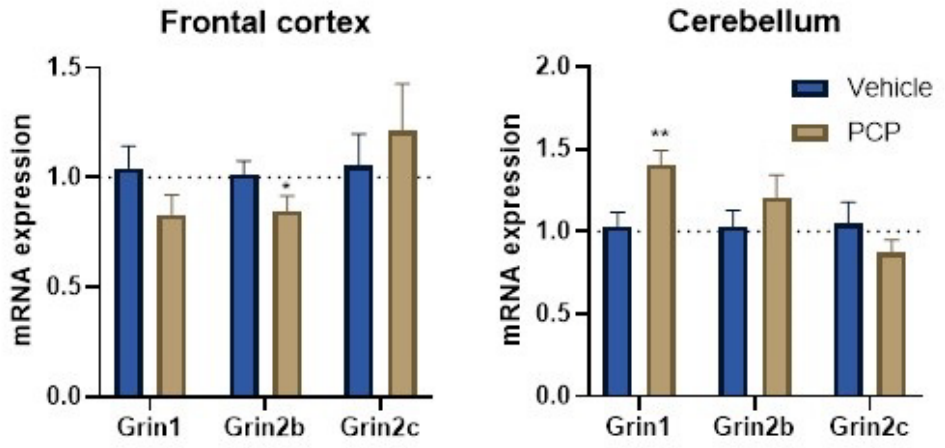

Figure 4-7 Regulation of *N*-methyl-D-aspartate receptor subunit genes expression. The graphs show an overall inverted trend of dysregulation of the 3 NMDA receptor subunit genes in the cerebellum and fontal cortex. Bars represent mean ± SEM. *, p < .05; **, *p* < .01 (unpaired t-test). N indicated in table 4-6.

4.4.3 Effect of subchronic PCP treatment on the cerebellum

Another component in validating the construct of an animal model may involve investigating the morphological correlates, and we, therefore, studied the effect of current PCP treatment on several features of the cerebellum. As mentioned in **Section 1.3.2**, cerebellar PCs are the most vulnerable type of neurons in the cerebellum; by using a PC-specific marker Calbindin D28K as a guide to differentiate PCs from other neuronal cell populations residing nearby (**Figure 4-8**) we examined whether the density and size of the Purkinje cells are affected by the subchronic PCP treatment, and the difference in the thickness of cerebellar cortex between the two groups was also investigated (**Figure 4-9**, **Table 4-7**).

Here we found that the linear cell density of the PCs was similar in the PCP-treated animals and the control animals (14.00 ± 0.84 vs. 15.01 ± 0.53; $p = .7949$). The PC size, however, was found significantly lower in the PCP group ($p < .0001$), with observably smaller average PC soma diameter in the PCP group compared to the control animals (21.16 ± 0.13 μm vs. 21.96 ± 0.14 μm). Further analysis revealed that this difference was the most significant in the right hemisphere ($p < .0001$), and then the vermis ($p = .0244$), whereas no change was observed in the left lateral hemisphere. We also saw a significant difference in cerebellar cortical thickness between the two groups ($p < .0001$), where the PCP-treated animals had a lower

cortical thickness compared to the control animals (155.5 ± 1.64 µm vs. 167.1 ± 2.38 µm). These observations were most significant in the vermis ($p < .0001$), followed by the right ($p = .0077$) and the left ($p = .0045$) cerebellar hemisphere.

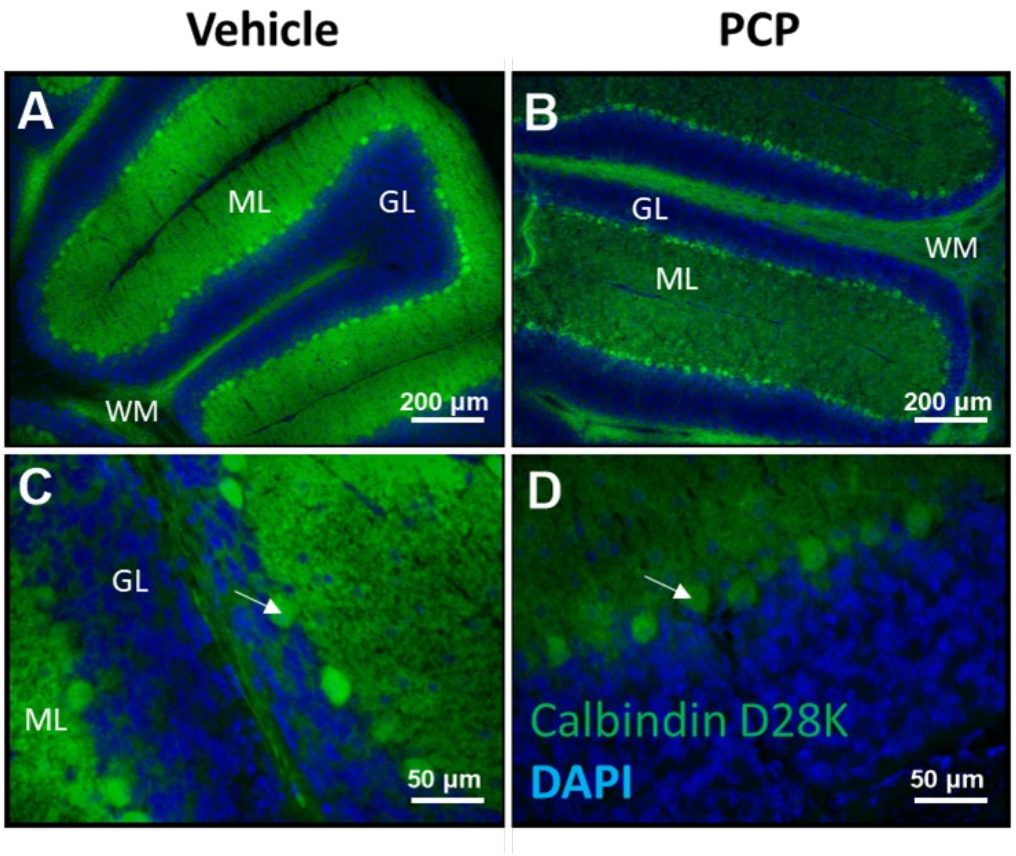

Figure 4-8 Micrograph images showing Purkinje cells in a section of cerebellar vermis.

PCs (green) were differentiated using anti-CalbindinD28 antibody. The olive-shaped PC soma (arrow) and dense dendritic trees extending into the ML are clearly visible. Nuclei (blue) were counter-stained using DAPI. Abbreviations: GL, granular cell layer; PC, Purkinje cell; ML, molecular layer; WM, white matter.

Table 4-7 Summary of the effects of PCP on cerebellar features.

		Purkinje cell density (count/ mm)
	Vehicle vs. PCP	**Significance**
Overall	15.01 ± 0.53, N = 27 vs. 14.78 ± 0.84, N = 27	$t_{(52)} = 0.26$, $p = .7949$
Left hemisphere	11.84 ± 0.85, N = 9 vs. 7.98 ± 1.10, N = 9	$t_{(16)} = 0.69$, $p = .4998$
Vermis	11.32 ± 0.99, N = 9 vs. 9.01 ± 1.63, N = 9	$t_{(16)} = 0.92$, $p = .3737$
Right hemisphere	10.63 ± 0.97, N = 9 vs. 10.03 ± 0.88, N = 9	$t_{(16)} = 1.57$, $p = 0.14$
		Purkinje cell soma diameter (µm)
	Vehicle vs. PCP	**Significance[$]**
Overall	21.96 ± 0.14, n = 337 vs. 21.16 ± 0.13, n = 389	$Z = 4.18$, $p < .0001$
Left hemisphere	20.99 ± 0.28, n = 112 vs. 16.00 ± 0.23, n = 129	$Z = 1.05$, $p = .2944$
Vermis	21.66 ± 1.97, n = 112 vs. 21.03 ± 2.45, n = 139	$Z = 2.26$, $p = .0244$
Right hemisphere	23.23 ± 2.43, n = 113 vs. 21.08 ± 2.31, n = 121	$Z = 6.91$, $p < .0001$
		Cortical thickness (µm)
	Vehicle vs. PCP	**Significance**
Overall	167.1 ± 2.38, n = 78 vs. 155.5 ± 1.64, n = 104	[$]$Z = 4.01$, $p < .0001$
Right hemisphere	168.8 ± 5.96, n = 16 vs. 156.7 ± 2.78, n = 21	$t_{(81)} = 2.77$, $p = .0077$
Vermis	170.4 ± 3.51, n = 33 vs. 158.8 ± 2.56, n = 50	[$]$Z = 6.35$, $p < .0001$
Right hemisphere	162.5 ± 3.77, n = 29 vs. 149.7 ± 2.74, n = 33	[^]$U = 279$, $p = .0045$

[$]Z-test; [^]Mann-Whitney U test.

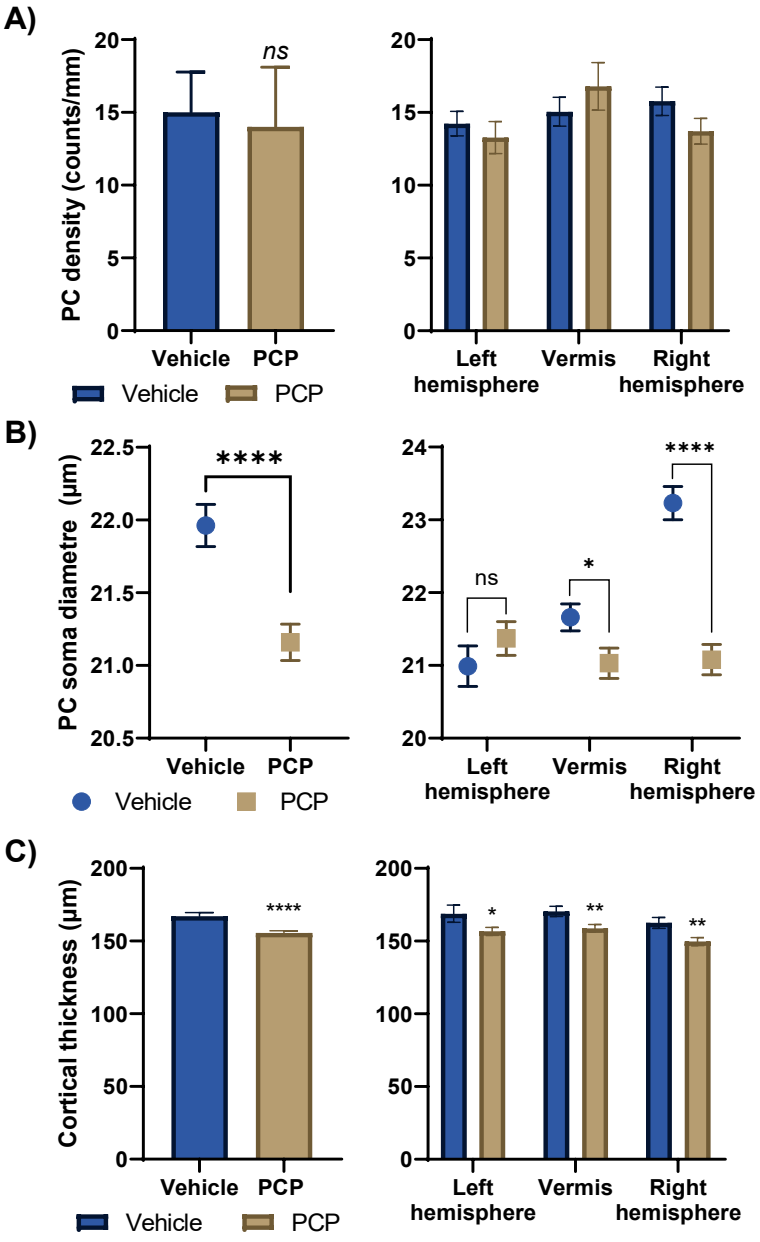

Figure 4-9 Effect of PCP on morphological features of the cerebellum.

Subchronic PCP induced lasting changes in the cerebellum 7 days after treatment. Although there was no overall effect on Purkinje cell number (A), the PCP animals had significantly smaller Purkinje cell soma (B) in the vermis and right cerebellar hemisphere. Significant reduction in cortical thickness was observed in both lateral hemispheres and the vermis (C). Bars represent mean ± SEM. *, $p < .05$; **, $p < .01$; ***, $p < .001$; ****, $p < .0001$; ns, not statistically significant (unpaired t-test). N indicated in table 4-7.

4.4.4 Effects of acute concomitant antipsychotic treatment on PCP-induced behavioural changes

The final part (and perhaps the most important one!) in testing animal models is the value they present for developing novel treatments. For that, the model should have a therapeutic response similar to that in human. As mentioned in **Section 1.1.4**, haloperidol (HAL) and clozapine (CLZ) are two commonly used antipsychotics. We therefore tested in another experiment whether a concomitant acute administration of these compounds with PCP may attenuate the behavioural alterations observed on day 1 in our subchronic study. Here, forty animals were randomly allocated into four treatment groups of equal group sizes (i.e., N = 10 per group).

HAL and CLZ normalise PCP-exacerbated grooming but only CLZ attenuates PCP-exacerbated rearing.

Kruskal-Wallis test detected significant differences in mean ranks of grooming ($\chi^2_{(3)}$ = 29.40, p < .0001) and rearing ($\chi^2_{(3)}$ = 25.36, p < .0001) events between treatment groups (**Table 4-8**; **Figure 4-10**). Dunn's post-hoc comparison further suggested that the grooming frequency increased significantly in the PCP group compared to saline group (5.80 ± 0.46 vs. 1.90 ± 0.23; Z = 5.33, p < .0001). Co-administration of PCP+HAL did not reverse the PCP effect (4.20 ± 0.25 vs 5.80 ± 0.46, p = .2940), and the grooming events remained significantly higher compared to SAL controls

(4.20 ± 0.25 vs. 1.90 ± 0.2; Z = 3.36, p = .0047). Simultaneously, co-administration of PCP+CLZ significantly reduced the PCP effect on grooming events (3.60 ± 0.27 vs. 5.80 ± 0.46; Z = 2.93, p = .0204).

Table 4-8 Summary of grooming and rearing in the acute study.

	Grooming
Comparison	**Mean ± SEM, Significance^**
SAL vs. PCP	1.90 ± 0.23 vs. 5.80 ± 0.46, $p < .0001$
SAL vs. PCP + HAL	1.90 ± 0.23 vs. 4.20 ± 0.25, $p = .0047$
SAL vs. PCP + CLZ	1.90 ± 0.23 vs. 3.60 ± 0.27, $p = .0985$
PCP vs. PCP + HAL	5.80 ± 0.46 vs. 4.20 ± 0.25, $p = .2940$
PCP vs. PCP + CLZ	5.80 ± 0.46 vs. 3.60 ± 0.27, $p = .0204$
PCP+HAL vs. PCP + CLZ	4.20 ± 0.25 vs. 3.60 ± 0.27, $p > .9999$
	Rearing
Comparison	**Mean ± SEM, Significance^**
SAL vs. PCP	1.78 ± 0.43 vs. 7.40 ± 0.43, $p = .0502$
SAL vs. PCP + HAL	1.78 ± 0.43 vs. 1.43 ± 0.20, $p = .8361$
SAL vs. PCP + CLZ	1.78 ± 0.43 vs. 1.14 ± 0.14, $p = .3028$
PCP vs. PCP + HAL	7.40 ± 0.43 vs. 1.43 ± 0.20, $p = .0004$
PCP vs. PCP + CLZ	7.40 ± 0.43 vs. 1.14 ± 0.14, $p < .0001$
PCP+HAL vs. PCP + CLZ	1.43 ± 0.20 vs. 1.14 ± 0.14, $p > .9999$

^Dunn's multiple comparison; N = 10 in each group.

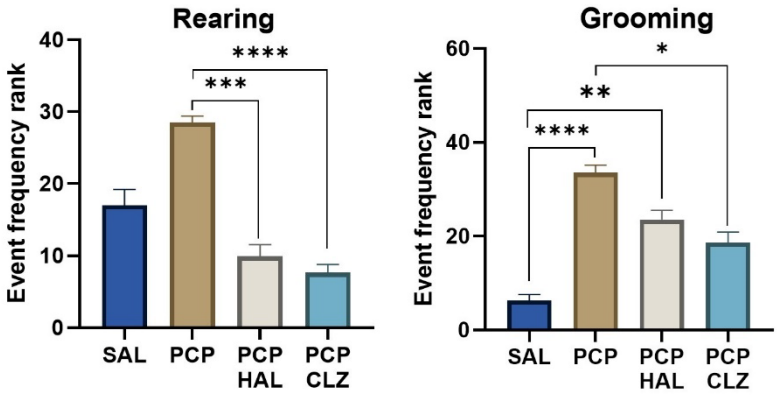

Figure 4-10 Effect of antipsychotics on acute PCP-enhanced grooming and rearing. On the left, rearing is reduced with HAL and CLZ. On the right, grooming is reduced with CLZ only. Bars show mean ranks ± SEM. *, $p < .05$; **, $p < .01$; ***, $p < .001$; ****, $p < .0001$ for Dunn's multiple comparison; N = 10 in each group.

HAL and CLZ attenuate PCP-induced stereotypical behaviours but exert no effect on PCP-induced changes in locomotor activity.

We found several effects of PCP administered concomitantly with HAL or CLZ on general locomotor activity, which are summarised in **Table 4-9**. First, we found a statistically significant difference between the treatment groups in travel distance and in travel speed ($F_{(3, 36)} = 14.21$, $p = .0001$; one-way ANOVA), and a post-hoc analysis with Tukey's multiple comparison test showed that the PCP-treated animals travelled significantly less (13.43 ± 1.15 m vs. 26.3 ± 3.4 m; q = 5.64, $p = .0017$) compared to the control animals. Moreover, neither concomitant PCP+HAL (13.43 ± 1.15 m vs. 7.12 ± 1.60 m; q = 2.77, $p = .22$) or PCP+CLZ (13.43 ± 1.15 m vs. 9.21 ± 2.24 m; q = 1.85, $p = .56$) normalised the PCP-induced effect **Figure 4-11**A.

On the contrary, treatment with both concomitant PCP+HAL (7.12 ± 1.60 m vs. 26.26 ± 3.44; q = 8.41¸ *p* = .0001) and PCP+CLZ (9.22 ± 2.34 m vs. 26.26 ± 3.44; q = 7.49, *p* = .0001) reduced the travel distance even further compared to control animals, and analogous effects were found for travel speed **Figure 4-11**B.

Although we found a significant difference in motion time/ trial duration between treatment groups ($F_{(3, 36)}$ = 19.70, *p* = .0002; Kruskal-Wallis), the Dunn's multiple comparison showed that the PCP treatment itself did not affect overall mobility (0.95 ± 0.02 vs. 0.94 ± 0.02; Z = 0.344, *p* = .99). However, concomitant HAL significantly decreased overall mobility as compared to control animals (0.61 ± 0.06 vs. 0.94 ± 0.02; Z = 3.43, *p* = .004) (**Figure 4-11**C).

In contrast, acute PCP-induced stereotypical circling was attenuated with both concomitant PCP+HAL and PCP+CLZ (**Figure 4-11**D). The one-way ANOVA analysis ($F_{(3, 36)}$ = 6.77, *p* = .001) on rotation counts with Tukey's multiple comparison test showed that PCP+HAL (38.7 ± 6.59 vs. 65.7 ± 4.20; q = 4.74, *p* = .0099) and PCP+CLZ (40.5 ± 7.40 vs. 65.7 ± 4.20; q = 4.42; *p* = .0176) statistically significantly reduced the number of rotations made compared to the control group.

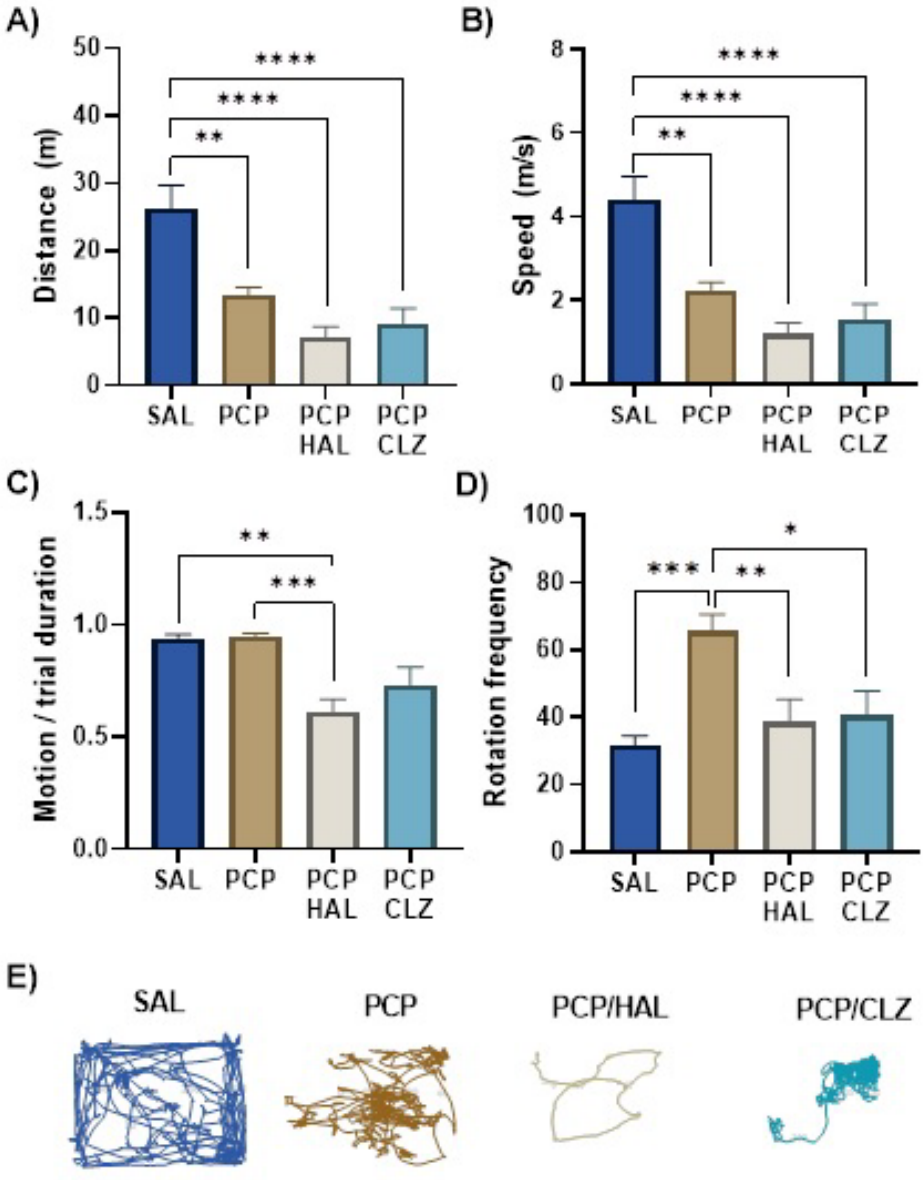

Figure 4-11 Effect of concomitant antipsychotic medication on locomotor activity changes induced by acute PCP treatment.

Graphs A-D represent mean values ± SEM. Panel E shows representative trajectories from a single animal in each treatment group. N = 10 in each group. **, p <.01; ***, p < .001, ****, p < .0001 (one-way ANOVA); N = 10 in each group. Abbreviations: SAL, saline; PCP, phencyclidine; HAL, haloperidol; CLZ, clozapine.

Table 4-9 Summary of locomotor activity in the acute reversal study.

	Overall mobility
Comparison	**Mean ± SEM, Significance^**
SAL vs. PCP	0.94 ± 0.02 vs. 0.95 ± 0.02, *p* > .9999
SAL vs. PCP + HAL	0.94 ± 0.02 vs. 0.61 ± 0.06, *p* = .0037
SAL vs. PCP + CLZ	0.94 ± 0.02 vs. 0.73 ± 0.08, *p* = .1370
PCP vs. PCP + HAL	0.95 ± 0.02 vs. 0.61 ± 0.06, *p* = .0010
PCP vs. PCP + CLZ	0.95 ± 0.02 vs. 0.73 ± 0.08, *p* = .0527
PCP + HAL vs. PCP + CLZ	0.61 ± 0.06 vs. 0.73 ± 0.08, *p* > .9999
	Travel distance (m)
Comparison	**Mean ± SEM, Significance$**
SAL vs. PCP	26.26 ± 3.41 vs. 13.4 ± 1.14, p = .0017
SAL vs. PCP + HAL	26.26 ± 3.41 vs. 7.12 ± 1.6, *p* < .0001
SAL vs. PCP + CLZ	26.26 ± 3.41 vs. 9.22 ± 2.24, *p* < .0001
PCP vs. PCP + HAL	13.41 ± 1.14 vs. 7.12 ± 1.60, *p* = .2215
PCP vs. PCP + CLZ	13.41 ± 1.41 vs. 9.22 ± 2.24, *p* = .5635
PCP + HAL vs. PCP + CLZ	7.12 ± 1.60 vs. 9.22 ± 2.24, *p* = .9140
	Travel speed (cm/s)
Comparison	**Mean ± SEM, Significance$**
SAL vs. PCP	4.38 ± 0.57 vs. 2.24 ± 0.19, p = .0017
SAL vs. PCP + HAL	4.38 ± 0.57 vs. 1.89 ± 0.27, *p* < .0001
SAL vs. PCP + CLZ	4.38 ± 0.57 vs. 1.54 ± 0.37, *p* < .0001
PCP vs. PCP + HAL	2.24 ± 0.19 vs. 1.89 ± 0.27, *p* = .2215
PCP vs. PCP + CLZ	2.24 ± 0.19 vs. 1.54 ± 0.37, *p* = .5635
PCP + HAL vs. PCP + CLZ	1.89 ± 0.27 vs. 1.54 ± 0.37, *p* = .9140

^, Dunn's multiple comparison; $, Tukey's comparison of means; N = 10 per group

We also investigated the ability of concomitant PCP+HAL or PCP+CLZ on attenuating stress- and anxiety related behaviours in the open field by analysing the locomotor activity in the outer and the centre zone of the test arena (**Table 4-10**; **Figure 4-12**). Our one-way ANOVA analysis detected no significant differences between treatment groups on time spent in the centre zone ($F_{(3, 33)}$ = 2.66, p = .0644) or the time spent in the outer zones ($F_{(3, 24)}$ = 1.37, p = .2762).

Table 4-10 Summary of locomotor activity in the centre and outer zones of test arena

	Time in centre (s)
Comparison	**Mean ± SEM, Significance^**
SAL vs. PCP	98.01 ± 3.37 vs. 268.0 ± 66.60, *p* > .05
SAL vs. PCP + HAL	98.01 ± 3.37 vs. 295.7 ± 71.49, *p* > .05
SAL vs. PCP + CLZ	98.01 ± 3.37 vs. 293.8 ± 73.01, *p* > .05
PCP vs. PCP + HAL	268.0 ± 66.60 vs. 295.7 ± 71.49, *p* > .05
PCP vs. PCP + CLZ	268.0 ± 66.60 vs. 293.8 ± 73.01, *p* > .05
PCP + HAL vs. PCP + CLZ	295.7 ± 71.49 vs. 293.8 ± 73.01, *p* > .05
	Time in outer zone (s)
Comparison	**Mean ± SEM, Significance^**
SAL vs. PCP	218.0 ± 24.51 vs. 303.1 ± 73.80, *p* > .05
SAL vs. PCP + HAL	218.0 ± 24.51 vs. 137.4 ± 75.28, *p* > .05
SAL vs. PCP + CLZ	218.0 ± 24.51 vs. 196.4 ± 60.73, *p* > .05
PCP vs. PCP + HAL	303.1 ± 73.80 vs. 137.4 ± 75.28, *p* > .05
PCP vs. PCP + CLZ	303.1 ± 73.80 vs. 196.4 ± 60.73, *p* > .05
PCP + HAL vs. PCP + CLZ	137.4 ± 75.28 vs. 196.4 ± 60.73, *p* > .05

^Tukey's multiple comparison; N for each group shown in Figure 4-12.

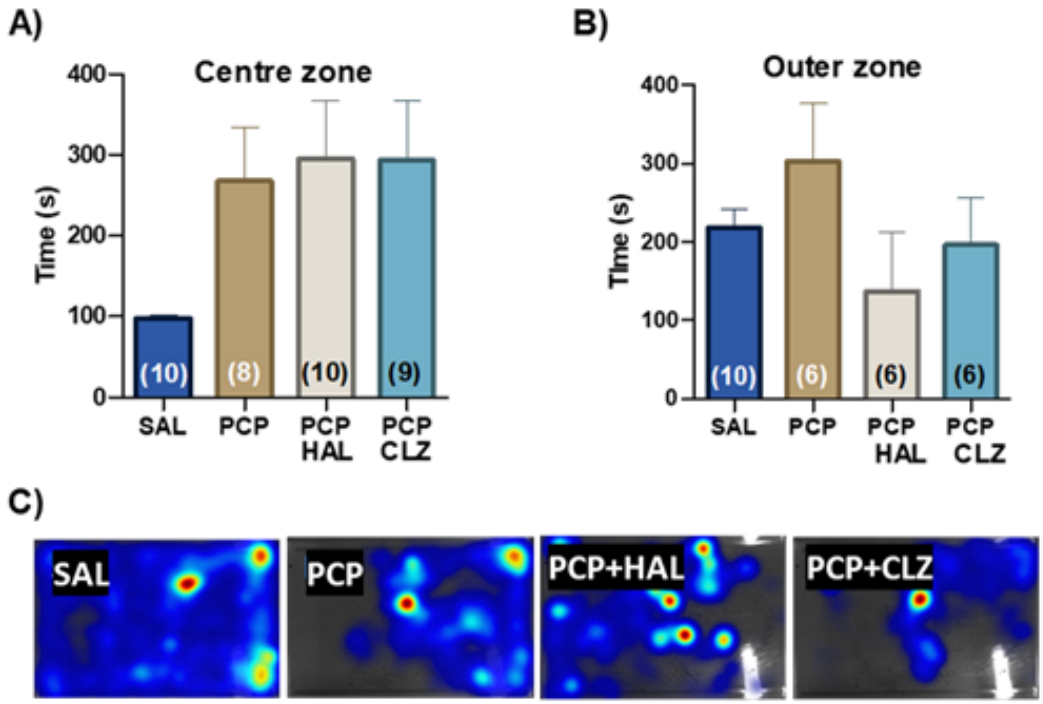

Figure 4-12 Effect of antipsychotic drugs on mouse activity in different zones of the open field test arena.

Graphs A and B show the mean time spent in the centre and the outer zones, respectively. C. The representative heatmap of an animal trajectory from each treatment group showing the activity location and times within the test arena. Statistical significance was measured using Kruskal-Wallis test with Tukey's multiple comparison. The number in each column indicate the number of animals used in the analysis.

4.4.5 Effect of antipsychotic drugs on PCP-induced changes in motor performance

As introduced in **Section 1.1.3**, there is ample evidence of cerebellar involvement in schizophrenia, and a considerable proportion of schizophrenia patients presents with neurological soft signs (NSS). We therefore employed cerebellar-specific challenges to test motor performance and coordination using the horizontal bar and vertical pole

tests (Filali et al., 2015), and the test results are summarised in **Table 4-11** and **Table 4-12**.

Our Kruskal-Wallis analysis detected significant differences in mean ranks between treatment groups in the horizontal bar challenge ($\chi^2_{(3)}$ = 29.87, p < .0001. $\chi^2_{(3)}$ = 13.99, p = .0029). The Dunn's multiple comparison test revealed that PCP-treated animals took a significantly longer time before righting compared to control animals (34.00 ± 9.73 s vs. 11.80 ± 0.65 s; Z = 4.15, p = .0002). This was improved by concomitant PCP+HAL injection (14.20 ± 0.87 s; p > .99) but not concomitant PCP+CLZ (27.60 ± 2.29 s; p < .0001). Furthermore, the concomitant PCP+CLZ-injected mice failed the bar challenge much faster compared to controls (25.40 ± 10.65 s vs. 110.1 ± 9.90 s; Z = 3.51, p = .0025) as well as the concomitant PCP+HAL injected animals (96.70 ± 15.53 s; Z = 2.584, p = .04) (**Figure 4-13**A).

Our analysis also showed significant difference between treatments in vertical pole climbing challenge ($\chi^2_{(3)}$ = 9.01, p = 0.029; $\chi^2_{(3)}$ = 23.71, p < .0001; Kruskal-Wallis). The animals administered with concomitant PCP+CLZ performed significantly worse compared to the control animal by taking a longer time to climb (99.50 ± 3.54 s vs. 78.20 ± 4.46 s; Z = 2.844, p = .0267). In addition, the animals co-administered with PCP+CLZ failed the climbing challenge significantly faster by taking less time to fall compared to

control animals (12.30 ± 2.02 s vs. 104.1 s; Z = 4.55, $p < .0001$) and compared to the concomitant PCP+HAL injected animals (12.30 ± 2.02 s vs. 78.70 ± 14.09 s; Z = 3.74, $p = .0011$) (**Figure 4-13**B).

The analysis also detected significant differences in the performance during the descend challenge ($\chi^2_{(3)} = 21.09$, $p = .0001$; $\chi^2_{(3)} = 8.62$, p = .0349; Kruskal-Wallis). Here the animals co-administered PCP+HAL performed significantly worse compared to the controls by taking a longer time to descend (20.60 ± 1.41 s vs. 13.00 ± 0.68 s; Z = 2.84, $p = .0273$), and similar result was found for the PCP+CLZ-treated animals (32.10 ± 0.68 s; Z = 6.04, $p = .0019$). Additionally, the group co-administered with PCP+CLZ failed the descend challenge significantly faster compared to control animals by taking less time to come down compared to controls (22.00 ± 11.03 s vs. 96.90 ± 15.40 s; Z = 2.316, $p = .0206$), compared to PCP+HAL-treated animals (22.00 ± 11.03 s vs. 97.60 ± 14.94 s; Z = 2.53, $p = .0116$) (**Figure 4-13**C)

Table 4-11 Summary of motor performance in the horizontal bar test.

	Time to righting
Comparison	**Mean ± SEM, Significance**
SAL vs. PCP	11.80 ± 0.65 s vs. 34.00 ± 9.73 s, $p = .0002$
SAL vs. PCP + HAL	11.80 ± 0.65 s vs. 14.20 ± 0.87 s, $p > .9999$
SAL vs. PCP + CLZ	11.80 ± 0.65 s vs. 27.60 ± 2.29 s, $p < .0001$
PCP vs. PCP + HAL	34.00 ± 9.73 s vs. 14.20 ± 0.87 s, $p = .0105$
PCP vs. PCP + CLZ	34.00 ± 9.73 s vs. 27.60 ± 2.29 s, $p > .9999$
PCP + HAL vs. PCP + CLZ	14.20 ± 0.87 s vs. 27.60 ± 2.29 s, $p = .0035$
	Time to fall
Comparison	**Mean ± SEM, Significance**
SAL vs. PCP	110.1 ± 9.90 s vs. 88.50 ± 16.05 s, $p > .9999$
SAL vs. PCP + HAL	110.1 ± 9.90 s vs. 96.70 ± 15.53 s, $p > .9999$
SAL vs. PCP + CLZ	110.1 ± 9.90 s vs. 25.40 ± 10.65 s, $p = .0025$
PCP vs. PCP + HAL	88.50 ± 16.05 s vs. 96.70 ± 15.53 s, $p > .9999$
PCP vs. PCP + CLZ	88.50 ± 16.05 s vs. 25.40 ± 10.65 s, $p = .0584$
PCP + HAL vs. PCP + CLZ	96.70 ± 15.53 s vs. 25.40 ± 10.65 s, $p = .0436$

Table 4-12 Summary of motor performance in the vertical pole test. N = 10 in each group

	Latency to climb (t)
Comparison	**Mean ± SEM, Significance**
SAL vs. PCP	78.20 ± 4.46 s vs. 96.90 ± 6.44 s, p = .2315
SAL vs. PCP + HAL	78.20 ± 4.46 s vs. 95.30 ± 4.33 s, p = .1963
SAL vs. PCP + CLZ	78.20 ± 4.46 s vs. 99.50 ± 3.55 s, p = .0267
PCP vs. PCP + HAL	96.90 ± 6.44 s vs. 95.30 ± 4.33 s, p > .9999
PCP vs. PCP + CLZ	96.90 ± 6.44 s vs. 99.50 ± 3.55 s, p > .9999
PCP + HAL vs. PCP + CLZ	95.30 ± 4.33 s vs. 99.50 ± 3.55 s, p > .9999
	Latency to fall while climbing (t)
Comparison	**Mean ± SEM, Significance**
SAL vs. PCP	104.1 ± 10.68 s vs. 53.60 ± 14.79 s, p = .2060
SAL vs. PCP + HAL	104.1 ± 10.68 s vs. 78.70 ± 14.09 s, p > .9999
SAL vs. PCP + CLZ	104.1 ± 10.68 s vs. 12.30 ± 2.02 s, p < .0001
PCP vs. PCP + HAL	53.60 ± 14.79 s vs. 78.70 ± 14.09 s, p > .9999
PCP vs. PCP + CLZ	53.60 ± 14.79 s vs. 12.30 ± 2.02 s, p = .0900
PCP + HAL vs. PCP + CLZ	78.70 ± 14.09 s vs. 12.30 ± 2.02 s, p = .0011
	Latency to descent (t)
Comparison	**Mean ± SEM, Significance**
SAL vs. PCP	13.00 ± 0.68 s vs. 12.10 ± 1.91 s, p > .9999
SAL vs. PCP + HAL	13.00 ± 0.68 s vs. 20.60 ± 1.41 s, p = .0273
SAL vs. PCP + CLZ	13.00 ± 0.68 s vs. 32.10 ± 10.05 s, p = .0129
PCP vs. PCP + HAL	12.10 ± 1.91 s vs. 20.60 ± 1.41 s, p = .0044
PCP vs. PCP + CLZ	12.10 ± 1.91 s vs. 32.10 ± 10.05 s, p = .0019
PCP + HAL vs. PCP + CLZ	20.60 ± 1.41 s vs. 32.10 ± 10.05 s, p > .9999
	Latency to fall while descending (t)
Comparison	**Mean ± SEM, Significance**
SAL vs. PCP	96.90 ± 15.40 vs. 62.50 ± 19.17, p = .1572
SAL vs. PCP + HAL	96.90 ± 15.40 vs. 97.60 ± 14.94, p = .8340
SAL vs. PCP + CLZ	96.90 ± 15.40 vs. 22.00 ± 11.03, p = .0206
PCP vs. PCP + HAL	62.50 ± 19.17 vs. 97.60 ± 14.94, p = .1044
PCP vs. PCP + CLZ	62.50 ± 19.17 vs. 22.00 ± 11.03, p = .3675
PCP + HAL vs. PCP + CLZ	97.60 ± 14.94 vs. 22.00 ± 11.03, p = .0116

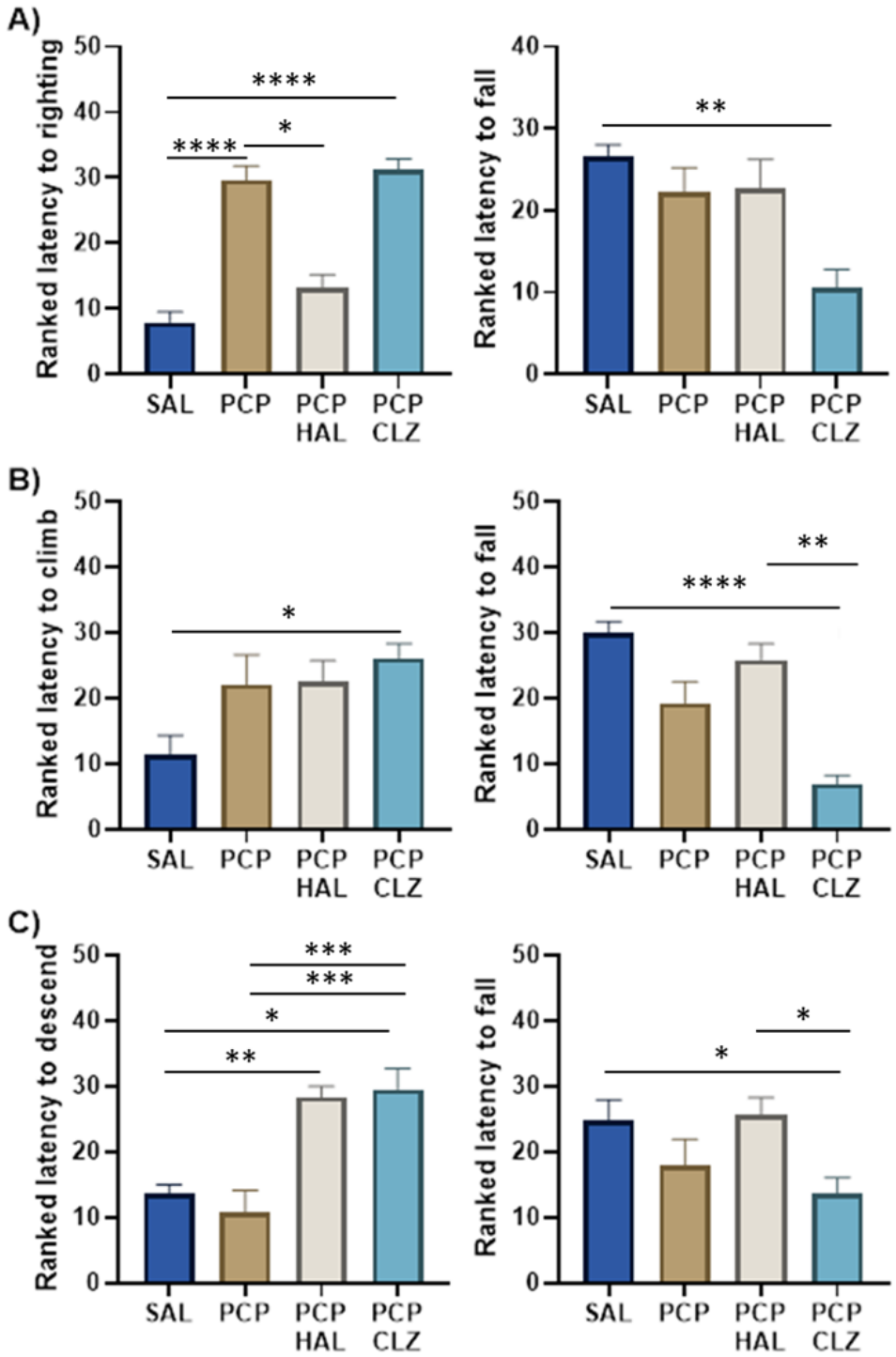

Figure 4-13 Mouse performance in motor coordination tests.

A. Horizontal bar challenge; B. Climbing up challenge; C. Climbing down challenge. Bars show mean ranks ± SEM. *, $p < .05$; **, $p < .01$; ***, $p < .001$; ****, < .0001. Kruskal-Wallis test with Dunn's multiple comparison; N = 10 in each group. Abbreviations: SAL, saline; PCP, phencyclidine; HAL, haloperidol; CLZ, clozapine.

4.4.6 Discussion

Face validity

As mentioned in the introduction, animal models are evaluated by a set of qualities in terms of face validity, construct validity, and predictive validity. The face validity refers to the phenotypic resemblance to schizophrenia where several behavioural traits, such as increased response to stimulants or stereotypical behaviours can be directly observed or measured. In this context, the present chapter investigated the overall behavioural phenotype produced by subchronic PCP treatment in CBA/Ca mice. In particular, we observed overall reduced mobility on day 1 of treatment which was accompanied by repetitive circling and increased grooming. This may seem paradoxical; however, overall mobility is a measure of movement / distance travelled, whereas rotation is a measure of circular motion around central axis. Therefore, while overall mobility is reduced, circular motions and otherwise stationary measures, such as rearing and grooming are present. On day 4 of treatment, we observed an exaggerated locomotor response to subsequent dose of PCP and this increase in locomotion was also accompanied by repetitive circling, and increased rearing. While no stereotypical behaviours were observed during the washout period, the mice were significantly less mobile on day 8 (first day of drug washout), and their mobility returned to normal on day 14.

Useful animal models of schizophrenia are expected to mimic, at least partially, the core symptoms observed in human subjects; however, these encompass uniquely human traits for which they are diagnosed using extensive interviews – a feat not possible in animals (Winship et al., 2019). A significant behavioural correlate is that systemic administration of NMDA antagonists in rodents induces hyperlocomotion and stereotypy that, as hallucinations or delusions in schizophrenia, are associated with increased serotonergic and dopaminergic neurotransmission (Giros et al., 1996; Jentsch et al., 1998), and therefore, are thought to potentially resemble the positive symptoms observed in man (F Sams-Dodd, 1996; Homayoun et al., 2004). Furthermore, these manifestations are analogous to those observed in human subjects with schizophrenia, such as disorganised behaviour and agitation, and the several repetitive motor behaviours observed in acute psychosis (Morrens et al., 2006). The behavioural sensitisation as manifested here by the exaggerated locomotor response on day 4 of treatment is commonly observed with dopaminergic compounds such as cocaine and amphetamine (Post and Rose, 1976; Pierce and Kalivas, 1997; Featherstone, Kapur and Fletcher, 2007; Robert E Featherstone et al., 2008). However, similar observations were made in C57BL/6N and C57BL/6J mouse strains following subchronic and chronic PCP regiments (Xu and Domino, 1994; Mouri et al., 2012). This hyperlocomotion might be partially mediated by an increase in striatal dopamine release, considering

that these effects in mice can be also reversed by dopamine receptor antagonists (Nagai et al., 2003; Chartoff, Heusner and Palmiter, 2005). The manifestation of repetitive grooming on day 1 but not day 4 of treatment may be partially attributed to sensitisation (Audet, Goulet and Doré, 2006). However, it is more probable that this is attributable to mediation of these behaviours differentially by D_1 and D_2 dopamine receptors, which will be discussed on later pages (Starr and Starr, 1986). Moreover, while rearing in rodents is a well-established index of curiosity, it may also indicate vigilance, whereas excessive grooming also occurs naturally after exposure to novelty and stress (Gispen and Isaacson, 1981; Kalueff and Tuohimaa, 2005; Audet, Goulet and Doré, 2006). Therefore, it can be speculated that in this context both grooming on day 1 combined with reduced overall mobility and increased rearing on day 4 are associated with stress and anxiety, considering that stress-related anxiety in rodents is also indicated by reduced exploration (Crawley and Bailey, 2008); however, this remains to be explored further with more rigorous testing. Subsequently, we observed a significant decrease in overall mobility on the first day of washout period. Withdrawal from chronic/subchronic PCP in rodents results in reduced performance in the social interaction and the novel object recognition tests (Seillier and Giuffrida, 2009), as well as increased immobility in several behavioural paradigms (Castañé, Santana and Artigas, 2015) which, as negative and cognitive symptoms in human, are associated with reduced

dopamine activity in several brain regions relevant to schizophrenia (Frank Sams-Dodd, 1998; Juckel et al., 2006; Amann et al., 2010). Although our NOR test was inconclusive, especially that identical treatment in C57BL/6 juvenile male mice produced robust deficits in spatial memory (Zain et al., 2018), our data on the first day of washout corresponds to the reduced performance in tail suspension and forced-swim tests, where mice during acute PCP withdrawal showed increased immobility scores, which may indicate negative- or depressive-lime symptoms in mice (Trullas and Skolnick, 1990; Wesolowska et al., 2010).

Construct validity

The construct generally refers to the extent to which a model is 'built' on the basis of disease aetiology. This may include induction of genetic alterations which are associated with an increased risk for developing schizophrenia, or a known pathophysiological process involved, such a targeted disruption of neurochemical system(s). To validate the model construct, we therefore investigated the consequences of PCP treatment on NMDAR gene expression in frontal cortex, as well as both the biomolecular and morphological consequences of this treatment on the cerebellum when PCP was no longer on board. Here we observed a differential regulation of NDMA receptor genes in the frontal cortex and the cerebellum. Specifically, we observed a non-significant downregulation of *Grin1* gene coding for the

compulsory subunit NR1 in the frontal cortex, and a significant upregulation was observed in the cerebellum. At the same time, the *Grin2b* gene coding for the NR2B receptor was significantly downregulated in the frontal cortex, whereas no changes were observed in the cerebellum, and no changes in *Grin2c* gene coding for the NR2C receptor were observed in neither frontal cortex nor the cerebellum.

NMDA receptors play pivotal roles in brain development, synaptic plasticity, and excitatory neurotransmission (Goff and Coyle, 2001). PCP increases both negative and positive symptoms in schizophrenia (Coyle, 2006) and evidence exists that abnormal NR1 subunits may allow schizophrenia to develop (Halene et al., 2009; Gordon, 2010). The behavioural manifestations in NR1-deficient mice generated by Mohn and colleagues (Mohn et al., 1999), which express only 5-10% of normal NR1 subunits, involved increased locomotor activity, stereotypy, and reduced sexual and social behaviours, and the former two were observed in our PCP-treated animals. We therefore expected to see a significant change in the regulation of *Grin1* in frontal cortex of the subchronic PCP model; however, our study saw only a non-significant downregulation of *Grin1* which might be partially due to small sample size, and thus should be confirmed by increasing number of animals used in further testing. While these findings do not correspond to the glutamate hypofunction observed in schizophrenia, a five-day chronic PCP treatment followed by a three-day

withdrawal and an acute challenge with a single dose of PCP results in the upregulation of *Grin1* in rat forebrain (Wang et al., 1999). This may suggest a staggered glutamatergic pathology where the initial hyperfunction elicits a compensatory mechanism that may lead to downstream hypofunction (Catts et al., 2016). This assumption could be partially supported by the significant upregulation of *Grin1* observed in the cerebellum of our model. Subsequently, we saw a significant downregulation in *Grin2b* gene in the frontal cortex. The NR2A-NR2D subunits bind glutamate, and the NR2B subunit is predominantly expressed in both excitatory neurons and interneurons of adult cortex, and together with the NR2A they are important players in synaptic plasticity. However, in human hippocampal formation, the expression of NR2B peaks around the time of birth and decreases with aging in parallel with increasing levels of NR2A (Law et al., 2003); therefore, it would be interesting to see whether differential regulation of these two subunits exists in our model, and whether their ratio is affected by the subchronic PCP treatment – considering that, compared to normal controls, both NR2A and NR2B are downregulated in preferontocortical *post-mortem* human samples of schizophrenia brains at both genetic (Beneyto et al., 2007) and protein level (Errico et al., 2013).

We also investigated the effect of subchronic PCP treatment on the cerebellum. As mentioned previously, the cerebellar PC is the most vulnerable cell type to cerebellar insult, including hypoxia or glutamate

toxicity (Koeppen, 2018). For the latter, early results showed that even brief exposure to increased concentrations of glutamate (100-300 μM for 30 min + 90 min recovery) induces PC degeneration in rats (Garthwaite, Williams and Garthwaite, 1992). As mentioned in **Section 1.3**, there is ample evidence of cerebellar abnormalities in schizophrenia. A large meta-analysis of brain volumes from schizophrenia of over 18, 000 subjects showed that the total cerebellar volume in schizophrenia was reduced compared to controls (Haijma et al., 2013). Furthermore, a fMRI study of 183 schizophrenia patients found volumetric reductions of both white and grey matter in schizophrenia brains compared to controls (Weinberg et al., 2016). Our investigation into cortical features of the cerebellum revealed that the size of PCs and the thickness of cerebellar cortex were significantly reduced in the PCP-treated animals, whereas the treatment had no effect on the number of PCs. Despite that no apparent loss of PCs was observed, our findings are consistent with cerebellar atrophy observed in schizophrenia (Nasrallah, Jacoby and Mccalley-Whitters, 1981; Luchins et al., 1981; Sandyk, Kay and Merriam, 1991). Furthermore, our data showed that PCs in the right lateral hemisphere of the PCP-treated animals were smaller compared to controls, whereas there was no change was observed in its left counterpart. Cerebellar asymmetry in schizophrenia has been reported in multiple studies in the past decades (Szeszko et al., 2003; Özbek et al., 2019).

Predictive validity

Finally, the value of a model to predict future therapeutic potential must also be assessed. Nevertheless, it must be stressed that predictive validity cannot be always ascertained in each and every aspect of a pathological condition. This is particularly applicable to schizophrenia due to its convoluted and multifaceted pathophysiology, and only certain aspects of the disorder may be modelled, which poses the greatest limitation to studying schizophrenia in non-human subjects. (Jones, Watson and Fone, 2011; Winship et al., 2019). In this work, we studied the ability of concomitant PCP administered with either haloperidol or clozapine on attenuating acutely induced changes in behaviour that are believed to be analogous to those observed in a psychotic episode. However, it is also important to note that psychosis and schizophrenia are not equal; acute psychosis may mark the onset of schizophrenia, but psychosis may also occur in other neuropsychiatric disorders, including depression or delusional disorder. Hence, the purpose of this study was to assess the ability of the two antipsychotic drugs to attenuate the drug-induced psychotic state, based on the fact that they are both ought to arise due to dysfunctional glutamate signalling. In this context, we observed a differential effect of haloperidol and clozapine on the PCP-induced non-significant increase in rearing, and the significantly increased grooming. Here, the concomitant PCP+HAL or PCP+CLZ attenuated exaggerated rearing,

whereas only PCP+CLZ attenuated increased grooming. Haloperidol is a selective D_1 receptor antagonist, whereas clozapine is a preferential D_2 receptor antagonist. Early research showed that locomotor activity, as well as grooming and rearing can be selectively modulated with D_1 and D_2 dopamine receptor agonists, respectively. Starr and Starr (1986) demonstrated that mice treated with D_1 agonist amphetamine show increased locomotor activity, rearing, and grooming. Simultaneously, the preferential D_2 receptor agonist apomorphine elicited no effect on locomotor activity but evoked increased rearing and grooming. This stipulates that the differential effect of haloperidol and clozapine on changes in grooming and rearing evoked by acute PCP can be attributed to the dopamine receptor subtypes to mediate these behaviours. This also supports the observed changes in locomotor activity. However, it must be reminded that the effect of PCP on locomotor activity is dose-dependent (Morris, Cochran and Pratt, 2005). The animals in this study received a single dose of PCP at 10 mg/ kg, whereas the subchronic treatment involved two daily injections at 5 mg/ kg. Because all behavioural tests in the subchronic study were conducted after first daily dose of PCP, the differential effects of acute PCP in this study and on day 1 in the subchronic study can attributed to the difference in PCP dosage. In the current study we observed no change in overall mobility in the PCP group, and this was significantly reduced in the animals administered with concomitant

PCP+HAL compared to control the animals, while no significant change was observed in the PCP+CLZ group – further suggesting the role of dopamine receptor subtypes in mediating the locomotor response. Additionally, both antipsychotic drugs attenuated stereotypical circling, which underlies the clinical effectiveness of both typical and atypical antipsychotics for treatment of positive symptoms in schizophrenia.

Neurological soft signs are subtle impairments in motor function, which reflect deficits in sensory integration (Quitkin et al., 1976), sequencing of complex motor actions (Buchanan and Heinrichs, 1989), and motor coordination (Ismail, Cantor-Graae and McNeil, 1998). Over fifty per-cent of schizophrenia patients present with NSS, compared to only about 5% of healthy individuals (Chen, Chen and Mak, 2000; Chan and Chen, 2007). Furthermore, limited findings suggest that these might have some measure of neuroanatomical localisation and could indicate dysfunctional neuronal circuitry (Keshavan et al., 2003; Boks et al., 2004). Therefore, we were interested to find out whether acute PCP treatment can induce any cerebellar-specific effects that could be attributed to dysfunctional cerebellar processing. Here we observed that the PCP animals were deficient on the horizontal bar challenge by taking more time to reach the upright position, which was attenuated with concomitant HAL+CLZ but not HAL. Whereas no deficiencies in mouse performance on the vertical pole challenge were observed. PCP-induced deficiencies in several motor

coordination paradigms were reported previously. For example, the first study on the effects of PCP on sensory-motor function described reduced righting and grasping reflexes in rat at doses of 12 mg/ kg and above (Kesner, Hardy and Calder, 1981), and dose-dependent reductions in indices of motor coordination was also reported in animals administered with other NMDA receptor antagonists, including ketamine and MK-801 (Carter, 1995). This may indicate that the current dose was insufficient to induce changes in performance on the climbing challenge. However, this also implies that the complexity of vertical climbing may be inferior to that of righting from an upside-down position. Additionally, while the role of dopamine D_2 receptors in vertical exploration may partially explain the increased latencies to complete vertical challenge by the clozapine-co-administered animals (Protais, Costentin and Schwartz, 1976), the similar observation in concomitant PCP and haloperidol-injected animals may also imply partial involvement of the D_1 receptor.

4.4.7 **Conclusion**

Here we investigated the behavioural changes evoked by PCP during subchronic and acute treatments, the effectiveness of antipsychotic medication on attenuating the acute effects of PCP, and some of the biological substrates present after the discontinuation of subchronic PCP administration. Our data showed that PCP induced positive symptom-like

effects (e.g., stereotypy) and negative/affective symptom-like effects (e.g., reduced mobility), and motor discoordination which can be attributed to early cerebellar impairments and analogous to the neurological soft signs observed in schizophrenia patients. Majority of effects were reversed with antipsychotic treatment, and the PCP regimen resulted in dysregulation of NMDAR subtypes and morphological changes in the cerebellum. These findings support several aspects of face, construct, and predictive validity; however, there are also many limitations. In particular, the NOR test which produced no conclusive results in this chapter should be repeated, ensuring special attention is given to eliminate potential stressors during acquisition. Furthermore, more testing is needed to confirm the face validity of negative symptoms, which could be achieved by employing the tail suspension test or sucrose preference test.

Chapter 5 Cerebellar Regulation of Kv2.1, Kv6.4, and Kv3.1b in The Subchronic PCP Model

5.1 Introduction

Voltage-gated potassium channels are critical components of neuronal excitability, thus playing fundamental roles in communicating information within the CNS. The diversity of Kv channel subtypes allows them to control discrete aspects of neuronal events, which are responsible for a plethora of biological functions, including movement or cognition (Rudy et al., 2009). However, because of this functional diversity, Kv channel dysfunction leads to an equally vast repertoire of neuronal disorders (Dworakowska and Dołowy, 2000; Imbrici, Camerino and Tricarico, 2013). For example, a dominantly inherited mutation in the Kv1.1 channel subunit at Val408Cys and Phe184Cys results in a three-fold reduction of channel opening duration thereby causing a shift in repolarisation to a more positive potential, which in observed in episodic ataxia with myokymia syndrome (Adelman et al., 1995; D'Adamo et al., 1999). While several mutations in the

KCNQ2 and *KCNQ3* genes coding for Kv7.2 and Kv7.3 subunits, respectively, alter the M currents which are involved in regulating subthreshold of neuronal excitability and their responsiveness to synaptic input, thereby leading to a form of epilepsy in the new-born (Steinlein, 2001).

Recently, several Kv channels, including the Kv2.1 and Kv3.1, were also implicated in the pathophysiology of schizophrenia (Imbrici, Camerino and Tricarico, 2013). For example, in an analysis of 313 protein-coding genes from a large schizophrenia genome-wide association study (Ripke et al., 2014), Ohi and colleagues (Ohi et al., 2016) found nine genes, including the Kv2.1-coding *KCNB1* gene, and *KCNV1* gene coding for the non-conductive Kv8.1 α subunit, that showed significant overexpression in the neocortex of schizophrenia subjects. Moreover, a *post-mortem* schizophrenia samples of 72 ion channel genes revealed a near 3-fold downregulation of *KCNB1* in a cerebellar lateral hemisphere (Smolin et al., 2012). Additionally, the amount of Kv2.1 and Kv9.3 were reduced in a *post-mortem* analysis of parvalbumin-positive pyramidal neurons of prefrontal cortex in schizophrenia subjects (Georgiev et al., 2014), whereas the Kv3.1 was significantly reduced in dorsolateral prefrontal cortex, parietal cortex, and occipital cortex of untreated schizophrenia subjects compared to normal controls, whereas no changes were present in medicated subject (Yanagi et al., 2014). Furthermore, in an animal study, the AMIGO protein

was demonstrated as an auxiliary subunit of the Kv2.1 channel (Peltola et al., 2011). It was later shown that AMIGO knock-out mice show reduced levels of Kv2.1 protein in the brain, and manifest with increased locomotion and an exaggerated locomotor response to a low dose of the NMDA receptor antagonist MK-801. In concurrent findings, the authors found a rare population-specific single nucleotide polymorphism in *KCNB1* gene that was enriched in schizophrenia, further implicating a genetic component of Kv2.1 to the development of the disorder (Peltola et al., 2016). Additionally, mutant mice lacking the *Kcnb1* gene show profound neuronal excitability, they are remarkably hyperactive, and they also display reduced spatial learning, and anxiety-like behaviours, reminiscent of schizophrenia like-phenotype (Speca et al., 2014).

In the early attempts at explaining the diversity of schizophrenia symptoms at neural level, researchers were mainly focused on relating the particular symptoms to the specific areas in the cerebral cortex with the capacity to produce such symptoms. For example, reduced cognitive abilities could potentially be explained by abnormalities in the frontal lobes (Goldman-Rakic, 1991), whereas auditory hallucinations cold be potentially explained by anomalies in the auditory cortex (Silbersweig et al., 1995). At approximately one-fifth of the total brain volume, the cerebellum contains around 80 percent of grey matter in the entire CNS combined (Haines and Mihailoff, 2018). The cerebellar cortex receives sensorimotor input from

numerous areas in the CNS, including the cerebral cortex (Hoover and Strick, 1999), spinal cord (Manzoni, 2007), brain stem (Nowak et al., 2007), and vestibular nuclei (Meng et al., 2014), and then communicates this information *via* the thalamus to various parts of cerebral cortex, including the parietal cortex, motor cortex, and frontal cortex (Middleton and Strick, 2000; Baldaçara et al., 2008). This vast interconnectivity between the cerebellum and other brain regions implicates important roles in influencing information processing, and may explain why so many individuals who suffered cerebellar damage also present with symptoms similar to those present in schizophrenia (Villanueva, 2012).

In this chapter, we considered the importance of the cerebellum to information processing, and the increasing body of evidence of Kv2.1, KvS and Kv3.1b subunits in the pathophysiology of schizophrenia and were interested in finding out whether their expression is altered in the cerebellum of our subchronic PCP model.

5.2 Aims

This chapter aims to investigate the regulation of voltage-gated potassium channels Kv2.1, Kv6.4, and Kv3.1b in the cerebellum of the subchronic PCP mouse model. Specifically, we are looking to compare the expression

changes in the three cerebellar cortical layers in the vermis and the lateral hemispheres.

5.3 Materials and Methods

In brief, this chapter used a total of 32 animals. Ten animals were used exclusively for western blotting, and 16 animals were used for combined western blotting and RT-qPCR. Additional six animals were used for immunohistochemistry. As previously, each method will be considered briefly unless specific changes were implemented, and this will be elaborated accordingly. For a full description of materials and methods used please refer to **Chapter 2.**

5.3.1 Animal work

Animals were subject to subchronic PCP treatment as described in **Section 4.1**. The mice were culled by cervical dislocation and tissues harvested for processing. The protein samples for western blotting were prepared by two methods: in the first method, the proteins were extracted from ten animals using RIPA buffer as summarised in **Section 3.3.2**. In the remaining samples from sixteen animals Trizol® was used to simultaneously extract protein and RNA material as described in **Section 2.2**.

5.3.2 Western blotting

The proteins extracted using RIPA buffer were mixed with an equal volume of electrophoresis sample buffer and heated for 10 minutes at 95°C, then allowed to reach RT before loading onto 12% polyacrylamide gels. The Trizol-extracted dry protein pellets were first solubilised in an optimised lysis buffer as described by Kopec (Kopec et al., 2017). In brief, the pellets were dislodged in the prepared lysis buffer and heated for a minimum of 30 minutes at 100°C. After estimating their protein concentrations, the samples were mixed with an equal volume of electrophoresis sample buffer as above and loaded onto 12% stain-free polyacrylamide gels. The ten RIPA-extracted protein samples were then resolved, transferred onto nitrocellulose membranes, and described in **Section 3.3.2**. The Trizol-extracted protein samples were resolved on stain-free gels, which were then activated and imaged using a Bio-Rad Gel-doc™ EZ® as described in **Section 2.3.6**, and the proteins transferred onto membranes as previously. The gel images were used to normalise the band densities of proteins of interest for analysis. The membranes were blocked and probed for Kv2.1 and Kv6.4 and incubated with appropriate HRP-conjugated secondary antibodies and prepared for imaging as in **Section 3.3.2**.

5.3.3 Immunohistochemistry

Immunohistochemistry was carried out as in **Section 3.3.3** with some minor changes. In brief, three vehicle- and three PCP-treated animals were used. Three sections per each animal from each lateral hemisphere, vermis, and right hemisphere were fixed, blocked, and probed for the Kv2.1, Kv6.4, or Kv3.1b (Rabbit-anti-Kv3.1b; 1:500 APC-014, Alomone) and incubated overnight in the cold room. The slides were then washed and incubated with appropriate AlexaFluor®488 secondary antibodies at RT. The slides were then washed, counterstained with DAPI, and preserved with cover slips and sealant as previously. Three fluorescence images were obtained from each slide using Leica fluorescence equipped with a x40 objective lens at constant acquisition parameters for each protein of interest. The images were then used to quantify the fluorescence signal as detailed **Section 2.4.7**. The raw data populated and analysed with IBM SPSS and GraphPad PRISM.

5.3.4 RT-qPCR

Cerebellar samples were homogenised, and RNA was extracted as described in **Section 2.2**. Complimentary DNA (cDNA) strands were synthesised using a High-Capacity cDNA Reverse Transcription Kit (ThermoFisher Scientific, UK) in a Hybaid thermal cycler (Thermo Scientific, UK). Real time-quantitative PCR was carried out as summarised in **Section**

4.3.4. The primer pairs used for the amplification of *Kcnb1* and *Kcng4* genes are listed in **Table 2.4**. A 10 µM PCR primer mix was prepared separately for each studied gene by diluting 10 µL of forward and reverse primer stock in 980 µL water. A reaction mix was then prepared for each gene by combining the primer mix for each gene with SYBR green assay reagent and DEPC-treated water. In triplicates, a 96-well plate was loaded with 1 µL of the previously synthesised cDNA and 10 µL of the reaction mixture was added to the corresponding wells. The plates were then sealed and centrifuged using a plate mixer for one minute before being placed in a StepOne Real-time PCR thermocycler (Applied Biosystems, UK). The thermocycler settings are presented in **Section 2.5.4**. Relative gene expression was calculated using the Livak method, as described in **Section 2.5.1.**

5.4 Results

Kv2.1, Kv6.4, and Kv3.1b are dysregulated in the subchronic PCP model

First, we studied the regulation of Kv2.1 and Kv6.4 subunits at protein level using western blotting and immunohistochemistry. Western blot analysis showed that the Kv2.1 was significantly reduced in the subchronic PCP model (1.21 ± 0.08 vs. 0.87 ± 0.06; $t_{(24)}$ = 3.61, p = .001), whereas a non-

significant increase in the amount of Kv6.4 was observed (0.93 ± 0.07 vs. 1.19 ± 0.10; U = 12, p = .07) (**Figure 5-1**).

Further immunohistochemistry revealed that reduction in Kv2.1 occurred in PCs and the GL. Analysis of ranked corrected total cell fluorescence (CTCF) in PCs showed that Kv2.1 was significantly reduced in the left lateral hemisphere (U =17974, p < .0001), vermis (U = 40873, p < .0001), and right lateral hemisphere (U = 45822, p < .0001) (**Figure 5-2**A; **Figure 5-3**). Meanwhile, the ranked CTCF in the GL was reduced in the vermis (U = 5074, p < .0001) and the right lateral hemisphere (U = 1631, p = .02).

Although western blot analysis only showed a non-significant increase in the amount of Kv6.4 in the subchronic PCP model, we hypothesised that statistical significance may be hindered in whole tissue lysates, and indeed, our immunohistochemistry data reinforced this assumption; the analysis revealed that Kv6.4 was significantly increased in both PCs and GL in the PCP model (**Figure 5-2**B; **Figure 5-4**). We observed a significant reduction of Kv6.4 in PCs of the left and right lateral hemispheres in the PCP model (p < 0.001), while no significant change was observed in the vermis. At the same time, the analysis in GL showed a significant increase of Kv6.4 in the left lateral hemisphere (p < 0.001), vermis (p < 0.001), and right lateral hemisphere (p < 0.001).

We also investigated the expression of Kv3.1b subunit in the PCP model. Here, the analysis of ranked CTCF in GL showed a significant reduction of Kv3.1b in the right lateral hemisphere, whereas no significant change was observed in left lateral hemisphere or vermis. Simultaneously, no significant change in the ranked CTCF in the ML was observed in either lateral hemisphere or the vermis (**Figure 5-2**C; **Figure 5-5**).

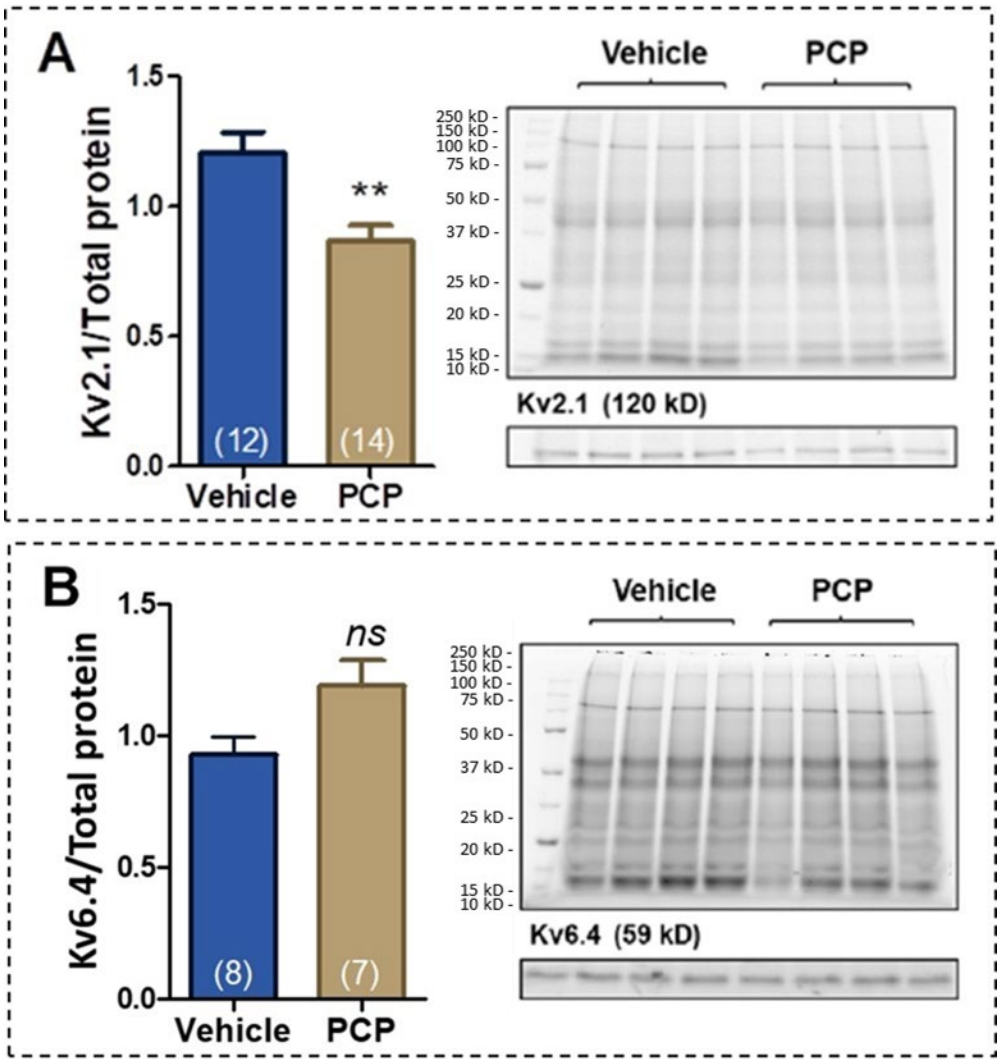

Figure 5-1 Effect of subchronic PCP treatment on the expression of Kv2.1 and Kv6.4 proteins in the cerebellum.

Graphs in panels A and B show the expression of Kv2.1 and Kv6.4 proteins in the cerebellum from vehicle treated and PCP treated animals, respectively. The images on the right are the representative stain-free gel images of total proteins (upper panels) and the immunoreactive bands for Kv2.1 and Kv6.4 on blotted membrane (lower panels). The number of animals used is indicated in each column.

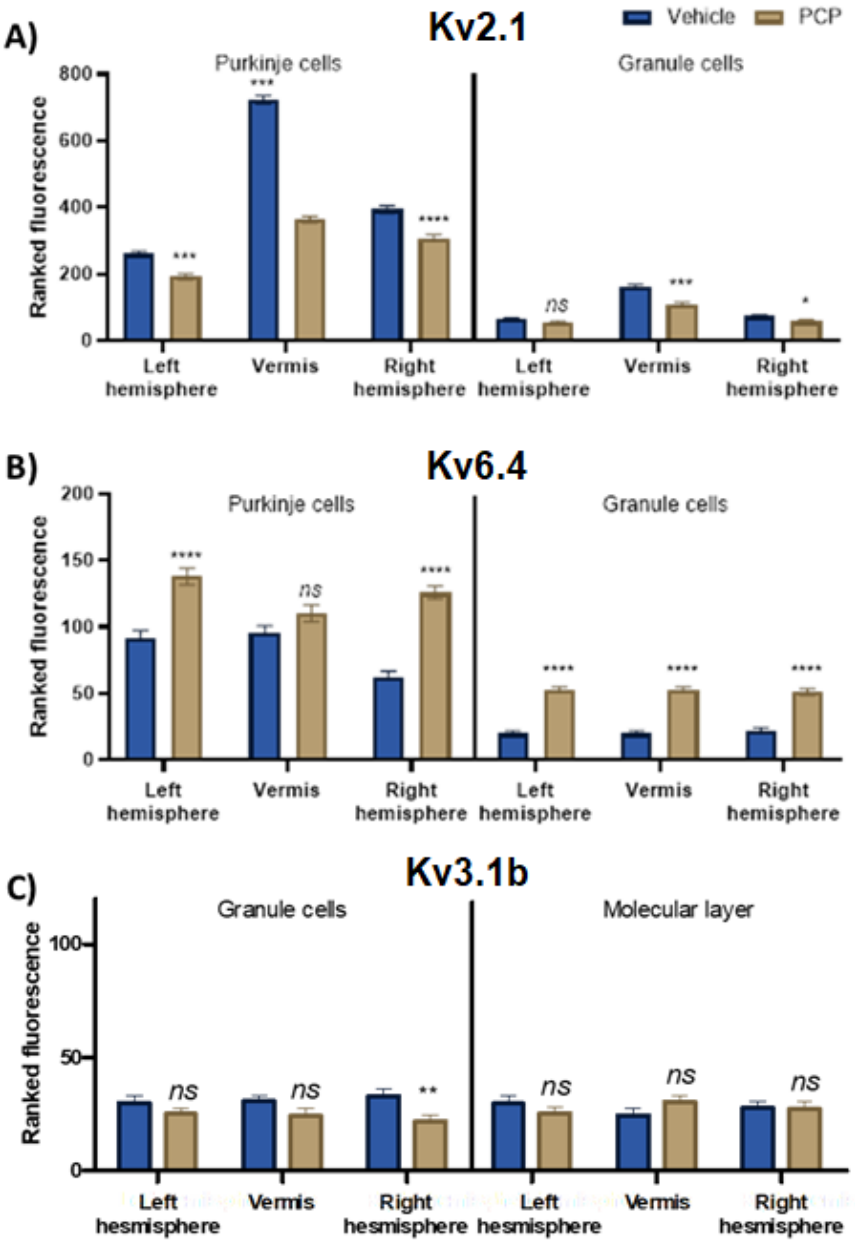

Figure 5-2 Effects of PCP subchronic treatment of Kv2.1, Kv6.4 and Kv3.1b protein expression quantified by fluorescence staining.

Graphs in Panel A, B, and C illustrate the fluorescence of Kv2.1, Kv6.4, and Kv3.1b, respectively. Values represent mean ranks ± SEM. Significance: **, $p < .02$; ***, $p < .001$; **** $p < .0001$ (Mann-Whitney U test). The numbers of cells/areas used in analysis are indicated in figures 5-3 – 5-5 on next pages.

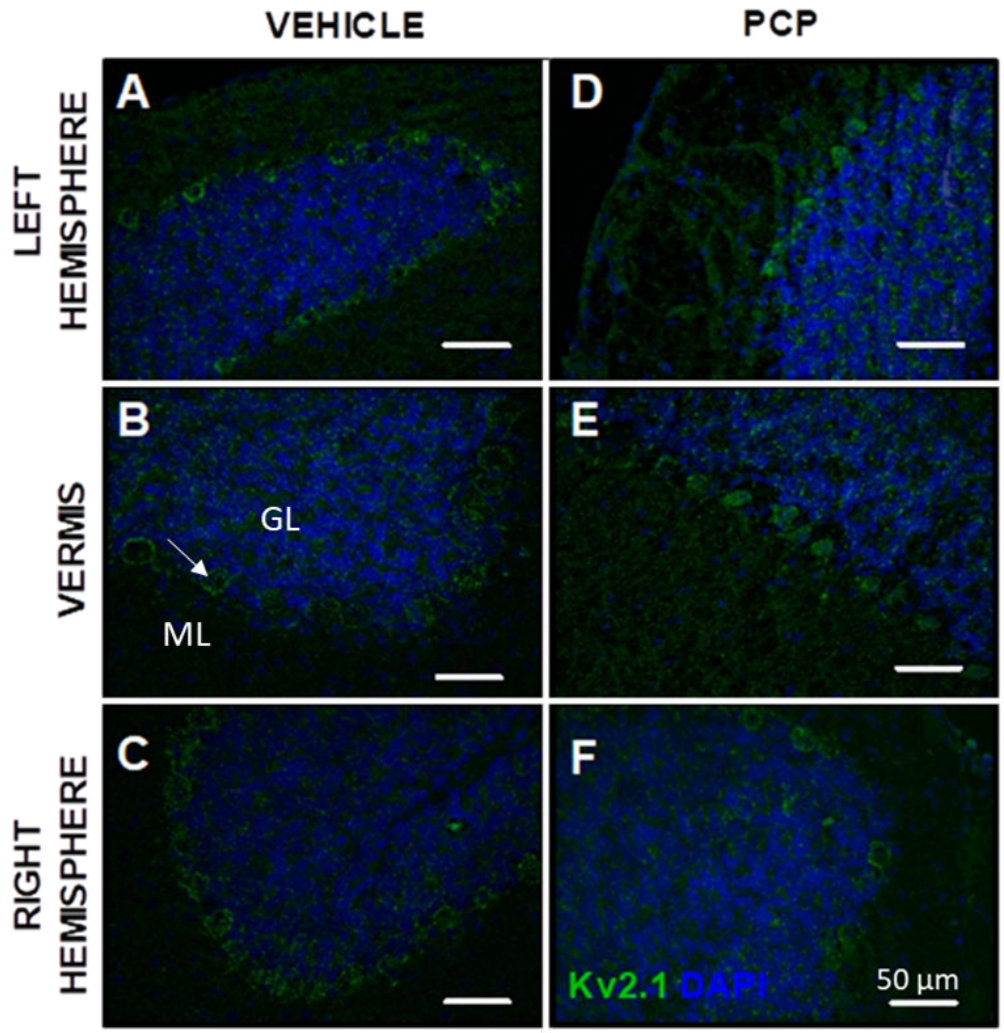

		Kv2.1 CTCF; mean rank ± SEM, n (cells)		
Region	**Group**	**Left hemisphere**	**Vermis**	**Right hemisphere**
PC	Veh	260.2 ± 8.4, 237	723.2 ± 12.3, 454	393. ± 11.3, 339
	PCP	191.8 ± 8.5, 217	362.9 ± 9.2, 586	307.6 ± 9.8, 359
GL	Veh	63.8 ± 4.7, 55	161.6 ± 6.7, 117	721.9 ± 4.6, 72
	PCP	54.7 ± 4.1, 62	108.3 ± 5.9, 146	57.6 ± 4.5, 59

Figure 5-3 Micrographs showing Kv2.1 in the PCP model and control animals.
The Kv2.1 (green) that is expressed in the Purkinje cells (arrow) and the granule cell layer (GL), was quantified, and is presented in the table. Nuclei (blue) were counterstained with DAPI. Abbreviations: ML, molecular layer.

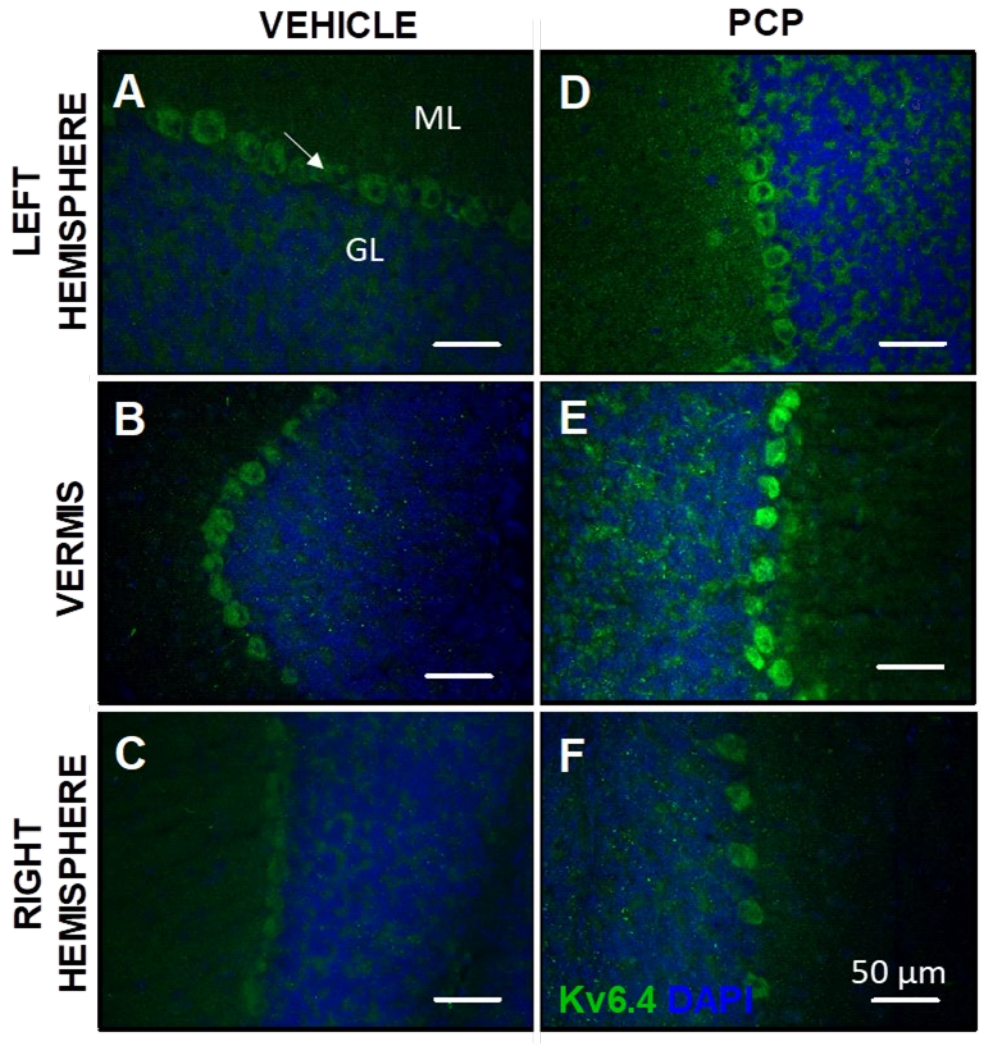

		Kv6.4 CTCF; mean rank ± SEM, n (areas)		
Region	**Group**	**Left hemisphere**	**Vermis**	**Right hemisphere**
PC	Veh	92.3± 6.0, 110	99.1± 5.7, 108	52.4 ± 3.7, 94
	PCP	139.7± 6.7, 121	108.5 ± 6.2, 96	119.2 ± 3.1, 93
GL	Veh	21.6 ± 1.3, 36	20.9 ± 1.2, 36	22.3 ± 1.9, 36
	PCP	50.5 ± 1.9, 36	51.2 ± 2.0, 36	49.9 ± 1.7, 36

Figure 5-4 Micrographs showing Kv6.4 in the PCP model and control animals.
The Kv6.4 (green) that is expressed in the Purkinje cells (arrow) and the granule cell layer (GL), was quantified and is presented in the table. Nuclei (blue) were counterstained with DAPI. Abbreviations: ML, molecular layer.

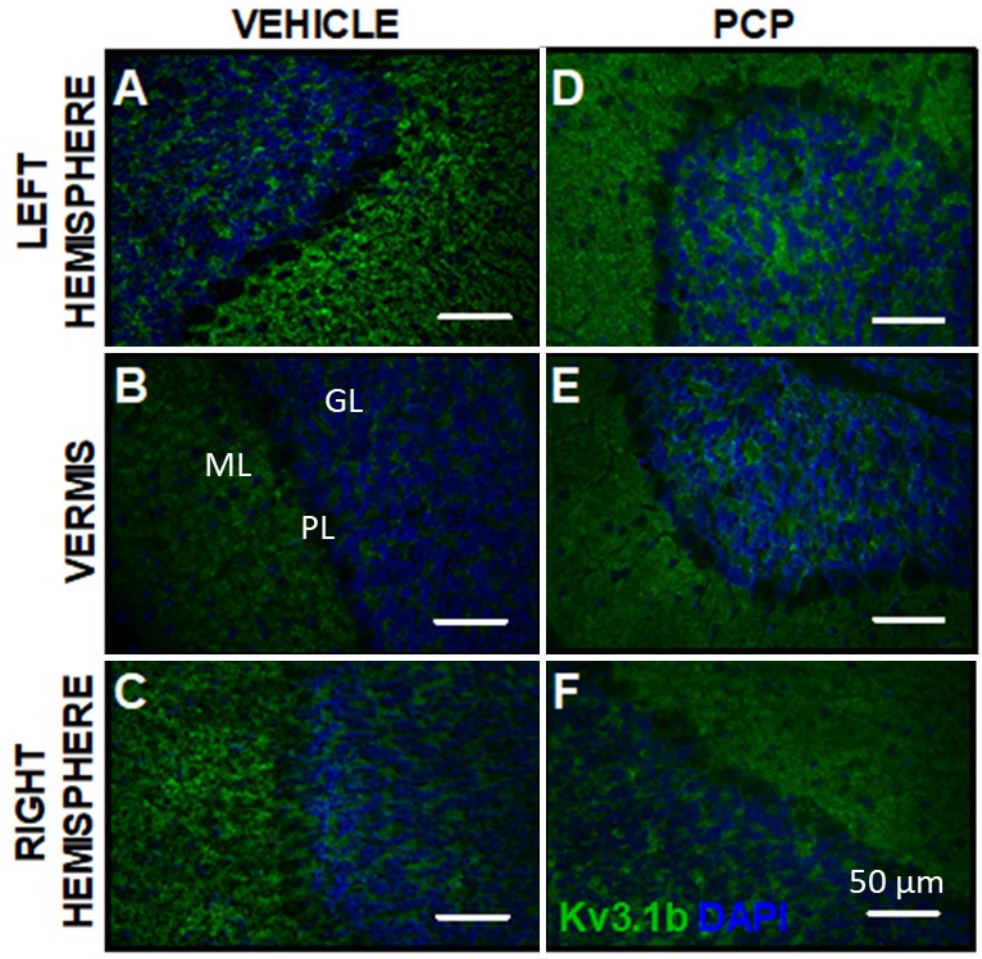

		Kv3.1b CTCF; mean rank ± SEM, n (areas)		
Region	**Group**	**Left hemisphere**	**Vermis**	**Right hemisphere**
GL	Veh	29.9 ± 3.2, 27	30.7 ± 2.5, 27	33.1 ± 3.0, 27
	PCP	25.1 ± 2.8, 27	24.3 ± 3.4, 27	21.9 ± 2.6, 27
ML	Veh	29.6 ± 3.4, 27	24.5 ± 3.2, 27	27.7 ± 3.3, 27
	PCP	25.3 ± 2.6, 27	30.5 ± 2.7, 27	27.3 ± 3.2, 27

Figure 5-5 Micrographs showing Kv3.1b in the subchronic PCP model and control animals.

The Kv3.1b (green) that is expressed in the granule cell layer (GL) and the molecular layer (ML) was quantified and is presented in the table. Nuclei (blue) were counterstained with DAPI. Abbreviations: PL, Purkinje cell layer.

Regulation of Kv2.1- and Kv6.4-coding genes

After establishing the regulation patterns of Kv2.1 and Kv6.4 at protein level, we then investigated the regulation of these two subunits at the gene level. We observed a non-statistically significant reduction in Kcnb1 gene product in the PCP-treated animals, a statistically significant increase in Kcng4 gene products was observed in PCP animals (**Figure 5-6**).

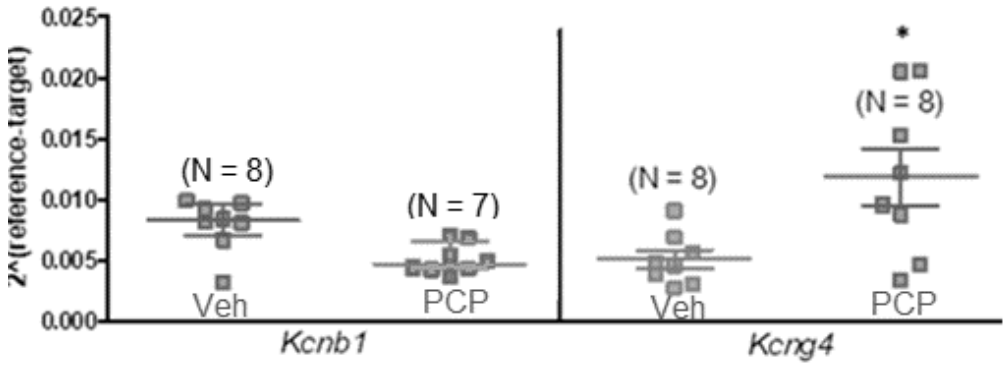

Figure 5-6 Regulation of *Kcnb1* and *Kcnb4* genes in the subchronic PCP model.
There was a non-significant downregulation of *Kcnb1* gene downregulation whereas the *Kcng4* gene was significantly upregulated in the PCP model. Significance: *, $p < .05$ (Mann-Whitney U test, *Kcnb1*; t-test, *Kcng4*).

5.5 Discussion

The cerebellar function is best interpreted as a 'forward controller' which utilises the internal memory to represent system state to enable predictive processing based on sensory information (Diedrichsen, Shadmehr and Ivry,

2010; Shadmehr and Mussa-Ivaldi, 2018). The GCs and PCs play an important role in this system, whereby the former integrate the sensorimotor information from various regions in the brain, whereas the latter generate an error signal to compensate for the mismatch between the anticipated outcome of sensory response and the predicted outcome stored in an internal reference copy (Moberget and Ivry, 2019), thus voltage-gated potassium channels are important facilitators of this neuronal communication because of their fundamental roles in the maintenance of membrane excitability (Hille, 2001).

The overall reduction in the level of Kv2.1 in our PCP model is consistent with existing studies in *post-mortem* human subjects (reviewed in the introduction), whereas the dysregulation in Kv3.1b observed in the granular layer of the right lateral hemisphere seems to be only partially consistent with another PCP study where subchronic and intermittent treatment resulted in reduced *KCNC1* mRNA expression in parvalbumin-positive interneurons in rat prefrontal cortex (Pratt et al., 2008). In **Chapter 3** of this thesis, we demonstrated that Kv2.1 exists primarily as clusters on the plasma membranes of proximal dendrites and the soma of PCs and GCs. The Kv2.1 clusters play a role in suppressing neuronal activity following several events, including glutamate stimulation, which suggests a protective function against sustained input (Misonou et al., 2004; Mohapatra et al., 2009). Moreover, we also showed in **Chapter 3** that Kv2.1 and Kv6.4

assemble together to form channels in the cerebellum, although majority of the Kv6.4 seems to be localised to cytosolic reservoirs in the PCs and GCs. Heteromeric Kv2.1/Kv6.4 configuration causes a hyperpolarising shift in voltage-dependant inactivation and reduces Kv2-mediated current density, thereby reducing neuronal excitability (Bocksteins et al., 2009; Bocksteins et al., 2012; Stas et al., 2015). In this work, the increased amount of Kv6.4 may indicate a compensatory employment of heteromeric Kv2.1/Kv6.4 channels to meet the physiological demands set out by Kv2.1 loss. The existence of this compensation could be supported by the observation that our PCP model did not manifest any changes in behaviour on day 14 as presented in **Section 4.4.1** of this work. Therefore, it would be interesting to study in the future whether a single dose of stimulant could induce an exaggerated locomotor response in the model animals that could implicate the involvement of compromised Kv2.1. Additionally, we also investigated changes in *Kcnb1* and *Kcng4* mRNA expression in the model animals. While we observed a significant increase in *Kcng4* expression that is consistent with the increased levels of Kv6.4, the *Kcnb1* showed a non-significant reduction in *Kcnb1* gene products in the PCP model; nonetheless, it is also consistent with our findings for decreased levels of Kv2.1. In contrast, the amount of Kv3.1b in granular layer was reduced in right lateral hemisphere only. The Kv3.1 channels activate at potential more positive than -10 mV thus remain closed at typical membrane potentials but open rapidly once

the action potentials reach their peak (Grissmer et al., 1994). Furthermore, they undergo little inactivation during depolarisation that last less than one second although their inactivation response is substantial once the depolarisation is extended to many seconds (Kanemasa et al., 1995), closing very rapidly once the membrane returned to resting state which results in a minimal refractory period in neurons in which Kv3.1 are responsible for repolarisation. Therefore, thy are expressed in those neuronal populations that are responsible for generating action potentials with millisecond precision to accurately represent the temporal patterns of synaptic stimuli (Rowan et al., 2016); therefore, a reducing functional expression of Kv3.1 could result in an insufficient information processing.

Recently, the notion that schizophrenia symptoms may onset as a result of a dysfunctional predictive mechanism gained momentum. Indeed, the cerebellar cortex receives multiple input and communicates it out *via* the deep cerebellar nuclei through three pathways: 1) form the cerebellar vermis to the pons, medulla, and the reticular formation; 2) from the intermediate zones to the thalamus and red nucleus; and 3) form the lateral hemispheres to the thalamus (Baldaçara et al., 2008). The input which arrives in the thalamus is then projected to different parts of the cerebral cortex, including motor cortex, parietal cortex, and the frontal cortex. In the context of the predictive model, the cerebellum therefore has significant influence over the information processing in those areas (Middleton and

Strick, 2000; Baldaçara et al., 2008; Sterzer et al., 2018). In our study we found that all Kv2.1, Kv6.4, and Kv3.1b are regulated differently across the cerebellum in the PCP model. For example, while the Kv2.1 decreased in the PCs in both lateral hemisphere and vermis, the Kv6.4 increased in lateral hemispheres but not in the vermis. In human, fMRI studies found correlates between cognitive performance and reduced vermal volume (Nopoulos et al., 1999; Crespo-Facorro et al., 2007; Andreasen, Calage and O'Leary, 2008). Such observation in Kv2.1/Kv6.4 regulation in human could lead to hyperexcitability of PCs in the vermis resulting in communicating incorrect erorr messages to the frontal cortex, tereby leading to reduced cognitive performance. However, it must be stressed that although cerbellar structure appears as unifrorm, regional differences in PC and GC pakcing and morphologies exist, which could profoundly affect the energy consumption and biophysical properties of individual cells located in distinct cortical regions (Cerminara et al., 2015). For example, in rat there are considerably more PCs located at the apex of of each cerbellar folium compared to the base (Braitenberg and Atwood, 1958; Armstrong and Schild, 1970), whereas the dimeter of PCs and volume of their organelles is larger in the vermis, compared to phylogenetically younger rgions of the cerbellum (Müller and Heinsen, 1984). Therefore, it can be speculated that the changes in regulaiton observed in the different parts of the cerebellum

in our model most likely reflect the functions ascribed to the particular region within these parts, as opposed to the them as a whole.

5.6 Conclusions

In this chapter we demonstrated that a differential regulation of Kv channels in a subchronic PCP model can persist for at least seven days after discontinuation of treatment – when a direct influence of PCP on Kv expression is no longer possible. Remarkably, we showed that reduction of Kv2.1 coincided with an increase in Kv6.4, and we speculated that this overexpression may compensate for the loss of Kv2.1 function. We also demonstrated that the regulation of Kv channels can be unique to individual regions of the cerebellum, which can be attributed to their distinct functions.

Chapter 6 Concluding Remarks and Future Perspectives

The overall aim of this thesis was to investigate the cerebellar regulation of three voltage-gated potassium channel α-subunits in a pharmacologically induced mouse model of schizophrenia with the end goal to shed light on their contribution to the pathophysiology of this disorder. The expression of two of these α-subunits in the cerebellum was not previously established, thus the focus in **Chapter 3** was to investigate the subcellular localisation of Kv2.1 and Kv6.4 in the two main cerebellar cortical neuronal populations. There, by using a combination of immunohistochemistry and microscopy techniques, we learnt that in the Purkinje cells, the Kv2.1 are primarily localised to clusters on the plasma membrane of soma and proximal dendrites, whereas in granule cells, we only observed these clusters in the soma. We also learnt that the silent subunit Kv6.4 appears to be localised to cytosolic reservoirs in the soma of both the Purkinje cells and the granule cells, and then by using proximity ligation assay we further demonstrated, for the very first time, the *in-situ* interaction between Kv2.1 and Kv6.4 in any neuron. Although the Kv2.1 have been studied extensively in both intact and

cultured neurons as well as in transfected cell lines, our findings provide the first simultaneous account on the expression of Kv2.1 and Kv6.4, and to best of our knowledge, it is the first reported attempt at demonstrating *in situ* interaction between these subunits using histology techniques. Nonetheless, we also identified several deficiencies which should be addressed in the future. First, neuronal nuclear antigen NeuN should be used to selectively stain the cerebellar granule cells to ensure the correct neurons in the granular layer are being investigated. Additionally, the neurites can be differentiated by selectively staining the dendrites and axons by using markers such as Map2 and Tau, respectively, and the axon initial segment may be distinguished specifically with Ankyrin G or Spectrin IV. Finally, to maximise the impact of this work, all imaging should be completed using confocal microscopy to enable the visualisation of fine structures.

To investigate the regulation of the above and the Kv3.1b in the disease state, we needed to generate a model that is relevant to the underlaying schizophrenia pathology. Therefore, in **Chapter 4** we subjected the CBA/Ca mouse strain to subchronic PCP regiment, providing the first account of the behavioural phenotype produced in CBA/Ca mice by repeated phencyclidine administration. By implementing several behavioural paradigms throughout the duration of treatment and after its discontinuation, we learnt that phencyclidine in CBA/Ca strain produces

aberrant locomotor activity, stimulant sensitisation, changes in grooming and rearing behaviours, as well as induced stereotypy, which are considered significant correlates to the positive symptoms observed in schizophrenia. While major changes in behaviour were not manifested during the withdrawal period, the treatment resulted in differential regulation of two NMDA receptor subtypes in the in frontal cortex and the cerebellum as well as altered cerebellar morphology. Lastly, by applying cerebellar specific motor test in a separate experiment, we showed that acute PCP affects cerebellar motor function, and that some of the effects together with select behavioural featured observed in the subchronic study can be attenuated by concomitant application of antipsychotic drugs clozapine and haloperidol. Collectively, our findings validated the model in several aspects of face, construct and predictivity; however, several additional aspects in the realms of negative and cognitive symptoms remain to be investigated.

At last, in the grand **Chapter 5**, by using a combination of histological and biomolecular analyses, we presented the differential regulation of the three Kv subunits in the cerebellar cortex in the lateral hemispheres and vermis of the pharmacological schizophrenia model. While the contribution of Kv3.1b in the cerebellar pathology of this disorder remains to be investigated further, we concluded that the reduction in amount of Kv2.1 accompanied by the increase in Kv6.4 in the PCP model may indicate a compensatory mechanism where Kv6.4 recuperates for the loss of Kv2.1

function by increased Kv2.1/Kv6.4 membrane expression. Additionally, we also hypothesised that, while effectively balancing the neuronal functionality, this compensatory mechanism might be responsible for producing exaggerated locomotor response to subsequent dose of PCP in animals, and perhaps the same mechanism might be responsible for exacerbating the positive symptoms in stabilised schizophrenia subjects by administering NMDA antagonists to humans. Therefore, a future study should seek to investigate the presence of this mechanism by using proximity ligation assay to compare the abundance of Kv2.1/Kv6.4 in the PCP model to control animas. Additional supporting evidence could be obtained by studying the electrophysiological profiles of Purkinje cells and granule cells in the PCP model and testing their reposes to various insults.

In conclusion, the overall aim of this thesis has been accomplished. At the same time, new avenues have been opened for this journey to cointinue…

Chapter 7 Bibliography

ABBOTT, L.C. and SOTELO, C. (2000) Ultrastructural analysis of catecholaminergic innervation in weaver and normal mouse cerebellar cortices. *Journal of Comparative Neurology*, 426(2), pp. 316–329.

ABI-DARGHAM, A. et al. (2000) Increased baseline occupancy of D2 receptors by dopamine in schizophrenia. *Proceedings of the National Academy of Sciences of the United States of America*, 97(14), pp. 8104–8109.

ADELMAN, J.P. et al. (1995) Episodic ataxia results from voltage-dependent potassium channels with altered functions. *Neuron*, 15(6), pp. 1449–1454.

AGNEW, W.S. et al. (1978) Purification of the tetrodotoxin-binding component associated with the voltage-sensitive sodium channel from Electrophorus electricus electroplax membranes. *Proceedings of the National Academy of Sciences of the United States of America*, 75(6), pp. 2606–2610.

AJNAKINA, O. et al. (2016) Impact of childhood adversities on specific symptom dimensions in first-episode psychosis. *Psychological Medicine*, 46(2), pp. 317–326.

AKSHOOMOFF, N.A. and COURCHESNE, E. (1992) A New Role for the Cerebellum in Cognitive Operations. *Behavioral Neuroscience*, 106(5), pp. 731–738.

ALEXANDER, S.P.H. et al. (2017) THE CONCISE GUIDE TO PHARMACOLOGY 2017/18: Voltage-gated ion channels. *British Journal of Pharmacology*, 174, pp. S160–S194.

ALLE, H., KUBOTA, H. and GEIGER, J.R.P. (2011) Sparse but highly efficient Kv3 outpace BKca channels in action potential repolarization at hippocampal mossy fiber boutons. *Journal of Neuroscience*, 31(22), pp. 8001–8012.

ALLEN, R.M. and YOUNG, S.J. (1978) Phencyclidine-induced psychosis. *American Journal of Psychiatry*, 135(9), pp. 1081–1084.

AMANN, L.C. et al. (2010) Mouse behavioral endophenotypes for schizophrenia. *Brain Research Bulletin*, 83(3–4), pp. 147–161.

AMARILLO, Y. et al. (2008) Ternary Kv4.2 channels recapitulate voltage-dependent inactivation kinetics of A-type K+ channels in cerebellar granule neurons. *Journal of Physiology*, 586(8), pp. 2093–2106.

AMBERG, G.C. and SANTANA, L.F. (2006) Kv2 channels oppose myogenic constriction of rat cerebral arteries. *American Journal of Physiology - Cell Physiology*, 291(2), [Online] Available from: doi.org/10.1152/ajpcell.00086.2006.

AMBOS *Cerebellum*. Available from : https://www.amboss.com/us/knowledge/Cerebellum [Accessed 20/02/20].

ANDERSON, K.K. et al. (2015) Incidence of psychotic disorders among first-generation immigrants and refugees in Ontario. *Cmaj*, 187(9), pp. E279–E286.

ANDERSON, P.A.V. and GREENBERG, R.M. (2001) Phylogeny of ion channels: Clues to structure and function. *Comparative Biochemistry and Physiology - B Biochemistry and Molecular Biology*, 129(1), pp. 17–28.

ANDREASEN, N.C. (1999) A Unitary Model of Schizophrenia: Bleuler's "Fragmented Phrene" as Schizencephaly. *Archives of General Psychiatry*, 56(9), pp. 781–787.

ANDREASEN, N.C., CALAGE, C.A. and O'LEARY, D.S. (2008) Theory of mind and schizophrenia: A positron emission tomography study of medication-free patients. *Schizophrenia Bulletin*, 34(4), pp. 708–719.

ANIS, N.A. et al. (1983) The dissociative anaesthetics, ketamine and phencyclidine, selectively reduce excitation of central mammalian neurones by N-methyl-aspartate. *British Journal of Pharmacology*, 79(2), pp. 565–575.

ANTICEVIC, A. et al. (2015) Association of Thalamic Dysconnectivity and Conversion to Psychosis in Youth and Young Adults at Elevated Clinical Risk. *JAMA Psychiatry*, 72(9), p. 882.

ANTONUCCI, D.E. et al. (2001) Dynamic localization and clustering of dendritic Kv2.1 voltage-dependent potassium channels in developing hippocampal neurons. *Neuroscience*, 108(1), pp. 69–81.

ARENDT, M. et al. (2005) Cannabis-induced psychosis and subsequent schizophrenia-spectrum disorders: Follow-up study of 535 incident cases. *British Journal of Psychiatry*, 187(DEC.), pp. 510–515.

ARMSTRONG, D.M. and SCHILD, R.F. (1970) A quantitative study of the purkinje cells in the cerebellum of the albino rat. *Journal of Comparative Neurology*, 139(4), pp. 449–456.

ARNONE, D. et al. (2009) Magnetic resonance imaging studies in bipolar disorder and schizophrenia: Meta-analysis. *British Journal of Psychiatry*, 195(3), pp. 194–201.

AUDET, M.C., GOULET, S. and DORÉ, F.Y. (2006) Repeated subchronic exposure to phencyclidine elicits excessive atypical grooming in rats. *Behavioural Brain Research*, 167(1), pp. 103–110.

BACOPOULOS, N.C. et al. (1979) Antipsychotic drug action in schizophrenic patients: Effect on cortical dopamine metabolism after long-term treatment. *Science*, 205(4413), pp. 1405–1407.

BAGCHI, S., FREDRIKSSON, R. and WALLÉN-MACKENZIE, Å. (2015) In Situ Proximity Ligation Assay (PLA). *Methods in Molecular Biology*, 1318, pp. 149–159.

BALDAÇARA, L. et al. (2008) Cerebellum and psychiatric disorders. *Revista Brasileira de Psiquiatria*, 30(3), pp. 281–289.

BALU, D.T. (2016) The NMDA Receptor and Schizophrenia. From Pathophysiology to Treatment. In: *Advances in Pharmacology*. pp. 351–382.

BASSETT, A.S. et al. (2005) Clinical features of 78 adults with 22q11 deletion syndrome. *American Journal of Medical Genetics*, 138 A(4), pp. 307–313.

BEARD, J. (2003) Iron deficiency alters brain development and functioning. *Journal of Nutrition*, 133(5 SUPPL. 2), [Online] Available from: doi.org/10.1093/jn/133.5.1468s.

BEARD, J.L. (2008) Why iron deficiency is important in infant development. *Journal of Nutrition*, 138(12), pp. 2534–2536.

BECKINGHAUSEN, J. and SILLITOE, R. V. (2019) Insights into cerebellar development and connectivity. *Neuroscience Letters*, 688, pp. 2–13.

BEKKERS, J.M. (2000) Distribution and activation of voltage-gated potassium channels in cell-attached and outside-out patches from large layer 5 cortical pyramidal neurons of the rat. *Journal of Physiology*, 525(3), pp. 611–620.

BENES, F.M. et al. (2007) Regulation of the GABA cell phenotype in hippocampus of schizophrenics and bipolars. *Proceedings of the National Academy of Sciences of the United States of America*, 104(24), pp. 10164–10169.

BENEYTO, M. et al. (2007) Abnormal glutamate receptor expression in the medial temporal lobe in schizophrenia and mood disorders. *Neuropsychopharmacology*, 32(9), pp. 1888–1902.

BERGERON, R. and T. COYLE, J. (2012) NAAG, NMDA Receptor and Psychosis. *Current Medicinal Chemistry*, 19(9), pp. 1360–1364.

BERNARD, J.A., ORR, J.M. and MITTAL, V.A. (2017) Cerebello-thalamo-cortical networks predict positive symptom progression in individuals at ultra-high risk for psychosis. *NeuroImage: Clinical*, 14, pp. 622–628.

BERTRON, J.L., SETO, M. and LINDSLEY, C.W. (2018) DARK Classics in Chemical Neuroscience: Phencyclidine (PCP). *ACS Chemical Neuroscience*, 9(10), pp. 2459–2474.

BEVINS, R.A. and BESHEER, J. (2006) Object recognition in rats and mice: a one-trial non-matching-to-sample learning task to study “recognition memory.” *Nature Protocols*, 1(3), pp. 1306–1311.

BIEDERMANN, F. and FLEISCHHACKER, W.W. (2016) Psychotic disorders in DSM-5 and ICD-11. *CNS Spectrums*, 21(4), pp. 349–354.

BISHOP, H.I. et al. (2015) Distinct cell-and layer-specific expression patterns and independent regulation of kv2 channel subtypes in cortical pyramidal neurons. *Journal of Neuroscience*, 35(44), pp. 14922–14942.

BLACK, J.A., WAXMAN, S.G. and SMITH, K.J. (2006) Remyelination of dorsal column axons by endogenous Schwann cells restores the normal pattern of Na v1.6 and K v1.2 at nodes of Ranvier. *Brain*, 129(5), pp. 1319–1329.

BLACKMAN, G. and MACCABE, J.H. (2020) Schizophrenia. *Medicine (United Kingdom)*, 48(11), pp. 704–708.

BOCKSTEINS, E. et al. (2009) Kv2.1 and silent Kv subunits underlie the delayed rectifier K+ current in cultured small mouse DRG neurons. *American Journal of Physiology - Cell Physiology*, 296(6), p. 1278.

BOCKSTEINS, E. (2016) Kv5, Kv6, Kv8, and Kv9 subunits: No simple silent bystanders. *Journal of General Physiology*, 147(2), pp. 105–125.

BOCKSTEINS, E. et al. (2012) The electrically silent Kv6.4 subunit confers hyperpolarized gating charge movement in Kv2.1/Kv6.4 heterotetrameric channels. *PLoS ONE*, 7(5), p. e37143.

BOCKSTEINS, E. et al. (2014) The subfamily-specific interaction between Kv2.1 and Kv6.4 subunits is determined by interactions between the N-And C-termini. *PLoS ONE*, 9(6), p. e98960.

BOCKSTEINS, E. and SNYDERS, D.J. (2012) Electrically silent Kv Subunits: Their Molecular and Functional Characteristics. *Physiology*, 27(2), pp. 73–84.

BOKS, M.P.M. et al. (2004) Neurological soft signs discriminating mood disorders from first episode schizophrenia. *Acta Psychiatrica Scandinavica*, 110(1), pp. 29–35.

BOUZA, A.A. and ISOM, L.L. (2018) Voltage-gated sodium channel β subunits and their related diseases. In: *Handbook of Experimental Pharmacology*. pp. 423–450.

BRAITENBERG, V. and ATWOOD, R.P. (1958) Morphological observations on the cerebellar cortex. *Journal of Comparative Neurology*, 109(1), pp. 1–33.

BRIGMAN, J.L. et al. (2009) Effects of subchronic phencyclidine (PCP) treatment on social behaviors, and operant discrimination and reversal learning in C57BL/6J mice. *Frontiers in Behavioral Neuroscience*, 3(FEB), [Online] Available from: doi.org/10.3389/neuro.08.002.2009.

BROOKS, J.X. and CULLEN, K.E. (2009) Multimodal integration in rostral fastigial nucleus provides an estimate of body movement. *Journal of Neuroscience*, 29(34), pp. 10499–10511.

BROWN, A.S. et al. (2007) Elevated prenatal homocysteine levels as a risk factor for schizophrenia. *Archives of General Psychiatry*, 64(1), pp. 31–39.

BUCHANAN, R.W. and HEINRICHS, D.W. (1989) The neurological evaluation scale (NES): A structured instrument for the assessment of neurological signs in schizophrenia. *Psychiatry Research*, 27(3), pp. 335–350.

BUSTIN, S.A. et al. (2005) Quantitative real-time RT-PCR - A perspective. *Journal of Molecular Endocrinology*, 34(3), pp. 597–601.

CADINU, D. et al. (2018) NMDA receptor antagonist rodent models for cognition in schizophrenia and identification of novel drug treatments, an update. *Neuropharmacology*, 142, pp. 41–62.

CALVO, M. et al. (2016) Altered potassium channel distribution and composition in myelinated axons suppresses hyperexcitability following injury. *eLife*, 5(APRIL2016), [Online] Available from: doi.org/10.7554/eLife.12661.

DEL CAMINO, D. et al. (2000) Blocker protection in the pore of a voltage-gated K+ channel and its structural implications. *Nature*, 403(6767), pp. 321–325.

CANNON, T.D. et al. (2008) Prediction of psychosis in youth at high clinical risk: A multisite longitudinal study in North America. *Archives of General Psychiatry*, 65(1), pp. 28–37.

CANNON, T.D. et al. (1998) The genetic epidemiology of schizophrenia in a Finnish twin cohort: A population-based modeling study. *Archives of General Psychiatry*, 55(1), pp. 67–74.

CANTOR-GRAAE, E. and SELTEN, J.P. (2005) Schizophrenia and migration: A meta-analysis and review. *American Journal of Psychiatry*, 162(1), pp. 12–24.

CAO, H. et al. (2018) Cerebello-thalamo-cortical hyperconnectivity as a state-independent functional neural signature for psychosis prediction and characterization. *Nature Communications*, 9(1), p. 3836.

CARDIN, J.A. et al. (2009) Driving fast-spiking cells induces gamma rhythm and controls sensory responses. *Nature*, 459(7247), pp. 663–667.

CARLSSON, A. and LINDQVIST, M. (1963) Effect of Chlorpromazine or Haloperidol on Formation of 3-Methoxytyramine and Normetanephrine

in Mouse Brain. *Acta Pharmacologica et Toxicologica*, 20(2), pp. 140–144.

CASTAÑÉ, A., SANTANA, N. and ARTIGAS, F. (2015) PCP-based mice models of schizophrenia: Differential behavioral, neurochemical and cellular effects of acute and subchronic treatments. *Psychopharmacology*, 232(21–22), pp. 4085–4097.

CATTABENI, F. and DI LUCA, M. (1997) Developmental models of brain dysfunctions induced by targeted cellular ablations with methylazoxymethanol. *Physiological Reviews*, 77(1), pp. 199–215.

CATTS, V.S. et al. (2016) A quantitative review of the postmortem evidence for decreased cortical N-methyl-d-aspartate receptor expression levels in schizophrenia: How can we link molecular abnormalities to mismatch negativity deficits? *Biological Psychology*, 116, pp. 57–67.

CERMINARA, N.L. et al. (2015) Re-defining the cerebellar cortex as an assembly of non-uniform Purkinje cell microcircuits *Nature Reviews Neuroscience*, 16(2), pp. 1–28.

CHAN, R.C.K. and CHEN, E.Y.H. (2007) Neurological abnormalities in Chinese schizophrenic patients. *Behavioural Neurology*, 18(3), pp. 171–181.

CHARLSON, F.J. et al. (2018) Global epidemiology and burden of schizophrenia: Findings from the global burden of disease study 2016. *Schizophrenia Bulletin*, 44(6), pp. 1195–1203.

CHARTOFF, E.H., HEUSNER, C.L. and PALMITER, R.D. (2005) Dopamine is not required for the hyperlocomotor response to NMDA receptor antagonists. *Neuropsychopharmacology*, 30(7), pp. 1324–1333.

CHEN, C. et al. (2005) Real-time quantification of microRNAs by stem-loop RT-PCR. *Nucleic Acids Research*, 33(20), [Online] Available from: doi.org/10.1093/nar/gni178.

CHEN, Y.L.R., CHEN, Y.H.E. and MAK, F.L. (2000) Soft neurological signs in schizophrenic patients and their nonpsychotic siblings. *Journal of Nervous and Mental Disease*, 188(2), pp. 84–89.

CHUNG, Y. and CANNON, T.D. (2015) Brain imaging during the transition from psychosis prodrome to Schizophrenia. *Journal of Nervous and Mental Disease*, 203(5), pp. 336–341.

CHUNG, Y.H. et al. (2001) Age-related changes in the distribution of Kv1.1 and Kv1.2 channel subunits in the rat cerebellum. *Brain Research*, 897(1–2), pp. 193–198.

CHUNG, Y.H. et al. (2005) Immunohistochemical study on the distribution of the voltage-gated potassium channels in the gerbil cerebellum. *Neuroscience Letters*, 374(1), pp. 58–62.

CLAGHORN, J. et al. (1987) The risks and benefits of clozapine versus chlorpromazine. *Journal of Clinical Psychopharmacology*, 7(6), pp. 377–384.

CLAPCOTE, S.J. et al. (2007) Behavioral Phenotypes of Disc1 Missense Mutations in Mice. *Neuron*, 54(3), pp. 387–402.

CLARK, R.E., ZHANG, A.A. and LAVOND, D.G. (1992) Reversible Lesions of the Cerebellar Interpositus Nucleus During Acquisition and Retention of a Classically Conditioned Behavior. *Behavioral Neuroscience*, 106(6), pp. 879–888.

COHEN, B.D. et al. (1962) Comparison of Phencyclidine Hydrochloride (Sernyl) with Other Drugs: Simulation of Schizophrenic Performance

with Phencyclidine Hydrochloride (Sernyl), Lysergic Acid Diethylamide (LSD-25), and Amobarbital (Amytal) Sodium; II. Symbolic and Sequential Think. *Archives of General Psychiatry*, 6(5), pp. 395–401.

COHEN, C.I. et al. (2012) The relationship between trauma and clinical outcome variables among older adults with schizophrenia spectrum disorders. *American Journal of Geriatric Psychiatry*, [Online] Available from: doi.org/10.1097/JGP.0b013e318211817e.

COLBERT, C.M. (2002) Back-propagating action potentials in pyramidal neurons: A putative signaling mechanism for the induction of Hebbian synaptic plasticity. *Restorative Neurology and Neuroscience*, 19(3–4), pp. 199–211.

COLELLA, A.D. et al. (2012) Comparison of Stain-Free gels with traditional immunoblot loading control methodology. *Analytical Biochemistry*, 430(2), pp. 108–110.

CONLEY, R.R. and BUCHANAN, R.W. (1997) Evaluation of treatment-resistant schizophrenia. *Schizophrenia Bulletin*, 23(4), pp. 663–674.

CONN, P.J., LINDSLEY, C.W. and JONES, C.K. (2009) Activation of metabotropic glutamate receptors as a novel approach for the treatment of schizophrenia. *Trends in Pharmacological Sciences*, 30(1), pp. 25–31.

CONTRERAS, P.C. et al. (1988) Biochemical and behavioral effects of sigma and PCP ligands. *Synapse*, 2(3), pp. 240–243.

COYLE, J. (2006) Glutamate and Schizophrenia: Beyond the Dopamine Hypothesis. *Cellular and Molecular Neurobiology*, 26(4), pp. 363–382.

COYLE, J.T. (1996) The glutamatergic dysfunction hypothesis for schizophrenia. *Harvard Review of Psychiatry*, 3(5), pp. 241–253.

CRAWLEY, J. and BAILEY, K. (2008) Anxiety-Related Behaviors in Mice. In: *Methods of Behavior Analysis in Neuroscience*. Taylor & Francis Group, LLC, pp. 77–101.

CREESE, I., BURT, D.R. and SNYDER, S.H. (1976) Dopamine receptor binding predicts clinical and pharmacological potencies of antischizophrenic drugs. *Science*, 192(4238), pp. 481–483.

CRILLY, J. (2007) The history of clozapine and its emergence in the US market: A review and analysis. *History of Psychiatry*, 18(1), pp. 39–60.

CROSSLEY, N.A. et al. (2009) Superior temporal lobe dysfunction and frontotemporal dysconnectivity in subjects at risk of psychosis and in first-episode psychosis. *Human Brain Mapping*, 30(12), pp. 4129–4137.

CULLEN, A.E. et al. (2014) Daily stressors and negative life events in children at elevated risk of developing schizophrenia. *British Journal of Psychiatry*, 204(5), pp. 354–360.

D'ADAMO, M.C. et al. (1999) Mutations in the KCNA1 gene associated with episodic ataxia type-1 syndrome impair heteromeric voltage-gated K + channel function . *The FASEB Journal*, 13(11), pp. 1335–1345.

DALMAU, J. et al. (2007) Paraneoplastic anti-N-methyl-D-aspartate receptor encephalitis associated with ovarian teratoma. *Annals of Neurology*, 61(1), pp. 25–36.

D'ANGELO, E. (2018) Physiology of the cerebellum. In: *Handbook of Clinical Neurology*. pp. 85–108.

DAVIES, G. et al. (2003) A Systematic Review and Meta-analysis of Northern Hemisphere Season of Birth Studies in Schizophrenia. *Schizophrenia Bulletin*, 29(3), pp. 587–593.

DAVIS, K.L. et al. (1991) Dopamine in schizophrenia: A review and reconceptualization. *American Journal of Psychiatry*, 148(11), pp. 1474–1486.

DEALBERTO, M.J. (2010) Ethnic origin and increased risk for schizophrenia in immigrants to countries of recent and longstanding immigration. *Acta Psychiatrica Scandinavica*, 121(5), pp. 325–339.

DELAY, J., DENIKER, P. and HARL, J.M. (1952) [Therapeutic use in psychiatry of phenothiazine of central elective action (4560 RP)]. *Annales medico-psychologiques*, 110(2 1), pp. 112–7.

DELISI, L.E. et al. (2006) Early detection of schizophrenia by diffusion weighted imaging. *Psychiatry Research - Neuroimaging*, 148(1), pp. 61–66.

DEUTSCH, E. et al. (2012) Kv2.1 cell surface clusters are insertion platforms for ion channel delivery to the plasma membrane. *Molecular Biology of the Cell*, 23(15), pp. 2917–2929.

DEVAUX, J. et al. (2003) Kv3.1b is a novel component of CNS nodes. *Journal of Neuroscience*, 23(11), pp. 4509–4518.

DICKERSON, D.D. et al. (2014) Association of aberrant neural synchrony and altered GAD67 expression following exposure to maternal immune activation, a risk factor for schizophrenia. *Translational Psychiatry*, 4, [Online] Available from: doi.org/10.1038/tp.2014.64.

DIEDRICHSEN, J., SHADMEHR, R. and IVRY, R.B. (2010) The coordination of movement: optimal feedback control and beyond. *Trends in Cognitive Sciences*, 14(1), pp. 31–39.

DIEUDONNÉ, S. (2001) Serotonergic neuromodulation in the cerebellar cortex: Cellular, synaptic, and molecular basis. *Neuroscientist*, 7(3), pp. 207–219.

DOMINO, E.F., MIRZOYAN, D. and TSUKADA, H. (2004) N-methyl-D-aspartate antagonists as drug models of schizophrenia: A surprising link to tobacco smoking. *Progress in Neuro-Psychopharmacology and Biological Psychiatry*, 28(5), pp. 801–811.

DONNELLY, P. et al. (2012) Genome-wide association study implicates HLA-C*01:02 as a risk factor at the major histocompatibility complex locus in schizophrenia. *Biological Psychiatry*, 72(8), pp. 620–628.

DU, J. et al. (2000) Frequency-dependent regulation of rat hippocampal somato-dendritic excitability by the K+ channel subunit Kv2.1. *Journal of Physiology*, 522(1), pp. 19–31.

DU, J. et al. (1998) The K+ channel, Kv2.1, is apposed to astrocytic processes and is associated with inhibitory postsynaptic membranes in hippocampal and cortical principal neurons and inhibitory interneurons. *Neuroscience*, 84(1), pp. 37–48.

DWORAKOWSKA, B. and DOŁOWY, K. (2000) Ion channels-related diseases. *Acta Biochimica Polonica*, 47(3), pp. 685–703.

E. MCCULLUMSMITH, R. et al. (2012) Recent Advances in Targeting the Ionotropic Glutamate Receptors in Treating Schizophrenia. *Current Pharmaceutical Biotechnology*, 13(8), pp. 1535–1542.

EAGLES, J. (2017) Eating disorders. In: *Psychiatry by Ten Teachers, Second Edition*. CRC Press, pp. 129–141.

EGERTON, A. et al. (2005) Impairment in perceptual attentional set-shifting following PCP administration: A rodent model of set-shifting deficits in schizophrenia. *Psychopharmacology*, 179(1), pp. 77–84.

ELLEGOOD, J. et al. (2014) Neuroanatomical phenotypes in a mouse model of the 22q11.2 microdeletion. *Molecular Psychiatry*, 19(1), pp. 99–107.

ELLENBROEK, B.A. (2016) Schizophrenia. *The Curated Reference Collection in Neuroscience and Biobehavioral Psychology*, pp. 188–195.

ENDLER, N.S. (1988) The origins of electroconvulsive therapy (ECT). *Convulsive Therapy*, 4(1), pp. 5–23.

ENGEMANN, K. et al. (2018) Childhood exposure to green space – A novel risk-decreasing mechanism for schizophrenia? *Schizophrenia Research*, 199, pp. 142–148.

EPPERSON, A. et al. (1999) Molecular diversity of K(v) α- and β-subunit expression in canine gastrointestinal smooth muscles. *American Journal of Physiology - Gastrointestinal and Liver Physiology*, 277(1 40-1), [Online] Available from: doi.org/10.1152/ajpgi.1999.277.1.g127.

VAN ERP, T.G.M. et al. (2016) Subcortical brain volume abnormalities in 2028 individuals with schizophrenia and 2540 healthy controls via the ENIGMA consortium. *Molecular Psychiatry*, 21(4), pp. 547–553.

ERRICO, F. et al. (2013) Decreased levels of d-aspartate and NMDA in the prefrontal cortex and striatum of patients with schizophrenia. *Journal of Psychiatric Research*, 47(10), pp. 1432–1437.

FAKHOURY, M. (2017) Role of the Endocannabinoid System in the Pathophysiology of Schizophrenia. *Molecular Neurobiology*, 54(1), pp. 768–778.

FEATHERSTONE, ROBERT E et al. (2008) A sensitizing regimen of amphetamine that disrupts attentional set-shifting does not disrupt working or long-term memory. *Behavioural Brain Research*, 189(1), pp. 170–179.

FEATHERSTONE, ROBERT E. et al. (2008) A sensitizing regimen of amphetamine that disrupts attentional set-shifting does not disrupt working or long-term memory. *Behavioural Brain Research*, 189(1), pp. 170–179.

FEATHERSTONE, R.E., KAPUR, S. and FLETCHER, P.J. (2007) The amphetamine-induced sensitized state as a model of schizophrenia. *Progress in Neuro-Psychopharmacology and Biological Psychiatry*, 31(8), pp. 1556–1571.

FEINSHREIBER, L. et al. (2010) Non-conducting function of the Kv2.1 channel enables it to recruit vesicles for release in neuroendocrine and nerve cells. *Journal of Cell Science*, 123(11), pp. 1940–1947.

FFRENCH-MULLEN, J.M.H. and ROGAWSKI, M.A. (1989) Interaction of phencyclidine with voltage-dependent potassium channels in cultured rat hippocampal neurons: Comparison with block of the NMDA receptor-ionophore complex. *Journal of Neuroscience*, 9(11), pp. 4051–4061.

FILALI, M. et al. (2015) Sensorimotor skills in Fxn KO/Mck mutants deficient for frataxin in muscle. *Brain Research*, 1608, pp. 91–96.

FISHER, H.L. et al. (2010) The varying impact of type, timing and frequency of exposure to childhood adversity on its association with adult psychotic disorder. *Psychological Medicine*, 40(12), pp. 1967–1978.

FLETCHER, P.J. et al. (2007) A sensitizing regimen of amphetamine impairs visual attention in the 5-choice serial reaction time test: Reversal by a

D1 receptor agonist injected into the medial prefrontal cortex. *Neuropsychopharmacology*, 32(5), pp. 1122–1132.

FLETCHER, P.J. et al. (2005) Sensitization to amphetamine, but not PCP, impairs attentional set shifting: Reversal by a D1 receptor agonist injected into the medial prefrontal cortex. *Psychopharmacology*, 183(2), pp. 190–200.

FLOURENS, P. (1842) *Recherches expérimentales sur les propriétés et les fonctions du système nerveux dans les animaux vertébrés*. Paris.

FOLEY, C., CORVIN, A. and NAKAGOME, S. (2017) Genetics of Schizophrenia: Ready to Translate? *Current Psychiatry Reports*, 19(9), [Online] Available from: doi.org/10.1007/s11920-017-0807-5.

FORNITO, A., BULLMORE, E.T. and ZALESKY, A. (2017).

FORREST, A.D., COTO, C.A. and SIEGEL, S.J. (2014) Animal Models of Psychosis: Current State and Future Directions. *Current Behavioral Neuroscience Reports*, 1(2), pp. 100–116.

FOX, P.D., LOFTUS, R.J. and TAMKUN, M.M. (2013) Regulation of Kv2.1 K+ conductance by cell surface channel density. *Journal of Neuroscience*, 33(3), pp. 1259–1270.

FRECH, G.C. et al. (1989) A novel potassium channel with delayed rectifier properties isolated from rat brain by expression cloning. *Nature*, 340(6235), pp. 642–645.

FREDRIKSSON, S. et al. (2002) Protein detection using proximity-dependent DNA ligation assays. *Nature Biotechnology*, 20(5), pp. 473–477.

FU, J. et al. (2017) Kv2.1 clustering contributes to insulin exocytosis and rescues human β-cell dysfunction. *Diabetes*, 66(7), pp. 1890–1900.

FUNK, A.J. et al. (2009) Decreased expression of NMDA receptor-associated proteins in frontal cortex of elderly patients with schizophrenia. *NeuroReport*, 20(11), pp. 1019–1022.

FUSAR-POLI, P. et al. (2013) The psychosis high-risk state: A comprehensive state-of-the-art review. *Archives of General Psychiatry*, 70(1), pp. 107–120.

FUSAR-POLI, P. and MEYER-LINDENBERG, A. (2013) Striatal presynaptic dopamine in schizophrenia, part II: Meta-analysis of [18F/11C]-DOPA PET studies. *Schizophrenia Bulletin*, 39(1), pp. 33–42.

GAREY, L.J. et al. (1998) Reduced dendritic spine density on cerebral cortical pyramidal neurons in schizophrenia. *Journal of Neurology Neurosurgery and Psychiatry*, 65(4), pp. 446–453.

GAREY, R.E. and HEATH, R.G. (1976) The effects of phencyclidine on the uptake of 3H-catecholamines by rat striatal and hypothalamic synaptosomes. *Life Sciences*, 18(10), pp. 1105–1110.

GARTHWAITE, G., WILLIAMS, G.D. and GARTHWAITE, J. (1992) Glutamate Toxicity: An Experimental and Theoretical Analysis. *European Journal of Neuroscience*, 4(4), pp. 353–360.

GEORGE, A.L. (2005) Inherited disorders of voltage-gated sodium channels. *Journal of Clinical Investigation*, 115(8), pp. 1990–1999.

GEORGIEV, D. et al. (2014) Lower Gene Expression for KCNS3 Potassium Channel Subunit in Parvalbumin-Containing Neurons in the Prefrontal Cortex in Schizophrenia. *American Journal of Psychiatry*, 171(1), pp. 62–71.

GEYER, M.A. and VOLLENWEIDER, F.X. (2008) Serotonin research: Contributions to understanding psychoses. *Trends in Pharmacological Sciences*, 29(9), pp. 445–453.

GHOSE, S. et al. (2009) Localization of NAAG-related gene expression deficits to the anterior hippocampus in schizophrenia. *Schizophrenia Research*, 111(1–3), pp. 131–137.

GILDA, J.E. and GOMES, A. V. (2013) Stain-Free total protein staining is a superior loading control to b-actin for Western blots. *Analytical Biochemistry*, 440(2), pp. 186–188.

GIROS, B. et al. (1996) Hyperlocomotion and indifference to cocaine and amphetamine in mice lacking the dopamine transporter. *Nature*, 379(6566), pp. 606–612.

GISPEN, W.H. and ISAACSON, R.L. (1981) ACTH-induced excessive grooming in the rat. *Pharmacology and Therapeutics*, 12(1), pp. 209–246.

GLANTZ, L.A. and LEWIS, D.A. (2000) Decreased dendritic spine density on prefrontal cortical pyramidal neurons in schizophrenia. *Archives of General Psychiatry*, 57(1), pp. 65–73.

GOFF, D.C. and COYLE, J.T. (2001).

GOGTAY, N. et al. (2012) Delayed white matter growth trajectory in young nonpsychotic siblings of patients with childhood-onset schizophrenia. *Archives of General Psychiatry*, 69(9), pp. 875–884.

GOLDBERG, E.M. et al. (2005) Specific functions of synaptically localized potassium channels in synaptic transmission at the neocortical GABAergic fast-spiking cell synapse. *Journal of Neuroscience*, 25(21), pp. 5230–5235.

GORDON, J.A. (2010) Testing the glutamate hypothesis of schizophrenia. *Nature Neuroscience*, 13(1), pp. 2–4.

GOULD, T.D., DAO, D.T. and KOVACSICS, C.E. (2009) The open field test. *Neuromethods*, 42, pp. 1–20.

GRAVES, T.C. (1928) Influenza in relation to the onset of acute psychoses. *Journal of Neurology, Neurosurgery and Psychiatry*, S1-9(34), pp. 97–112.

GREGGOR, A.L., THORNTON, A. and CLAYTON, N.S. (2015) Neophobia is not only avoidance: Improving neophobia tests by combining cognition and ecology. *Current Opinion in Behavioral Sciences*, 6, pp. 82–89.

GREITZER-ANTES, D. et al. (2018) Kv2.1 clusters on -cell plasma membrane act as reservoirs that replenish pools of newcomer insulin granule through their interaction with syntaxin-3. *Journal of Biological Chemistry*, 293(18), pp. 6893–6904.

GRISSMER, S. et al. (1994) Pharmacological characterization of five cloned voltage-gated K+ channels, types Kv1.1, 1.2, 1.3, 1.5, and 3.1, stably expressed in mammalian cell lines. *Molecular Pharmacology*, 45(6), pp. 1227–1234.

GRUBE, S. et al. (2011) A CAG repeat polymorphism of KCNN3 predicts SK3 channel function and cognitive performance in schizophrenia. *EMBO Molecular Medicine*, 3(6), pp. 309–319.

GUAN, D., ARMSTRONG, W.E. and FOEHRING, R.C. (2013) Kv2 channels regulate firing rate in pyramidal neurons from rat sensorimotor cortex. *The Journal of physiology*, 591(19), pp. 4807–4825.

GUTIÉRREZ-FERNÁNDEZ, J. et al. (2015) Different presence of chlamydia pneumoniae, herpes simplex virus type 1, human herpes virus 6, and

toxoplasma gondii in schizophrenia: Meta-analysis and analytical study. *Neuropsychiatric Disease and Treatment*, 11, pp. 843–852.

HABAS, C. et al. (2009) Distinct Cerebellar Contributions to Intrinsic Connectivity Networks. *Journal of Neuroscience*, 29(26), p. 8586.

HAIJMA, S. V. et al. (2013) Brain volumes in schizophrenia: A meta-analysis in over 18 000 subjects. *Schizophrenia Bulletin*, 39(5), pp. 1129–1138.

HAINES, D.E. and MIHAILOFF, G.A. (2018) The Cerebellum. In: *Fundamental Neuroscience for Basic and Clinical Applications: Fifth Edition*. Elsevier Inc., pp. 394-412.e1.

HALENE, T.B. et al. (2009) Assessment of NMDA receptor NR1 subunit hypofunction in mice as a model for schizophrenia. *Genes, Brain and Behavior*, 8(7), pp. 661–675.

HALL, C. and L, E. (1932) A study of the rat's behavior in a field. A contribution to method in comparative psychology. *University of California Publications in Psychology*, 6, pp. 1–12.

HAMMOND, J.C. et al. (2014) Evidence of glutamatergic dysfunction in the pathophysiology of schizophrenia. In: *Synaptic Stress and Pathogenesis of Neuropsychiatric Disorders*. pp. 265–294.

HANANIA, T., HILLMAN, G.R. and JOHNSON, K.M. (1999) Augmentation of locomotor activity by chronic phencyclidine is associated with an increase in striatal NMDA receptor function and an upregulation of the NR1 receptor subunit. *Synapse*, 31(3), pp. 229–239.

HANSEN, D.K. and INSELMAN, A.L. (2014) Folic Acid. In: *Encyclopedia of Toxicology: Third Edition*. pp. 616–618.

HAO, Y. et al. (2009) Schizophrenia patients and their healthy siblings share disruption of white matter integrity in the left prefrontal cortex and the hippocampus but not the anterior cingulate cortex. *Schizophrenia Research*, 114(1–3), pp. 128–135.

HARRISON, C.L. and FOWLER, D. (2004) Negative symptoms, trauma, and autobiographical memory: An investigation of individuals recovering from psychosis. *Journal of Nervous and Mental Disease*, 192(11), pp. 745–753.

HARRISON, G. et al. (1997) Increased incidence of psychotic disorders in migrants from the Caribbean to the United Kingdom. *Psychological Medicine*, 27(4), pp. 799–806.

HASHIMOTO, K. and KANO, M. (2005) Postnatal development and synapse elimination of climbing fiber to Purkinje cell projection in the cerebellum. *Neuroscience Research*, 53(3), pp. 221–228.

HECKERS, S. et al. (2013) Structure of the psychotic disorders classification in DSM-5. *Schizophrenia Research*, 150(1), pp. 11–14.

HEINRICHS, D.W. and BUCHANAN, R.W. (1988) Significance and meaning of neurological signs in schizophrenia. *American Journal of Psychiatry*, 145(1), pp. 11–18.

HENRIKSEN, M.G., NORDGAARD, J. and JANSSON, L.B. (2017) Genetics of schizophrenia: Overview of methods, findings and limitations. *Frontiers in Human Neuroscience*, 11, [Online] Available from: doi.org/10.3389/fnhum.2017.00322.

HESS, E.J. et al. (1987) Dopamine receptor subtype imbalance in schizophrenia. *Life Sciences*, 40(15), pp. 1487–1497.

HIKIDA, T. et al. (2007) Dominant-negative DISC1 transgenic mice display schizophrenia-associated phenotypes detected by measures translatable to humans. *Proceedings of the National Academy of Sciences of the United States of America*, 104(36), pp. 14501–14506.

HINTON, P. (2014) *SPSS Explained*. 2nd Editio. London and New York: Routledge Taylor & Francis Group.

HITCH, P.J. and RACK, P.H. (1980) Mental illness among Polish and Russian refugees in Bradford. *British Journal of Psychiatry*, 137(3), pp. 206–211.

HIYOSHI, T. et al. (2014) Differential effects of NMDA receptor antagonists at lower and higher doses on basal gamma band oscillation power in rat cortical electroencephalograms. *Neuropharmacology*, 85, pp. 384–396.

HO, C.S., GRANGE, R.W. and JOHO, R.H. (1997) Pleiotropic effects of a disrupted K+ channel gene: Reduced body weight, impaired motor skill and muscle contraction, but no seizures. *Proceedings of the National Academy of Sciences of the United States of America*, 94(4), pp. 1533–1538.

HODGKIN, A.L. and HUXLEY, A.F. (1952) Currents carried by sodium and potassium ions through the membrane of the giant axon of Loligo. *The Journal of Physiology*, 116(4), pp. 449–472.

HOFFMAN, E.A. et al. (2015) Formaldehyde crosslinking: A tool for the study of chromatin complexes. *Journal of Biological Chemistry*, 290(44), pp. 26404–26411.

HOFMANN, S.G. et al. (2012).

HOLLANDER, A.C. et al. (2016) Refugee migration and risk of schizophrenia and other non-affective psychoses: Cohort study of 1.3 million people

in Sweden. *BMJ (Online)*, 352, [Online] Available from: doi.org/10.1136/bmj.i1030.

HOMAYOUN, H. et al. (2004) Functional interaction between NMDA and mGlu5 receptors: Effects on working memory, instrumental learning, motor behaviors, and dopamine release. *Neuropsychopharmacology*, 29(7), pp. 1259–1269.

HONEA, R. et al. (2005) Regional deficits in brain volume in schizophrenia: A meta-analysis of voxel-based morphometry studies. *American Journal of Psychiatry*, 162(12), pp. 2233–2245.

HOOVER, J.E. and STRICK, P.L. (1999) The organization of cerebellar and basal ganglia outputs to primary motor cortex as revealed by retrograde transneuronal transport of herpes simplex virus type 1. *Journal of Neuroscience*, 19(4), pp. 1446–1463.

HOPPA, M.B. et al. (2014) Control and plasticity of the presynaptic action potential waveform at small CNS nerve terminals. *Neuron*, 84(4), pp. 778–789.

HOPTMAN, M.J. et al. (2008) A DTI study of white matter microstructure in individuals at high genetic risk for schizophrenia. *Schizophrenia Research*, 106(2–3), pp. 115–124.

HORWITZ, T. et al. (2019) A decade in psychiatric GWAS research. *Molecular Psychiatry*, 24(3), pp. 378–389.

HOWES, O., MCCUTCHEON, R. and STONE, J. (2015) Glutamate and dopamine in schizophrenia: An update for the 21st century. *Journal of Psychopharmacology*, 29(2), pp. 97–115.

HOWLAND, J.G., CAZAKOFF, B.N. and ZHANG, Y. (2012) Altered object-in-place recognition memory, prepulse inhibition, and locomotor activity in the

offspring of rats exposed to a viral mimetic during pregnancy. *Neuroscience*, 201, pp. 184–198.

HUGNOT, J.P. et al. (1996) Kv8.1, a new neuronal potassium channel subunit with specific inhibitory properties towards Shab and Shaw channels. *EMBO Journal*, 15(13), pp. 3322–3331.

HUMPHRIES, C. et al. (1996) NMDA receptor mRNA correlation with antemortem cognitive impairment in schizophrenia. *NeuroReport*, 7(12), pp. 2051–2055.

HWANG, P.M. et al. (1992) A novel K+ channel with unique localizations in mammalian brain: Molecular cloning and characterization. *Neuron*, 8(3), pp. 473–481.

HWANG, P.M., CUNNINGHAM, A.M., et al. (1993) CDRK and DRK1 K+ channels have contrasting localizations in sensory systems. *Neuroscience*, 55(3), pp. 613–620.

HWANG, P.M., FOTUHI, M., et al. (1993) Contrasting immunohistochemical localizations in rat brain of two novel K+ channels of the Shab subfamily. *Journal of Neuroscience*, 13(4), pp. 1569–1576.

IMBRICI, P., CAMERINO, D.C. and TRICARICO, D. (2013) Major channels involved in neuropsychiatric disorders and therapeutic perspectives. *Frontiers in genetics*, 4(MAY), p. 76.

IRANI, S.R. et al. (2010) N-methyl-d-aspartate antibody encephalitis: Temporal progression of clinical and paraclinical observations in a predominantly non-paraneoplastic disorder of both sexes. *Brain*, 133(6), pp. 1655–1667.

ISHIKAWA, T. et al. (2003) Distinct Roles of Kv1 and Kv3 Potassium Channels at the Calyx of Held Presynaptic Terminal. *Journal of Neuroscience*, 23(32), pp. 10445–10453.

ISMAIL, B., CANTOR-GRAAE, E. and MCNEIL, T.F. (1998) Neurological abnormalities in schizophrenic patients and their siblings. *American Journal of Psychiatry*, 155(1), pp. 84–89.

ITO, M. (2008) Control of mental activities by internal models in the cerebellum. *Nature Reviews Neuroscience*, 9, pp. 304–313.

IVRY, R.B. et al. (2002) The cerebellum and event timing. *Annals of the New York Academy of Sciences*, 978(1), pp. 302–317.

JAARO-PELED, H. (2009) Gene models of schizophrenia: DISC1 mouse models. *Progress in Brain Research*, 179(C), pp. 75–86.

JAARSMA, D. et al. (1997) Cholinergic innervation and receptors in the cerebellum. *Progress in Brain Research*, 114, pp. 67–96.

JÄÄSKELÄINEN, E. et al. (2013) A systematic review and meta-analysis of recovery in schizophrenia. *Schizophrenia Bulletin*, 39(6), pp. 1296–1306.

JABLENSKY, A. (2010) The diagnostic concept of schizophrenia: its history, evolution, and future prospects. *Dialogues in clinical neuroscience*, 12(3), pp. 271–87.

JACOMY, H. and TALBOT, P.J. (2003) Vacuolating encephalitis in mice infected by human coronavirus OC43. *Virology*, 315(1), pp. 20–33.

JALALI, MEHDI, ZABOROWSKA, J. and JALALI, MORTEZA (2017) The Polymerase Chain Reaction: PCR, qPCR, and RT-PCR. In: *Basic Science Methods for Clinical Researchers*. Elsevier Inc., pp. 1–18.

JAN, L.Y. and JAN, Y.N. (2012) Voltage-gated potassium channels and the diversity of electrical signalling. *Journal of Physiology*, 590(11), pp. 2591–2599.

JAUHAR, S. et al. (2014) Cognitive-behavioural therapy for the symptoms of schizophrenia: systematic review and meta-analysis with examination of potential bias. *The British journal of psychiatry : the journal of mental science*, 204(1), pp. 20–29.

JĘDRYCHOWSKA, J. and KORZH, V. (2019) Kv2.1 voltage-gated potassium channels in developmental perspective. *Developmental Dynamics*, 248(12), pp. 1180–1194.

JENTSCH, J.D. et al. (1998) Prefrontal cortical involvement in phencyclidine-induced activation of the mesolimbic dopamine system: Behavioral and neurochemical evidence. *Psychopharmacology*, 138(1), pp. 89–95.

JIAO, S. et al. (2007) cAMP/protein kinase A signalling pathway protects against neuronal apoptosis and is associated with modulation of Kv2.1 in cerebellar granule cells. *Journal of Neurochemistry*, 100(4), pp. 979–991.

JOHNSON, B., LEEK, A.N. and TAMKUN, M.M. (2019) Kv2 channels create endoplasmic reticulum / plasma membrane junctions: a brief history of Kv2 channel subcellular localization. *Channels*, 13(1), pp. 88–101.

JOHO, R.H. et al. (2006) Behavioral motor dysfunction in Kv3-type potassium channel-deficient mice. *Genes, Brain and Behavior*, 5(6), pp. 472–482.

JONES, C. (2018) α;7 Nicotinic Acetylcholine Receptor: A Potential Target in Treating Cognitive Decline in Schizophrenia. *Journal of Clinical Psychopharmacology*, 38(3), pp. 247–249.

JONES, C., WATSON, D. and FONE, K. (2011) Animal models of schizophrenia. *British Journal of Pharmacology*, 164(4), pp. 1162–1194.

JUCKEL, G. et al. (2006) Dysfunction of ventral striatal reward prediction in schizophrenia. *NeuroImage*, 29(2), pp. 409–416.

KALINICHEV, M. et al. (2008) Comparison between intraperitoneal and subcutaneous phencyclidine administration in Sprague-Dawley rats: A locomotor activity and gene induction study. *Progress in Neuro-Psychopharmacology and Biological Psychiatry*, 32(2), pp. 414–422.

KALUEFF, A. V. and TUOHIMAA, P. (2005) The grooming analysis algorithm discriminates between different levels of anxiety in rats: Potential utility for neurobehavioural stress research. *Journal of Neuroscience Methods*, 143(2), pp. 169–177.

KANE, J. et al. (1988) Clozapine for the Treatment-Resistant Schizophrenic: A Double-blind Comparison With Chlorpromazine. *Archives of General Psychiatry*, 45(9), pp. 789–796.

KANEMASA, T. et al. (1995) Electrophysiological and pharmacological characterization of a mammalian Shaw channel expressed in NIH 3T3 fibroblasts. *Journal of Neurophysiology*, 74(1), pp. 207–217.

KARAYIORGOU, M., SIMON, T.J. and GOGOS, J.A. (2010) 22q11.2 microdeletions: Linking DNA structural variation to brain dysfunction and schizophrenia. *Nature Reviews Neuroscience*, 11(6), pp. 402–416.

KARCHER, N.R. et al. (2019) Resting-State Functional Connectivity and Psychotic-like Experiences in Childhood: Results From the Adolescent Brain Cognitive Development Study. *Biological Psychiatry*, 86(1), pp. 7–15.

KATCHALSKI, E., GROSSFELD, I. and FRANKEL, M. (1947) Poly-lysine. *Journal of the American Chemical Society*, 69(10), p. 2564.

KEELE, S.W. and IVRY, R. (1990) Does the cerebellum provide a common computation for diverse tasks? A timing hypothesis. *Annals of the New York Academy of Sciences*, 608(1 The Developme), pp. 179–211.

KELLER, A. et al. (2003) Progressive loss of cerebellar volume in childhood-onset schizophrenia. *American Journal of Psychiatry*, 160(1), pp. 128–133.

KELLY, R.M. and STRICK, P.L. (2003) Cerebellar loops with motor cortex and prefrontal cortex of a nonhuman primate. *Journal of Neuroscience*, 23(23), pp. 8432–8444.

KERSCHENSTEINER, D., SOTO, F. and STOCKER, M. (2005) Flourescence measurements reveal stoichiometry of K+ channels formed by modulatory and delayed rectifier α-subunits. *Proceedings of the National Academy of Sciences of the United States of America*, 102(17), pp. 6160–6165.

KESHAVAN, M.S. et al. (2003) Diagnostic specificity and neuroanatomical validity of neurological abnormalities in first-episode psychoses. *American Journal of Psychiatry*, 160(7), pp. 1298–1304.

KESNER, R.P., HARDY, J.D. and CALDER, L.D. (1981) Phencyclidine and behavior: I. Sensory-motor function, activity level, taste aversion and water intake. *Pharmacology, Biochemistry and Behavior*, 15(1), pp. 7–13.

KESSELS, H.W. and MALINOW, R. (2009) Synaptic AMPA Receptor Plasticity and Behavior. *Neuron*, 61(3), pp. 340–350.

KIM, HYUNA et al. (2018) Familial cases of progressive myoclonic epilepsy caused by maternal somatic mosaicism of a recurrent KCNC1 p.Arg320His mutation. *Brain and Development*, 40(5), pp. 429–432.

KIM, J.B. (2014) Channelopathies. *Korean Journal of Pediatrics*, 57(1), pp. 1–18.

KIM, K.X. and RUTHERFORD, M.A. (2016) Maturation of nav and kv channel topographies in the auditory nerve spike initiator before and after developmental onset of hearing function. *Journal of Neuroscience*, 36(7), pp. 2111–2118.

KITZINGER, H. and ARNOLD, D.G. (1949) A preliminary study of the effects of glutamic acid on catatonic schizophrenics. *Rorschach research exchange and journal of projective techniques*, 13(2), pp. 210–218.

KLEMIC, K.G. et al. (1998) Inactivation of Kv2.1 potassium channels. *Biophysical Journal*, 74(4), pp. 1779–1789.

KNUTSON, B., BURGDORF, J. and PANKSEPP, J. (2002) Ultrasonic vocalizations as indices of affective states in rats. *Psychological Bulletin*, 128(6), pp. 961–977.

KOEPPEN, A.H. (2018) The neuropathology of the adult cerebellum. In: *Handbook of Clinical Neurology*. pp. 129–149.

KÖHLING, R. and WOLFART, J. (2016) Potassium channels in epilepsy. *Cold Spring Harbor Perspectives in Medicine*, 6(5), p. 24.

KONOPASKE, G.T. et al. (2014) Prefrontal cortical dendritic spine pathology in schizophrenia and bipolar disorder. *JAMA Psychiatry*, 71(12), pp. 1323–1331.

KOPEC, A.M. et al. (2017) Optimized solubilization of TRIzol-precipitated protein permits Western blotting analysis to maximize data available from brain tissue. *Journal of Neuroscience Methods*, 280, pp. 64–76.

KORNGREEN, A. and SAKMANN, B. (2000) Voltage-gated K+ channels in layer 5 neocortical pyramidal neurones from young rats: Subtypes and gradients. *Journal of Physiology*, 525(3), pp. 621–639.

KOZIOL, L.F. et al. (2014a) Consensus paper: The cerebellum's role in movement and cognition. *Cerebellum*, [Online] Available from: doi.org/10.1007/s12311-013-0511-x.

KOZIOL, L.F. et al. (2014b) Consensus paper: The cerebellum's role in movement and cognition. *Cerebellum*, 13(1), pp. 151–177.

KRAMER, J.W. et al. (1998) Modulation of potassium channel gating by coexpression of Kv2.1 with regulatory Kv5.1 or Kv6.1 α-subunits. *American Journal of Physiology - Cell Physiology*, 274(6 43-6), [Online] Available from: doi.org/10.1152/ajpcell.1998.274.6.c1501.

KRISTENSEN, L. V., SANDAGER-NIELSEN, K. and HANSEN, H.H. (2012) K v7 (KCNQ) channel openers normalize central 2-deoxyglucose uptake in a mouse model of mania and increase prefrontal cortical and hippocampal serine-9 phosphorylation levels of GSK3β. *Journal of Neurochemistry*, 121(3), pp. 373–382.

KRISTIANSEN, L. V. et al. (2006) Changes in NMDA receptor subunits and interacting PSD proteins in dorsolateral prefrontal and anterior cingulate cortex indicate abnormal regional expression in schizophrenia. *Molecular Psychiatry*, 11(8), pp. 737–747.

KRISTIANSEN, L. V. et al. (2007) NMDA receptors and schizophrenia. *Current Opinion in Pharmacology*, 7(1), pp. 48–55.

KRUPA, D.J. and THOMPSON, R.F. (1997) Reversible inactivation of the cerebellar interpositus nucleus completely prevents acquisition of the classically conditioned eye-blink response. *Learning and Memory*, 3(6), pp. 545–556.

KRYSTAL, JOHN H et al. (1994) Subanesthetic Effects of the Noncompetitive NMDA Antagonist, Ketamine, in Humans: Psychotomimetic, Perceptual, Cognitive, and Neuroendocrine Responses. *Archives of General Psychiatry*, 51(3), pp. 199–214.

KRYSTAL, JOHN H. et al. (1994) Subanesthetic Effects of the Noncompetitive NMDA Antagonist, Ketamine, in Humans: Psychotomimetic, Perceptual, Cognitive, and Neuroendocrine Responses. *Archives of General Psychiatry*, 51(3), pp. 199–214.

KULLMANN, D.M. (2010) Neurological channelopathies. *Annual Review of Neuroscience*, 33, pp. 151–172.

KUMAR, G. et al. (2015) Refinement of schizophrenia GWAS loci using methylome-wide association data. *Human Genetics*, 134(1), pp. 77–87.

KURIEN, B.T. and SCOFIELD, R.H. (2006) Western blotting. *Methods*, 38(4), pp. 283–293.

KURYSHEV, Y.A. et al. (2000) KChAP as a chaperone for specific K+ channels. *American Journal of Physiology - Cell Physiology*, 278(5 47-5), [Online] Available from: doi.org/10.1152/ajpcell.2000.278.5.c931.

KUSHIMA, I. et al. (2017) High-resolution copy number variation analysis of schizophrenia in Japan. *Molecular Psychiatry*, 22(3), pp. 430–440.

LABRIE, V., DUFFY, S., et al. (2009) Genetic inactivation of D-amino acid oxidase enhances extinction and reversal learning in mice. *Learning and Memory*, 16(1), pp. 28–37.

LABRIE, V., FUKUMURA, R., et al. (2009) Serine racemase is associated with schizophrenia susceptibility in humans and in a mouse model. *Human Molecular Genetics*, 18(17), pp. 3227–3243.

LABRIE, V., WONG, A.H.C. and RODER, J.C. (2012) Contributions of the d-serine pathway to schizophrenia. *Neuropharmacology*, 62(3), pp. 1484–1503.

LABRO, A.J. et al. (2003) Gating of Shaker-type Channels Requires the Flexibility of S6 Caused by Prolines. *Journal of Biological Chemistry*, 278(50), pp. 50724–50731.

LAFRENIÈRE, R.G. and ROULEAU, G.A. (2012) Identification of novel genes involved in migraine. *Headache*, 52 Suppl 2, pp. 107–110.

LAI, H.C. and JAN, L.Y. (2006) The distribution and targeting of neuronal voltage-gated ion channels. *Nature Reviews Neuroscience*, 7(7), pp. 548–562.

LANZENBERGER, R. and KASPER, S. (2005) Neuroimaging bei schizophrenen Erkrankungen. In: *Fortschritte der Neurologie Psychiatrie*.

LARRAMENDI, L.M.H. and LEMKEY-JOHNSTON, N. (1970) The distribution of recurrent purkinje collateral synapses in the mouse cerebellar cortex: An electron microscopic study. *Journal of Comparative Neurology*, 138(4), pp. 451–482.

LARUELLE, M. et al. (1999) Increased dopamine transmission in schizophrenia: relationship to illness phases. *Biological psychiatry*, 46(1), pp. 56–72.

LARUELLE, M. et al. (1996) Single photon emission computerized tomography imaging of amphetamine-induced dopamine release in drug-free schizophrenic subjects. *Proceedings of the National*

Academy of Sciences of the United States of America, 93(17), pp. 9235–9240.

LATYPOVA, X. et al. (2017) Novel KCNB1 mutation associated with non-syndromic intellectual disability. *Journal of Human Genetics*, 62(5), pp. 569–573.

LAW, A.J. et al. (2003) Expression of NMDA receptor NR1, NR2A and NR2B subunit mRNAs during development of the human hippocampal formation. *European Journal of Neuroscience*, 18(5), pp. 1197–1205.

LEE, C. (2007a) Coimmunoprecipitation assay. *Methods in Molecular Biology*, 362, pp. 401–406.

LEE, C. (2007b) Western blotting. *Methods in Molecular Biology*, 362, pp. 391–399.

LEE, M.C. et al. (2020) Human Labour Pain is Influenced by the Voltage-Gated Potassium Channel K_v6.4 Subunit. *SSRN Electronic Journal*, [Online] Available from: doi.org/10.2139/ssrn.3553404.

LEE, S.H. et al. (2012) Estimating the proportion of variation in susceptibility to schizophrenia captured by common SNPs. *Nature Genetics*, 44(3), pp. 247–250.

LEE, S.M. et al. (2009) Down-regulation of delayed rectifier K+ channels in the hippocampus of seizure sensitive gerbils. *Brain Research Bulletin*, 80(6), pp. 433–442.

LEE, T. and TANG, S.W. (1984) Loxapine and clozapine decrease serotonin (S2) but do not elevate dopamine (D2) receptor numbers in the rat brain. *Psychiatry Research*, 12(4), pp. 277–285.

LEGER, M. et al. (2013) Object recognition test in mice. *Nature Protocols*, 8(12), pp. 2531–2537.

LESH, T.A. et al. (2011) Cognitive control deficits in schizophrenia: Mechanisms and meaning. *Neuropsychopharmacology*, 36(1), pp. 316–338.

LEUNG, A.T., IMAGAWA, T. and CAMPBELL, K.P. (1987) Structural characterization of the 1,4-dihydropyridine receptor of the voltage-dependent Ca2+ channel from rabbit skeletal muscle. Evidence for two distinct high molecular weight subunits. *Journal of Biological Chemistry*, 262(17), pp. 7943–7946.

LEVITT, J.J. et al. (1999) Quantitative volumetric MRI study of the cerebellum and vermis in schizophrenia: Clinical and cognitive correlates. *American Journal of Psychiatry*, 156(7), pp. 1105–1107.

LEWIS, A., MCCROSSAN, Z.A. and ABBOTT, G.W. (2004) MinK, MiRP1, and MiRP2 Diversify Kv3.1 and Kv3.2 Potassium Channel Gating. *Journal of Biological Chemistry*, 279(9), pp. 7884–7892.

LEWIS, D.A. et al. (1999) Altered GABA neurotransmission and prefrontal cortical dysfunction in schizophrenia. In: *Biological Psychiatry*. pp. 616–626.

LEWIS, D.A. et al. (2012) Cortical parvalbumin interneurons and cognitive dysfunction in schizophrenia. *Trends in Neurosciences*, 35(1), pp. 57–67.

LEWIS, D.A. and GONZALEZ-BURGOS, G. (2006) Pathophysiologically based treatment interventions in schizophrenia. *Nature Medicine*, 12(9), pp. 1016–1022.

LI, W., KACZMAREK, L.K. and PERNEY, T.M. (2001) Localization of two high-threshold potassium channel subunits in the rat central auditory system. *Journal of Comparative Neurology*, 437(2), pp. 196–218.

LI, Y. et al. (2013) Association between antibodies to multiple infectious and food antigens and new onset schizophrenia among US military personnel. *Schizophrenia Research*, 151(1–3), pp. 36–42.

LI, Y., SUNG, Y.U. and MCDONALD, T. V. (2006) Voltage-gated potassium channels: Regulation by accessory subunits. *Neuroscientist*, 12(3), pp. 199–210.

LICHTENSTEIN, P. et al. (2009) Common genetic determinants of schizophrenia and bipolar disorder in Swedish families: a population-based study. *The Lancet*, 373(9659), pp. 234–239.

LINDEN, D.E.J. (2012) The Challenges and Promise of Neuroimaging in Psychiatry. *Neuron*, 73(1), pp. 8–22.

LINDENMAYER, J.P. et al. (2013) A systematic review of psychostimulant treatment of negative symptoms of schizophrenia: Challenges and therapeutic opportunities. *Schizophrenia Research*, 147(2–3), pp. 241–252.

LIPINA, T. V. et al. (2013) Maternal immune activation during gestation interacts with Disc1 point mutation to exacerbate schizophrenia-related behaviors in mice. *Journal of Neuroscience*, 33(18), pp. 7654–7666.

LIU, SI QIONG J. and KACZMAREK, L.K. (1998) Depolarization selectively increases the expression of the Kv3.1 potassium channel in developing inferior Colliculus neurons. *Journal of Neuroscience*, 18(21), pp. 8758–8769.

LIU, S. Q.J. and KACZMAREK, L.K. (1998) The expression of two splice variants of the Kv3.1 potassium channel gene is regulated by different signaling pathways. *Journal of Neuroscience*, 18(8), pp. 2881–2890.

LIVAK, K.J. and SCHMITTGEN, T.D. (2001) Analysis of relative gene expression data using real-time quantitative PCR and the 2-ΔΔCT method. *Methods*, 25(4), pp. 402–408.

LÓPEZ-MUÑOZ, F. et al. (2005) History of the discovery and clinical introduction of chlorpromazine. *Annals of Clinical Psychiatry*, 17(3), pp. 113–135.

LOZOFF, B. et al. (2006) Long-lasting neural and behavioral effects of iron deficiency in infancy. *Nutrition Reviews*, 64(5 SUPPL. 1), [Online] Available from: doi.org/10.1301/nr.2006.may.S34-S43.

LU, H., HARTMANN, M.J. and BOWER, J.M. (2005) Correlations between purkinje cell single-unit activity and simultaneously recorded field potentials in the immediately underlying granule cell layer. *Journal of Neurophysiology*, 94(3), pp. 1849–1860.

LUBY, E.D. et al. (1959) Study of a New Schizophrenomimetic Drug—Sernyl. *Archives of Neurology And Psychiatry*, 81(3), pp. 363–369.

LUCHINS, D.J. et al. (1981) Cerebral asymmetry and cerebellar atrophy in schizophrenia: A controlled postmortem study. *American Journal of Psychiatry*, 138(11), pp. 1501–1503.

LUKOWSKI, A.F. et al. (2010) Iron deficiency in infancy and neurocognitive functioning at 19 years: Evidence of long-term deficits in executive function and recognition memory. *Nutritional Neuroscience*, 13(2), pp. 54–70.

LUNEAU, C.J. et al. (1991) Alternative splicing contributes to K+ channel diversity in the mammalian central nervous system. *Proceedings of the National Academy of Sciences of the United States of America*, 88(9), pp. 3932–3936.

LYSAKER, P.H. et al. (2005) Associations of anxiety-related symptoms with reported history of childhood sexual abuse in schizophrenia spectrum disorders. *Journal of Clinical Psychiatry*, 66(10), pp. 1279–1284.

LYSAKER, P.H. and LAROCCO, V.A. (2008) The prevalence and correlates of trauma-related symptoms in schizophrenia spectrum disorder. *Comprehensive Psychiatry*, 49(4), pp. 330–334.

MACHADO, C.J. et al. (2015) Maternal immune activation in nonhuman primates alters social attention in juvenile offspring. *Biological Psychiatry*, 77(9), pp. 823–832.

MACKAY, A.V.P. et al. (1982) Increased Brain Dopamine and Dopamine Receptors in Schizophrenia. *Archives of General Psychiatry*, 39(9), pp. 991–997.

MAGEE, J.C. and JOHNSTON, D. (2005) Plasticity of dendritic function. *Current Opinion in Neurobiology*, 15(3 SPEC. ISS.), pp. 334–342.

MAILMAN, R. and MURTHY, V. (2010) Third Generation Antipsychotic Drugs: Partial Agonism or Receptor Functional Selectivity? *Current Pharmaceutical Design*, 16(5), pp. 488–501.

MALHOTRA, A.K. et al. (1996) NMDA Receptor Function and Human Cognition: The Effects of Ketamine in Healthy Volunteers. *Neuropsychopharmacology*, 14(5), pp. 301–307.

MALIN, S.A. and NERBONNE, J.M. (2002) Delayed rectifier K+ currents, IK, are encoded by Kv2 α-subunits and regulate tonic firing in mammalian

sympathetic neurons. *Journal of Neuroscience*, 22(23), pp. 10094–10105.

MANSBACH, R. (1989) Effects of phencyclidine and phencyclidine biologs on sensorimotor gating in the rat*1. *Neuropsychopharmacology*, 2(4), pp. 299–308.

MANZONI, D. (2007) The cerebellum and sensorimotor coupling: Looking at the problem from the perspective of vestibular reflexes. *Cerebellum*, 6(1), pp. 24–37.

MARCELIS, M. et al. (1998) Urbanization and psychosis: A study of 1942-1978 birth cohorts in The Netherlands. *Psychological Medicine*, 28(4), pp. 871–879.

MATSUMOTO, H. and HIGA, H.H. (1966) Studies on methylazoxymethanol, the aglycone of cycasin: methylation of nucleic acids in vitro. *The Biochemical journal*, 98(2), [Online] Available from: doi.org/10.1042/bj0980020C.

MCCROSSAN, Z.A. et al. (2009) Regulation of the Kv2.1 potassium channel by MinK and MiRP1. *Journal of Membrane Biology*, 228(1), pp. 1–14.

MCGRATH, J. et al. (2008) Schizophrenia: A concise overview of incidence, prevalence, and mortality. *Epidemiologic Reviews*, 30(1), pp. 67–76.

MCGRATH, J. et al. (2004) Vitamin D supplementation during the first year of life and risk of schizophrenia: A Finnish birth cohort study. *Schizophrenia Research*, 67(2–3), pp. 237–245.

MCGRATH, J., BROWN, A. and ST CLAIR, D. (2011) Prevention and schizophrenia - The role of dietary factors. *Schizophrenia Bulletin*, [Online] Available from: doi.org/10.1093/schbul/sbq121.

McKetin, R. et al. (2013) Dose-related psychotic symptoms in chronic methamphetamine users: Evidence from a prospective longitudinal study. *JAMA Psychiatry*, 70(3), pp. 319–324.

McKetin, R. et al. (2010) The risk of psychotic symptoms associated with recreational methamphetamine use. *Drug and Alcohol Review*, 29(4), pp. 358–363.

McLean, S., Woolley, M. and Neill, J.C. (2010) Effects of subchronic phencyclidine on behaviour of female rats on the elevated plus maze and open field. *Journal of Psychopharmacology*, 24(5), pp. 787–790.

Meng, H. et al. (2014) Diversity of vestibular nuclei neurons targeted by cerebellar nodulus inhibition. *Journal of Physiology*, 592(1), pp. 171–188.

Merritt, K. et al. (2016) Nature of glutamate alterations in schizophrenia a meta-analysis of proton magnetic resonance spectroscopy studies. *JAMA Psychiatry*, 73(7), pp. 665–674.

Meyer, U. (2014) Prenatal Poly(I:C) exposure and other developmental immune activation models in rodent systems. *Biological Psychiatry*, 75(4), pp. 307–315.

Meyer-Lindenberg, A. et al. (2002) Reduced prefrontal activity predicts exaggerated striatal dopaminergic function in schizophrenia. *Nature Neuroscience*, 5(3), pp. 267–271.

Mezey, A.G. (1960) Psychiatric Illness in Hungarian Refugees. *Journal of Mental Science*, 106(443), pp. 628–637.

Michael Owens, S. et al. (1990) Phencyclidine pharmacokinetics and concentration-response relationships in the pigeon. *Pharmacology, Biochemistry and Behavior*, 35(4), pp. 797–801.

MIDDLETON, F.A. and STRICK, P.L. (2000) Basal ganglia and cerebellar loops: motor and cognitive circuits. *Brain Research Reviews*, 31(2), pp. 236–250.

MIGNARRI, A. et al. (2014) Cerebellum and neuropsychiatric disorders: Insights from ARSACS. *Neurological Sciences*, 35(1), pp. 95–97.

MISONOU, H. et al. (2006) Bidirectional activity-dependent regulation of neuronal ion channel phosphorylation. *Journal of Neuroscience*, 26(52), pp. 13505–13514.

MISONOU, H. et al. (2004) Regulation of ion channel localization and phosphorylation by neuronal activity. *Nature Neuroscience*, 7(7), pp. 711–718.

MISONOU, H., MOHAPATRA, D.P. and TRIMMER, J.S. (2005) Calcium- and metabolic state-dependent modulation of the voltage-dependent Kv2.1 channel regulates neuronal excitability in response to ischemia. *NeuroToxivology*, 26, pp. 734–752.

MISONOU, H., THOMPSON, S.M. and CAI, X. (2008) Dynamic Regulation of the Kv2.1 Voltage-Gated Potassium Channel during Brain Ischemia through Neuroglial Interaction. *Journal of Neuroscience*, 28(34), pp. 8529–8538.

MOBERGET, T. and IVRY, R.B. (2019) Prediction, Psychosis, and the Cerebellum. *Biological Psychiatry: Cognitive Neuroscience and Neuroimaging*, 4(9), pp. 820–831.

MOGHADDAM, B. et al. (1997) Activation of Glutamatergic Neurotransmission by Ketamine: A Novel Step in the Pathway from NMDA Receptor Blockade to Dopaminergic and Cognitive Disruptions Associated with the Prefrontal Cortex. *Journal of Neuroscience*, 17(8), p. 2921.

MOHAPATRA, D.P. et al. (2009) Regulation of intrinsic excitability in hippocampal neurons by activity-dependent modulation of the KV2.1 potassium channel. *Channels*, 3(1), pp. 46–56.

MOHN, A.R. et al. (1999) Mice with reduced NMDA receptor expression display behaviors related to schizophrenia. *Cell*, 98(4), pp. 427–436.

MÖLLER, L. et al. (2020) Determining the correct stoichiometry of Kv2.1/Kv6.4 heterotetramers, functional in multiple stoichiometrical configurations. *Proceedings of the National Academy of Sciences of the United States of America*, 117(17), pp. 9365–9376.

MOLLICA, R.F. et al. (1999) Disability associated with psychiatric comorbidity and health status in Bosnian refugees living in Croatia. *Journal of the American Medical Association*, 282(5), pp. 433–439.

MONROE, J.M., BUCKLEY, P.F. and MILLER, B.J. (2015) Meta-Analysis of Anti-Toxoplasma gondii IgM Antibodies in Acute Psychosis. *Schizophrenia Bulletin*, 41(4), pp. 989–998.

MOORE, H. et al. (2006) A Neurobehavioral Systems Analysis of Adult Rats Exposed to Methylazoxymethanol Acetate on E17: Implications for the Neuropathology of Schizophrenia. *Biological Psychiatry*, 60(3), pp. 253–264.

MORGAN, C. and CURRAN, H. (2006) Acute and chronic effects of ketamine upon human memory: a review. *Psychopharmacology*, 188(4), pp. 408–424.

MORGAN, C.J.A., MUETZELFELDT, L. and CURRAN, H.V. (2009) Ketamine use, cognition and psychological wellbeing: a comparison of frequent, infrequent and ex-users with polydrug and non-using controls. *Addiction*, 104(1), pp. 77–87.

MORRENS, M. et al. (2006) Stereotypy in schizophrenia. *Schizophrenia Research*, 84(2–3), pp. 397–404.

MORRIS, B.J., COCHRAN, S.M. and PRATT, J.A. (2005) PCP: From pharmacology to modelling schizophrenia. *Current Opinion in Pharmacology*, 5(1), pp. 101–106.

MOURI, A. et al. (2012) Mouse strain differences in phencyclidine-induced behavioural changes. *International Journal of Neuropsychopharmacology*, 15(6), pp. 767–779.

MUENNICH, E.A.L. and FYFFE, R.E.W. (2004) Focal aggregation of voltage-gated, Kv2.1 subunit-containing, potassium channels at synaptic sites in rat spinal motoneurones. *Journal of Physiology*, 554(3), pp. 673–685.

MUGNAINI, E., SEKERKOVÁ, G. and MARTINA, M. (2011).

MULHOLLAND, P.J. et al. (2008) Glutamate transporters regulate extrasynaptic NMDA receptor modulation of Kv2.1 potassium channels. *Journal of Neuroscience*, 28(35), pp. 8801–8809.

MÜLLER, U. and HEINSEN, H. (1984) Regional differences in the ultrastructure of Purkinje cells of the rat. *Cell and Tissue Research*, 235(1), pp. 91–98.

MUÑOZ MANIEGA, S. et al. (2008) A diffusion tensor MRI study of white matter integrity in subjects at high genetic risk of schizophrenia. *Schizophrenia Research*, 106(2–3), pp. 132–139.

MUONA, M. et al. (2015) A recurrent de novo mutation in KCNC1 causes progressive myoclonus epilepsy. *Nature Genetics*, 47(1), pp. 39–46.

MURAKOSHI, H. and TRIMMER, S. (1999) Identification of the Kv2.1 K+ Channel as a Major Component of Delayed Rectifier K+ Current in Rat

Hippocampal Neurons. *The Journal of Neuroscience*, 19(5), pp. 1728–1735.

NAGAI, T. et al. (2003) Effect of AD-5423 on animal models of schizophrenia: Phencyclidine-induced behavioral changes in mice. *NeuroReport*, 14(2), pp. 269–272.

NAKAMURA, Y. and TAKAHASHI, T. (2007) Developmental changes in potassium currents at the rat calyx of Held presynaptic terminal. *Journal of Physiology*, 581(3), pp. 1101–1112.

NASCIMENTO, F.A. and ANDRADE, D.M. (2016) Myoclonus epilepsy and ataxia due to potassium channel mutation (MEAK) is caused by heterozygous KCNC1 mutations. *Epileptic Disorders*, 18, pp. S135–S138.

NASRALLAH, H.A., JACOBY, C.G. and MCCALLEY-WHITTERS, M. (1981).

NEILL, J.C. et al. (2014) Acute and chronic effects of NMDA receptor antagonists in rodents, relevance to negative symptoms of schizophrenia: A translational link to humans. *European Neuropsychopharmacology*, 24(5), pp. 822–835.

NIEMI-PYNTTÄRI, J.A. et al. (2013) Substance-induced psychoses converting into schizophrenia: A register-based study of 18,478 finnish inpatient cases. *Journal of Clinical Psychiatry*, 74(1), pp. e94–e99.

NODA, M. et al. (1984) Primary structure of Electrophorus electricus sodium channel deduced from cDNA sequence. *Nature*, 312(5990), pp. 121–127.

NOLDUS, L.P.J.J., SPINK, A.J. and TEGELENBOSCH, R.A.J. (2001) EthoVision: A versatile video tracking system for automation of behavioral experiments. *Behavior Research Methods, Instruments, and Computers*, 33(3), pp. 398–414.

NOPOULOS, P.C. et al. (1999) An MRI study of cerebellar vermis morphology in patients with schizophrenia: Evidence in support of the cognitive dysmetria concept. *Biological Psychiatry*, 46(5), pp. 703–711.

NOPOULOS, P.C. et al. (2001) An MRI study of midbrain morphology in patients with schizophrenia: Relationship to psychosis, neuroleptics, and cerebellar neural circuitry. *Biological Psychiatry*, 49(1), pp. 13–19.

NOWAK, D.A. et al. (2007) The role of the cerebellum for predictive control of grasping. *Cerebellum*, 6(1), pp. 7–17.

NUMATA, S. et al. (2015) Evaluation of an association between plasma total homocysteine and schizophrenia by a Mendelian randomization analysis. *BMC Medical Genetics*, 16(1), [Online] Available from: doi.org/10.1186/s12881-015-0197-7.

NÚÑEZ, L.A. and GURPEGUI, M. (2002) Cannabis-induced psychosis: A cross-sectional comparison with acute schizophrenia. *Acta Psychiatrica Scandinavica*, 105(3), pp. 173–178.

O'CALLAGHAN, E. et al. (1991) Schizophrenia after prenatal exposure to 1957 A2 influenza epidemic. *The Lancet*, 337(8752), pp. 1248–1250.

O'CONNELL, D.J. et al. (2010) Integrated protein array screening and high throughput validation of 70 novel neural calmodulin-binding proteins. *Molecular and Cellular Proteomics*, 9(6), pp. 1118–1132.

O'CONNELL, K.M.S. et al. (2006) Kv2.1 potassium channels are retained within dynamic cell surface microdomains that are defined by a perimeter fence. *Journal of Neuroscience*, 26(38), pp. 9609–9618.

O'CONNELL, K.M.S., WHITESELL, J.D. and TAMKUN, M.M. (2008) Localization and mobility of the delayed-rectifer K+ channel Kv2.1 in adult cardiomyocytes. *American Journal of Physiology - Heart and*

Circulatory Physiology, 294(1), [Online] Available from: doi.org/10.1152/ajpheart.01038.2007.

ÖDEGAARD, ÖRNULV (1933) Emigration and Insanity. *The Journal of Nervous and Mental Disease*, 78(6), p. 666.

O'DONOVAN, M.C. et al. (2008) Identification of loci associated with schizophrenia by genome-wide association and follow-up. *Nature Genetics*, 40(9), pp. 1053–1055.

OHI, K. et al. (2016) Specific gene expression patterns of 108 schizophrenia-associated loci in cortex. *Schizophrenia research*, 174(1–3), pp. 35–38.

OKUGAWA, G. et al. (2002) Selective reduction of the posterior superior vermis in men with chronic schizophrenia. *Schizophrenia Research*, 55(1), pp. 61–67.

O'MALLEY, H.A. and ISOM, L.L. (2015) Sodium channel β subunits: Emerging targets in channelopathies. *Annual Review of Physiology*, 77, pp. 481–504.

OSWALD, R.E., BAMBERGER, M.J. and MCLAUGHLIN, J.T. (1984) Mechanism of phencyclidine binding to the acetylcholine receptor from Torpedo electroplaque. *Molecular Pharmacology*, 25(3), pp. 360–368.

OTTE, D.M. et al. (2009) Behavioral changes in G72/G30 transgenic mice. *European Neuropsychopharmacology*, 19(5), pp. 339–348.

OTTSCHYTSCH, N. et al. (2005) DOmain analysis of Kv6.3, an electrically silent channel. *Journal of Physiology*, 568, pp. 737–747.

OTTSCHYTSCH, N. et al. (2002) Obligatory heterotetramerization of three previously uncharacterized Kv channel α-subunits identified in the

human genome. *Proceedings of the National Academy of Sciences of the United States of America*, 99(12), pp. 7986–7991.

OZAITA, A. et al. (2002) Differential subcellular localization of the two alternatively spliced isoforms of the Kv3.1 potassium channel subunit in brain. *Journal of Neurophysiology*, 88(1), pp. 394–408.

ÖZBEK, A. et al. (2019) Cerebellar volume in early-onset schizophrenia and its association with severity of symptoms. *Journal of International Medical Research*, 47(1), pp. 411–419.

PASSINGHAM, R.E., TONI, I. and RUSHWORTH, M.F.S. (2000) Specialisation within the prefrontal cortex: the ventral prefrontal cortex and associative learning. *Experimental Brain Research*, 133(1), pp. 103–113.

PATEL, K.R. et al. (2014) Schizophrenia: Overview and treatment options. *P and T*, 39(9), pp. 638–645.

PAYLOR, J.W. et al. (2016) Developmental disruption of perineuronal nets in the medial prefrontal cortex after maternal immune activation. *Scientific Reports*, 6, [Online] Available from: doi.org/10.1038/srep37580.

PEDERSEN, C.B. and MORTENSEN, P.B. (2006) Urbanization and traffic related exposures as risk factors for Schizophrenia. *BMC Psychiatry*, 6, [Online] Available from: doi.org/10.1186/1471-244X-6-2.

PELTOLA, M.A. et al. (2011) AMIGO is an auxiliary subunit of the Kv2.1 potassium channel. *EMBO Reports*, 12(12), pp. 1293–1299.

PELTOLA, M.A. et al. (2016) AMIGO-Kv2.1 Potassium Channel Complex Is Associated with Schizophrenia-Related Phenotypes. *Schizophrenia Bulletin*, 42(1), pp. 191–201.

PERALS, D. et al. (2017) Revisiting the open-field test: what does it really tell us about animal personality? *Animal Behaviour*, 123, pp. 69–79.

PERNEY, T.M. et al. (1992) Expression of the mRNAs for the Kv3.1 potassium channel gene in the adult and developing rat brain. *Journal of Neurophysiology*, 68(3), pp. 756–766.

PICCHIONI, M.M. and MURRAY, R.M. (2007) Schizophrenia. *British Medical Journal*, 335(7610), pp. 91–95.

PIERCE, R.C. and KALIVAS, P.W. (1997) A circuitry model of the expression of behavioral sensitization to amphetamine-like psychostimulants. *Brain Research Reviews*, 25(2), pp. 192–216.

PILOWSKY, L.S. et al. (2006) First in vivo evidence of an NMDA receptor deficit in medication-free schizophrenic patients. *Molecular psychiatry*, 11(2), pp. 118–119.

PISUPATI, A. et al. (2018) The S6 gate in regulatory Kv6 subunits restricts heteromeric K+ channel stoichiometry. *Journal of General Physiology*, 150(12), pp. 1702–1721.

PISUPATI, A. et al. (2020).

POCKLINGTON, A.J. et al. (2015) Novel Findings from CNVs Implicate Inhibitory and Excitatory Signaling Complexes in Schizophrenia. *Neuron*, 86(5), pp. 1203–1214.

POELS, E.M.P. et al. (2014) Imaging glutamate in schizophrenia: Review of findings and implications for drug discovery. *Molecular Psychiatry*, 19(1), pp. 20–29.

POLYAKOVA, S.A. and PACQUIAO, D.F. (2006) Psychological and Mental Illness Among Elder Immigrants From the Former Soviet Union. *Journal of Transcultural Nursing*, 17(1), pp. 40–49.

POST, M.A., KIRSCH, G.E. and BROWN, A.M. (1996) Kv2.1 and electrically silent Kv6.1 potassium channel subunits combine and express a novel current. *FEBS Letters*, 399(1–2), pp. 177–182.

POST, R.M. and ROSE, H. (1976) Increasing effects of repetitive cocaine administration in the rat. *Nature*, 260(5553), pp. 731–732.

POWELL, S.B., RISBROUGH, V.B. and GEYER, M.A. (2003) Potential use of animal models to examine antipsychotic prophylaxis for schizophrenia. *Clinical Neuroscience Research*, 3(4–5), pp. 289–296.

PRATT, J.A. et al. (2008) Modelling prefrontal cortex deficits in schizophrenia: Implications for treatment. In: *British Journal of Pharmacology*.

PROTAIS, P., COSTENTIN, J. and SCHWARTZ, J.C. (1976) Climbing behavior induced by apomorphine in mice: a simple test for the study of dopamine receptors in striatum. *Psychopharmacology*, 50(1), pp. 1–6.

PUBILL, D. et al. (1998) Characterization of [3H]nisoxetine binding in rat vas deferens membranes: Modulation by sigma and PCP ligands. *Life Sciences*, 62(8), pp. 763–773.

PURCELL, S.M. et al. (2009) Common polygenic variation contributes to risk of schizophrenia and bipolar disorder. *Nature*, 460(7256), pp. 748–752.

RAMOS-VARA, J.A. (2017) Principles and methods of immunohistochemistry. In: *Methods in Molecular Biology*. pp. 115–128.

RAMSAY, I.S. (2019) An Activation Likelihood Estimate Meta-analysis of Thalamocortical Dysconnectivity in Psychosis. *Biological Psychiatry: Cognitive Neuroscience and Neuroimaging*, 4(10), pp. 859–869.

RANJAN, R. et al. (2019) A Kinetic Map of the Homomeric Voltage-Gated Potassium Channel (Kv) Family. *Frontiers in Cellular Neuroscience*, 13, [Online] Available from: doi.org/10.3389/fncel.2019.00358.

RASBAND, M.N. et al. (1998) Potassium channel distribution, clustering, and function in remyelinating rat axons. *Journal of Neuroscience*, 18(1), pp. 36–47.

RASETTI, R. et al. (2009) Evidence that altered amygdala activity in schizophrenia is related to clinical state and not genetic risk. *American Journal of Psychiatry*, 166(2), pp. 216–225.

RECTOR, N.A. and BECK, A.T. (2012) Cognitive behavioral therapy for schizophrenia: An empirical review. In: *Journal of Nervous and Mental Disease*. pp. 832–839.

REES, E. et al. (2014) Analysis of copy number variations at 15 schizophrenia-associated loci. *British Journal of Psychiatry*, 204(2), pp. 108–114.

REGNIER, G. et al. (2017) Targeted deletion of the Kv6.4 subunit causes male sterility due to disturbed spermiogenesis. *Reproduction, Fertility and Development*, 29(8), pp. 1567–1575.

REISINGER, S. et al. (2015) The Poly(I:C)-induced maternal immune activation model in preclinical neuropsychiatric drug discovery. *Pharmacology and Therapeutics*, 149, pp. 213–226.

REYNOLDS, G.P. (1983) Increased concentrations and lateral asymmetry of amygdala dopamine in schizophrenia. *Nature*, 305(5934), pp. 527–529.

RICHELSON, E. (1984) Neuroleptic affinities for human brain receptors and their use in predicting adverse effects. *Journal of Clinical Psychiatry*, 45(8), pp. 331–336.

RIPKE, S. et al. (2014) Biological insights from 108 schizophrenia-associated genetic loci. *Nature*, 511(7510), pp. 421–427.

RIPOLL, N., BRONNEC, M. and BOURIN, M. (2004).

RITZAU-JOST, A. et al. (2014) Ultrafast action potentials mediate kilohertz signaling at a central synapse. *Neuron*, 84(1), pp. 152–163.

RIVERO-GUTIÉRREZ, B. et al. (2014) Stain-free detection as loading control alternative to Ponceau and housekeeping protein immunodetection in Western blotting. *Analytical Biochemistry*, 467, pp. 1–3.

ROBERTS, R.C. et al. (1996) Reduced striatal spine size in schizophrenia: A postmortem ultrastructural study. *NeuroReport*, 7(6), pp. 1214–1218.

ROBIN, M. (2006) What Are the Differences Between. *Social Indicators Research*, pp. 363–404.

ROGNLI, E.B. et al. (2015) Long-term risk factors for substance-induced and primary psychosis after release from prison. A longitudinal study of substance users. *Schizophrenia Research*, 168(1–2), pp. 185–190.

ROSE, S.A. et al. (2013) Rett syndrome: An eye-tracking study of attention and recognition memory. *Developmental Medicine and Child Neurology*, 55(4), pp. 364–371.

ROSOKLIJA, G. et al. (2000) Structural abnormalities of subicular dendrites in subjects with schizophrenia and mood disorders: Preliminary findings. *Archives of General Psychiatry*, 57(4), pp. 349–356.

ROTHMAN, D.L. et al. (2003) In vivo NMR studies of the glutamate neurotransmitter flux and neuroenergetics: Implications for brain function. *Annual Review of Physiology*, 65(1), pp. 401–427.

ROUX, B. (2017) Ion channels and ion selectivity. *Essays in Biochemistry*, 61(2), pp. 201–209.

ROWAN, M.J.M. et al. (2016) Synapse-Level Determination of Action Potential Duration by K+ Channel Clustering in Axons. *Neuron*, 91(2), pp. 370–383.

ROWLAND, L.M. et al. (2005) Effects of Ketamine on Anterior Cingulate Glutamate Metabolism in Healthy Humans: A 4-T Proton MRS Study. *American Journal of Psychiatry*, 162(2), pp. 394–396.

RUDY, B. et al. (2009) Voltage Gated Potassium Channels: Structure and Function of Kv1 to Kv9 Subfamilies. In: SQUIRE, L.R. (ed.) *Encyclopedia of Neuroscience*. Encyclopedia of Neuroscience. Oxford: Academic Press, pp. 397–425.

SAHA, S. et al. (2006) The incidence and prevalence of schizophrenia varies with latitude. *Acta Psychiatrica Scandinavica*, 114(1), pp. 36–39.

ŞAHIN, S. et al. (2013) The history of childhood trauma among individuals with ultra high risk for psychosis is as common as among patients with first-episode schizophrenia. *Early Intervention in Psychiatry*, 7(4), pp. 414–420.

SAITSU, H. et al. (2015) De novo KCNB1 mutations in infantile epilepsy inhibit repetitive neuronal firing. *Scientific reports*, 5, p. 15199.

SALINAS, M. et al. (1997) New modulatory α subunits for mammalian Shab K+ channels. *Journal of Biological Chemistry*, 272(39), pp. 24371–24379.

SAMS-DODD, F (1998) A test of the predictive validity of animal models of schizophrenia based on phencyclidine and D-amphetamine. *Neuropsychopharmacology : official publication of the American College of Neuropsychopharmacology*, 18(4), pp. 293–304.

SAMS-DODD, FRANK (1998) A test of the predictive validity of animal models of schizophrenia based on phencyclidine and d-amphetamine. *Neuropsychopharmacology*, 18(4), pp. 293–304.

SAMS-DODD, F. (1996) Phencyclidine-induced stereotyped behaviour and social isolation in rats: a possible animal model of schizophrenia. *Behavioural pharmacology*, 7(1), pp. 3–23.

SAMS-DODD, F (1996) Phencyclidine-induced stereotyped behaviour and social isolation in rats: a possible animal model of schizophrenia. *Behavioural Pharmacology*, 7(1), pp. 3–23.

SAMSON, A.L. et al. (2015) MouseMove: An open source program for semi-automated analysis of movement and cognitive testing in rodents. *Scientific Reports*, 5, p. 16171.

SANDERS, S.J. et al. (2012) De novo mutations revealed by whole-exome sequencing are strongly associated with autism. *Nature*, 485(7397), pp. 237–241.

SANDYK, R., KAY, S.R. and MERRIAM, A.E. (1991) Atrophy of the cerebellar vermis: Relevance to the symptoms of schizophrenia. *International Journal of Neuroscience*, 57(3–4), pp. 205–212.

SARMIERE, P.D., WEIGLE, C.M. and TAMKUN, M.M. (2008) The Kv2.1 K+ channel targets to the axon initial segment of hippocampal and cortical neurons in culture and in situ. *BMC Neuroscience*, 9(112), pp. 1–15.

SCALIA, C.R. et al. (2017) Antigen Masking During Fixation and Embedding, Dissected. *Journal of Histochemistry and Cytochemistry*, 65(1), pp. 5–20.

SCALZO, F.M. and HOLSON, R.R. (1992) The ontogeny of behavioral sensitization to phencyclidine. *Neurotoxicology and Teratology*, 14(1), pp. 7–14.

SCHMITTGEN, T.D. and LIVAK, K.J. (2008) Analyzing real-time PCR data by the comparative CT method. *Nature Protocols*, 3(6), pp. 1101–1108.

SCHNITZLER, M.M. et al. (2009) Mutation of histidine 105 in the T1 domain of the potassium channel Kv2.1 disrupts heteromerization with Kv6.3 and Kv6.4. *Journal of Biological Chemistry*, 284(7), pp. 4695–4704.

SCOTT, V.E.S. et al. (1994) Primary structure of a β subunit of α-dendrotoxin-sensitive K+ channels from bovine brain. *Proceedings of the National Academy of Sciences of the United States of America*, 91(5), pp. 1637–1641.

SEEGER, T.F., THAL, L. and GARDNER, E.L. (1982) Behavioral and biochemical aspects of neuroleptic-induced dopaminergic supersensitivity: Studies with chronic clozapine and haloperidol. *Psychopharmacology*, 76(2), pp. 182–187.

SEEMAN, P. et al. (1987) Human brain D1 and D2 dopamine receptors in schizophrenia, Alzheimer's, Parkinson's, and Huntington's diseases. *Neuropsychopharmacology*, 1(1), pp. 5–15.

SEEMAN, P. and LEE, T. (1975) Antipsychotic drugs: direct correlation between clinical potency and presynaptic action on dopamine neurons. *Science*, 188(4194), pp. 1217–1219.

SEILLIER, A. and GIUFFRIDA, A. (2009) Evaluation of NMDA receptor models of schizophrenia: Divergences in the behavioral effects of sub-chronic PCP and MK-801. *Behavioural Brain Research*, 204(2), pp. 410–415.

SEKAR, A. et al. (2016) Schizophrenia risk from complex variation of complement component 4. *Nature*, 530(7589), pp. 177–183.

SEKIRNJAK, C. et al. (1997) Subcellular localization of the K+ channel subunit Kv3.1b in selected rat CNS neurons. *Brain Research*, 766(1–2), pp. 173–187.

SELTEN, J.P. et al. (2001) Incidence of psychotic disorders in immigrant groups to the Netherlands. *British Journal of Psychiatry*, 178(APR.), pp. 367–372.

SELTEN, J.P., SLAETS, J.P.J. and KAHN, R.S. (1997) Schizophrenia in Surinamese and Dutch Antillean immigrants to The Netherlands: Evidence of an increased incidence. *Psychological Medicine*, 27(4), pp. 807–811.

SENSKY, T. et al. (2000) A randomized controlled trial of cognitive-behavioral therapy for persistent symptoms in schizophrenia resistant to medication. *Archives of General Psychiatry*, 57(2), pp. 165–172.

SEVERANCE, E.G. and YOLKEN, R.H. (2020) From Infection to the Microbiome: An Evolving Role of Microbes in Schizophrenia. *Current topics in behavioral neurosciences*, 44, pp. 67–84.

SHADMEHR, R. and MUSSA-IVALDI, S. (2018) Optimal Feedback Control. In: *Biological Learning and Control*.

SHENG, M. et al. (1993) Presynaptic A-current based on heteromultimeric K+ channels detected in vivo. *Nature*, 365(6441), pp. 72–75.

SHI, J. et al. (2009) Common variants on chromosome 6p22.1 are associated with schizophrenia. *Nature*, 460(7256), pp. 753–757.

SHINN, A.K. et al. (2015) Aberrant cerebellar connectivity in motor and association networks in schizophrenia. *Frontiers in Human Neuroscience*, 9, [Online] Available from: doi.org/10.3389/fnhum.2015.00134.

SICCA, F. et al. (2011) Autism with Seizures and Intellectual Disability: Possible Causative Role of Gain-of-function of the Inwardly-Rectifying K + Channel Kir4.1. *Neurobiology of Disease*, 43(1), pp. 239–247.

SIDDI, S. et al. (2019) Depression, auditory-verbal hallucinations, and delusions in patients with schizophrenia: Different patterns of association with prefrontal gray and white matter volume. *Psychiatry Research - Neuroimaging*, 283, pp. 55–63.

SILBERSWEIG, D.A. et al. (1995) A functional neuroanatomy of hallucinations in schizophrenia. *Nature*, 378(6553), pp. 176–179.

SILLITOE, R. V. and JOYNER, A.L. (2007) Morphology, Molecular Codes, and Circuitry Produce the Three-Dimensional Complexity of the Cerebellum. *Annual Review of Cell and Developmental Biology*, 23(1), pp. 549–577.

SIMPSON, E.H., KELLENDONK, C. and KANDEL, E. (2010) A Possible Role for the Striatum in the Pathogenesis of the Cognitive Symptoms of Schizophrenia. *Neuron*, 65(5), pp. 585–596.

SINCLAIR, D.J.M. et al. (2019) Electroconvulsive therapy for treatment-resistant schizophrenia. *Cochrane Database of Systematic Reviews*, 2019(3), [Online] Available from: doi.org/10.1002/14651858.CD011847.pub2.

SINGER-LAHAT, D. et al. (2007) K+ channel facilitation of exocytosis by dynamic interaction with syntaxin. *Journal of Neuroscience*, 27(7), pp. 1651–1658.

SKLAR, P. et al. (2011) Large-scale genome-wide association analysis of bipolar disorder identifies a new susceptibility locus near ODZ4. *Nature Genetics*, 43(10), pp. 977–985.

SMOLIN, B. et al. (2012) Differential expression of genes encoding neuronal ion-channel subunits in major depression, bipolar disorder and schizophrenia: Implications for pathophysiology. *International Journal of Neuropsychopharmacology*, 15(7), pp. 869–882.

SÖDERBERG, O. et al. (2008) Characterizing proteins and their interactions in cells and tissues using the in situ proximity ligation assay. *Methods*, 45(3), pp. 227–232.

SÖDERBERG, O. et al. (2006) Direct observation of individual endogenous protein complexes in situ by proximity ligation. *Nature Methods*, 3(12), pp. 995–1000.

SOKOLOV, B.P. (1998) Expression of NMDAR1, GluR1, GluR7, and KA1 glutamate receptor mRNAs is decreased in frontal cortex of "neuroleptic-free" schizophrenics: Evidence on reversible up-regulation by typical neuroleptics. *Journal of Neurochemistry*, 71(6), pp. 2454–2464.

SOMMER, I.E.C. et al. (2008) Auditory verbal hallucinations predominantly activate the right inferior frontal area. *Brain*, 131(12), pp. 3169–3177.

SOUTHAN, A.P. and ROBERTSON, B. (2000) Electrophysiological characterization of voltage-gated K+ currents in cerebellar basket and

Purkinje cells: Kv1 and Kv3 channel subfamilies are present in basket cell nerve terminals. *Journal of Neuroscience*, 20(1), pp. 114–122.

SPECA, D.J. et al. (2014) Deletion of the Kv2.1 delayed rectifier potassium channel leads to neuronal and behavioral hyperexcitability. *Genes, Brain and Behavior*, 13(4), pp. 394–408.

SQUIRE, L.R. and DEDE, A.J.O. (2015) Conscious and unconscious memory systems. *Cold Spring Harbor Perspectives in Medicine*, 5(1), [Online] Available from: doi.org/10.1101/cshperspect.a021667.

ST CLAIR, D. et al. (2005) Rates of adult schizophrenia following prenatal exposure to the Chinese famine of 1959-1961. *Journal of the American Medical Association*, 294(5), pp. 557–562.

STACHOWIAK, M.K. et al. (2013) Schizophrenia: A neurodevelopmental disorder - Integrative genomic hypothesis and therapeutic implications from a transgenic mouse model. *Schizophrenia Research*, 143(2–3), pp. 367–376.

STAHL, S.M. (2013) Neurotransmitters and circuits in schizophrenia. Stahl's essential psychopharmacology: neuroscientific basis and practical applications. In: *Essential psychopharmacology*. Cambridge: Cambridge Medicine, pp. 90–96.

STARK, K.L. et al. (2008) Altered brain microRNA biogenesis contributes to phenotypic deficits in a 22q11-deletion mouse model. *Nature Genetics*, 40(6), pp. 751–760.

STARR, B.S. and STARR, M.S. (1986) Differential effects of dopamine D1 and D2 agonists and antagonists on velocity of movement, rearing and grooming in the mouse. Implications for the roles of D1 and D2 receptors. *Neuropharmacology*, 25(5), pp. 455–463.

STAS, J.I. et al. (2015) Modulation of closed-state inactivation in Kv2.1/Kv6.4 heterotetramers as mechanism for 4-AP induced potentiation. *PLoS ONE*, 10(10), [Online] Available from: doi.org/10.1371/journal.pone.0141349.

STEINLEIN, O.K. (2001) Ion channels and epilepsy. *American Journal of Medical Genetics - Seminars in Medical Genetics*, 106(2), pp. 146–159.

STĘPNICKI, P., KONDEJ, M. and KACZOR, A.A. (2018) Current concepts and treatments of schizophrenia. *Molecules*, 23(8), [Online] Available from: doi.org/10.3390/molecules23082087.

STERZER, P. et al. (2018).

STOCKER, M., HELLWIG, M. and KERSCHENSTEINER, D. (1999) Subunit assembly and domain analysis of electrically silent K+ channel α-subunits of the rat Kv9 subfamily. *Journal of Neurochemistry*, 72(4), pp. 1725–1734.

STOODLEY, C.J., VALERA, E.M. and SCHMAHMANN, J.D. (2012) Functional topography of the cerebellum for motor and cognitive tasks: An fMRI study. *NeuroImage*, 59(2), pp. 1560–1570.

STRANGE, P.G. (2001) Antipsychotic drugs: Importance of dopamine receptors for mechanisms of therapeutic actions and side effects. *Pharmacological Reviews*, 53(1), pp. 119–133.

STRASSLE, B.W. et al. (2005) Light and electron microscopic analysis of KChIP and Kv4 localization in rat cerebellar granule cells. *Journal of Comparative Neurology*, 484(2), pp. 144–155.

SULLIVAN, P.F., KENDLER, K.S. and NEALE, M.C. (2003) Schizophrenia as a Complex Trait: Evidence from a Meta-analysis of Twin Studies. *Archives of General Psychiatry*, 60(12), pp. 1187–1192.

SUSSER, E.S. and LIN, S.P. (1992) Schizophrenia After Prenatal Exposure to the Dutch Hunger Winter of 1944-1945. *Archives of General Psychiatry*, 49(12), pp. 983–988.

SWEET, R.A. et al. (2009) Reduced dendritic spine density in auditory cortex of subjects with schizophrenia. *Neuropsychopharmacology*, 34(2), pp. 374–389.

SZESZKO, P.R. et al. (2003) Reversed cerebellar asymmetry in men with first-episode schizophrenia. *Biological Psychiatry*, 53(5), pp. 450–459.

TAKAHASHI, M. et al. (1987) Subunit structure of dihydropyridine-sensitive calcium channels from skeletal muscle. *Proceedings of the National Academy of Sciences of the United States of America*, 84(15), pp. 5478–5482.

TAMMINGA, C.A. (2002) Partial dopamine agonists in the treatment of psychosis. *Journal of Neural Transmission*, 109(3), pp. 411–420.

TAVIAN, D., DE GIORGIO, A. and GRANATO, A. (2011) Selective underexpression of Kv3.2 and Kv3.4 channels in the cortex of rats exposed to ethanol during early postnatal life. *Neurological Sciences*, 32(4), pp. 571–577.

TEMPEL, B.L. et al. (1987) Sequence of a probable potassium channel component encoded at Shaker locus of Drosophila. *Science*, 237(4816), pp. 770–775.

TERASAKI, O. et al. (1997) Decreased prefrontal dopamine D1 receptors in schizophrenia revealed by PET. *Nature*, 385(6617), pp. 634–636.

THIFFAULT, I. et al. (2015) A novel epileptic encephalopathy mutation in KCNB1 disrupts Kv2.1 ion selectivity, expression, and localization. *Journal of General Physiology*, 146(5), pp. 399–410.

THOMAS L. SCHWARTZ, SHILPA SACHDEVA and STEPHEN M. STAHL (2012) Genetic Data Supporting the NMDA Glutamate Receptor Hypothesis for Schizophrenia. *Current Pharmaceutical Design*, 18(12), pp. 1580–1592.

TIAN, C. et al. (2014) Molecular identity of axonal sodium channels in human cortical pyramidal cells. *Frontiers in Cellular Neuroscience*, 8, [Online] Available from: doi.org/10.3389/fncel.2014.00297.

TORKAMANI, A. et al. (2014) De novo KCNB1 mutations in epileptic encephalopathy. *Annals of Neurology*, 76, pp. 529–540.

TORU, M. et al. (1988) Neurotransmitters, receptors and neuropeptides in post-mortem brains of chronic schizophrenic patients. *Acta Psychiatrica Scandinavica*, 78(2), pp. 121–137.

TRÉHOUT, M. et al. (2019) Dandy-walker malformation-like condition revealed by refractory schizophrenia: A case report and literature review. *Neuropsychobiology*, 77(2), pp. 59–66.

TRIKAMJI, B., SINGH, P. and MISHRA, S. (2015) Spinocerebellar ataxia-10 with paranoid schizophrenia. *Annals of Indian Academy of Neurology*, 18(1), pp. 93–95.

TRIMMER, J.S. (2015) Subcellular localization of K+ channels in mammalian brain neurons: Remarkable precision in the midst of extraordinary complexity. *Neuron*, 85(2), pp. 238–256.

TRULLAS, R. and SKOLNICK, P. (1990) Functional antagonists at the NMDA receptor complex exhibit antidepressant actions. *European Journal of Pharmacology*, 185(1), pp. 1–10.

TSAI, G. et al. (1995) Abnormal Excitatory Neurotransmitter Metabolism in Schizophrenic Brains. *Archives of General Psychiatry*, 52(10), pp. 829–836.

TSANTOULAS, C. et al. (2014) Kv2 dysfunction after peripheral axotomy enhances sensory neuron responsiveness to sustained input. *Experimental neurology*, 251, pp. 115–126.

TSANTOULAS, C. et al. (2012) Sensory neuron downregulation of the Kv9.1 potassium channel subunit mediates neuropathic pain following nerve injury. *Journal of Neuroscience*, 32(48), pp. 17502–17513.

TSENG, K.Y., CHAMBERS, R.A. and LIPSKA, B.K. (2009).

TU, L.W. and DEUTSCH, C. (1999) Evidence for dimerization of dimers in K+ channel assembly. *Biophysical Journal*, 76(4), pp. 2004–2017.

ÜÇOK, A. et al. (2015) History of childhood physical trauma is related to cognitive decline in individuals with ultra-high risk for psychosis. *Schizophrenia Research*, 169(1–3), pp. 199–203.

UHLHAAS, P.J. and SINGER, W. (2010) Abnormal neural oscillations and synchrony in schizophrenia. *Nature Reviews Neuroscience*, 11(2), pp. 100–113.

UJIKE, H. and SATO, M. (2004) Clinical features of sensitization to methamphetamine observed in patients with methamphetamine dependence and psychosis. In: *Annals of the New York Academy of Sciences*. pp. 279–287.

UNO, Y. and COYLE, J.T. (2019) Glutamate hypothesis in schizophrenia. *Psychiatry and Clinical Neurosciences*, 73(5), pp. 204–215.

VARESE, F. et al. (2012) Childhood adversities increase the risk of psychosis: A meta-analysis of patient-control, prospective-and cross-sectional cohort studies. *Schizophrenia Bulletin*, 38(4), pp. 661–671.

VEYE, K., SNYDERS, D. and DE SCHUTTER, E. (2013) Kv3.3b expression defines the shape of the complex spike in the Purkinje cell. *Frontiers in Cellular Neuroscience*, 6(NOV), [Online] Available from: doi.org/10.3389/fncel.2013.00205.

VILARIÑO-GÜELL, C. et al. (2019) Exome sequencing in multiple sclerosis families identifies 12 candidate genes and nominates biological pathways for the genesis of disease. *PLoS Genetics*, 15(6), [Online] Available from: doi.org/10.1371/journal.pgen.1008180.

VILLANUEVA, R. (2012) The cerebellum and neuropsychiatric disorders. *Psychiatry Research*, 198(3), pp. 527–532.

VINCENT, J.P. et al. (1983) Identification and properties of phencyclidine-binding sites in nervous tissues. *Federation Proceedings*, 42(9), pp. 2570–2573.

VOOGD, J. and MARANI, E. (2016) Gross anatomy of the cerebellum. In: *Essentials of Cerebellum and Cerebellar Disorders: A Primer for Graduate Students*. pp. 33–38.

VOS, T. et al. (2017) Global, regional, and national incidence, prevalence, and years lived with disability for 328 diseases and injuries for 195 countries, 1990-2016: A systematic analysis for the Global Burden of Disease Study 2016. *The Lancet*, 390(10100), pp. 1211–1259.

WALTER, T. et al. (1989) Iron deficiency anemia: Adverse effects on infant psychomotor development. *Pediatrics*, 84(1), pp. 7–17.

WANG, C. et al. (1999) Chronic phencyclidine increases NMDA receptor NR1 subunit mRNA in rat forebrain. *Journal of Neuroscience Research*, 55(6), pp. 762–769.

WANG, C.Y. et al. (2014) GDF15 regulates Kv2.1-mediated outward K+ current through the Akt/mTOR signalling pathway in rat cerebellar granule cells. *Biochemical Journal*, 460(1), pp. 35–47.

WANG, H. et al. (2002) Chronic neuropathic pain is accompanied by global changes in gene expression and shares pathobiology with neurodegenerative diseases. *Neuroscience*, 114(3), pp. 529–546.

WANG, H. et al. (1993) Heteromultimeric K+ channels in terminal and juxtaparanodal regions of neurons. *Nature*, 365(6441), pp. 75–79.

WANG, L.Y. et al. (1998) Activation of Kv3.1 channels in neuronal spine-like structures may induce local potassium ion depletion. *Proceedings of the National Academy of Sciences of the United States of America*, 95(4), pp. 1882–1887.

WANG, L.Y. and KACZMAREK, L.K. (1998) High-frequency firing helps replenish the readily releasable pool of synaptic vesicles. *Nature*, 394(6691), pp. 384–388.

WARREN, N., SISKIND, D. and O'GORMAN, C. (2018) Refining the psychiatric syndrome of anti-N-methyl-d-aspartate receptor encephalitis. *Acta Psychiatrica Scandinavica*, 138(5), pp. 401–408.

WASSEF, A., BAKER, J. and KOCHAN, L.D. (2003) GABA and Schizophrenia: A Review of Basic Science and Clinical Studies. *Journal of Clinical Psychopharmacology*, 23(6), pp. 601–640.

DE WEIJER, A.D. et al. (2013) Aberrations in the arcuate fasciculus are associated with auditory verbal hallucinations in psychotic and in non-psychotic individuals. *Human Brain Mapping*, 34(3), pp. 626–634.

WEINBERG, D. et al. (2016) Cognitive subtypes of schizophrenia characterized by differential brain volumetric reductions and cognitive decline. *JAMA Psychiatry*, 73(12), pp. 1251–1259.

WELTER, D. et al. (2014) The NHGRI GWAS Catalog, a curated resource of SNP-trait associations. *Nucleic Acids Research*, 42(D1), [Online] Available from: doi.org/10.1093/nar/gkt1229.

WESOLOWSKA, A. et al. (2010) Atypical antipsychotics with clinical antidepressant activity do not produce anti immobility effect in the mouse tail suspension test. *International journal of neuropsychopharmacology*, Conference(var.pagings), p. 69.

WHO: WORLD HEALTH ORGANIZATION (2013) *Refugee and migrant health Refugee and migrant health : definitions*. [Online] Who: World Health Organization. Available from : http://www.who.int/migrants/definitions/en/ [Accessed 16/04/20].

WINSHIP, I.R. et al. (2019) An Overview of Animal Models Related to Schizophrenia. *Canadian Journal of Psychiatry*, 64(1), pp. 5–17.

WONG, M.L. and MEDRANO, J.F. (2005).

WRIGHT, I.C. et al. (2000) Meta-analysis of regional brain volumes in schizophrenia. *American Journal of Psychiatry*, 157(1), pp. 16–25.

XU, M. et al. (2007) The axon-dendrite targeting of Kv3 (Shaw) channels is determined by a targeting motif that associates with the T1 domain and ankyrin G. *Journal of Neuroscience*, 27(51), pp. 14158–14170.

XU, M.Q. et al. (2009) Prenatal malnutrition and adult Schizophrenia: Further evidence from the 1959-1961 chinese famine. *Schizophrenia Bulletin*, 35(3), pp. 568–576.

XU, X. and DOMINO, E.F. (1994) Phencyclidine-induced behavioral sensitization. *Pharmacology, Biochemistry and Behavior*, 47(3), pp. 603–608.

YAMADA, K. et al. (2012) Association study of the KCNJ3 gene as a susceptibility candidate for schizophrenia in the Chinese population. *Human Genetics*, 131(3), pp. 443–451.

YANAGI, M. et al. (2014) Kv3.1-containing K+ channels are reduced in untreated schizophrenia and normalized with antipsychotic drugs. *Molecular Psychiatry*, 19(5), pp. 573–579.

YANG, A.C. and TSAI, S.J. (2017) New targets for schizophrenia treatment beyond the dopamine hypothesis. *International Journal of Molecular Sciences*, 18(8), [Online] Available from: doi.org/10.3390/ijms18081689.

YAVIN, E. and YAVIN, Z. (1974) Attachment and culture of dissociated cells from rat embryo cerebral hemispheres on poly lysine-coated surface. *Journal of Cell Biology*, 62(2), pp. 540–546.

YAZULLA, S. and STUDHOLME, K.M. (1998) Differential distribution of Shaker-like and Shab-like K+-channel subunits in goldfish retina and retinal bipolar cells. *Journal of Comparative Neurology*, 396(1), pp. 131–140.

YOKOYAMA, S. et al. (1989) Potassium channels from NG108-15 neuroblastoma-glioma hybrid cells. Primary structure and functional expression from cDNAs. *FEBS Letters*, 259(1), pp. 37–42.

YOLKEN, R.H. and TORREY, E.F. (2008).

YOUNG, J.W., ZHOU, X. and GEYER, M.A. (2010) Animal models of schizophrenia. *Current Topics in Behavioral Neurosciences*, 4, pp. 391–433.

YU, Y. et al. (2018) Rare loss of function mutations in N-methyl-d-aspartate glutamate receptors and their contributions to schizophrenia susceptibility. *Translational Psychiatry*, 8(1), [Online] Available from: doi.org/10.1038/s41398-017-0061-y.

ZAHN, R.K. et al. (2012) Reduced ictogenic potential of 4-aminopyridine in the hippocampal region in the pilocarpine model of epilepsy. *Neuroscience Letters*, 513(2), pp. 124–128.

ZAHN, R.K. et al. (2008) Reduced ictogenic potential of 4-aminopyridine in the perirhinal and entorhinal cortex of kainate-treated chronic epileptic rats. *Neurobiology of Disease*, 29(2), pp. 186–200.

ZAIN, M.A. et al. (2018) *Phencyclidine dose optimisation for induction of spatial learning and memory deficits related to schizophrenia in c57bl/6 mice*.

ZANDI, M.S. et al. (2011) Disease-relevant autoantibodies in first episode schizophrenia. *Journal of Neurology*, 258(4), pp. 686–688.

ZHANG, B. et al. (2019) Social-valence-related increased attention in rett syndrome cynomolgus monkeys: An eye-tracking study. *Autism Research*, 12(11), pp. 1585–1597.

ZHANG, Y. et al. (2012) Prenatal exposure to a viral mimetic alters behavioural flexibility in male, but not female, rats. *Neuropharmacology*, 62(3), pp. 1299–1307.

ZHANG, Y. and KACZMAREK, L.K. (2016) Kv3.3 potassium channels and spinocerebellar ataxia. *Journal of Physiology*, 594(16), pp. 4677–4684.

ZHANG, Y.X. et al. (2013) An Exploratory Study of the Association between KCNB1 rs1051295 and Type 2 Diabetes and Its Related Traits in

Chinese Han Population. *PLoS ONE*, 8(2), [Online] Available from: doi.org/10.1371/journal.pone.0056365.

ZHU, X.R. et al. (1999) Structural and functional characterization of Kv6.2, a new γ-subunit of voltage-gated potassium channel. *Receptors and Channels*, 6(5), pp. 337–350.

ZHUANG, J.L. et al. (2012) TGF-β1 enhances Kv2.1 potassium channel protein expression and promotes maturation of cerebellar granule neurons. *Journal of Cellular Physiology*, 227(1), pp. 297–307.

ZOLKOWSKA, K., CANTOR-GRAAE, E. and MCNEIL, T.F. (2001) Increased rates of psychosis among immigrants to Sweden: Is migration a risk factor for psychosis? *Psychological Medicine*, 31(4), pp. 669–678.

Appendices

A1 Comparison of the diagnostic criteria for schizophrenia in ICD-10 and DSM-5.

ICD-10	DSM-5
a. Thought echo, thought insertion or withdrawal, and thought broadcasting. b. Delusions of control, influence, or passivity, clearly refereed to body or limb movements or specific thoughts, actions, or sensations, delusional perception. c. Hallucinatory voices giving a running commentary on the patient's behaviour or discussing patients among themselves, or other types if hallucinatory voices coming from some part of the body. d. persistent delusions of other kinds that are culturally inappropriate and completely impossible, such as religious	A. Characteristic symptoms: Two (or more) of the following, each present for a significant portion of time during a one-month period (or less if successfully treated): • Delusions • Hallucinations • Disorganised speech (e.g., frequent t derailment or incoherence) • Grossly disorganised or catatonic behaviour • Negative symptoms (e.g., affective flattening, alogia, or avolition) Only one criterion A symptom is required if delusions or

ICD-10	DSM-5
or political identity, or superhuman powers and abilities (e.g., being able to control the weather, or being in communication with aliens from another world). e. persistent hallucinations in any modality, when accompanied either by fleeting or half-formed delusions without clear affective content, or by persistent over-valued f. ideas, or when occurring every day for weeks or months on end. g. breaks or interpolations in the train of thought, resulting in incoherence or irrelevant speech, or neologisms. h. catatonic behaviour, such as excitement, posturing, or waxy flexibility, negativism, mutism, and stupor. i. "negative" symptoms such as marked apathy, paucity of speech, and blunting or incongruity of emotional responses, usually resulting in social withdrawal and lowering of social performance; it must be clear that these are not due to depression or to neuroleptic medication. j. a significant and consistent change in the overall quality of some aspects of personal behaviour, manifest as loss of interest, aimlessness, idleness, a self-absorbed attitude, and social withdrawal. A minimum of one very clear symptom (and usually two or	bizarre hallucinations consist of a voice giving a running commentary on the person's behaviour or thought, or two or more voices conversing with each other B. Social/occupational dysfunction: For a significant portion of the time since the onset of the disturbance, one or more major areas functioning such as work, interpersonal relations, or self-care are markedly below the level achieved or prior to the onset (or when the onset is in childhood or adolescence, failure to achieve expected level of interpersonal, academic, or occupational achievement). C. Duration: Continuous signs of the disturbance persists for at least 6 months. This 6-month period must include at least 1 month of symptoms (or less if successfully treated) that meet criterion A (i.e., active-phase symptoms) and may include periods of prodromal or residual symptoms, during which the signs of the disturbance may be manifested by only negative symptoms or two or more symptoms listed in criterion A present in an attenuated form (e.g., odd beliefs, unusual perceptual experiences). D. Schizoaffective ad Mood Disorder exclusion: schizoaffective and Mood Disorder with Psychotic features have been ruled out because either (1) no Major Depressive Episode, Manic

ICD-10	DSM-5
more if less clear) belonging to any one of the groups listed as (a) to (d) below, or symptoms from at least two of the groups listed as (e) to (h), should have been clearly present for most of the time during a period of one month or more. Conditions meeting such symptomatic requirements but of duration less than 1 month (weather treated or not) should be diagnosed in the first instance as acute schizophrenia-like psychotic disorder and are classified as schizophrenia if the assumption persists for longer periods. Viewed retrospectively, it may be clear that a prodromal phase in which symptoms and behaviour, such as loss of interest in work, social activities, and personal appearance and hygiene, together with generalized anxiety and mild degrees of depression and preoccupation, preceded the onset of psychotic symptoms by weeks or even months. Because of the difficulty in timing onset, the 1-month duration criterion applies only to the specific symptoms listed above and not to any prodromal nonpsychotic phase. The diagnosis of schizophrenia should not be made in the presence of extensive depressive or manic symptoms unless it is clear that schizophrenic symptoms antedated the affective	Episode, or Mixed Episode have occurred concurrently with the active-phase symptoms; or (2) if mood episodes have occurred during active-phase symptoms, their total duration has been briefed relative to the duration of the active and residual phases. E. Substance/general medical condition exclusion: the disturbance is not due to the direct physiological effects of a substance (e.g., a drug of abuse, a medication) or a general medical condition. F. Relationship to a Pervasive Developmental Disorder: If there is a history of Autistic Disorder or another Pervasive developmental Disorder, the additional diagnosis of Schizophrenia is made only if prominent delusions or hallucinations are also present for at least a month (or less if successfully treated)

ICD-10	DSM-5
disturbance. If both schizophrenic and affective symptoms develop together and are evenly balanced, the diagnosis of schizoaffective disorder should be made, even if the schizophrenic symptoms by themselves would have justified the diagnosis of schizophrenia. Schizophrenia should not be diagnosed in the presence of overt brain disease or during states of drug intoxication or withdrawal.	

A2 Cerebellar mRNA expression levels by in-situ hybridisation experiments published by Allen Brain Atlas

Ion channel	Experiment	Raw value	log_2
Kv2.1	**74047856**	**1.22**	**0.28**
Kv5.1	68798944	2.14	1.10
Kv6.1	71489812	0	0
Kv6.2	74431065	0	0
Kv6.3	70278129	0	0
Kv6.4	**68845825**	**7.35**	**2.88**
Kv8.1	71232860	0	0
Kv8.2	1764	1.27	0.34
Kv9.1	No data	-	-
Kv9.2	70303701	0	0
Kv9.3	71488701	0	0

A3 Additional observations during PCP treatment

PCP slows animal growth.

Initially, the mice in both groups were of similar weight at baseline, with marginally higher weight in the PCP group (21.22 ± 0.27 g vs. 21.49 ± 0.22 g) compared to control animals, and both groups showed steady growth until day 4 of treatment. On day 5, the average weight of control animals significantly surpassed that of PCP animals (22.76 ± 0.29 g vs. 21.87 ± 0.24), and the growth of PCP mice was hampered until cessation of treatment and until day 8. The growth of PCP-treated animals resumed from day 9 but remained low compared to the saline-treated animals until the end of study on day 14 (24.72 ± 0.33 g vs. 23.58 ± 0.29 g). We used a two-way mixed ANOVA, which revealed a significant effect of interaction between treatment groups across study duration ($F_{(4.70,\ 371.27)} = 7.48$, $p < 0.001$), and subsequent univariate analysis on the simple main effects showed this interaction was significant from day 5 ($p < .05$), except for day 11 and day 12.

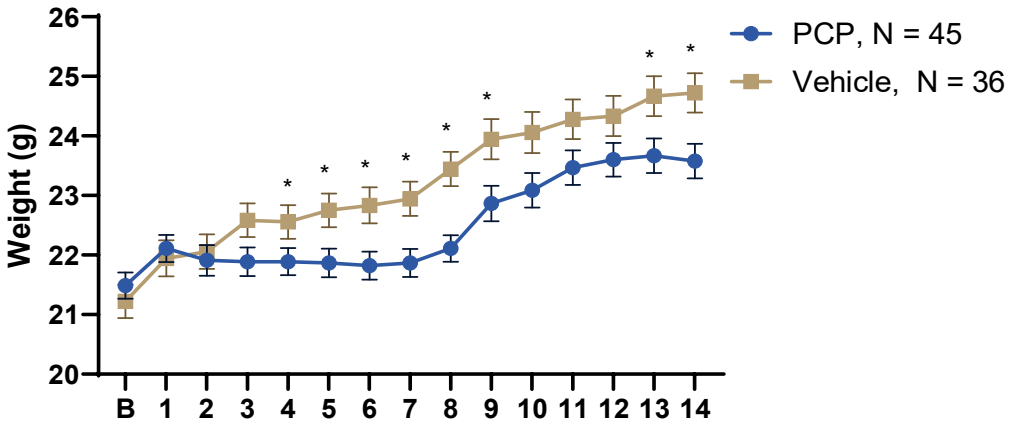

Figure A3-1 Animal weight plot in the subchronic study.

The trend shows hampered growth in the PCP cohort, resulting in average lower body weight at day 14. Data shows mean ± SEM.* $p < .05$ (Pairwise comparison).

PCP reduced the frequency of bowel movements.

We also recorded the frequency of faecal droppings after each trial throughout the study (**Table A3-1**). We observed a statistically significant difference in the frequency of faecal boli production in the PCP group ($\chi^2_{(4)} = 40.13$, $p = .0001$, Friedman test), and a post-hoc analysis with Dunn's multiple comparison revealed that the PCP animals produced droppings significantly less frequently on day 1 (mean frequency, 0.94 ± 0.21 vs. 8.13 ± 0.41; Z = 4.58, $p = .0001$) compared to baseline, and on day 4 of treatment (0.69 ± 0.15 vs. 8.13 ± 0.41; Z = 5.20, $p = .0001$), as well as during the washout period on days 8 (1.00 ± 0.16 vs. 8.13 ± 0.41; Z = 4.47, $p = .0001$) and 14 (1.76 ± 0.37 vs. 8.13 ± 0.41, Z = 3.63, $p = .003$), whereas no statistical significance across study duration in bowel movements within the control group was observed ($\chi^2_{(4)} = 5.21$, $p = .27$).

Table A3-1 Bowel movement frequency in the PCP animals across the study duration.

	Faecal droppings
Comparison	**Mean ± SEM, Significance^**
Baseline vs. Day 1	8.13 ± 0.41 vs. 0.94 ± 0.21, $p < .0001$
Baseline vs. Day 4	8.13 ± 0.41 vs. 0.69 ± 0.15, $p < .0001$
Baseline vs. Day 8	8.13 ± 0.41 vs. 1.00 ± 0.16, $p = .0003$
Baseline vs. Day 14	8.13 ± 0.41 vs. 1.76 ± 0.37, $p = .0031$

^, Dunn's correction within PCP groups.

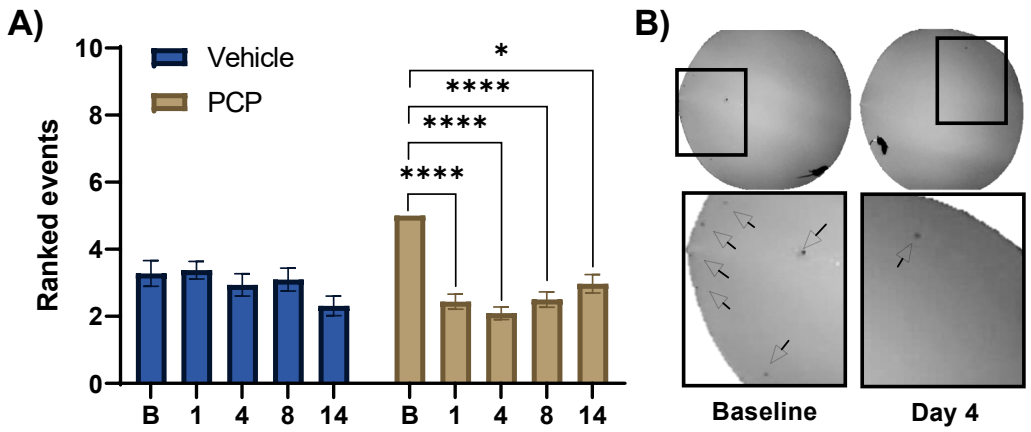

Figure A3-2 Frequency of bowel movements throughout the study duration.
The bars show ranks ± SEM of bowel movement frequencies listed in Table 4-2. *, $p = .03$; ****, $p = .0001$ (Dunn's multiple comparison). Representative images of the last frames of video recordings (B). Arrows showing the number of droppings at baseline and on day 4 in the PCP group.

Neither haloperidol nor clozapine attenuate PCP-induced decreased bowel movement frequency.

Although Kruskal-Wallis test detected significant difference in mean rank frequency between treatment groups ($\chi^2_{(3)} = 22.75$, $p < .0001$). The Dunn's

multiple comparison post-hoc analysis showed that PCP-treated mice defaecated statistically significantly lower than the control animals (mean frequency, 8.40 ± 0.48 vs. 1.20 ± 0.20; Z = 3.64, p = .0016). Additionally, both the haloperidol and clozapine co-administered animals not only failed to normalise the PCP-induced reduction in bowel movement frequency, but similarly to PCP animals, the haloperidol co-administered group (2.00 ± 0.31 vs. 8.40 ± 0.48; Z = 2.71, p = .002) and the clozapine co-administered group (1.43 ± 0.79 vs. 8.40 ± 0.48; Z = 4.14, p = .0002) defaecated significantly less frequently compared to the animals in the control group.

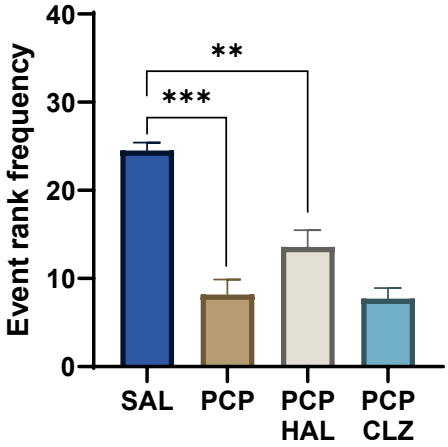

Figure A3-3 Effect of concomitant antipsychotic drug administration on PCP-reduced bowel movement frequency.

Neither concomitant PCP+HAL nor PCP+CLZ normalised normal bowel movement frequency. Bars show mean ranks ± SEM. **, p < .01; ***, p < .001. Dunn's multiple comparison. Abbreviations: HAL. Haloperidol; CLZ, clozapine.

Table A3-2 Dunn's multiple comparison of defaecation frequency between treatment groups

	Defaecation frequency
Comparison	**Mean ± SEM, Significance^**
SAL vs. PCP	8.40 ± 0.48 vs. 1.20 ± 0.20, p = .0016
SAL vs. PCP + HAL	8.40 ± 0.48 vs. 2.00 ± 0.31, p = .0037
SAL vs. PCP + CLZ	8.40 ± 0.48 vs. 1.43 ± 0.79, p = .1370
PCP vs. PCP + HAL	1.20 ± 0.20 vs. 2.00 ± 0.31, p > .9999
PCP vs. PCP + CLZ	1.20 ± 0.20 vs. 1.43 ± 0.79, p > .9999
PCP + HAL vs. PCP + CLZ	2.00 ± 0.31 vs. 1.43 ± 0.79, p > .9999

^, Dunn's multiple comparison

PCP evokes audible vocalisations during subchronic treatment

Our first direct observation involved audible vocalisations which were apparent approximately 15 minutes following each PCP injection. This phenomenon preceded any other directly observable changes in behaviour, and it did not occur following saline injection. Although the frequency at which these vocalisations were emitted nor the duration of these events were measured, a Cochran-Armitage test revealed a significant trend in vocalisation events within the PCP group ($\chi^2_{(1)}$ = 39.65, p = .0001). During treatment days, 85.7% (N = 48) of animals exhibited audible vocalisation following PCP injection, whereas 14.3% of mice (N = 8) did not vocalise (**Figure A3-3**). The vocalisations did not occur at baseline or during the washout period.

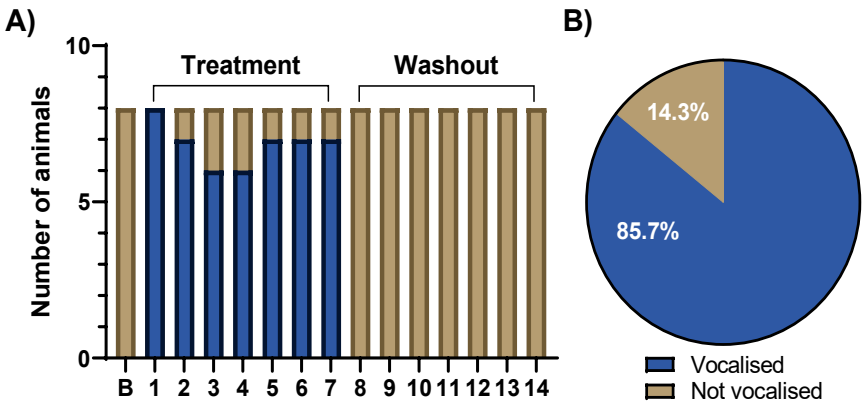

Figure A3-4 Vocalisation evetns in the PCP animals.

The stacked bar graph in A illustrates the vocalisation events across study duration in the PCP group. Out of 56 counts in total days of treatment (days 1-7), 48 volcalisation events (85.7%) were reported. The proportion of total events is shown in the pie chart shown in B. Vehicle group not considered.

HAL and CLZ attenuate PCP-induced vocalisations.

As in the subchronic study, we report that acute PCP treatment induced vocalisations in 90% of animals. Concomitant PCP+HAL injection prevented PCP-induced vocalisations in all animals, whereas PCP+CLZ reduced vocalisation from 90% to 10%.

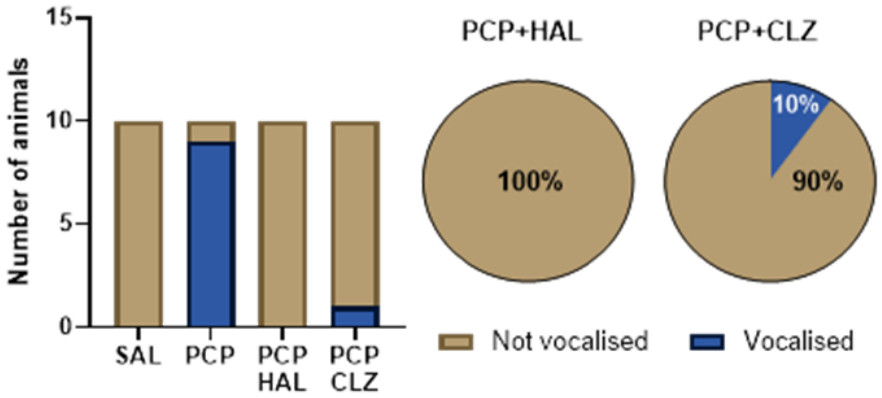

Figure A3-5 Effect of APDs on PCP-evoked audible vocalisations.

No animals in the control group produced vocalisations following saline injection, while 90% of PCP-treated mice vocalised after injection. Concomitant HAL prevented vocalisation in all animals, whereas CLZ was effective in attenuating vocalisation events in 90% of the subjects.